New Insights into Mitochondrial Quality Control Mechanisms in Neurons and Astrocytes

Jack Hartley Howden

A thesis submitted to University College London

for the degree of Doctor of Philosophy

September 2021

Department of Neuroscience, Physiology and Pharmacology

I, Jack Hartley Howden, confirm that the work presented in this thesis is my own.

Where information has been derived from other sources, I confirm that this has been indicated in the thesis.

Abstract

Mitochondria play essential roles in ATP generation, calcium buffering and apoptotic signalling. In complex neuronal networks of the CNS, mitochondrial quality control systems are essential to maintain a functional mitochondrial network in neurons and glia. The clearance of dysfunctional mitochondria is termed mitophagy and mutations in this pathway are linked to Parkinson's Disease. This thesis investigated the mitophagy pathway in astrocytes and neurons and identified clear differences in the spatiotemporal regulation, showing that mitophagy occurs quicker and is less spatially restricted in astrocytes compared to neurons. Additionally, it was found that astrocytic mitophagy is dependent on glycolysis. Furthermore, with the use of genetic mouse models, the role of Miro1 in mitophagy in astrocytes and neurons was investigated. This thesis identified a redundancy in the requirement of Miro1 for the mitophagic process in astrocytes yet highlighted its importance for neuronal mitochondrial homeostasis *in vitro* and *in vivo*. The loss of Miro1 delayed neuronal mitophagy *in vitro* and the long-term disruption of mitochondrial quality control in principal neurons lacking Miro1 *in vivo* led to upregulation of Mfn1/2, remodelling of the mitochondrial network and induction of the integrated stress response. Altogether, this thesis provides important new insights into the cell type-specific regulation of mitochondrial quality control in astrocytes and neurons and outlines how disrupted mitochondrial homeostasis in the CNS can lead to neurodegenerative pathology.

Impact Statement

Clinical genetics has identified a clear role for mitochondrial dynamics and quality control mechanisms in the aetiology of human neurodegenerative disease, particularly Parkinson's Disease. The work contained within this thesis further contributes to our understanding of these mechanisms in two important cell types of the central nervous system: neurons and astrocytes, with relevance for neuroscientists, cell biologists, clinicians, geneticists and others. This work will be disseminated through publication in peer-reviewed journals and presentations at conferences.

Acknowledgements

I would first like to thank Josef for his constant supply of knowledge, help and support over the years. Secondly, I would like to thank all the past and present members of the Kittler lab. You guys have helped me enormously over the last 5 years, I could not have done it without you. Georgina, Christian and Nathalie for taking me under their wings when I first arrived and providing me with the knowledge and techniques I needed. Davor, Viktoriya and James (x2) for making office life so easy and enjoyable. Flavie and Guillermo for being the constants during my time in the lab. I have learnt so much from both of them and I cannot thank them enough.

I would like to thank my family for their unwavering support, I hope I have made them proud. I can (nearly) finally say I have more degrees than my father…

Last but not least, I would like to thank Jess. She has made the last 5 years in London so happy and enjoyable. Her daily love and support have made this PhD attainable.

Table of Contents

Abbreviations

2DG – 2-Deoxy-D-glucose

6-OHDA – 6-hydroxydopamine

AA – Antimycin-A

AD – Alzheimer's Disease

ADOA – Autosomal dominant optic atrophy

ALS – Amyotrophic Lateral Sclerosis

AMBRA1 - Autophagy And Beclin 1 Regulator 1

AMPA – a-amino-3-hydroxy-5-methyl-4-isoxazolepropionic acid

AMPK – AMP-activated protein kinase

APV - Amino-5-phosphonovaleric acid

ASD – Autism Spectrum Disorders

ATP – Adenosine triphosphate

BNIP3 - BCL2 interacting protein 3

BNIP3L - BCL2 Interacting Protein 3 Like

Ca^{2+} - Calcium

CCCP - Carbonyl cyanide m-chlorophenyl hydrazone

CMT2A – Charcot-Marie-Tooth Subtype 2A

CNS – Central nervous system

CRISPR – Clustered regularly interspaced short palindromic repeats

DA – Dopaminergic

DAPI – 4,6-diamidino-2-phenylindole

DHODH – Dihydroorotate dehydrogenase

DMSO – Dimethyl sulfoxide

DNA – Deoxyribonucleic acid

DNQX – 6,7-dinitroquinoxalin-2,3-dione

DRP1 – Dynamin-related protein 1

ER – Endoplasmic reticulum

FCCP - Carbonyl cyanide-p-trifluoromethoxyphenylhydrazone

FIS1 – Mitochondrial fission protein 1

FUNDC1 - FUN14 domain containing 1

GCN2 – General control non-derepressible

GFAP – Glial fibrillary acidic protein

GFP – Green fluorescent protein

GLAST – Glutamate/aspartate transporter

GLT1 – Glutamate transporter 1

HD – Huntington’s Disease

HRI – Heme-regulated eIF2α kinase

IFNγ – Interferon gamma

IMM – Inner mitochondrial membrane

IP3 – Inositol triphosphate receptor

iPSC – Induced pluripotent stem cells

ISR – Integrated stress response

K^+ - Potassium

KIF – Kinesin-related protein

KO – Knockout

LC3 – Light chain 3

LPS – Lipopolysaccharide

LTCC – L-type calcium channels

LTP – Long-term potentiation

MAP2 – Microtubule associated protein 2A

MCU – Mitochondrial Ca^{2+} uniporter

MERCS – Mitochondrial-ER contact sites

MFF – Mitochondrial fission factor

Mfn – Mitofusin

mGluR – Metabotropic glutamate receptor

MPTP – Mitochondrial permeability transition pore

MtDNA – Mitochondrial deoxyribonucleic acid

MUL1 – Mitochondrial ubiquitin ligase activator of NFKB1

Na^{+} - Sodium

NCLX – Na^{+}/Ca^{2+} exchanger

NDUFS4 – NADH:ubiquinone oxidoreductase subunit 4

NMDA – N-methyl-D-aspartate

NMJ – Neuromuscular junction

OMM – Outer mitochondrial membrane

OPA1 – Optic atrophy 1

OPC – Oligodendrocyte precursor cell

OPTN – Optineurin

OXPHOS – Oxidative phosphorylation

PAP – Peripheral astrocyte process

PBS – Phosphate-buffered saline

PCR – Polymerase chain reaction

PD – Parkinson’s Disease

PERK – PKR-like ER kinase

PFA – Paraformaldehyde

PI – Propidium iodide

PINK1 – PTEN-induced kinase 1

PKR – Double-stranded RNA-dependent protein kinase

PPV – Pulse to pulse variability

RGC - Retinal ganglion cell

ROS – Reactive oxygen species

SN – Substantia Nigra

SNPH – Syntaphilin

STING – Stimulator of interferon genes

TBC1D15 - TBC1 Domain Family Member 15

TCA – Tricarboxylic acid

TMRM – Tetramethyl rhodamine

TRAK – Trafficking kinesin-binding protein

TRPML1 - Transient receptor potential mucolipin 1

TTX – Tetrodotoxin

VDAC – Voltage-dependent anion-selective channel

WT – Wild-type

YFP – Yellow fluorescent protein

Publications directly arising from the work in this thesis.

Guillermo López-Doménech*, Jack H. Howden*, Christian Covill-Cooke, Corinne Morfill, Jigna V. Patel, Roland Burli, Damian Crowther, Nicol Birsa, Nicholas J. Brandon, Josef T. Kittler (2021) Loss of neuronal Miro1 disrupts mitophagy and induces hyper-activation of the ISR. *The EMBO Journal EMBO J. 2021 Jun 21:e100715.*

Jack H. Howden, Guillermo López-Doménech, Josef T. Kittler (2021) Mitochondrial Dynamics in CNS Health and Disease. *Nature communications (pre-publication).*

Christian Covill-Cooke, Jack H Howden, Nicol Birsa, Josef T Kittler (2018) Ubiquitination at the mitochondria in neuronal health and disease. *Neurochem Int. 2018 Jul;117:55-64.*

* - denotes joint first author

Chapter 1 - Introduction

1.1 Summary

Mitochondria are vital organelles that play critical roles in ATP generation, calcium buffering and apoptotic signalling. In complex neuronal networks of the Central Nervous System (CNS), mitochondrial trafficking is crucial to match mitochondrial positioning to localised energy demands at synapses, while correct mitochondrial dynamics and quality control systems are essential to maintain a functional mitochondrial network. The extreme spatial variability in metabolic demand and need for tight calcium (Ca^{2+}) regulation makes mitochondria and their dynamics perfectly suited to regulating CNS formation and function (MacAskill and Kittler, 2010, Seager et al., 2020).

Synapses enable neurons to communicate by electrical and chemical means. At chemical synapses, neurotransmitters are released from vesicles into the synaptic cleft in response to action potentials triggering the influx of Ca^{2+} ions through voltage gated ion channels (Jahn and Fasshauer, 2012). Filling and releasing of vesicles and regulating electrochemical gradients are highly energy-demanding processes that are tightly regulated by Ca^{2+} dynamics. Therefore, it is unsurprising that mitochondria are actively recruited to and reside at synapses (Devine and Kittler, 2018). Neurons are highly complex and polarised cells that require organized positioning of synapses to carry out the process of information required for CNS function. Thus, mitochondria are required to be transported, often over very long distances, to synapses

positioned at various locations away from the soma, where the nucleus resides, and the majority of mitochondrial biogenesis takes place (Davis and Clayton, 1996).

Traditionally, synapses were simply thought of as a point of communication between two neurons, but it is now widely accepted that astrocytes and microglia, types of glial cell, play a key role in synaptic function. This has been termed the tetrapartite synapse due to all four components contributing to synapse formation and function (Dityatev and Rusakov, 2011). Thus, there is a growing belief that astrocytic and microglial mitochondria and their dynamics and quality control mechanisms are also extremely important to synaptic function.

In this section, the mechanisms underpinning mitochondrial trafficking, dynamics and quality control in neuronal and glial cells and their role in CNS function will be outlined. Next, the main canonical roles of mitochondria; ATP production and Ca^{2+} buffering will be explored in the context of synaptic development, function, and plasticity and how dysfunctional mitochondria could contribute to neurodegenerative disease. Additionally, more putative roles for mitochondria in CNS health and disease will be looked at, including ROS-dependent synaptic pruning and transcellular mitochondrial transfer.

1.2 Mitochondrial recruitment to- and stabilisation at the synapse

Neurons are highly complex and polarised cells that require organized positioning of synapses to carry out the communication between other

neurons required for CNS function. Thus, mitochondria are required to be transported, often over exceptionally long distances, to synapses positioned at various locations away from the soma, where the nucleus resides, and the majority of mitochondrial biogenesis takes place (Davis and Clayton, 1996) (Figure 1).

In primary mature neurons, 10-20% of axonal and 5-10% of dendritic mitochondria are motile and are transported over distances up to 1m at velocities up to 2µm per second (Morris and Hollenbeck, 1993, Martin et al., 1999, Chen et al., 2007, Kang et al., 2008, Russo et al., 2009, Chen and Sheng, 2013, Faits et al., 2016, Zhou et al., 2016). The percentage of motile mitochondria decreases *in vivo* (Smit-Rigter et al., 2016) and with maturation (Faits et al., 2016, Lewis et al., 2016, Zhou et al., 2016). In the early developmental stages (DIV7) up to 50% of axonal mitochondria are motile with a progressive decline to ~20% at maturity (DIV18) which is accompanied by an increased mitochondrial occupancy at presynaptic boutons and dendritic spines (Zhou et al., 2016, Faits et al., 2016, Lewis et al., 2016).

Long distanced mitochondrial trafficking is, in the main, fulfilled by movement along microtubules via interaction with motor proteins. In axons, microtubules display directional polarity with the + end placed distally and the – end placed somatically (Baas et al., 1988). Of the axonal mitochondria in motion, approximately half are those are moving in the anterograde direction (away from the soma) and half are moving in the retrograde direction (towards the

soma). Anterograde movement is controlled by kinesin motors whereas dynein motors control retrograde trafficking (Glater et al., 2006). Conversely in dendrites, microtubules are non-uniformly orientated with both + and – ends placed somatically and distally (Baas et al., 1988), and mitochondrial transport is primarily dynein-dependent (Zheng et al., 2008). Various cargoes are transported by kinesin/dynein motors throughout neuronal processes and are bound to the motors through interactions with cargo-specific adaptor proteins (Karcher et al., 2002).

Mitochondrial motility along microtubules is tightly regulated by its adaptors, the membrane bound mitochondrial RhoGTPases (Miros), which link with kinesin/dynein motors via the trafficking kinesin-binding proteins (TRAKs), TRAK1 and TRAK2 (Stowers et al., 2002). TRAK1 is, in the main, localised to axons and can bind to both kinesin and dynein motors, whereas TRAK2 preferentially binds with dynein motors and is localised to the dendrites (van Spronsen et al., 2013). The importance of the TRAKs is highlighted by a recent study showing that kinesin-1 movement along microtubules is entirely dependent on its interaction with TRAK1 (Henrichs et al., 2020).

Miros are made up of 2 isoforms, Miro1 and Miro2, that contain 2 GTPase domains flanking 2 Ca^{2+}-binding EF-hand domains and an outer mitochondrial membrane targeted carboxy-terminal domain (Birsa et al., 2013, Devine et al., 2016). Miros are found in almost all eukaryotic cells but their role takes on particular importance in neurons where mitochondria are transported over long

microtubule tracts throughout axons and dendrites to pre- and post-synapses (Saxton and Hollenbeck, 2012, Schwarz, 2013, Maeder et al., 2014, Sheng, 2014). The drosophila orthologue of the mammalian Miros, dMiro, is required for both kinesin-driven and dynein-driven axonal trafficking of mitochondria to and from presynapses and dynein-driven trafficking of mitochondria into dendrites (Guo et al., 2005, Russo et al., 2009). All these processes are dependent on N-terminal GTPase activity of Miro (Babic et al., 2015) and interaction with the TRAK orthologue, Milton. Further studies in mammalian cells have highlighted Miro1 as the key isoform when it comes to mitochondrial trafficking along microtubules. The Ca^{2+}-sensing EF-hand domains of Miro1 allow coordination of mitochondrial transport with intracellular Ca^{2+} concentrations and although the exact mechanism is somewhat disputed, this relationship is key for the positioning of mitochondria at neuronal synapses. One possible mechanism is that increasing Ca^{2+} concentrations inhibit an interaction between Miro1 and the kinesin motor, KIF5, thereby releasing mitochondria from the microtubules (Macaskill et al., 2009). An alternative model suggests that Ca^{2+} causes a conformational change in KIF5 itself, to release it from the microtubules, in turn releasing mitochondria (Wang and Schwarz, 2009). A third mechanism includes the presence of an anchoring protein, that upon the presence of increased Ca^{2+} concentrations, binds to mitochondria, thereby stopping its movement. In axons, the protein Syntaphilin (SNPH) has been identified as a mitochondrial anchor that is able to bind to mitochondria, independently of Miro1, to facilitate mitochondrial stopping

(Chen and Sheng, 2013) (Figure 1). How/if dendritic mitochondria are stabilised in a similar manner remains to be established.

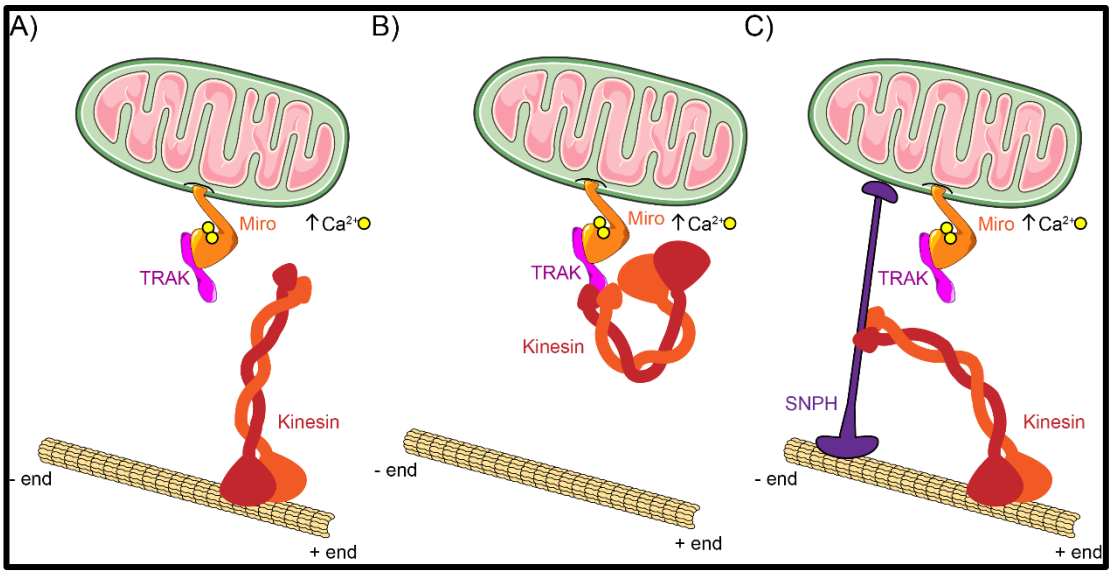

Figure 1: Proposed mechanisms for Ca^{2+} dependent stopping of mitochondria. A) Ca^{2+} binds to the EF-hand domains of Miro1 to inhibit an interaction between Miro1 and the kinesin motor, KIF5, thereby releasing mitochondria from the microtubules (Macaskill et al., 2009). B) Increasing Ca^{2+} concentrations cause a conformational change in KIF5 itself, to release it from the microtubules, in turn releasing mitochondria (Wang and Schwarz, 2009). C) Upon the presence of increased Ca^{2+} concentrations, a microtubular anchoring protein binds to mitochondria, stopping its movement. In axons, the protein Syntaphilin (SNPH) has been identified as a mitochondrial anchor that is able to bind to mitochondria, independently of Miro1, to facilitate mitochondrial stopping (Chen and Sheng, 2013). Schematic adapted from (Birsa et al., 2013).

On top of microtubular-based transport, mitochondria also couple to the actin cytoskeleton - an interaction that may be key to the stabilisation of mitochondria at synapses. Presynaptic boutons and postsynaptic spines are highly enriched for filamentous actin (f-actin) (D'Este et al., 2015, Nirschl et al., 2017) and actin-dependent motility, mediated by myosin motors, tends to be more localised than microtubular-dependent motility (Morris and Hollenbeck, 1995, Hirokawa and Takemura, 2005, Quintero et al., 2009, Saxton and Hollenbeck, 2012). Consequently, f-actin could act as the ideal mitochondrial scaffold at synapses. At presynapses, it has recently been proposed that axonal mitochondria can be anchored to the actin cytoskeleton via an interaction between SNPH and myosin VI (Li et al., 2020). Presynaptic captured mitochondria become mobilised and released back into the axonal tract following myosin XI depletion or treatment with latrunculin B, an actin depolymeriser (Li et al., 2020). A similar interaction may also occur between mitochondria and the actin cytoskeleton at postsynaptic spines. Dendritic mitochondria shorten and become more dynamic following actin disassembly (Rangaraju et al., 2019) although little is known mechanistically about the interaction between dendritic mitochondria and f-actin.

Miros have also been shown to couple mitochondria to the actin cytoskeleton, via interaction with myosin XIX (Lopez-Domenech et al., 2018) and hence Miro may provide a linker for mitochondria to disengage from long distance microtubular-based transport and switch to localised actin-based transport.

Despite this, the role of Miro-myosin XIX-actin coupling at synapses is yet to be established and warrants further research. Could Miro-dependent actin coupling provide a mechanism for synaptic stabilisation of mitochondria in dendrites?

The importance of Miro and mitochondrial trafficking for CNS health and function is highlighted by the fact that Miro1 knockout is lethal postnatally (Nguyen et al., 2014, Lopez-Domenech et al., 2016). Conditional knockout strategies have shown that neuronal knockout of Miro1 leads to defects in dendritic mitochondrial distribution and decreased dendritic branching leading to progressive neurodegeneration (Lopez-Domenech et al., 2016). Neuronal death in this model occurs in the absence of defects in mitochondrial ATP production or Ca^{2+} buffering (Nguyen et al., 2014), thus highlighting that neuronal mitochondrial trafficking and placement are a prerequisite for CNS health.

1.3 Mitochondrial trafficking in glia

Traditionally, synapses were simply thought of as a point of communication between two neurons, but it is now widely accepted that glia, in particular astrocytes, are present at synapses and play a key role in synaptic function. Thus, there is a growing belief that astrocytic mitochondria and their dynamics are also extremely important to synaptic function. Glial cells make up roughly half of all cells in the brain and are essential for neuronal homeostasis (Allen and Lyons, 2018), yet in contrast to mitochondrial dynamics in neurons, the

role of glial mitochondria and their dynamics in CNS function and disease has been somewhat underappreciated (Figure 1).

1.3.1 Astrocytes

Astrocytes are the most abundant glial cells in the central nervous system (Kettenmann and Verkhratsky, 2008). Termed astro (star) -cytes (cells) due to their star-like structure, they extend vast numbers of highly ramified processes from a central cell body that together from a dense meshwork engulfing neurons, vasculature and other glia (Oberheim et al., 2006). Astrocytes are involved in numerous CNS functions, including neuronal and synaptic plasticity, ionic homeostasis, glucose metabolism, glutamate uptake & clearance and the control of blood flow in the brain. These functions are supported by ultrafine processes that contact vast numbers of synapses and end-feet that ensheath blood vessels (Bushong et al., 2004, Halassa et al., 2007). This specialised morphology allows astrocytes to couple neuronal activity with rapid metabolic changes. Astrocytes respond to neuronal activity by increasing their intracellular Ca^{2+} and releasing glutamate, ATP, thrombospondins, cholesterol, and glypicans to refine synapse structure and function in the developing and adult brain meaning astrocyte function is intimately related to brain wiring, plasticity and pathology (Allen, 2014).

A single astrocyte in the rodent brain can contact up to 100,000 synapses increasing to 2 million in the human brain (Oberheim et al., 2009). The finest of these processes, known as peripheral astrocytic processes (PAPs), can be

as small as 20nm in diameter and contain almost no cytoplasm. It was originally thought that PAPs were too narrow to accommodate mitochondria, however new imaging capabilities have identified the presence of mitochondria within PAPs *in situ* and *in vivo* (Oberheim et al., 2009, Jackson et al., 2014, O'Donnell et al., 2016, Derouiche et al., 2015, Stephen et al., 2015, Agarwal et al., 2017, Jackson and Robinson, 2018, Lovatt et al., 2007, Mathiisen et al., 2010). Thus, mitochondria are required to be transported to these distal regions as mitochondrial biogenesis is likely not possible in such small areas. Yet, unlike in neurons, less is known about the mechanisms underlying the trafficking of astrocytic mitochondria to and from synapses.

Primary astrocytes alone in culture vary greatly in appearance from their counterparts *in vivo*. Without the need for synaptic contacts, they are morphologically simple and do not contain ramified processes (Matsutani and Yamamoto, 1997). Therefore, most studies into mitochondrial trafficking and dynamics in astrocytes have been done in neuron-astrocyte co-cultures, organotypic slice cultures, acute slices and *in vivo*. Direct comparisons between neurons and astrocytes have shown that astrocytic mitochondria are generally less motile than their neuronal counterparts. In organotypic hippocampal slices *in situ,* two studies have similarly shown that only 20-30% of mitochondria are motile in astrocytic processes compared to ~50% in neuronal processes from the same preparation. Of those moving, neuronal mitochondria move around 3 times quicker than astrocytic mitochondria

(Jackson et al., 2014, Stephen et al., 2015). The percentage of motile mitochondria and the velocity of those moving decreases when imaging astrocytes *in vivo* (Jackson and Robinson, 2018).

As with neurons, astrocytic mitochondria are trafficked to and stabilised at sites of elevated activity including synapses (Jackson et al., 2014, Stephen et al., 2015). Astrocytic activity is heavily linked to neuronal and synaptic activity, particularly excitatory (glutamatergic) activity, and coincides with localised increases in intracellular Ca^{2+} concentrations (Dani et al., 1992). Blockade of neuronal activity through treatment with TTX (blocks action potential generation) or DNQX, APV and bicuculline (AMPAR, NMDAR and GABAR antagonists, respectively) increase the percentage of motile mitochondria in astrocytes threefold from 15 to 45% *in situ*. Adversely, increasing neuronal activity with 4-AP or glutamate treatment decreases mitochondrial mobility and reduces the distance between mitochondria and synapses (Stephen et al., 2015). Consequently, glutamate transmission has been implicated in the mechanism underlying mitochondrial arrest in astrocytes.

Synaptic glutamate can be taken up into astrocytes, via GLT1 and GLAST, or bind to glutamate receptors (mGluRs, AMPARs and NMDARs) present on astrocytic membranes. Inhibition of glutamate uptake with TFB-TBOA increases the percentage of motile mitochondria in astrocytes and decreases their localisation with synapses (Jackson et al., 2014). Additionally, pharmacological blockade of mGluRs and NMDARs (with D-APV), but not

AMPARs (with NBQX), blocks glutamate-induced mitochondrial stopping in astrocytes *in situ* (Stephen et al., 2015). AMPAR and NMDAR activation results in the influx of Na+ and Ca^{2+} ions, respectively and mGluR results in the release of Ca^{2+} from intracellular stores. Thus, it makes sense that astrocytic mitochondria are recruited to synapses following mGluR and NMDAR activation and Ca^{2+} elevation but not AMPAR activation.

As in neurons, the Ca^{2+}-dependent arrest of mitochondria in astrocytes is facilitated by Miro and TRAK. Both Miro isoforms are expressed in astrocytes and localise to mitochondria present throughout astrocyte processes (Stephen et al., 2015). In the case of TRAKs, TRAK2 is the main isoform present in astrocytes (Ugbode et al., 2014). This points to similarities between the mitochondrial trafficking machinery present in astrocytes and dendrites; a phenomenon that may explain the reduced mitochondrial mobility in astrocytes when compared to neurons as a whole (axons and dendrites).

In the case of Miro, Miro1 has once again been identified as the predominant isoform when it comes to mitochondrial mobility and arrest in astrocytes (Stephen et al., 2015, Jackson et al., 2014). Overexpression of Miro1 increases the percentage of motile mitochondria in astrocytes *in situ*. Expression of a Ca^{2+}-insensitive Miro1 mutant, $Miro1^{\Delta EF}$, also increases mitochondrial motility but blocks their arrest following glutamate application (Stephen et al., 2015). Therefore, Miro1, through its Ca^{2+} sensing EF-hand domains, appears to mediate the activity/Ca^{2+}-dependent arrest of

mitochondria in astrocytes. However, a full mechanism is yet to be elucidated and less is known regarding the other trafficking machinery involved in astrocytes.

The speed of mitochondrial movement in astrocytes is more akin to actin-coupled mitochondrial movement than the kinesin/dynein-dependent microtubular-coupled movement seen in neurons (Morris and Hollenbeck, 1995). In fact, the actin cytoskeleton has been shown to be involved in the Ca^{2+}-dependent arrest of astrocytic mitochondria (Kremneva et al., 2013). However, mitochondria in astrocytes are still required to be transported long distances to synapses and to reside in PAPs, which is likely dependent on microtubules. Thus, could the presence of different motors, adaptor proteins or cytoskeletons underlie the differences in mitochondrial trafficking between astrocytes and neurons? In addition to microtubular and actin networks, astrocytes contain three types of intermediate filaments (IF): glial fibrillary acidic protein (GFAP), vimentin and nestin (Lepekhin et al., 2001). So, could these IFs contribute to mitochondrial trafficking and stabilisation at synapses in astrocytes?

1.3.2 Microglia

Microglia are resident immune cells of the CNS and account for 10-15% of all cells found within the brain (Lawson et al., 1992). As a specialised population of macrophages, they act as the principal form of immune defence in the CNS. Microglia also play key roles in brain development and homeostasis including

synaptic organisation and pruning, myelin turnover, control of neuronal excitability and providing neurotrophic support. They respond to CNS insult by shifting to a reactive phenotype, altering their morphology, proliferation rates, phagocytic activity, antigen presentation and the release of inflammatory mediators. Microglial physiology is tightly regulated by its surrounding microenvironment and interactions with neurons, astrocytes and other glia. Microglia constantly survey their microenvironment through the extension and retraction of highly ramified, ultrafine processes; monitoring for foreign bodies including bacteria, fungi and viruses and the release of ATP from damaged neurons. Microglial surveillance is also key to synaptic development and homeostasis [Reviewed in (Li and Barres, 2018)].

As with astrocytes, microglia are less morphologically complex when cultured alone *in vitro* and due to their small size, the visualisation of mitochondria within microglia *in vivo* or *in situ* has been a challenge. However, with new imaging capabilities it has recently been shown that microglial processes are heavily populated with mitochondria both *in situ* and *in vivo* (Katoh et al., 2017, McWilliams et al., 2018). Nevertheless, mitochondrial trafficking and stabilisation in microglia and the molecular mechanisms underpinning these have not been well studied and various intriguing questions remain including: Do microglial mitochondria position themselves at sites apposed to synapses? Are these mechanisms similar to those in astrocytes? And how is

mitochondrial trafficking altered as microglia change from a non-reactive to a reactive phenotype?

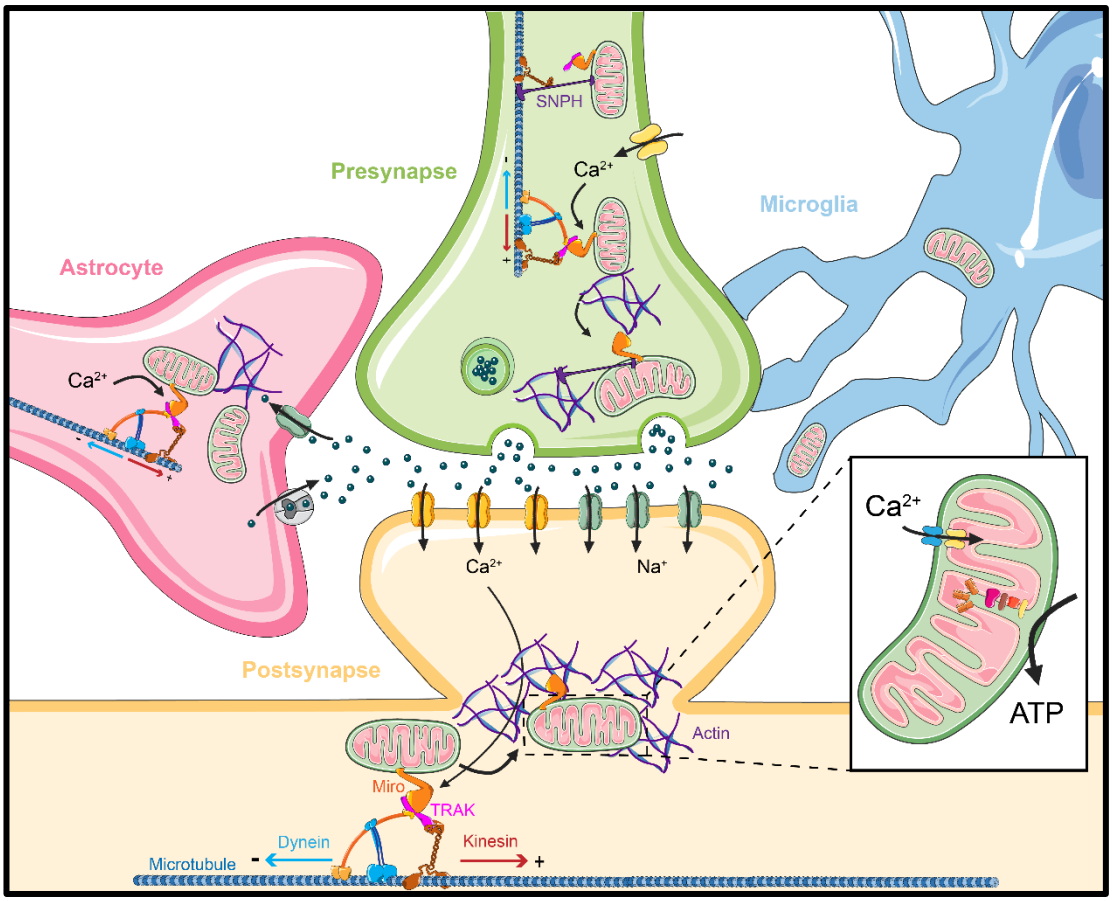

Figure 2: Mitochondrial recruitment to- and stabilisation at the synapse in neurons and glia. Miro interacts with kinesin and dynein motors in complex with TRAK motor adaptors to traffic mitochondria along microtubules. Miro's Ca^{2+}-sensing EF-hand domains facilitate the activity-dependent stopping of mitochondria at synapses. Miro can also couple mitochondria to the actin cytoskeleton which may play a role in the synaptic anchoring of mitochondria. In axons, the mitochondrial anchor protein, syntaphilin (SNPH), can stabilise mitochondria on microtubules and actin. Once present at synapses, mitochondria regulate synaptic function via ATP provision and buffering of intracellular Ca^{2+}.

1.4 Provision of ATP

CNS functions pose a large energetic burden. The brain constitutes around 2% of the mass of the human body, yet it utilises up to 20% of the ATP produced (Attwell and Laughlin, 2001). Glycolysis is capable of rapidly producing cellular energy directly from the breakdown of glucose and is the preferred form of fuel generation for certain neuronal functions including the fast-axonal transport of vesicles. In fact, axonal vesicles are decorated with their own set of glycolytic enzymes (Zala et al., 2013). However, glycolysis is only capable of generating only 2 molecules of ATP per molecule of glucose whereas mitochondrial oxidative phosphorylation generates around 30 (Kety, 1963). Thus, oxidative phosphorylation is the main source of fuel generation for the majority of CNS processes and mitochondria generate more than 90% of cellular ATP in the brain (Rolfe and Brown, 1997). Maintaining synaptic function is highly energy demanding for both neurons and astrocytes with synapses believed to be the principal sights of ATP consumption within the brain (Harris et al., 2012). So, once at the synapse, how do mitochondria go about meeting these demands? And what happens when mitochondria are not present at synapses? (Table 1)

1.4.1 At the presynapse

Following inhibition of neuronal activity (eg. with TTX), mitochondria become more mobile with reduced occupancy at presynapses (Chang et al., 2006, Rangaraju et al., 2014). In the absence of neuronal activity, presynaptic ATP

levels remain relatively stable and pharmacological inhibition of OXPHOS has little to no effect on ATP levels (Rangaraju et al., 2014). Whereas, increasing synaptic activity (through stimulation or glutamate application) decreases the percentage of motile neuronal mitochondria in axons and increases their presence at boutons. During long-term stimulation, presynaptic ATP concentrations increase and OXPHOS inhibition compromises synaptic neurotransmission (Rangaraju et al., 2014). This indicates that synaptic activity drives mitochondrial ATP production, which in turn fuels further synaptic activity and highlights a key role for mitochondria in sustaining long-term synaptic transmission. This is substantiated by findings in drosophila, where ablation of Miro depletes mitochondria from presynapses and leads to synaptic depression after long-term activity (Guo et al., 2005).

Intriguingly, the motility of axonal mitochondria has also been shown to be key to presynaptic plasticity by altering presynaptic ATP homeostasis. A study showed that reducing axonal mitochondrial motility, via knockdown of the KIF5B adaptor protein, syntabulin, impaired short-term plasticity and caused synaptic dysfunction (Ma et al., 2009). Additionally, the same group later showed that mitochondria in axons that do not express the mitochondrial anchor, SNPH, are more motile and show considerably more variability in presynaptic strength (Sun et al., 2013). This is termed pulse to pulse variability (PPV) and is key to synaptic plasticity. Overexpression of SNPH reduces mitochondrial motility and PPV. Inhibition of ATP synthesis with oligomycin

reduces vesicular release and causes mitochondria-containing boutons to behave similarly to those without mitochondria (Sun et al., 2013). Thus, motile mitochondria can pass through presynaptic boutons to alter synaptic vesicle release and contribute to PPV via altering presynaptic ATP homeostasis; a process that is key to synaptic plasticity.

Mitochondrial ATP synthesis is also required for synaptic vesicle recycling and filling (Pathak et al., 2015). In fact, vesicular release (exocytosis) uses comparatively less ATP than vesicular recycling (endocytosis) (Rangaraju et al., 2014). When presynaptic ATP levels drop below the required threshold for endocytosis, vesicular recycling is stopped. In a mouse model of Leigh Disease, the loss of the mitochondrial respiratory protein, NDUFS4, inhibits vesicle endocytosis and impairs synaptic function (Pathak et al., 2015). Taken together, these findings highlight that mitochondrial localisation and ATP provision has profound effects on presynaptic activity and vice versa (Cai et al., 2011).

1.4.2 At the postsynapse

Increasing synaptic activity also decreases the motion of dendritic mitochondria (Macaskill et al., 2009) and they become clustered at the base of spines (Li et al., 2004). On the other hand, suppression of neuronal activity increases mitochondrial length and motility and reduces occupancy at spines.

Dendritic spine development and maintenance requires the local translation of synaptic proteins, which is a highly energy demanding process (Harris et al.,

2012). Inhibition of OXPHOS, with oligomycin and antimycin, drastically reduces protein translation in dendrites, whereas inhibiting glycolysis with 2DG has little to no effect (Rangaraju et al., 2019). Depletion of mitochondria from dendrites during development leads to the loss of synapses and dendritic spines and conversely increasing dendritic mitochondrial content enhances the number of spines and synapses. The loss in synapses can be rescued by application of creatine, which provides an exogenous source of ATP by activating ATP-phosphocreatine exchange (Li et al., 2004) and suggests that dendritic synaptogenesis and spine development are fuelled by mitochondrial ATP synthesis.

Mitochondrial positioning at the base of spines also drives activity-dependent postsynaptic plasticity. A recent study has shown that mitochondria exist in temporally stable spatial compartments of around 30 µm that drive activity-dependent spine growth in dendrites. As in presynaptic boutons, ATP produced by glycolysis is sufficient to power local translation in the absence of neuronal activity and localised depletion of mitochondria has no effect on local translation rates. Yet, following long-term stimulation, spine head width increases by ~50% and is accompanied with a sharp increase in rates of local protein translation; a process that does not occur following localised depletion or fragmentation of these mitochondrial compartments (Rangaraju et al., 2019).

In addition to the local translation of proteins vital for dendritic spine growth and plasticity, mitochondrial respiratory proteins are synthesised locally at the synapse following glutamatergic stimulation. These proteins are imported into the mitochondria and incorporated into respiratory chain complexes to boost mitochondrial ATP production (Kuzniewska et al., 2020). Consequently, these findings reveal a positive feedback mechanism whereby synaptic activity triggers the positioning of mitochondria at postsynapses/the base of spines where they fuel the synthesis of proteins critical to dendritic spine growth and plasticity as well as the synthesis of mitochondrial respiratory proteins which in turn fuels further ATP production and further local protein translation.

The decreasing motility of dendritic mitochondria with age may also be key to spine maturation. In retinal ganglion cells (RGCs), dendritic mitochondria all but stop moving by postnatal day 21 and are stabilised at branch points and synapses (Faits et al., 2016). In a mouse model of retinal degeneration (Crx KO), dendritic mitochondria are hypermotile in mature neurons which leads to the pathological hyperactivity of RGCs and dendritic degeneration (Faits et al., 2016). Additionally, dendrite outgrowth is dependent on mitochondrial positioning at branch points (Lopez-Domenech et al., 2016, Fukumitsu et al., 2015). Depletion of mitochondria from dendrites leads to defects in both dendritic development and dendritic degeneration, eventually resulting in neuronal death. In Purkinje cells, this can be partially rescued by application of creatine. Conversely, inhibiting cytosolic creatine kinases (CKs) decreases

dendritic ATP levels and also disrupts dendrite development (Fukumitsu et al., 2015).

Taken together, these studies suggest that mitochondrial ATP synthesis in dendrites is key to fuelling dendritic and spine growth, function and plasticity and disrupted mitochondrial positioning can lead to defects in neurotransmission and dendritic degeneration.

1.4.3 Astrocytes

In contrast to neurons, astrocytes were classically believed to rely on glycolysis as their primary energy source. In fact, astrocytes can function purely glycolytically and mice expressing respiration-deficient astrocytes display no severe signs of pathology (Supplie et al., 2017). Yet, astrocytes contain just as many mitochondria (per μm^2) as neurons and studies have highlighted the ability of astrocytes to display high rates of mitochondrial oxidative phosphorylation (Hertz et al., 2007). In response to increased synaptic activity the motility of astrocytic mitochondria decreases and the distance between mitochondria and synapses is reduced (Jackson et al., 2014, Stephen et al., 2015). Once positioned at synapses, astrocytic mitochondria are thought to be key to fuelling synaptic glutamate uptake.

Astrocytes uptake almost the entirety of excess glutamate from the synaptic cleft post neurotransmission; a process that is key to inhibiting neurotransmission and preventing excitotoxicity. Glutamate uptake against its concentration gradient is believed to be one of the most energy-consuming

processes in the CNS (Pellerin et al., 2007). The two main sites of glutamate uptake in astrocytes are GLT1 and GLAST, which are heavily reliant on the influx of Na+ ions (Danbolt, 2001). The influx of Na+ triggers the Na+/K+-ATPase and the efflux of Na+ back into the synaptic space. This in turn causes local reversal of the Na+/Ca^{2+}-exchanger (NCX) and a rise in intracellular Ca^{2+} concentration (Danbolt, 2001). Overall, each molecule of glutamate taken up comes at the cost of over 1 molecule of ATP. Thus, it comes as no surprise that mitochondria are trafficked to and reside at sites of glutamate uptake as the primary source of ATP. Inhibition of glutamate uptake with TFB-TBOA increases the percentage of motile mitochondria in astrocytes and decreases their localisation with synapses and sites of glutamate uptake (Jackson et al., 2014). Accordingly, another study has shown that following the application of titanium dioxide (TiO_2), which depolarises mitochondria, glutamate uptake into primary astrocytes is markedly reduced (Wilson et al., 2015). Taken together, this suggests that local mitochondrial ATP production at GLAST and GLT1 fuels astrocyte glutamate uptake at synapses. Therefore, astrocytic mitochondrial dysfunction, specifically defects in respiratory capacity/ATP production, has potential implications in astrocyte-mediated synaptic and neuronal dysfunction.

1.4.4 Microglia

Non-reactive microglia utilise both oxidative and glycolytic energy *in situ* (Orihuela et al., 2016) but switch to glycolysis in a reactive state to produce

ATP at a faster rate (Volobоeva et al., 2013, Ghosh et al., 2018, Lauro and Limatola, 2020). In fact, microglia express more OXPHOS-related genes than both astrocytes and neurons (Ghosh et al., 2018).

Non-reactive microglia are highly dynamic and through extension and retraction of their processes are constantly surveying their local microenvironment including brief contacts with synapses; a process that is highly energy demanding (Madry et al., 2018). Thus, it comes as no surprise that mitochondrial ATP production is required for microglial dynamics and recently it has been shown that inhibition of glycolysis has no effect on microglial surveillance and response to non-inflammatory stimuli (laser-induced lesion) in acute slices *in situ* (Bernier et al., 2020). So, although non-reactive microglia display high rates of glycolysis, their surveillance and process motility can be fuelled entirely by mitochondrial ATP production. On the other hand, pharmacological inhibition of the electron transport chain induces microglial activation *in vitro*, as shown by the release of pro-inflammatory cytokines (Ye et al., 2016).

Taken together, it is clear that the functions of non-reactive microglia heavily rely on mitochondrial ATP production, however various questions remain; including what happens to microglial surveillance and chemotaxis *in situ* and/or *in vivo* when mitochondrial ATP production is blocked? How would depletion of mitochondria from microglial processes affect their motility and

response to non-inflammatory stimuli? And what would be the effect on synaptic function?

1.5 Calcium buffering

Ca^{2+} plays a key role in mediating spatiotemporal intracellular signalling and is vital to a variety of CNS functions, particularly synaptic transmission. Along with the ER, mitochondria contribute to intracellular Ca^{2+} homeostasis through the uptake and release of Ca^{2+}, meaning that cytosolic Ca^{2+} concentrations are intimately related to mitochondrial Ca^{2+} buffering capabilities. Ca^{2+} is taken up into the mitochondrial matrix through two channels: the OMM-localised voltage-dependent anion-selective channel (VDAC) (Freitag et al., 1982) and the IMM-localised mitochondrial Ca^{2+} uniporter (MCU) (Kirichok et al., 2004). The N-terminal domain of MCU has been suggested to bridge between mitochondrial membranes to interact with Miro and could link mitochondrial Ca^{2+} buffering to transport and vice versa (Niescier et al., 2018).

Ca^{2+} efflux from mitochondria is governed by the mitochondrial Na+/Ca^{2+} exchanger (NCLX) and through transient opening of the mitochondrial permeability transition pore (MPTP). Mitochondrial Ca^{2+} efflux is a prerequisite for normal health with induced deletion of NCLX causing sudden death in mice (Luongo et al., 2017). So, how does mitochondrial Ca^{2+} buffering alter neurotransmission? And what happens when mitochondria are unable to buffer Ca^{2+} at synapses in neurons and glia? (Table 1)

1.5.1 At the presynapse

At rest (without neuronal activity), presynaptic Ca^{2+} concentrations remain stable at ~100nM. Mitochondrial Ca^{2+} concentration sits at around the same level and there is no difference in cytosolic Ca^{2+} concentrations between boutons that do or do not contain mitochondria (Vaccaro et al., 2017). However, during neuronal activity and presynaptic depolarisation, inward-facing voltage-gated Ca^{2+} channels open to allow the influx of Ca^{2+} ions into presynaptic boutons which facilitates vesicular release (Reviewed in (Sudhof, 2012)). This causes presynaptic Ca^{2+} concentrations to increase sharply by ~20-fold and is accompanied by a large increase in mitochondrial Ca^{2+} influx (~5-fold) (Werth and Thayer, 1994). This is followed by a rapid exponential decay in presynaptic Ca^{2+} and the cessation of neurotransmission. Inhibition of mitochondrial Ca^{2+} influx extends the length of this decay (Billups and Forsythe, 2002).

Recent work has shown that in hippocampal (Vaccaro et al., 2017) and cortical (Kwon et al., 2016) neurons during stimulation, mitochondrial occupancy at synapses decreases presynaptic Ca^{2+} concentrations and vesicular release is reduced in the presence of mitochondria (Kwon et al., 2016, Vaccaro et al., 2017). Inhibition of mitochondrial Ca^{2+} uptake, via pharmacological blockade of MCU, diminished the difference in cytosolic Ca^{2+} between boutons with and without mitochondria (Vaccaro et al., 2017, Kwon et al., 2016). These findings are in agreement with a previous study into the neuromuscular junction (NMJ)

of drosophila, which shows that disrupted mitochondrial Ca^{2+} influx disrupts neurotransmission during high frequency stimulation at NMJs (Verstreken et al., 2005). On the other hand, recent evidence has shown that increasing mitochondrial Ca^{2+} buffering, via inhibition of mitochondrial dihydroorotate dehydrogenase (DHODH), stably decreases the mean firing rate set point during spiking activity in the hippocampus *in vivo* and reduces susceptibility to induced seizures (Styr et al., 2019). Thus, these findings illustrate that mitochondrial Ca^{2+} buffering is vital to presynaptic Ca^{2+} homeostasis and modulation of synaptic transmission which is key to maintaining neuronal health.

As well as altering cytosolic Ca^{2+} concentrations, mitochondrial Ca^{2+} influx and accumulation stimulates mitochondrial ATP production by modulating the activity of the enzymes involved in the tricarboxylic acid cycle (TCA cycle) (Denton et al., 1972, Denton, 2009, Balaban, 2009, Glancy and Balaban, 2012). The rate of mitochondrial ATP synthesis is proportionate to changes in matrix Ca^{2+} concentrations and thus, mitochondrial Ca^{2+} buffering can modulate local neuronal ATP production (Llorente-Folch et al., 2015). A recent study has shown that activity-dependent increases in presynaptic ATP correlate with a rise in nearby mitochondrial Ca^{2+} concentrations (Ashrafi et al., 2020). Blockade of Ca^{2+} uptake into mitochondria via knockdown of MCU or MICU3, a neuronal specific enhancer of MCU (Patron et al., 2019), blocks presynaptic ATP production and results in the impairment of synaptic function

and plasticity (Ashrafi et al., 2020). These findings suggest that presynaptic mitochondrial Ca^{2+} influx drives local ATP production as well as regulating presynaptic Ca^{2+} homeostasis in order to modulate vesicular release from axonal boutons.

Mitochondrial Ca^{2+} efflux has also been shown to play a role in presynaptic homeostasis. A study showed that during basal synaptic transmission in hippocampal neurons, blockade of the MPTP causes increased presynaptic release due to a rapid uptake of Ca^{2+} into mitochondria and an increased resting presynaptic Ca^{2+} concentration. However, following neuronal stimulation, MPTP inhibition has no effect on presynaptic Ca^{2+} levels and synaptic transmission suggesting that mitochondrial efflux through the MPTP is more important for regulating basal Ca^{2+} levels at the presynapse (Levy et al., 2003). Taken together, multiple lines of evidence highlight an extremely vital role for mitochondrial Ca^{2+} homeostasis in the modulation of neurotransmission at the neuronal presynapse.

1.5.2 At the postsynapse

The role of mitochondrial Ca^{2+} buffering in the modulation of postsynaptic function and spine plasticity is considerably less well known. A recent study has shown that dendritic mitochondrial Ca^{2+} transients increase in frequency following NMDAR-dependent LTP induction. Reducing Ca^{2+} uptake into mitochondria, by preventing mitochondrial fission, impaired LTP-induced dendritic spine growth and surface expression of AMPARs in culture and

suppressed electrophysiological LTP in slice (Divakaruni et al., 2018). Additionally, reduction in activity-driven local protein translation following mitochondrial depletion from the base of spines is accompanied with a reduction in postsynaptic Ca^{2+} transients (Rangaraju et al., 2019). Taken together, this suggests that Ca^{2+} influx into mitochondria may be key to regulating postsynaptic plasticity, including LTP, and warrants further research.

1.5.2 Astrocytes

Unlike neurons, astrocytes do not communicate electrically via the generation of action potentials. Instead, activation of astrocytic synaptic receptors is commonly coupled with intracellular rise in Ca^{2+} (Fields and Stevens-Graham, 2002). As a result, astrocytic processes contain functionally isolated microdomains that exhibit both activity dependent and spontaneous Ca^{2+} transients. Mitochondria frequently colocalise with these microdomains and recent studies have implicated mitochondrial Ca^{2+} buffering in the regulation of astrocytic Ca^{2+} transients (Agarwal et al., 2017, Montagna et al., 2019).

Early evidence in primary astrocyte cultures *in vitro* showed that damaging mitochondria through application of the mitochondrial uncoupler FCCP alongside oligomycin prevented mitochondrial Ca^{2+} influx and increased the rate of decay of cytosolic Ca^{2+} concentrations (Boitier et al., 1999). These findings were later confirmed in astrocyte processes *in situ* where application of FCCP extended the rate of decay of cytosolic Ca^{2+} transients in astrocytic

processes (Jackson and Robinson, 2015). Depletion of mitochondria from individual astrocyte processes, either by expression of Ca^{2+} insensitive Miro1 or photo-ablation, resulted in increased frequency and prolonged decay of Ca^{2+} transients in the processes not containing mitochondria (Jackson and Robinson, 2015, Stephen et al., 2015).

Initially, it was believed that intracellular Ca^{2+} rises in astrocytes were the result of Ca^{2+} release from the ER, mediated by IP3 receptors, and entry from the extracellular space through store-operated Ca^{2+} channels. However, recent evidence suggests that mitochondrial Ca^{2+} efflux may also act as a source of Ca^{2+} transient generation in astrocytes. *In vivo* imaging of cortical astrocytes lacking a subset of IP_3 receptors (IP_3R_2 KO) showed that spontaneous Ca^{2+} transients within astrocytic microdomains remain and are facilitated by the transient opening of the MPTP. Increasing neuronal activity, with picrotoxin, increased Ca^{2+} efflux from mitochondria and increased the number and activity of microdomains. Both spontaneous and activity-dependent microdomain Ca^{2+} activity was blocked by MPTP inhibition (Agarwal et al., 2017) and thus places mitochondria alongside the ER as a source of Ca^{2+} transients in astrocytes.

On top of the uptake of glutamate from the synaptic cleft, astrocytes also release glutamate at synapses which can bind to postsynaptic receptors and contribute to neurotransmission. The exocytosis of glutamate and other neurotransmitters from glia is known as gliotransmission and, as at the neuronal presynapse, vesicular exocytosis from astrocytes is heavily

regulated by mitochondrial Ca^{2+} homeostasis (Agulhon et al., 2012). Blockade of MCU in cortical astrocytes results in a rise in cytosolic Ca^{2+} concentration and increased glutamate release (Reyes and Parpura, 2008). On the other hand, inhibiting mitochondrial Ca^{2+} efflux through NCLX, both pharmacologically (Reyes and Parpura, 2008) and genetically (Parnis et al., 2013), reduced cytoplasmic Ca^{2+} concentrations and decreased exocytotic glutamate release.

These findings heavily implicate mitochondrial Ca^{2+} influx and efflux mechanisms in the regulation of cytosolic Ca^{2+} concentrations at synapses and microdomains in astrocytes which are vital to astrocytic and synaptic function.

1.5.3 Microglia

It has recently been shown that microglial Ca^{2+} signalling is attuned to neuronal activity *in vivo* and that microglial processes contain microdomains that exhibit spontaneous Ca+ activity that increases during neuronal hyperactivity (Umpierre et al., 2020). Additionally, microglia regulate neuronal Ca^{2+} activity. Selective depletion of microglia from the mouse brain leads to disrupted neuronal Ca^{2+} responses basally and neuronal Ca^{2+} overload and hyperactivity following cerebral ischemia and exposure to neurostimulants, respectively (Szalay et al., 2016, Badimon et al., 2020). This highlights a key role for microglia in shaping neuronal and synaptic function through regulation of neuronal Ca^{2+} homeostasis. Yet, unlike in astrocytes, less is known about

the role microglial mitochondria play in the regulation of intra- and inter-cellular Ca^{2+} homeostasis.

Mitochondrial Ca^{2+} influx could be involved in the inflammatory activation of microglia (Culmsee et al., 2018). In macrophages, Ca^{2+} influx via L-type calcium channels (LTCC) and P2X7 purinergic receptors results in increased mitochondrial Ca^{2+} concentrations, the loss of mitochondrial membrane potential (↓Ψm) and enhanced mitochondrial reactive oxygen species (ROS) formation. This contributes to the activation of macrophages via formation of the inflammasome (Sorbara and Girardin, 2011, Yaron et al., 2015). However, whether such a mechanism exists in microglia remains to be seen.

	ATP provision	Ca^{2+} buffering
Presynapse	Vesicular release (exocytosis) Synaptic plasticity Vesicular recycling (endocytosis)	Vesicular release Mitochondrial ATP production
Postsynapse	Spine development Spine maturation Synaptic plasticity Dendritic outgrowth	Long-term potentiation Synaptic plasticity
Astrocyte	Glutamate uptake Gliotransmission	Spontaneous and activity dependent Ca^{2+} transients Gliotransmission Inflammatory activation?
Microglia	Process surveillance	Inflammatory activation? Synaptic transmission?

Table 1: The roles of synaptic mitochondria in the CNS.

1.6 Synaptic pruning

During neurodevelopment, excessive synapses are removed. This targeted elimination of synapses and spines has been termed ‘synaptic pruning’ and disrupted synaptic pruning can lead to hyperexcitation through an excess of excitatory synapses which has been implicated in the pathophysiology of neurodevelopmental disorders including autism spectrum disorders (ASD),

schizophrenia and epilepsy (Sakai, 2020). Neuronal activity is a key regulator of synaptic pruning and, although no over-arching hypothesis exists, mitochondria have also been suggested to play a vital role (Li et al., 2004, Erturk et al., 2014, Meng et al., 2015, Cobley, 2018, Gyorffy et al., 2018, Baranov et al., 2019).

One possible mechanism involves a localised apoptotic-like process governed by mitochondrial ROS production and activation of caspase 3 in dendritic spines (Erturk et al., 2014, Baranov et al., 2019). A similar caspase 3-dependent mechanism has been identified in the elimination of synaptic components from axonal boutons in *C.elegans* (Meng et al., 2015). Caspase 3 deficient mice display increased spine density and synaptic strength but show a reduction in spine plasticity in response to NMDA stimulation (Erturk et al., 2014). In this study, localised mitochondrial ROS production was induced optogenetically with Mito-KillerRed photostimulation, but synaptic inactivity has also been shown to be a driver of ROS production (Sidlauskaite et al., 2018). Consistent with this, mitochondria present at distal synapses produce more ROS and induce more focal caspase-3 activation than their proximal counterparts (Baranov et al., 2019). Thus, mitochondria may be acting as a sensor of synaptic inactivity to trigger synaptic pruning through ROS production.

A distinct mechanism involves microglia phagocytically removing synapses (Paolicelli et al., 2011). Microglia respond to the secretion of specific signalling

molecules from excess synapses by engulfing and degrading the synaptic compartments (Paolicelli et al., 2011, Stephan et al., 2012). Intriguingly, new evidence suggests that the positioning and activity of neuronal mitochondria could be key to facilitating interactions between neurons and microglia *in vivo* (Cserep et al., 2020). In this study, microglial process recruitment to neuronal somas was shown to be linked to the metabolic activity of neuronal mitochondria through communication with microglial purinergic receptors (Cserep et al., 2020). So, could a similar mechanism exist whereby mitochondria position themselves at excess synapses to trigger microglial recruitment and phagocytosis? Notwithstanding, these findings further underline the importance of mitochondrial presence at synapses, this time in the context of synaptic pruning.

1.7 Mitochondrial fission/fusion

Mitochondrial membranes are highly dynamic, constantly undergoing fission and fusion events that alter the size of individual mitochondria (Scott and Youle, 2010). Mitochondrial function is highly dependent on its morphology with larger mitochondria generally able to produce more ATP and buffer more Ca^{2+} due to their increased surface area to volume ratio. On the other hand, smaller mitochondria are more motile and more suited to smaller cellular compartments eg. Synaptic boutons, dendritic spines and distal processes. Moreover, it is key to CNS function to strike a balance between motility and

metabolism by altering the fusion/fission balance of mitochondria (Ferree and Shirihai, 2012).

Mitochondrial fission is principally governed by the cytosolic GTPase protein, dynamin-related protein 1 (DRP1) (Smirnova et al., 2001) and its interaction with the mitochondrial adaptor proteins, Mitochondrial fission protein 1 (FIS1) (Mozdy et al., 2000), Mitochondrial fission factor (MFF) (Otera et al., 2010) and mitochondrial dynamics proteins of 49 and 51 kDa (MID49 and MID51) (Otera et al., 2016). In brief, DRP1 is recruited to the OMM, polymerizes around the membrane, constricts both the OMM and IMM and, in collaboration with dynamin 2 (Dyn2) (Lee et al., 2016a), performs a scission event to form two daughter mitochondria (Reviewed in (Tilokani et al., 2018, Kraus et al., 2021)). The interaction between mitochondria and the actin cytoskeleton is key to regulating mitochondrial fission and the endoplasmic reticulum (ER) is often used as a platform for initiating mitochondrial constriction (Kraus et al., 2021). The importance of mitochondrial fission for neurodevelopment is highlighted by the fact that neuronal DRP1 knockout in mice is lethal in the early prenatal stage (Wakabayashi et al., 2009, Ishihara et al., 2009).

Mitochondrial fusion is mediated by the mitofusin proteins, Mfn1 and Mfn2 (Ishihara et al., 2004). Located on the OMM, the Mfns bridge between adjacent mitochondria via the formation of homo- and heterodimers on opposing membranes to facilitate membrane fusion. Optic Atrophy 1 (OPA1) then facilitates fusion of the IMM (Cipolat et al., 2004), ultimately resulting in the

mixing of matrix contents and the formation of a single mitochondrion. Mitochondrial fusion is also a prerequisite for normal development with Mfn1, Mfn2 or OPA1 knockout mice dying embryonically (Chen et al., 2003, Davies et al., 2007). Interestingly, the fusion machinery is intrinsically linked to the trafficking machinery through physical interactions between the Mfns, Miros and TRAKs (Misko et al., 2010). Accordingly, the loss of Mfn2 disrupts axonal mitochondrial transport (Misko et al., 2010) and conversely, the loss of Miro triggers mitochondrial fragmentation (Covill-Cooke et al., 2020).

1.7.1 Altered fission/fusion balance in axons and dendrites

Recent studies have shown that the mitochondrial network is distinctly regulated in different neuronal compartments by altering the fusion/fission balance. Axonal mitochondria are smaller than their dendritic counterparts (Lewis et al., 2018); a phenomenon that has recently been shown to be driven by axonal-specific activity of the mitochondrial fission adaptor protein, MFF. Forced extension of axonal mitochondria, via knockdown of MFF, results in increased Ca^{2+} uptake by presynaptic mitochondria, lower levels of presynaptic cytosolic Ca^{2+} and a reduction in vesicular release (Lewis et al., 2018). On the other hand, dendritic mitochondria are long in comparison to axonal mitochondria (Chicurel and Harris, 1992, Li et al., 2004, Chen et al., 2007, Dickey and Strack, 2011, Kasthuri et al., 2015, Lewis et al., 2018, Rangaraju et al., 2019) but undergo rapid DRP1-dependent fission events following sustained neuronal activation (Divakaruni et al., 2018). Neurons

expressing inactive DRP1 showed less dendritic spine growth and AMPAR trafficking after LTP stimulation (Divakaruni et al., 2018).

The alterations in the size of dendritic and axonal mitochondria are a prime example of mitochondrial optimisation within different subcellular compartments of the same cell. This optimisation could reflect the difference in timescale between the metabolic needs in axons and dendrites. Mitochondria are longer in dendrites and less mobile, making them more suited to fuelling protein translation at numerous postsynaptic compartments over longer timescales (Rangaraju et al., 2019). Whereas, in axons, mitochondria are smaller and more motile, yet still retain a high surface area to volume ratio (Perkins et al., 2010), which suits movement between boutons supporting presynaptic plasticity (PPV), rapid ATP production and tempered Ca^{2+} buffering to modulate vesicular release.

1.7.2 Mitochondrial fission and glial activation

Although microglia are the principal immune cells of the brain, both microglia and astrocytes can respond to CNS insult, injury and disease by switching to a reactive phenotype that triggers changes in morphology, proliferation and the secretion of pro- and anti-inflammatory factors. This is accompanied by a metabolic reprogramming from mitochondrial oxidative phosphorylation to glycolysis (Lauro and Limatola, 2020, Brown et al., 1995, Almeida et al., 2001, Motori et al., 2013, Gimeno-Bayon et al., 2014) and recently, it has been shown that this switch coincides with- and is dependent on- altering the

fission/fusion balance of their mitochondria (Katoh et al., 2017, Nair et al., 2019, Motori et al., 2013).

Cortical stab wound and exposure to proinflammatory stimuli triggers DRP1-dependent mitochondrial fragmentation and a reduction in mitochondrial respiration in astrocytes (Motori et al., 2013) and more recently, these findings have been mirrored in microglia. Pharmacological activation of astrocytes and microglia via the application of lipopolysaccharide (LPS) triggers rapid fission of glial mitochondria and a metabolic switch from oxidative phosphorylation to glycolysis (Motori et al., 2013, Katoh et al., 2017, Nair et al., 2019). Blockade of LPS-induced mitochondrial fission through application of Mdivi1, which inhibits DRP1, blocks this metabolic switch and attenuates the release of proinflammatory cytokines and chemokines (Katoh et al., 2017, Nair et al., 2019). Intriguingly, increasing mitochondrial fusion in neurons, via the overexpression of Mfn2, is also capable of blocking LPS-induced microglial activation and suggests that changes in mitochondrial fission/fusion balance in the CNS are not exclusively cell autonomous (Harland et al., 2020). Following LPS treatment over longer timescales, glial mitochondria re-fuse and mitochondrial length is restored (Katoh et al., 2017, Motori et al., 2013). This is believed to be the result of enhanced ROS production by fragmented mitochondria which triggers AMPK-dependent phosphorylation, inactivation of DRP1 and inhibition of fission (Park et al., 2015, Katoh et al., 2017).

This biphasic remodelling of mitochondria likely reflects the changing metabolic/bioenergetic needs of microglia and astrocytes as they alter their phenotype from a non-activated state to an activated state and finally a regenerative state following prolonged CNS insult. The initial mitochondrial fragmentation triggers the switch from oxidative phosphorylation to glycolysis and enables activated glia to produce ATP at a faster rate to fuel rapid cytokine production (Chang et al., 2013). The subsequent elongation of mitochondria could then indicate increased mitochondrial ATP production and a metabolic switch back to oxidative phosphorylation in order to restore CNS homeostasis (Schett and Neurath, 2018).

1.7.3 Mitochondrial hyper-fission/fusion in neurodegenerative disease

Dysregulation in the fusion/fission balance of mitochondria can be detrimental to the CNS. Hyper-fission of mitochondria is a common hallmark of neurodegenerative pathology and has been observed in patient post-mortem brains and mouse models of dementia, Alzheimer's Disease (AD), Parkinson's Disease (PD), Huntington's Disease (HD) and Amyotrophic Lateral Sclerosis (ALS) (Itoh et al., 2013, Joshi et al., 2018, Reddy et al., 2011, Reddy, 2014, Knott et al., 2008, Joshi et al., 2019). In addition, loss of function mutations in mitochondrial fusion proteins are directly linked to neurodegenerative disease with mutations in Mfn2 leading to Charcot-Marie-Tooth subtype 2A (CMT2A) (Zuchner et al., 2004, Chung et al., 2006, Zuchner et al., 2006, Feely et al., 2011, Pham et al., 2012, Lee et al., 2012, El Fissi et al., 2018) and mutations

in OPA1 leading to autosomal dominant optic atrophy (ADOA) (Alexander et al., 2000, Delettre et al., 2000).

Consequently, inhibiting excessive mitochondrial fission has been suggested as a potential therapeutic strategy in combating neurodegenerative disease. Genetic silencing or pharmacological inhibition of DRP1, with Mdivi1, confers neuroprotection against glutamate-induced excitotoxicity *in vitro* and ischemia *in vivo* (Grohm et al., 2012) and more recently, a novel and selective inhibitor of excessive mitochondrial fission, P110, has been developed which alleviates neurodegeneration in patient-derived and mouse models of AD, PD, HD and ALS (Joshi et al., 2018, Filichia et al., 2016, Guo et al., 2013, Disatnik et al., 2016). P110, selectively inhibits the interaction between DRP1 and FIS1, while the interaction between DRP1 and its other mitochondrial adaptors remains, so physiological mitochondrial fission is less affected (Qi et al., 2013). Furthermore, increasing mitochondrial fusion has also been proposed as a strategy to prevent neurodegeneration (Chen et al., 2007, Harland et al., 2020).

Glial activation can be both beneficial and detrimental to the CNS. The chronic activation of microglia and astrocytes leads to excessive secretion of proinflammatory factors ultimately resulting in neurotoxicity and has been linked to the pathophysiology of a variety of neurodegenerative diseases (Lull and Block, 2010). Recent evidence suggests that hyper-fission of glial mitochondria could underpin the pathomechanism (Joshi et al., 2019). The

expression of neurotoxic proteins associated with AD, ALS and HD in microglia alone is capable of triggering neuronal death. This is mediated by the release of fragmented mitochondria from microglia which are taken up by astrocytes to trigger their own activation which in turn propagates cytokine-mediated neuronal cell death (Joshi et al., 2019). Inhibiting excessive mitochondrial fission in microglia, with P110, reduces astrocytic activation and neuronal death. Additionally, P110 application reduces chronic microglia and astrocyte activation and proinflammatory responses in genetic mouse models of AD, ALS and HD *in vivo* (Joshi et al., 2019).

On the other hand, decreased mitochondrial fission and mitochondrial hyper-fusion is also associated with neurodegenerative disease. Loss of function mutations in DRP1 are associated with ADOA (Gerber et al., 2017) and gain of function mutations in Mfn2 are associated with CMT2A (El Fissi et al., 2018), both of which result in the hyper-fusion of neuronal mitochondria. Moreover, reducing mitochondrial fragmentation in neurodegenerative disease is an intriguing therapeutic avenue to explore yet caution needs to be exercised in order to not tip the intricate balance of mitochondrial fission and fusion in the CNS.

1.8 Mitochondria-endoplasmic reticulum contact sites

Mitochondria are associated with the endoplasmic reticulum (ER) at regions called mitochondria-ER contact sites (MERCS), which comprise 5–20% of the mitochondrial surface (Giacomello and Pellegrini, 2016). MERCS facilitate

inter-organellar communication between mitochondria and the ER that can modulate a wide range of physiological processes, including ATP synthesis, Ca^{2+} homeostasis, autophagy, mitochondrial trafficking and apoptosis (Paillusson et al., 2016). The formation of MERCS is dependent on the formation of molecular bridges, comprised of tethering protein complexes of both mitochondrial and ER proteins, between the OMM and the ER membrane.

The first tethering complex discovered forms between VDAC on the mitochondria and IP3R on the ER to modulate the transfer of Ca^{2+} from the ER to the mitochondria. This interaction is facilitated by the proteins, Glucose-regulated protein 75 (GRP75) and Protein deglycase (DJ-1), which are specifically expressed at the mitochondria-associated membrane (MAM) interface. Together, VDAC, IP3R, GRP75 and DJ-1 form a tetramer complex and the loss of either GRP75, or DJ-1 abolishes the Ca^{2+} influx into the mitochondria (Liu et al., 2019, Basso et al., 2020, Szabadkai et al., 2006). A second tethering complex forms between protein tyrosine phosphatase-interacting protein-51 (PTPIP51) in the OMM and vesicle-associated membrane protein B (VAPB) in the ER (De Vos et al., 2012). This interaction is believed to be involved in the physical formation of MERCS as loss of VAPB or PTPIP51 is accompanied by a reduction in the proportion of ER in contact with the mitochondria, as seen by electron microscopy (Stoica et al., 2014).

Interestingly, alongside its role in facilitating mitochondrial fusion, Mfn2 is also localised to the ER. Although its role at MERCS is not entirely clear, Mfn2 has been suggested to tether between mitochondria and the ER through the formation of homodimers or heterodimers between Mfn2 on the ER and Mfn1 on the mitochondria. Knockdown of Mfn2 disrupts Ca^{2+} transfer between the ER and mitochondria (Naon et al., 2016, de Brito and Scorrano, 2008). On the other hand, Mfn2 has been suggested to act as an ER-mitochondrial tethering antagonist. Overexpression and dysregulation of Mfn2, through knockdown of the mitochondrial E3 ubiquitin ligase MUL1, disrupts MERCS and reduces mitochondrial Ca^{2+} uptake from the ER in neurons (Puri et al., 2019). More recent evidence indicates that Miro1 is also present at MERCS and plays a role in their regulation (Modi et al., 2019, Lee et al., 2016b, Kornmann et al., 2011). Fibroblasts and induced pluripotent stem cell (iPSC) neurons derived from PD patients carrying Miro1 mutations display dysregulations in MERCS organization and tethering (Berenguer-Escuder et al., 2019, Grossmann et al., 2019, Grossmann et al., 2020) although if and how it forms tethers and its function at MERCS is yet to be fully elucidated.

Despite their role in shaping both mitochondrial and ER function, the role of MERCS in the CNS has not been well studied. Recently, it has been shown that MERCS regulate synaptic activity through the formation of VAPB-PTPIP51 tethers in neuronal synapses (Gomez-Suaga et al., 2019) and that MERCS are present throughout astrocytes *in vivo (Bergami and Motori, 2020).*

Additionally, dysfunctional MERCS are associated with neurodegenerative disease including Alzheimer's disease (AD), Parkinson's disease (PD) and specifically, mutations in VAPB cause an autosomal-dominant form of ALS (Wilson and Metzakopian, 2020). Thus, going forward it will be important to further establish how MERCS in neurons and glia are involved in the regulation of synaptic function.

1.9 Mitochondria-lysosome contacts

Mitochondria are also associated with lysosomes (Gordaliza-Alaguero et al., 2019). Lysosomes play vital roles in cellular signalling and energy metabolism alongside degrading and recycling cellular waste, including damaged mitochondria (Ballabio and Bonifacino, 2020); a process which will be described later in this chapter. Notwithstanding, recent advances in imaging technology have identified physical contacts between lysosomes and mitochondria in healthy cells in the absence of mitochondrial damage (Valm et al., 2017, Han et al., 2017). Mitochondrial-lysosomal (M-L) contacts play vital roles in the regulation of mitochondrial and lysosomal dynamics and are principally regulated by the lysosomal protein Rab7 and the mitochondrial GTPase TBC1D15 (Zhang et al., 2005). GTP-bound Rab7 promotes the formation of M-L contacts, whereas the recruitment of TBC1D15 to mitochondria causes Rab7 GTP hydrolysis, the separation of mitochondria from lysosomes and mitochondrial division via an interaction with FIS1 (Wong

et al., 2018). Defective modulation of TBC1D15 prolongs M-L contacts and has been linked to the aetiology of PD (Kim et al., 2021).

Lysosomes are a primary intracellular Ca^{2+} stores and recent evidence suggests that M-L contacts can regulate mitochondrial Ca^{2+} dynamics (Peng et al., 2020). Efflux of Ca^{2+} via the lysosomal calcium efflux channel, transient receptor potential mucolipin 1 (TRPML1), is taken up by mitochondria at M-L contacts via VDAC1 and MCU to increase mitochondrial Ca^{2+} concentrations (Peng et al., 2020). The loss of TRPML1 alters M-L contact sites and disrupts mitochondrial Ca^{2+} uptake (Peng et al., 2020).

The importance of M-L contacts in the CNS is highlighted by mutations in Rab7 leading to the neurodegenerative disease, Charcot-Marie-Tooth. Expression of these disease-associated mutations results in mitochondrial hyperfusion, mitochondrial depolarisation and dysfunctional mitochondrial protein translation in the axons of xenopus RGCs (Cioni et al., 2019).

1.10 Mitophagy

Alongside trafficking and membrane dynamics, mitochondria also regulate their network through quality control mechanisms. Damaged mitochondria are unable to meet their ATP production and Ca^{2+} buffering demands and produce excess reactive oxygen species that are harmful to the cell and therefore need to be removed (Youle and Narendra, 2011, Wang and Klionsky, 2011).

Mitochondrial autophagy (mitophagy) is the selective process by which damaged and dysfunctional mitochondria are degraded by the lysosome following loss of their membrane potential (ψ) (Figure 3). The selective nature of mitophagy is, in the main, governed by the serine/threonine-protein kinase, PINK1 (PTEN-induced putative kinase protein 1) and the E3 ubiquitin ligase, Parkin (Youle and Narendra, 2011, Covill-Cooke et al., 2018). In the case of healthy mitochondria, PINK1 is imported into the mitochondria where it is cleaved and then degraded by the proteosome in the cytosol (Yamano and Youle, 2013). Yet, upon mitochondrial depolarisation (↓ψ), PINK1 is not imported into the mitochondria but rather stabilises on the OMM where it phosphorylates ubiquitin (Kane et al., 2014) and the ubiquitin-like domain of Parkin (Kondapalli et al., 2012). The phosphorylation of Parkin activates its E3 ligase activity and Parkin ubiquitinates various OMM proteins (Sarraf et al., 2013). This triggers a feed-forward mechanism whereby further Parkin is recruited the OMM leading to the mass ubiquitination and proteasomal degradation of OMM proteins (Chan et al., 2011, Ordureau et al., 2014a). Phospho-ubiquitin chains decorate the damaged mitochondrion to engage the autophagic machinery allowing engulfment by the autophagosome and subsequent lysosomal degradation (Narendra et al., 2008, Okatsu et al., 2015). To date, five autophagy receptors have been reported: p62, Optineurin, NDP52, NBR1 and TAX1BP1 (Pickrell and Youle, 2015, Lazarou et al., 2015). Via their ubiquitin binding and LC3 interacting regions, these proteins have been proposed to bridge phospho-ubiquitinated cargoes and LC3 decorated

autophagosomal membranes (Roberts et al., 2016). Although all five autophagy receptors have been shown to translocate to the mitochondria following damage, only Optineurin and NDP52 are required for the clearance of mitochondria (Lazarou et al., 2015, Padman et al., 2019).

Mitophagy has also been shown to occur in the absence of PINK1 stabilisation on- and Parkin recruitment to depolarised mitochondria (Villa et al., 2018). This process involves LC3-interacting region (LIR) containing autophagic receptors that are localised at the OMM and can directly bind to LC3 on the autophagosomal membrane. This is known as receptor-mediated mitophagy, and it bypasses the need for the formation of ubiquitin chains on OMM Parkin substrates (Liu et al., 2014). The PINK1/Parkin-independent mitophagy receptors identified thus far include NIX/BNIP3L, BNIP3, AMBRA1 and FUNDC1 (Liu et al., 2014, Strappazzon et al., 2015). Additionally, the IMM localised phospholipid, cardiolipin, can externalise to the OMM and bind to LC3 in the absence of PINK1 and Parkin to induce mitophagy in neurons (Chu et al., 2013).

In the CNS, defective mitophagy has been heavily linked to the pathogenesis of neurodegenerative disease with mutations in Parkin (Kitada et al., 1998) and PINK1 (Valente et al., 2004) being the first and second most frequent causes of familial Parkinson’s Disease (PD), respectively. PD is the second most common neurodegenerative disease and the most common neurodegenerative movement disorder characterised by motor deficits,

including slowness of movement (bradykinesia), rigidity and tremors (Houlden and Singleton, 2012) that are the result of the loss of midbrain dopaminergic (DA) neurons from the substantia nigra (SN), although precisely how and why neurons are lost is not fully understood (Giguere et al., 2018).

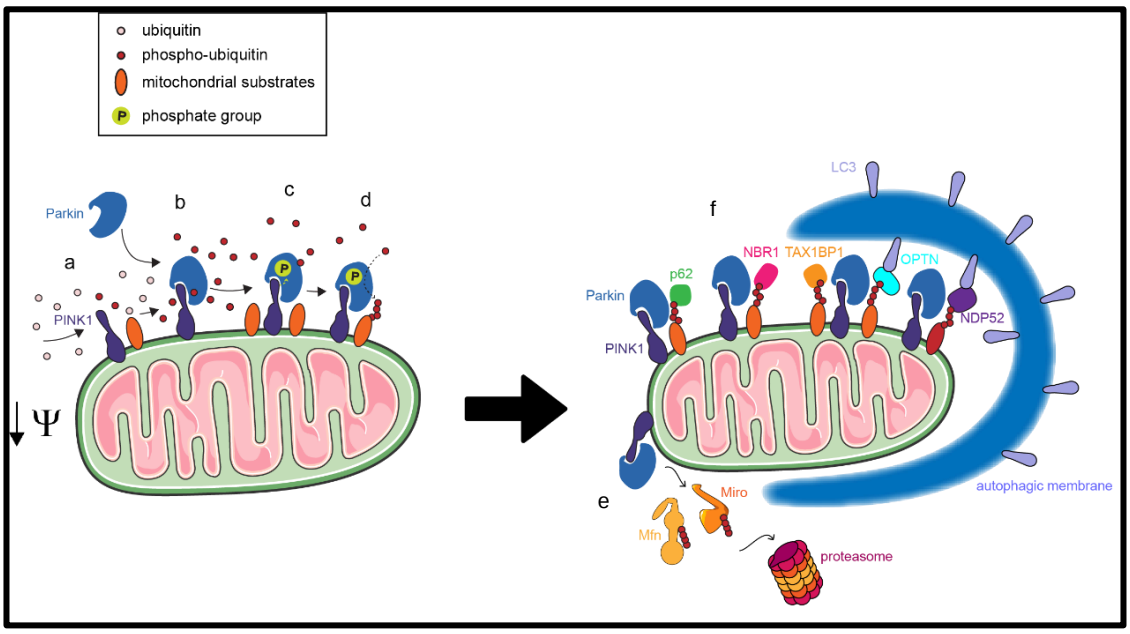

Figure 3: Mechanism of PINK1/Parkin-dependent mitophagy. Depolarisation of mitochondria stabilises PINK1 on the outer mitochondrial membrane (a) and recruits Parkin (b). PINK1 then phosphorylates ubiquitin and Parkin (c). Phosphorylated Parkin then ubiquitinates around 100 mitochondrial substrates to trigger mitophagy (d). Parkin-ubiquitination leads to the degradation of mitochondrial proteins including Miro and Mfn via the proteasome (e). Mass mitochondrial ubiquitination leads to the engagement of the autophagy machinery. Poly-ubiquitin chains on mitochondrial substrates bridge to LC3 decorated autophagosomal membranes via autophagy receptors, including NDP52 and OPTN (f).

1.10.1 Mitophagy in neurons

Despite the obvious pathological relevance, the knowledge of mitophagy in neurons is relatively poor and the majority of mechanistic insight has been gleaned from studies in non-neuronal cells. This could be due to the difference in bioenergetic state between neurons and cell lines (Van Laar et al., 2011). Cultured cell lines generally utilise glycolysis as their primary source of ATP (Gogvadze et al., 2010) meaning that, unlike neurons, they are less reliant on mitochondria to meet their metabolic demands and readily undergo mitophagy following application of mitochondrial depolarising agents (Van Laar et al., 2011). On the other hand, the large scale loss of mitochondria from neurons could result in an energy deficit and may explain why mitophagy is less readily observed (Van Laar et al., 2011). Notwithstanding, a number of studies have developed mitochondrial depolarising conditions to trigger mitophagy in neurons in the absence of widespread neurotoxicity (Martinez-Vicente, 2017, Doxaki and Palikaras, 2020).

Early evidence from primary cortical neurons treated with the mitochondrial depolarising agent, cyanide m-chlorophenylhydrazone (CCCP) in the presence of apoptotic inhibitors, suggests that neuronal mitophagy is spatially restricted (Cai et al., 2012). Following cell-wide mitochondrial depolarisation, Parkin-positive mitochondria accumulate in the somatodendritic regions where they are cleared through the autophagosomal-lysosomal pathway. This is accompanied by increased retrograde and reduced anterograde trafficking

of Parkin-positive mitochondria and suggests that damaged mitochondria are transported back to the soma, where the majority of lysosomes are present (Becker et al., 1960, Parton et al., 1992, Yap et al., 2018, Lie et al., 2021), for degradation (Cai et al., 2012). This is consistent with an earlier report showing that axonal mitochondrial transport is correlated to its potential with polarised mitochondria generally transported towards the growth cone and depolarised mitochondria towards the cell body (Miller and Sheetz, 2004). These findings have recently been replicated in neurons following ischemia where the retrograde movement of axonal mitochondria was required for their mitophagy in the soma; a process that protects from ischemic neuronal injury (Zheng et al., 2019). Additionally, mild oxidative stress triggers recruitment of the autophagy receptor, optineurin (OPTN), specifically to damaged mitochondria in the soma (Evans and Holzbaur, 2020). The increased retrograde transport of damaged mitochondria could be the result of the loss of the mitochondrial anchor, SNPH, following mitochondrial damage. Axonal mitochondria from neurons treated with a low dose of the complex III inhibitor, Antimycin-A (AA), to induce mild stress, release SNPH to selectively enhance their retrograde transport prior to the activation of Parkin-mediated mitophagy (Lin et al., 2017).

On the other hand, it has been shown that mitochondria can be degraded within distal axons following localised damage induced by AA or Mito-KillerRed photostimulation (Ashrafi et al., 2014). This is dependent on PINK1 and Parkin and the recruitment of autophagosomes, which are formed within the distal

regions of neurons (Maday and Holzbaur, 2016, Maday et al., 2012, Hollenbeck, 1993). Accordingly, although mitochondrial biogenesis primarily takes place in the soma, evidence suggests this can also occur locally within distal axons *in vitro* and *in vivo* (Lin et al., 2021, Amiri and Hollenbeck, 2008). This may serve as a mechanism to maintain energy supply following mitochondrial depletion in distal axons.

Consistent with this, Miro1 has been shown to be rapidly degraded in a PINK1/Parkin-dependent manner following mitochondrial depolarisation to arrest axonal mitochondrial movement (Wang et al., 2011b, Liu et al., 2012). Interestingly, Miro1 degradation is impaired in PD patient induced pluripotent stem cell (iPSC)-derived neurons following mitochondrial damage (Hsieh et al., 2016) and pharmacologically reducing the levels Miro1 is neuroprotective (Hsieh et al., 2019). In addition, recent evidence suggests that Miro1 could act as a receptor for Parkin on mitochondria (Safiulina et al., 2019, Birsa et al., 2014, Shlevkov et al., 2016) and the loss of Miro1 delays Parkin recruitment and the degradation of damaged mitochondria (Safiulina et al., 2019). This highlights a potentially important role for Miro1 in the mitophagic pathway in neurons whereby the presence of Miro1 on the OMM and the subsequent Parkin-dependent degradation of Miro1 are both required for the clearance of damaged mitochondria. Halting mitochondrial fusion has also been shown to be a key step preceeding mitophagy. Mfn1 and 2 are rapidly ubiquitinated and degraded upon mitochondrial damage. This is dependent on PINK1 and

Parkin and prevents the re-fusion of damaged mitochondria in order to faciliate their clearance (Gegg et al., 2010, Tanaka et al., 2010, Chen and Dorn, 2013). In the case of Mfn2, its rapid ubiquitination is also required for the p97-dependent disassembly of Mfn2 complexes at MERCS to trigger the release of damaged mitochondria from the ER prior to mitophagy (McLelland et al., 2018, Puri et al., 2019).

The evidence of neuronal mitophagy *in vivo* is scarce although it has recently started to gain momentum with the development of genetic fluorescent mitophagy reporters (Katayama et al., 2011, Katayama et al., 2020, Sun et al., 2015, McWilliams et al., 2016). Mito-Keima and Mito-QC utilise the pH-sensitive nature of certain fluorescent proteins to identify when mitochondria are present within the acidic environment of the lysosome. Work with these reporters have shown that mitophagy is widespread *in vivo* and varies between tissues and cell types (Sun et al., 2015, McWilliams et al., 2016). Use of the Mito-Keima probe in drosophila illustrated that mitophagy occurs in a PINK1/Parkin-dependent manner in dopaminergic neurons *in vivo* and increases with aging (Cornelissen et al., 2018). Yet, evidence from crossing the MitoQC reporter indicated that basal levels of mitophagy can occur in neurons *in vivo* even in the absence of PINK1 in mice (McWilliams et al., 2018) and Parkin in drosophila (Lee et al., 2018). However, the development of a new fluorescent mitophagy reporter, mito-SRAI, suggests that these findings could be an artefact of the MitoQC reporter (Katayama et al., 2020). Mito-SRAI

is targetted to the mitochondrial matrix, whereas MitoQC is targetted to the OMM meaning it could be more susceptible to proteosomal attack and thus not a true readout of mitophagy. In mito-SRAI-expressing mice, the rates of basal mitophagy appeared to be low even in PINK1-expressing neurons *in vivo* but increased following midbrain injection of the neurotoxin, 6-OHDA, which induces mitochondrial damage (Katayama et al., 2020). Intriguingly, 6-OHDA-induced mitophagy was detected within non-dopaminergic neurons but not dopaminergic neurons. This could explain the selective susceptibility of dopaminergic neurons to degeneration in PD due to their inability to sufficiently perform mitophagy in response to insult (Katayama et al., 2020).

1.10.2 Mitophagy in astrocytes

Mitochondrial quality control mechanisms in glia have not been well studied, although recent evidence suggests both astrocytes and microglia display relatively high levels of basal mitophagy *in vivo* (McWilliams et al., 2018). Interestingly, direct comparisons between primary neurons, astrocytes, microglia, and another glial cell type, oligodendrocyte progenitor cells (OPCs), showed that astrocytes exhibit considerably more mitophagic activation than other CNS cell types *in vitro* (Barodia et al., 2019). Following treatment with the pottasium (K+) ionophore, valinomycin, which depolorises mitochondria, the expression of phosphorylated ubiquitin was significantly increased in primary astrocytes compared to neurons, microglia and OPCs (Barodia et al., 2019). This agrees with a previous study showing that mitochondria are readily

cleared from astrocytes following ischemia *in situ* (O'Donnell et al., 2016). Intriguingly, mitochondria present in both the cell body and the distal processes of astrocytes colocalised with autophagosomal markers prior to their clearance and could imply that, unlike in neurons, mitophagy in astrocytes may not be spatially restricted to the cell body following cell-wide mitochondrial depolarisation (O'Donnell et al., 2016). On top of this, astrocytes cultured from PINK1 and Parkin-null mice exhibit markedly reduced proliferation and descreased neurotrophic capacity (Solano et al., 2008, Choi et al., 2013, Choi et al., 2016) and more recently, it's been found that there is reduced astrocytic reactivity in the SN of human brains carrying PD-causing Parkin mutations (Kano et al., 2020). Additionally, Parkin dysfunction has been shown to impair astrocyte mitochondrial function and contribute to the pathogenesis of PD through astrocytic, but not neuronal, upregulation of the unfolded protein response (Ledesma et al., 2002). This suggests that PINK1/Parkin-dependent mitophagy is regulated in a cell-type specific manner and could take on particular importance in astrocytes.

1.10.3 Transcellular mitophagy (Transmitophagy)

Mitochondrial quality control mechanisms were classically believed to be cell autonomous but now there is a growing body of evidence suggesting that neurons and glia engage in the intercellular transfer of mitochondria to facilitate their clearance. Remarkably, recent studies have shown that mitochondria can be released from neurons extracellularly and taken up and

internalised by nearby astrocytes (Gao et al., 2019, Davis et al., 2014, Morales et al., 2020) and microglia (Cserep et al., 2020). In the case of mitochondrial transfer to astrocytes, the internalised neuronal mitochondria can be degraded by the autophagy-lysosomal system. This has been shown to occur under basal conditions in the retina (Davis et al., 2014) and following 6-OHDA-induced mitochondrial damage in the striatum (Morales et al., 2020). For the latter, damaged mitochondria were released from degenerating dopaminergic axons in spheroids, where the early PINK1/Parkin-dependent steps of mitophagy are initiated, and subsequently taken up by neighbouring astrocytes to complete their degradation (Morales et al., 2020). This has been termed transmitophagy and may be a key process in conferring neuroprotection following neuronal insult.

Conversely, mitochondria can also be transported to neurons from astrocytes (Hayakawa et al., 2016, English et al., 2020, Gao et al., 2019) and microglia (Joshi et al., 2019) to support neuronal viability. Following ischemic stress, astrocytic mitochondria are transferred extracellularly to neurons via a Ca^{2+} and CD38-dependent mechanism to promote dendritic extension (Hayakawa et al., 2016). Knockdown of CD38, a glycoprotein found on the surface of glia that catalyses the synthesis of a Ca^{2+} messenger, cyclic ADP-ribose (cADPR) (Bruzzone et al., 2004), worsened neurological outcomes in an *in vivo* model of stroke (Hayakawa et al., 2016). This is substantiated by findings showing that the transfer of damaged mitochondria from microglia is neurotoxic,

whereas healthy mitochondria are neuroprotective (Joshi et al., 2019, Hayakawa et al., 2016). In addition to CD38, the astrocytic intermediate filament, GFAP, has been shown to be involved in the mitochondrial transfer from astrocytes to neurons. On the other hand, Miro1 and Miro2, alongside CD38, contribute to the transfer of mitochondria from neurons to astrocytes (Gao et al., 2019).

These findings and the apparent high rates of mitophagy in astrocytes previously mentioned (Barodia et al., 2019, O'Donnell et al., 2016) suggest that astrocytes could act as a hub for mitochondrial clearance and replenishment in the CNS. Therefore, targeting mitophagy in astrocytes and/or the transcellular transfer of mitochondria between neurons and glia may provide a novel therapeutic avenue in the treatment of CNS disease.

1.10.4 Dysfunctional mitophagy in neurodegenerative disease

On top of its direct links to the aetiology of PD, dysfunctional mitophagy has been implicated in numerous neurodegenerative diseases including AD, HD and ALS (Palikaras and Tavernarakis, 2012, Khalil et al., 2015, Kerr et al., 2017, Evans and Holzbaur, 2019, Santos et al., 2010). Yet, exactly how dysfunctional mitophagy results in neurodegeneration is less clear. It has been suggested that inadequate mitophagy can lead to neuronal death through bioenergetic deficiencies, imbalanced intracellular Ca^{2+} homeostasis and oxidative stress as a result of mitochondrial dysfunction that builds up over time (Lin and Beal, 2006). However, there is inconsistent evidence when it

comes to recapitulating neurodegenerative pathology in genetic animal models. On one hand, PINK1 and Parkin KO rats and flies display significant dopaminergic neuron loss (Cha et al., 2005, Clark et al., 2006, Yang et al., 2006, Whitworth et al., 2005, Dave et al., 2014) yet, on the other hand, there is an absence of any major phenotype, with no gross dopaminergic neuron loss in mice lacking PINK1 and Parkin (Kitada et al., 2007, Kitada et al., 2009, Goldberg et al., 2003, Akundi et al., 2011, Perez and Palmiter, 2005). This suggests there could be additional compensatory pathways counteracting defects in mitophagy *in vivo* and that neurodegenerative pathology may be the result of more than dysfunctional mitophagy alone.

1.10.4.1 Alpha-synuclein and Lewy Bodies

SNCA (encoding α-synuclein) was the first gene to be linked to familial PD (Polymeropoulos et al., 1996), and α-synuclein is the principal protein component of Lewy bodies; intracellular inclusions that are a pathological hallmark of PD. α-Synuclein is important in PD pathogenesis, whether sporadic or familial, but precisely how remains poorly understood. Intriguingly, recent evidence suggests that α-synuclein and mitochondrial dysfunction may act in concert with one another to contribute to PD pathogenesis (Zaltieri et al., 2015).

Numerous lines of evidence indicate that mutant α-synuclein induces mitochondrial damage (Wang et al., 2019b, Park et al., 2020, Luth et al., 2014, Ganjam et al., 2019) that is further exacerbated in PINK1/Parkin mutants that

are unable to clear their dysfunctional mitochondria (Creed and Goldberg, 2018, Creed and Goldberg, 2020, Oliveras-Salva et al., 2014, Chung et al., 2020). Additonally, mutant α-synuclein itself has been shown to inhibit mitophagy in iPSC-derived neurons (Shaltouki et al., 2018). Interestingly, evidence also suggests that mitochondrial dysfunction could precede pathology in PD and other related synucleinopathies by triggering α-synuclein aggregation (Scudamore and Ciossek, 2018, Nistico et al., 2011). Therefore, a “double hit” of aberrant a-synuclein formation and mitochondrial dysfunction could act together to contribute towards PD pathology (Gispert et al., 2015).

1.10.4.2 MtDNA mutations and STING-induced inflammation

Recently a role for inflammation has been identified in PINK1 and Parkin PD pathology (Pickrell and Youle, 2015). Inducing mitochondrial stress in PINK1 and Parkin ko mice, that usually exhibit no major signs of pathology, with exhaustive exercise and introduction of MtDNA mutations, respectively, results in the loss of DA neurons from the SN and motor defects that are accompanied by an increase in serum concentrations of inflammatory cytokines (Sliter et al., 2018). These defects can be rescued by the concurrent loss of STING, a central regulator of the innate immune response, suggesting that inflammation facilitates this phenotype. Accordingly, enhancing nucleotide metabolism to prevent build up of MtDNA mutations has previously been shown to protect against mitochondrial dysfunction in PINK1 mutant models of PD (Tufi et al., 2014). However, a recent study in drosophila found no

involvement of STING-induced inflammation in the behavioral and mitochondrial phenotypes of PINK1 and Parkin mutant flies (Lee et al., 2020) which suggests there could be inter-species variability and further research is warranted.

1.10.4.3 MERCS and the integrated stress response

Additionally, the integrated stress response (ISR) has been implicated PINK1 and Parkin PD pathology. The ISR is a protective homeostatic pathway which leads to a decrease in global protein synthesis upon the activation of one of four discrete kinases, PKR-like ER kinase (PERK), double-stranded RNA-dependent protein kinase (PKR), heme-regulated eIF2α kinase (HRI), and general control non-derepressible 2 (GCN2), that each sense different cellular stresses (Pakos-Zebrucka et al., 2016, Costa-Mattioli and Walter, 2020). However, chronic activation of this pathway in the CNS can lead to neuronal death due to the sustained repression of protein translation (Halliday and Mallucci, 2015, Smith and Mallucci, 2016).

In PINK1 and Parkin mutant drosophila, the ISR is activated due to the failure of degrading Mfn from MERCS following mitochondria damage (Celardo et al., 2016). Following the induction of mitophagy, the rapid ubiquitination and degradation of Mfn2 mediates the Valosin-containing protein (VCP/P97) - dependent release of damaged mitochondria from the ER which gates the wholesale ubiquitination of mitochondrial substrates and the clearance of dysfunctional mitochondria (McLelland et al., 2018). However, in PINK1 and

Parkin mutant flies, dysfunctional mitochondria remain attached to the ER and trigger the ISR via PERK activation, which senses ER stress (Munoz et al., 2013). Knockdown of Mfn and inhibition of PERK prevented ISR activation and was neuroprotective, irrespective of the mitochondrial dysfunction that remained (Celardo et al., 2016). Accordingly, ALS-causing pathogenic mutations in VCP/P97 have been shown to induce mitochondrial dysfunction (Bartolome et al., 2013) which highlights the importance of regulating MERCS for mitochondrial and CNS function.

Recently it's been indentifed that mitochondrial dysfunction can directly trigger the ISR through the HRI (Guo et al., 2020, Fessler et al., 2020) and GCN2 (Mick et al., 2020) branches of the ISR yet the role of these pathways in the pathogenesis of neurodegenerative disease is less clear.

1.11 Conclusions

Metabolic demand varies wildly across the CNS and the localisation and function of mitochondria is crucial to meeting these demands. Here, how neuronal and glial mitochondria position themselves at synapses and once present how they engage in vital roles in modulating neurotransmission and synaptic plasticity is explained. Mitochondria mainly achieve this through the provision of ATP and the regulation of Ca^{2+} yet the need for these functions changes greatly between cell types, subcellular compartments and cell phenotype. Consequently, how mitochondrial fusion/fission dynamics and quality control systems are tailored for these specific requirements, how

disruptions in these processes can result in CNS dysfunction and disease and how targeting these disruptions offer a promising target for therapeutic intervention is discussed. Despite these advances, numerous questions remain unanswered, particularly when it comes to how the mitochondrial network is regulated within glia in health and disease. Greater understanding of mitochondrial trafficking, dynamics and quality control in glia and how they impact glial and neuronal function could be key to elucidating novel therapeutic strategies in the treatment of mitochondrial dysfunction in neurodegenerative disease.

1.11 Thesis aims

1. Extensively characterise the spatiotemporal regulation of the PINK1/Parkin-mediated mitophagy pathway in astrocytes and compare that to the same pathway in neurons.

2. Define the role of Miro1 and its ubiquitination in the PINK1/Parkin-mediated mitophagy pathway in astrocytes and neurons.

3. Investigate the functional consequences of knocking out Miro1 in principal neurons *in vivo*.

Chapter 2 - Materials and methods

2.1 Animals

Animals were maintained under controlled conditions (temperature 20 ± 2°C; 12-hour light-dark cycle). Food and water were provided ad libitum. All breeding and experimental procedures were carried out in accordance with institutional animal welfare guidelines and licensed by the UK Home Office in accordance with the Animals (Scientific Procedures) Act 1986.

2.1.1 Mouse strains

The *Pink1* KO mouse line (Pink1tm1b(EUCOMM)Wtsi) was obtained from Harwell (UK). The *Rhot1* KO (Miro1 KO) (Rhot1tm1a(EUCOMM)Wtsi) and the *Rhot2* KO (Miro2 KO) mouse lines were obtained from the Wellcome Trust Sanger Institute as part of the International Knockout Mouse Consortium (IKMC) (Skarnes et al., 2011). *Rhot1* (Miro1) conditional-KO animals were generated following the Knockout-First strategy on C57BL/6J-TyrcBrd and subsequently backcrossed in C57BL/6N Taconic Denmark strain (Skarnes et al., 2011; White et al., 2013). The CAMKIIα-CRE strain was obtained from The Jackson Laboratory and has been described previously (Mantamadiotis et al., 2002). MitoDendra (B6;129S-Gt(ROSA)26Sortm1(CAGCOX8a/Dendra2)Dcc/J) line was obtained from The Jackson Laboratory and was previously described (Pham, McCaffery et al., 2012). All transgenic mice were bred on C57BL/6N Taconic USA background.

2.1.2 Genotyping

DNA was extracted from ear biopsies or tail biopsies using the Hot Shot method (Truett et al., 2000). Genotyping PCR was carried out using a standard PCR reaction (table 1) using the appropriate primers (table 2), to a final volume of 20µl per reaction containing: 0.8µl forward and reverse primers, 0.125µL Taq Polymerase (NEB), 5µl Taq buffer (4X) and Xµl ddH20. 10µl of the PCR product was run on a 1.5% agarose gel to determine the size of the PCR products.

Step	**Temperature**	**Time**	**Repeat**
Melting	95ºC	5m	
Melting	95ºC	30s	25-35x cycle
Annealing	58ºC	30s	
Extension	72ºC	40s	
Hold	4ºC	∞	

Table 2: PCR cycling conditions

Primer name	Sense	Sequence
PINK1	Forward	TGGAACAAATGCCATGTGAC
	Reverse	GGCTGTCCTGGAACTCACTC
PINK1 Mutant	Forward	TGGAACAAATGCCATGTGAC
	Reverse	GAACTTCGGAATAGGAACTTCG
Rhot1	Forward	TTAGGATTTGTACTTTGCCCCTG
	Reverse	AAAACCCTTCCTGCATCACC
Rhot1 Mutant	Forward	TTAGGATTTGTACTTTGCCCCTG
	Reverse	TCGTGGTATCGTTATGCGCC
Rhot1 Floxed	Forward	GGAGTAGAGAAGTCAGATTCCAG
	Reverse	GAAGGCGTCAGATCACATTG
LacZ	Forward	ATCACGACGCGCTGTATC
	Reverse	ACATCGGGCAAATAATATCG

Table 3: Genotyping primer sequences

2.1.3 Transcardial PFA perfusion

For all relevant experiments, brains were fixed by transcardial perfusion of 4% PFA (4% PFA, PBS). Animals were given terminal anaesthesia via intraperitoneal injection of 1µl/g pentobarbital solution. When fully anaesthetised, the chest cavity was opened, and diaphragm cut to reveal the heart. A 21-gauge needle was inserted into the posterior end of the left ventricle and clamped in place. In quick succession, a cut in the right atrium

was made and the PFA perfusion pump was started. After 10-15ml of ice-cold 4% PFA has circulated, perfusion was stopped, the animal decapitated and brain removed and placed in ice-cold 4% PFA prior to cryosectioning.

2.2 Reagents and constructs

2.2.1 Constructs

cDNA constructs encoding ^{YFP}Parkin (23955; Youle et al., 2008), MtDsRed (Addgene 55838), pRK5-myc-Miro1 (Addgene 47888; Fransson et al., 2003) and pRK5-myc-Miro1$^{\Delta EF}$ (47888; Fransson et al., 2003) were from Addgene. pRK5-myc-Miro1^{5R} was generated in-house by site directed mutagenesis of pRK5-myc-Miro1. pRK5-myc-Miro1^{AllR} was made commercially.

2.2.2 Antibodies

Primary antibodies used for immunofluorescence (IF) and western blotting (WB) were as follows: Guinea pig anti-MAP2 (1:2000; Synaptic systems; 188004), Rabbit anti-GFAP (1:1000; Dako; z0334), Mouse anti-GFAP (1:2000; Sigma; G3893), Rat anti- GFP (1:1000; Nacalai Tesque; 10013361), Rabbit anti-Actin (1:2000; Sigma; A2066), Rabbit anti-S65-phospho-ubiquitin (1:300; Merck; ABS1513), Mouse anti-Ubiquitin (1:500; Enzo; P4D1), Mouse anti-PINK1 (1:3; Neuromab; 73-346), Mouse anti-Miro1 (1:100; Atlas; AMAb90852), Mouse anti-Miro2 (1:500; Neuromab; N384/63), Rabbit anti-Mfn1 (1:500; Abcam; ab57602), Mouse anti-Mfn2 (1:500; Abcam; ab56889), Rabbit anti-Myc (1:1000; Abcam; ab32072), Rabbit anti-eIF2a (1:500; Cell

Signalling Technologies; 9722), Rabbit anti-S51-phospho-eIF2a (1:300 IF; 1:500 WB; Abcam; ab32157), Mouse anti-VDAC1 (1:1000; Neuromab; 75-204), Mouse anti-Parkin (1:500; Cell Signalling Technologies; 4211), Mouse anti-DRP1 (1:500; BD Biosciences; 611113), Mouse anti-Tuj1 (1:1000; Covance; MMS-435P). Fluorescent secondary antibodies (all from Thermo Fisher Scientific, 1:1,000) were as follows: Donkey anti-Rat Alexa Fluor 488 (A21208), Goat anti-Rabbit Alexa Fluor 555 (A21430), Donkey anti-Mouse Alexa Fluor 647 (A31571), Goat anti-Guinea pig Alexa Fluor 647 (A21450), Goat anti-Mouse Alexa Fluor 405 (A31553), Goat anti-Rabbit Alexa Fluor 405 (A31556), Goat anti-Rabbit Alexa Fluor 488 (A110088), Goat anti-Mouse Alexa Fluor 555 (A28180). HRP-conjugated secondary antibodies for western blotting were as follows: Goat anti-Rabbit IgG-HRP conjugate (1:10,000; Bio-Rad; 1706515), Goat anti-Mouse IgG-HRP conjugate (1:10,000; Rockland; 610-103-121).

2.2.3 Drugs

Drugs used for experimentation were as follows: Valinomycin (Sigma V0627) FCCP (Sigma C2920), Antimycin A (Sigma A8674), L-Glutamate (Sigma G1251), Glycine (Sigma G7126), MG132 (Calbiochem 474790), 2-Deoxy-D-Glucose (Sigma D8375), Tetramethylrhodamine (TMRM) dye (Invitrogen T668).

2.3 Molecular Biology

2.3.1 PCR

Amplification of DNA for the purpose of cloning was carried out using Phusion High Fidelity DNA Polymerase (New England Biolabs) following manufacturer's instructions. Briefly, this involved the addition of dNTPs, plasmid DNA, Forward and reverse primer, high fidelity buffer and Phusion (see table for concentrations). This reaction mixture was then subjected to cycles of heating and finally analysed by agarose electrophoresis for presence of DNA product.

2.3.2 Transformation

Plasmid DNA was transformed into chemically-competent cells. Briefly, plasmid DNA was incubated on ice with the bacteria for 30 minutes. Cells were then heat shocked at 42 degrees for 30 seconds. SOC media was added, and the cells recovered by shaking at 37 degrees. The cells were then plated onto agar plates containing the appropriate antibiotic.

2.3.3 Site-directed mutagenesis by reverse PCR

Primers were designed so that the nucleotide changes were in the middle of the forward primer (which was approximately 20 nucleotides long). The reverse primer started with its 5-prime most nucleotide being the next nucleotide upstream of the forward primer. Following PCR, as described above, the PCR product was purified using the Qiagen kit, phosphorylated by

PNK (New England Biolabs) and ligated by T4 DNA ligase, as manufacturer's instructions (New England Biolabs). DNA was then transformed, colonies picked, DNA extracted and sequenced.

2.3.4 Reverse Transcriptional Quantitative PCR (RT-qPCR)

One hippocampus per animal was dissected and RNA extracted and treated with DNase I (Amplification grade; ThermoFisher Scientific) to remove any remaining trace amounts of DNA. cDNA was generated with 20 ng of RNA by using the Qiagen Whole Transcriptome Amplification Kit as described in the manufacturer's protocol. Primers for qPCR were designed by Primerabbitank (Massachusetts General Hospital, Boston, US) and are as follows: *Gapdh* (GenBank accession NM_008084; forward ATGACATCAAGAAGGTGGTG; reverse CATACCAGGAAATGAGCTTG), *Hprt* (GenBank accession NM_013556; forward GTTGGATACAGGCCAGACTTTGTTG; reverse GAGGGTAGGCTGGCCTATAGGCT), *Mfn1* (GenBank accession NM_024200; forward CCTACTGCTCCTTCTAACCCA; reverse AGGGACGCCAATCCTGTGA), *Mfn2* (GenBank accession NM_133201; forward CCAACTCCAAGTGTCCGCTC; reverse GTCCAGCTCCGTGGTAACATC). qPCR reactions were performed by using Sybr Green reagent (Merck, UK) on a CFX96 Real-Time System (Bio-Rad, Hercules,CA). PCR conditions were 94°C for 2 minutes, followed by 40 three-step cycles of 94°C for 15 seconds, 60°C for 30 seconds and 72°C for 30 seconds. *Gapdh* and *Hprt* were used as housekeeping gene controls. Primers

were validated by PCR and agarose gel electrophoresis and had similar amplification efficiencies when validated by using a serial dilution of representative cDNA. Samples were obtained from 4 WT and 4 Miro1^{cKO} animals, the experiment was repeated 3 times, and, in each experiment, samples were amplified in triplicate. Relative quantification was determined according to the deltadelta c(t) method (Livak and Schmittgen, 2001).

2.4 Cell Culture

2.4.1 Primary neuronal/glial culture

Mouse hippocampal and cortical astrocyte-neuron cultures were obtained from E16.5 C57BL/6 mice of the relevant genotype. Following dissection of the respective regions, the tissue was added to trypsin and DNase for 15 minutes. After washing off the trypsin in attachment media (Minimal Essential Medium, 10% Horse Serum, 1 mM Sodium Pyruvate and 0.6% Glucose), the tissue was homogenised by passing the tissue through a pipette. Cells were plates at a density of 500,000 per 6cm^2 in attachment media. After 24 hours attachment media was replaced with maintenance media (Neurobasal Medium, B27 supplement, Glutamax, 0.6% Glucose, Penstrep). Cells were grown in a humidified incubator at 37 degrees and 5% CO_2 and O_2.

2.4.2 Primary astrocyte culture

Mouse pure astrocyte cultures were obtained from E16.5 C57BL/6 mice of the relevant genotype. Cortices were dissected and added to trypsin and DNase

for 15 minutes. After washing off the trypsin, the tissue was homogenised by passing the tissue through a pipette. Cells were maintained in Dulbecco's modified Eagle's medium (DMEM) with 10% foetal bovine serum (FBS) (GIBCO) and 1% Pen-Strep (10 U/ml, 100 µg/ml) at 37°C with 5% CO_2 in a humidified incubator. Media was changed initially the day after plating and subsequently every 2 days until confluency was reached (7-10 days after plating). Cells were passaged after reaching 80-90 % confluency.

2.4.3 Passaging/splitting astrocytes

Once grown to confluency (around 90%) trypsin solution was added (137 mM NaCl, 2.7 mM KCL, 8 mM Na2HPO4, 1.5 mM KH_2PO_4, 2.5 g/L trypsin (from porcine pancreas, Sigma), 0.2 g/L EDTA, 0.0015 g/L phenol red) at 37°C with 5% CO^2 for 5 minutes to detach cells from the dish surface. Fresh culture medium (Dulbecco's modified Eagle's medium (DMEM) with 10% foetal bovine serum (FBS) (GIBCO) and 1% Pen-Strep (10 U/ml, 100 µg/ml)), preheated to 37°C, was applied to quench the trypsin and the cells were then pelleted by centrifugation and resuspended the appropriate medium before being re-plated in line with experimental needs.

2.4.4 Transfection by lipofection

Lipofectamine 2000® (Life Technologies) was used to transfect astrocyte-neuron cultures (at DIV10) as previously described (Al Awabdh et al., 2016) with some modifications. For every two 13 mm coverslips 2 µg DNA was added to 2 µl of Lipofectamine reagent, each diluted in Neurobasal and incubated at

room temperature for 30 minutes to ensure the formation of DNA-lipo complexes. Neurobasal + glucose was then added to the DNA-Lipofectamine mix before adding to cultures for 2 hours, after which the media was replaced with the previously conditioned media. Lipofectamine 2000® (Life Technologies) was used to transfect pure astrocyte cultures. For every two 13 mm coverslips 2 µg DNA was added to 2 µl of Lipofectamine reagent, diluted in Opti-MEM (GIBCO), and added to the culture medium (Dulbecco's modified Eagle's medium (DMEM) with 10% foetal bovine serum (FBS) (GIBCO) and 1% Pen-Strep (10 U/ml, 100 µg/ml)). Culture medium was replaced the following day.

2.5 Biochemistry

2.5.1 Cryosectioning

PFA-fixed brain tissue was serially cryosectioned in a Bright OTF-AS Cryostat (Bright Instrument, Co. Ltd.) at 30µm thickness, in the coronal plane and stored in cryoprotective solution (30% PEG, 30% glycerol in PBS) at -20°C until used.

2.5.2 Preparation of brain region lysates

Mice were sacrificed using a Schedule 1 method and brains placed in ice-cold HBSS. Cortex, hippocampi and cerebella were dissected and placed in 500µl, 250µl and 300µl ice-cold HEPES buffer respectively (50mM HEPES pH 7.5, 0.5% Triton X-100, 150mM NaCl, 1mM EDTA, 1mM PMSF, 10µg/ml antipain, pepstatin and leupeptin) and kept on ice. Tissue was solubilised by sonication

to aid lysis, centrifuged at 14000 rpm for 15 minutes and the supernatant collected. Protein concentration was quantified using the Bradford assay following the manufacturer's protocol (BioRad). Western blot samples were generated from these lysates by adding 1/3 volume of Sample Buffer (3X) and boiling samples for 5 minutes. Samples were stored at -80°C until use.

2.5.3 Western Blotting

20 µg of protein from lysates were loaded on 8-12% acrylamide gels (depending on size of target) and transferred to nitrocellulose membranes (GE Healthcare Biosciences) using a Bio-Rad system. Membranes were blocked in 4% powder skimmed milk in PBS-T for 1-2 hours. Primary antibody was diluted in blocking solution and incubated on the membrane overnight at 4 degrees. The membrane was then washed three times for five minutes in PBS-T and then the appropriate anti-IgG-HRP was added to the membrane (diluted in blocking solution) and incubated at room temperature for 45 minutes. Following three more five-minute washes the membranes were imaged after the addition of Luminata Crescendo (Millipore) using an ImageQuant LAS 4000 CCD camera system (GE Healthcare).

2.5.4 Coimmunoprecipitation

Cells were lysed in lysis buffer (50 mM Tris-HCl pH 7.5, 0.5% Triton X-100, 150 mM NaCl, 1 mM EDTA, 1 mM PMSF and protease inhibitor cocktail) for 45 minutes at 4°C with rotation. The cell debris was then cleared by centrifuging the lysate at 13,000 g for 10 minutes with the resulting supernatant

collected for inputs and subsequent immunoprecipitation. 1 µg of primary antibody was added to lysate for 3 hours, with rotation at 4°C. Following incubation with antibody, Protein A/G sepharose beads were added for one hour with rotation at 4°C. The beads were then washed five times with lysis buffer and finally added to Laemmli buffer and boiled at 100 degrees for five minutes. This was loaded directly into an SDS-PAGE gel for analysis by western blotting.

2.5.5 Immunocytochemistry

Astrocyte-neuron and pure astrocyte cultures on glass coverslips were fixed in 4% PFA (4% paraformaldehyde, 4% sucrose, PBS, pH 7) for 7 minutes prior to blocking and permeabilization in blocking solution (10% horse serum, 0.5% BSA, 0.2% Triton X-100, PBS). Coverslips were incubated in primary antibody for 1 hour, washed 5x in PBS+0.2% Triton X-100, then incubated for 1 hour in secondary antibody. Antibody solutions were both diluted in blocking solution. Coverslips were mounted with Prolong Gold antifade mountant (Invitrogen). If coverslips were not stained immediately after fixation, they were stored at -20C in cryoprotect solution (30% ethylene glycol, 30% glycerol, 40% PBS).

2.5.6 Immunohistochemistry

Free floating brain sections were washed in PBS before permeabilization in blocking solution (10% horse serum, 0.5% BSA, 0.2% Triton X-100, PBS) for 4-6 hours then incubated with primary antibody diluted in block solution overnight at 4°C. For mouse primary antibodies, slices were first incubated

overnight at 4°C with mouse F(ab) fragment (1:50 with block solution; 115007-003, Jackson ImmunoResearch, West Grove, PA, USA). Slices were washed 5 times in PBS for 2 hours then incubated for 3-4 hours with secondary antibody at room temperature. Slices were then washed 5 times in PBS for 2 hours and mounted onto glass slides using ProLong™ Gold Antifade mounting medium (Invitrogen).

2.6 Fluorescence Microscopy

2.6.1 Image Acquisition

Images (1024 x 1024) were acquired on a Zeiss LSM700 upright confocal microscope. The following objectives were used:

10x Zeiss EC Plan-NEOFLUAR NA=0.3 Air (WD=5.3mm)

20x Zeiss W Plan-Apochromat NA =1.0 Water (WD 1.7mm)

63x Zeiss Plan-Apochromat NA=1.40 Oil (WD=0.19mm)

63x Zeiss W Plan-Apochromat NA=1.0 Water (WD=2.1mm)

2.6.2 Fixed Confocal Imaging

Confocal images (1024 x 1024) were acquired on a Zeiss LSM700 upright confocal microscope using the 10x, 20x and 63x oil objectives and digitally captured using the Zen LSM acquisition software. For brain sections, a low magnification region of the cortex was captured using a 63x oil objective and 0.5 zoom to confirm position. For analysis, 4 zoomed regions were imaged in

various cortical areas. Acquisition settings and laser power were kept constant within experiments. Image acquisition was performed blind to experimental condition/genotype. For high-resolution imaging, a 63X oil immersion objective (NA: 1.4) coupled to a Zeiss LSM880 inverted confocal microscope with Airyscan technology was used.

2.6.3 Live confocal imaging

TMRM in astrocyte-neuron cultures was imaged live using an upright Zeiss LSM700 confocal microscope with a 63× (1 NA) water objective. Coverslips were transferred to a recording chamber perfused with aCSF imaging media (125 mm NaCl, 10 mm d-glucose, 10 mm HEPES, 5 mm KCl, 2 mm CaCl2, 1 mm MgCl2, pH 7.4) at a rate of 5 ml/min, heated to 35–37°C. Perfusion was supplemented with valinomycin for 15 mins. Images were acquired pre- and post-drug treatment.

2.7 Image Analysis

Integrated intensity of fluorescent signal was calculated in ImageJ. Colocalisation of YFP-Parkin and MtDsRed was analysed using the integrated colocalisation plugin in MetaMorph. Mitochondrial area was measured by quantification of thresholded MtDsRed signal in ImageJ. Mitochondrial morphology was measured using a custom Matlab script to measure the circularity and Feret's diameter of individual mitochondria. Sholl analysis was performed using a custom ImageJ plugin, which quantified the amount of Phospho-Ub or MtDsRed pixels within shells radiating out from the cell body

at one-pixel intervals. Western blot images were analysed using QuantityOne software (Bio-Rad).

2.8 Statistical analysis

GraphPad Prism was used for all statistical tests. Data was first tested for normality using the Kosglomorov-Smirnov test. Normal data sets were analysed for statistical significance with either a two-tailed Student's t-test (for two groups), one-way ANOVA with a Tukey *post hoc* test (for three or more groups) or two-way ANOVA with a Tukey *post-hoc* test (for two groups with multiple conditions). Non-normal or discrete data sets were analysed with a Mann-Whitney U test (for two groups) or Kruskall-Wallis (for three or more groups). In all cases, *, **, *** and **** represent $p<0.05$, $p<0.01$, $p<0.001$ and $p<0.0001$, respectively. Statistical tests used are stated throughout the thesis in the figure legends.

Chapter 3 – Differences in the spatiotemporal regulation of PINK1/Parkin-mediated mitophagy in astrocytes and neurons

3.1 Introduction

Mitochondria are trafficked to and stabilised at synapses in astrocytes where they buffer Ca^{2+}, to modulate intracellular Ca^{2+} homeostasis, and provide ATP for glutamate uptake, a process key to preventing excitotoxicity and maintaining synaptic function (Stephen et al., 2014, Jackson and Robinson, 2018). Yet how astrocytes regulate their mitochondrial network to ensure these functionalities are performed correctly is less clear. Depolarised mitochondria are unable to meet their ATP production and Ca^{2+} buffering demands and produce excess reactive oxygen species that are harmful to the cell and therefore need to be removed. To date, the majority of research into mitochondrial quality control in the CNS has focussed on neurons, however, neuronal mitophagy has been suggested to occur less readily than in non-neuronal cells (Cai et al., 2012, Van Laar et al., 2011). Despite this, very little is known about the mitophagy pathway in the other cell types of the brain, including astrocytes.

Recent evidence suggests both astrocytes and microglia display relatively high levels of basal mitophagy *in vivo* (McWilliams et al., 2018) yet, interestingly, direct comparisons between primary neurons, astrocytes,

microglia, and another glial cell type, oligodendrocyte progenitor cells (OPCs), showed that astrocytes exhibit considerably more mitophagic activation than other CNS cell types *in vitro* (Barodia et al., 2019). This agrees with a previous study showing that mitochondria are readily cleared from astrocytes following ischemia *in situ* (O'Donnell et al., 2016). Additionally, it's been shown that damaged neuronal mitochondria can be transferred to astrocytes to facilitate their clearance (Gao et al., 2019, Davis et al., 2014, Morales et al., 2020) and that healthy mitochondria can be sent in the other direction, from astrocytes to neurons (Hayakawa et al., 2016, English et al., 2020, Gao et al., 2019). This indicates that astrocytes could act as a principal site of mitochondrial turnover in the CNS, although how and why this would be the case is not clear.

Mitophagy is, in the main, controlled by the serine/threonine-protein kinase, PINK1 (PTEN-induced putative kinase protein 1) and the E3 ubiquitin ligase, Parkin, both of which are genetically linked to the aetiology of PD (Youle and Narendra, 2011, Covill-Cooke et al., 2018). Although, astrocytes and neurons express similar levels of PINK1 and Parkin at the mRNA level (Zhang et al., 2014, Zhang et al., 2016), they appear to be regulated distinctly between cell types. For example, Parkin dysfunction has been shown to impair astrocyte mitochondrial function and contribute to the pathogenesis of PD through astrocytic, but not neuronal, upregulation of the unfolded protein response (Ledesma et al., 2002) which suggests that PINK1/Parkin-dependent

mitophagy is regulated in a cell-type specific manner and could take on particular importance in astrocytes.

Another difference between the two cell types is their altered bioenergetic/metabolic state. Astrocytes are extremely metabolically flexible and have a high glycolytic capacity due to contact with vasculature *in vivo*, which provides a rapid source of glucose, and through increased expression of specific glycolytic enzymes (Herrero-Mendez et al., 2009, Zhang et al., 2014, Zhang et al., 2016). On the other hand, neuronal glycolysis is limited, and neurons rely heavily on mitochondrial respiration to meet their energy demands (Hall et al., 2012). Previous evidence suggests that Parkin activity is dependent on cellular ATP levels and that some level of glycolysis is required to adequately perform mitophagy upon loss of mitochondrial ATP production (Van Laar et al., 2011). However, research into the mitophagic process in astrocytes remains scarce, especially when it comes to direct comparisons between the rates of mitophagy in astrocytes to those in neurons present within the same biological system.

Therefore, the main aim of this chapter will be to further characterise the PINK1/Parkin mitophagic pathway in astrocytes and understand how and why this may differ from the mitophagic pathway in neurons. Additionally, with the use of a genetic knockout mouse line, the role of PINK1 in mitophagy in astrocytes and neurons will be explored.

3.2 Results

3.2.1 Generation of astrocyte-neuron cultures.

In order to visualise and quantify readouts of mitophagy in astrocytes and neurons, a primary culture system containing comparable amounts of both cell types was developed. To do this, E16.5 mouse primary brain cells were cultured in serum-containing attachment medium for at least 24 hours following plating, to encourage astrocyte proliferation, before being switched to B-27-supplemented Neurobasal medium, to aid neuronal survival. To assess the composition of the cultures, cells were fixed at DIV14 and stained with GFAP and MAP2 antibodies which are markers of astrocytes and neurons, respectively (Figure 1A). As desired, there was a comparable number of astrocytes and neurons per field of view (Figure 1A).

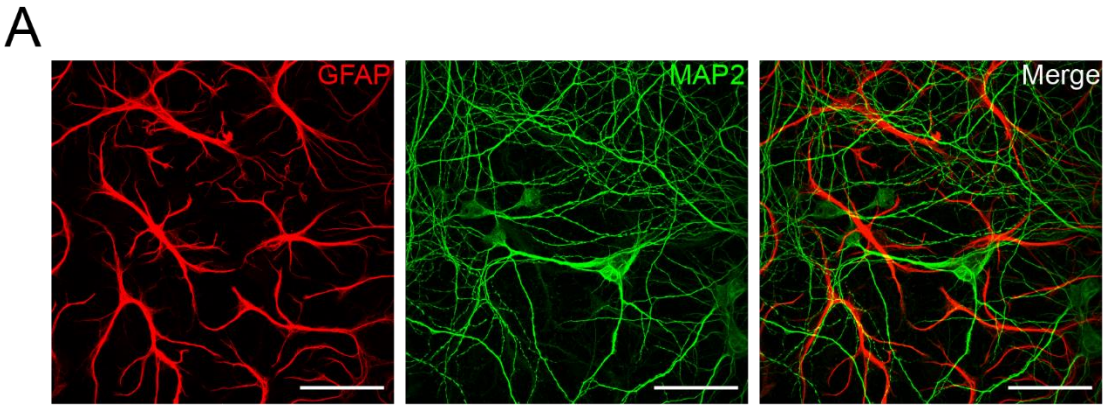

Figure 1: Generation of primary astrocyte-neuron mixed cultures. A. Representative confocal images of astrocyte-neuron cultures stained with GFAP and MAP2. (Scale bars = 50µm). This experiment was repeated but not quantified.

3.2.2 Low dose (1µM) valinomycin exerts minimal cytotoxicity in astrocyte-neuron cultures.

To establish a robust method for inducing neuronal and astrocytic mitophagy, options for damaging the mitochondrial network in both neurons and astrocytes of the same system were explored. There is controversy with respect to the optimal conditions and timescales that enable Parkin translocation without significant cytotoxicity (Cai et al., 2012, Joselin et al., 2012, Van Laar et al., 2011, Wang et al., 2011b, Barodia et al., 2019) and without the need of using caspase inhibitors (Cai et al., 2012, Lazarou et al., 2015) which can potentially interfere with the very process in study (Wang et al., 2011a). Therefore, conditions favourable for driving mitophagy in mouse primary astrocyte-neuron cultures, without leading to significant cell death were initially investigated (Figure 2). Firstly, the cytotoxicity of known mitochondrial-depolarising pharmacological agents were compared to minimise significant cellular damage following treatment. Antimycin A, a complex III inhibitor, FCCP, an oxidative phosphorylation uncoupler and valinomycin, a potassium ionophore, were chosen due to previous use in studies of neuronal mitophagy (Cai et al., 2012, Puschmann et al., 2017, Ashrafi et al., 2014). A previous study used Antimycin-A at a very low dose (5nM) to gradually and reversibly reduce mitochondrial membrane potential in neurons (Lin et al., 2017), yet the aim in this study was to rapidly depolarise the mitochondrial network in astrocytes and neurons. Therefore, DIV14 astrocyte-neuron cultures were treated with a low concentration (1µM) and a

high concentration (10µM) of each drug for 3 hours and cell death was measured as a ratio of dead cells (PI) to all cells (DAPI) (Figure 2). High dose treatment with any of the three drugs resulted in high levels of cytotoxicity; more than doubling the amount of death when compared to control (Figure 2B). This amount of death was comparable to a 3-hour treatment with 100µM glutamate and 1µM glycine; a treatment regimen used to induce high levels of excitotoxicity and neuronal death. Treatment with commonly used concentrations of FCCP or antimycin-A led to a significant amount of cell death within 3 hours, close to the levels of death induced by an excitotoxic glutamate insult (Figure 2B). 10µM FCCP has previously been used to induce mitophagy in dissociated cortical neurons however this was used in conjunction with caspase inhibitors to prevent the initiation of neuronal apoptosis (Cai et al., 2012). Low dose (1µM) treatments with valinomycin and FCCP were the least cytotoxic with cell death rates comparable to treatment with a control vehicle (DMSO) (Figure 2B). However, previous evidence suggests that traditional uncouplers, such as FCCP, lack mitochondrial specificity and can exhibit a protonophoric activity on other membranes, including the plasma membrane, which may mediate a variety of off-target effects (Park et al., 2002). Whereas valinomycin has been shown to be highly lipophilic and to exert minimal protonophoric activity at the plasma membrane which increases its mitochondrial specificity (Felber and Brand, 1982). Once present at the mitochondria, valinomycin increases K+ transport across the IMM to induce mitochondrial matrix depolarisation without altering the pH gradient of

mitochondria (Kenwood et al., 2014, Puschmann et al., 2017). Consequently, valinomycin at a concentration of 1µM was taken forward for further experimentation.

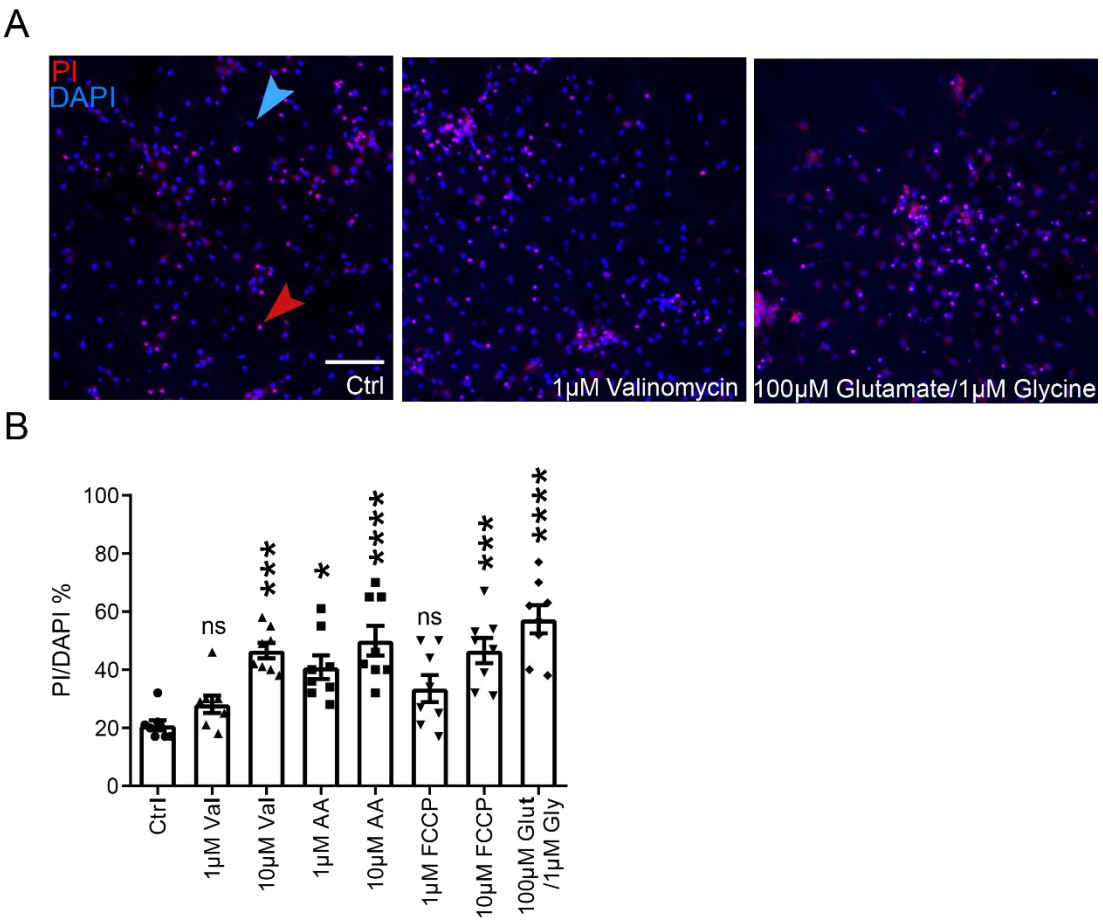

Figure 2: Cytotoxicity of known mitochondrial depolarising agents on primary astrocyte-neuron cultures. A. Example confocal images of cultures stained with DAPI (all nuclei) and PI (nuclei of dead cells) after 3 hours of drug treatment. Blue arrow indicates a viable cell. Red arrow indicates a dead cell (scale bars =100 µm). B. Quantification of the cytotoxicity of each drug, calculated as the number of dead (PI+) cells as a percentage of total (DAPI+) cells. Data collected from 4 different neuronal preparations (n=8 different replicates belonging to 8 different embryos: one-way ANOVA). Error bars represent s.e.m. Significance: *p<0.05, **p<0.01 and ***p<0.001.

3.2.3 Valinomycin induces mitochondrial depolarisation in neurons and astrocytes.

The induction of PINK1/Parkin dependent mitophagy is triggered by the dissipation of mitochondrial membrane potential (↓ψm). Therefore, it was established whether treatment with 1µM valinomycin depolarised the mitochondrial network in primary astrocyte-neuron cultures. To do this, a cell-permeable fluorescent mitochondrial dye, tetramethylrhodamine methyl ester (TMRM), that accumulates in healthy mitochondria with their membrane potential intact was utilised. Upon ↓ψm TMRM is no longer taken up into mitochondria and the fluorescent signal dissipates (Scaduto and Grotyohann, 1999). TMRM diluted in culture medium was added to DIV14 astrocyte-neuron cultures 30 minutes prior to imaging to allow the dye to be taken up into mitochondria (Figure 3). Astrocytes and neurons present on the same coverslip were then imaged live both before and after 15 minutes of 1µM valinomycin application and the intensity of TMRM signal was measured (Figure 3A). For this experiment, astrocytes and neurons were identified based on their morphology with the use of a GFP cell fill to allow for imaging of both cell types on the same coverslip. Prior to valinomycin treatment, TMRM signal intensity was high in both neurons (5489±836.6 AU) and astrocytes (7954±1397 AU) and there was no significant difference in fluorescence between cell types. Following application of valinomycin, TMRM signal intensity was significantly diminished in both neurons (610.7±202.5 AU) and astrocytes (1160±319.2 AU) (Figure 3B). Therefore, application of 1µM

valinomycin was deemed to depolarise the mitochondrial network in neurons and astrocytes present within the same culture system.

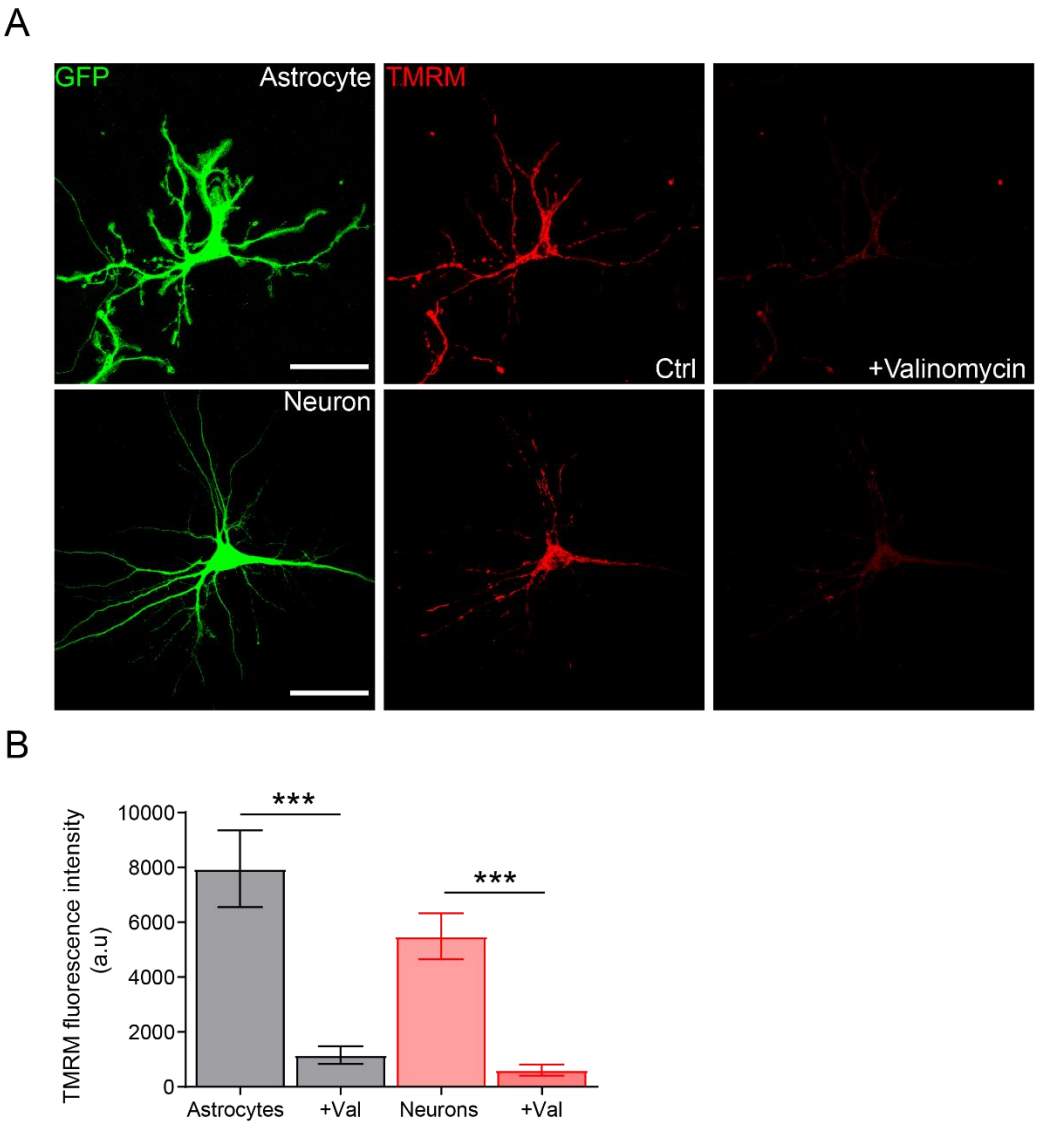

Figure 3: Valinomycin depolarises the mitochondrial network in astrocytes and neurons. A. Example confocal images of an astrocyte and a neuron expressing GFP stained with TMRM dye before and after 15 minutes of 1uM valinomycin treatment. (Scale bars = 50µm) B. Quantification of TMRM fluorescence intensity in neurons and astrocytes before and after 15 minutes of 1uM valinomycin treatment. (n=12 neurons and 12 astrocytes imaged over 3 different preparations; Unpaired t-test.) Error bars represent s.e.m. Significance: ***p<0.001.

3.2.4 Parkin translocation occurs quicker in astrocytes compared to neurons following mitochondrial depolarisation.

To establish whether mitochondrial depolarisation induces mitophagy in cultured astrocytes and neurons the translocation of Parkin to mitochondria following valinomycin treatment was visualised. Astrocyte-neuron cultures were transfected with a YFP-tagged Parkin (^{YFP}Parkin) and a DsRed targeted to the mitochondrial matrix (MtDsRed). At DIV14 astrocyte-neuron cultures were treated with 1µM valinomycin for various timepoints ranging from 30 minutes to 5 hours prior to fixation. As expected, ^{YFP}Parkin was diffuse in the cytosol of untreated astrocytes and neurons and redistributed to MtDsRed expressing mitochondria following treatment with valinomycin (Figure 4).

Following fixation, ^{YFP}Parkin and MtDsRed expressing astrocyte-neuron cultures were immunostained with anti-MAP2 and anti-GFAP antibodies to label neurons and astrocytes, respectively, in order to directly compare the rates of mitophagy between cell types. Intriguingly, it was found that Parkin began to translocate from the cytosol to mitochondria after just 30 minutes of valinomycin treatment in GFAP-positive astrocytes. In contrast, Parkin signal in MAP2-positive neurons remained entirely cytoplasmic for shorter treatment times (0.5 and 1h) (Figure 4A and B) and only began to translocate to mitochondria following 2 hours of valinomycin treatment (Figure 4A and C). Colocalization between ^{YFP}Parkin and MtDsRed signal in neurons was only significantly increased from control after 5 hours of valinomycin treatment

(Figure 4C). In astrocytes, ^{YFP}Parkin and MtDsRed signal colocalization increased significantly from control by around 4-fold after only 1 hour of valinomycin treatment. This was comparable to ^{YFP}Parkin and MtDsRed colocalization after 2, 3 and 5 hours of treatment suggesting that Parkin was fully translocated onto mitochondria in astrocytes after only 1 hour of valinomycin treatment (Figure 4C). In neurons, however, colocalisation of ^{YFP}Parkin and MtDsRed signal never reached the levels seen in astrocytes, even 5 hours after valinomycin treatment (Figure 4C).

Importantly, the robust and rapid recruitment of Parkin to depolarised mitochondria in astrocytes correlated with a significantly increased reduction of mitochondrial area, compared to neurons, at later valinomycin treatment timepoints (Figure 4D and E). Mitochondrial area was reduced in both astrocytes and neurons at early timepoints, yet this could be the result of mitochondrial fragmentation that occurs rapidly following ↓ψm (Miyazono et al., 2018) (Figure 4D). Consequently, the subsequent reduction in mitochondrial area seen between 3 and 5 hours of valinomycin treatment is likely indicative of increased mitochondrial clearance by the mitophagic process (Figure 4D and E). Between these timepoints, there was a significant reduction of mitochondrial area in astrocytes compared to neurons which strongly supports the notion of increased mitophagy rates in astrocytes compared to neurons.

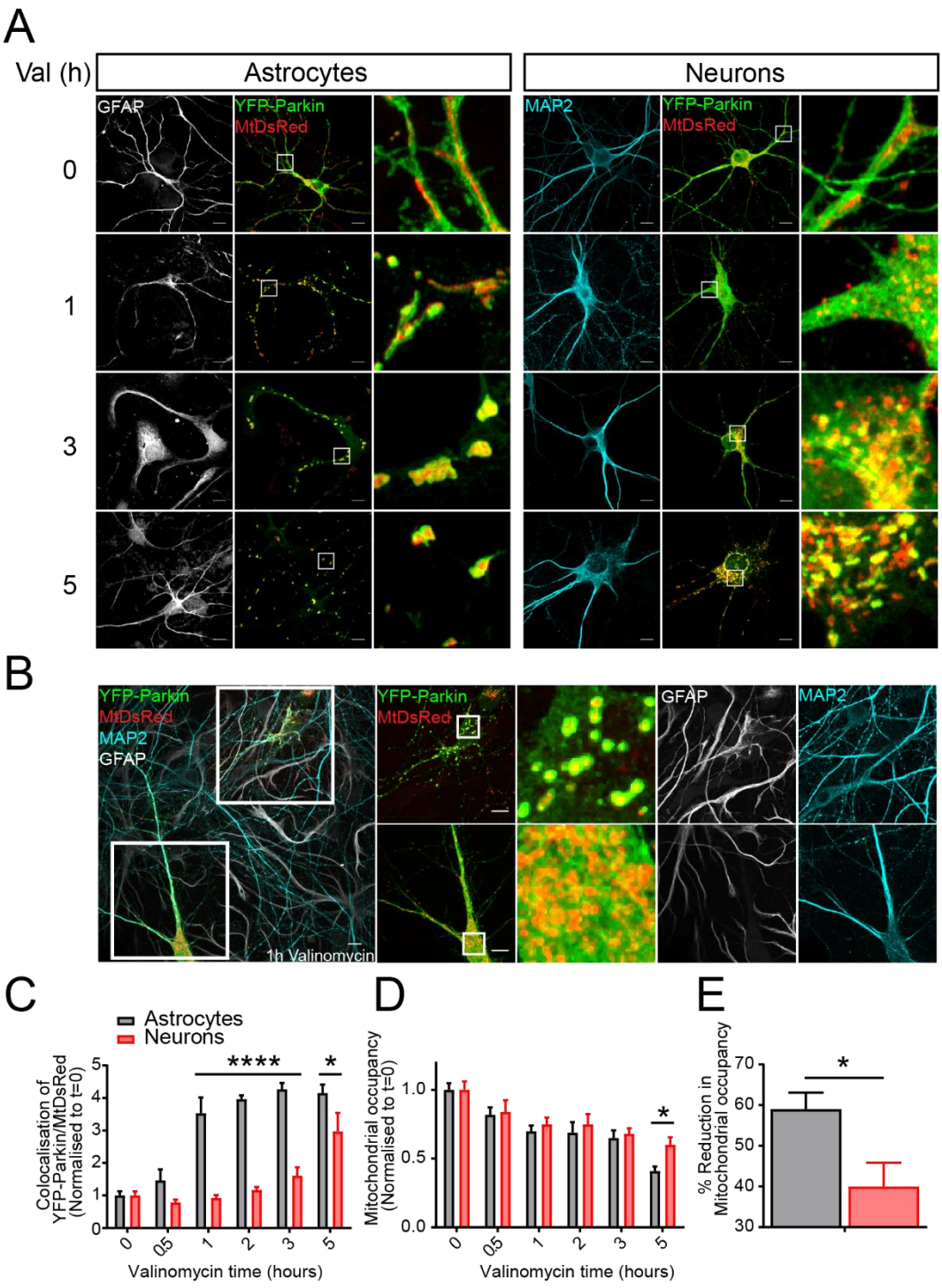

Figure 4: Parkin recruitment and mitophagy occurs quicker in astrocytes compared to neurons following mitochondrial damage. A. Representative confocal images of GFAP-positive astrocytes and MAP2-positive neurons present in an astrocyte-neuron mixed culture expressing YFP-Parkin and MtDsRed after valinomycin treatment. (Scale bars = 10µm) B. Representative 0.5x confocal image

of astrocyte-neuron mixed culture expressing YFP-Parkin and MtDsRed and immunostained with GFAP and MAP2 following 1h of valinomycin treatment. Zooms taken from showing an astrocyte and a neuron expressing YFP-Parkin and MtDsRed following 1h of valinomycin treatment. (Scale bars = 10μm) C. Quantification of Parkin recruitment to mitochondria (Integrated YFP-Parkin signal overlapping MtDsred signal normalised to t=0) in astrocytes and neurons following valinomycin treatment (two-way ANOVA, n≥15 cells all conditions over 4 different preparations). D. Quantification of mitochondrial occupancy (Area of MtDsRed signal in GFAP/MAP2 signal/area of cell) in astrocytes and neurons following valinomycin treatment (two-way ANOVA, n≥15 cells all conditions over 4 different preparations). E. Percentage reduction in mitochondrial occupancy (Area of MtDsRed signal in GFAP/MAP2 signal/area of cell) in astrocytes and neurons over 5 hours of valinomycin treatment. Error bars represent s.e.m. Significance: *$p<0.05$ and ****$p<0.0001$.

3.2.5 Translocation of Parkin precedes mitochondrial remodelling in astrocytes but not neurons.

Healthy mitochondria form a reticular network and are tubular in shape. As previously mentioned, upon mitochondrial damage they begin to fragment and become rounded in shape due to upregulation of the mitochondrial fission machinery. After analysing the length and shape of mitochondria following valinomycin treatment it was found that the neuronal mitochondrial network underwent damage-induced remodelling at a quicker rate than astrocytic mitochondria (Figure 5). Within 30 mins of valinomycin treatment, the length of neuronal mitochondria had almost halved (Figure 5B) and they had become much more circular (Figure 5C); indicative of rapid mitochondrial fission. Whereas in astrocytes, mitochondria were significantly less changed in their shape and size (Figure 5). Over time astrocytic mitochondria rounded and fragmented but never to the extent of neuronal mitochondria even after 5 hours of valinomycin treatment (Figure 5B and C). Interestingly, the recruitment of Parkin occurs prior to fragmentation of the mitochondrial network following damage in astrocytes but not in neurons. Hence, this could suggest that, unlike astrocytes, neurons prioritise fission over mitophagy as their principal method of maintaining mitochondrial fidelity following ↓ψm and only proceed to whole organellar clearance following prolonged mitochondrial damage.

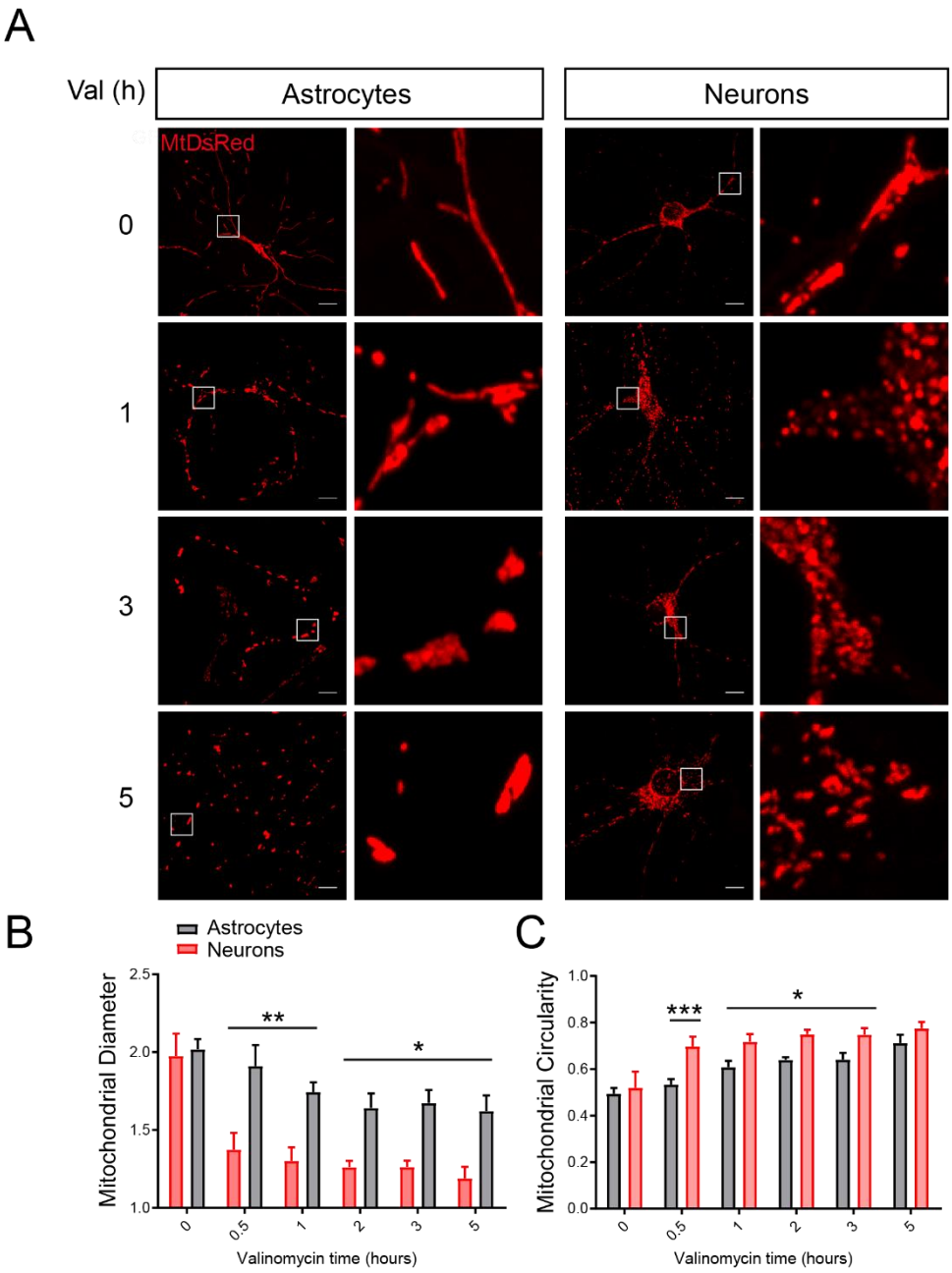

Figure 5: Damage-induced mitochondrial remodelling occurs quicker in neurons compared to astrocytes. A. Representative confocal images of astrocytes and neurons expressing MtDsRed after valinomycin treatment. (Scale bars = 10µm) B. Quantification of mitochondrial diameter in astrocytes and neurons following valinomycin treatment (two-way ANOVA, n≥15 cells all conditions over 4 different preparations). C. Quantification of mitochondrial circularity in astrocytes and neurons following valinomycin treatment (two-way ANOVA, n≥15 cells all conditions over 4 different preparations). Error bars represent s.e.m. Significance: *p<0.05, **p<0.01 and ***p<0.001.

3.2.6 Mitophagy occurs more quickly in astrocytes than neurons under endogenous conditions.

As PINK1 is the only known kinase that phosphorylates ubiquitin, antibodies specific to pS65-Ub can be used as a measure of PINK1-dependent mitophagy (Fiesel and Springer, 2015, Kane et al., 2014, Hou et al., 2018, Barodia et al., 2019) without the need for exogenous expression of fluorescently tagged Parkin, which could interfere with mitophagy kinetics. Therefore, DIV14 astrocyte-neuron cultures were treated with valinomycin as described above and, following fixation, the cells were immunostained with anti-GFAP, anti-MAP2 and anti-pS65-Ub antibodies (Figure 6). As described in introduction figure 3, phosphorylated ubiquitin chains decorate OMM proteins to initiate engagement of the autophagosomal machinery following mitochondrial damage. Therefore, a build-up of phospho-Ub on mitochondria suggests it is undergoing mitophagy.

It was found that valinomycin treatment of cultures induced accumulations of phospho-Ub in both neurons and astrocytes (Figure 6A and B). Importantly, however, there was a delay in the appearance of these accumulations in neurons compared to astrocytes. In astrocytes, there was zero signal when untreated however, phospho-Ub puncta began to appear 1 hour after valinomycin treatment and increased in number with increasing treatment time. In neurons, sparse accumulations of phospho-Ub began to appear after 2 hours of valinomycin treatment, yet never reached the amount seen in

astrocytes even after 5 hours of valinomycin treatment (Figure 6C). This data backs up the previous Parkin recruitment data and suggests that damage-induced PINK1/Parkin-dependent mitophagy occurs quicker in astrocytes than in neurons of the same culture expressing endogenous levels of Parkin.

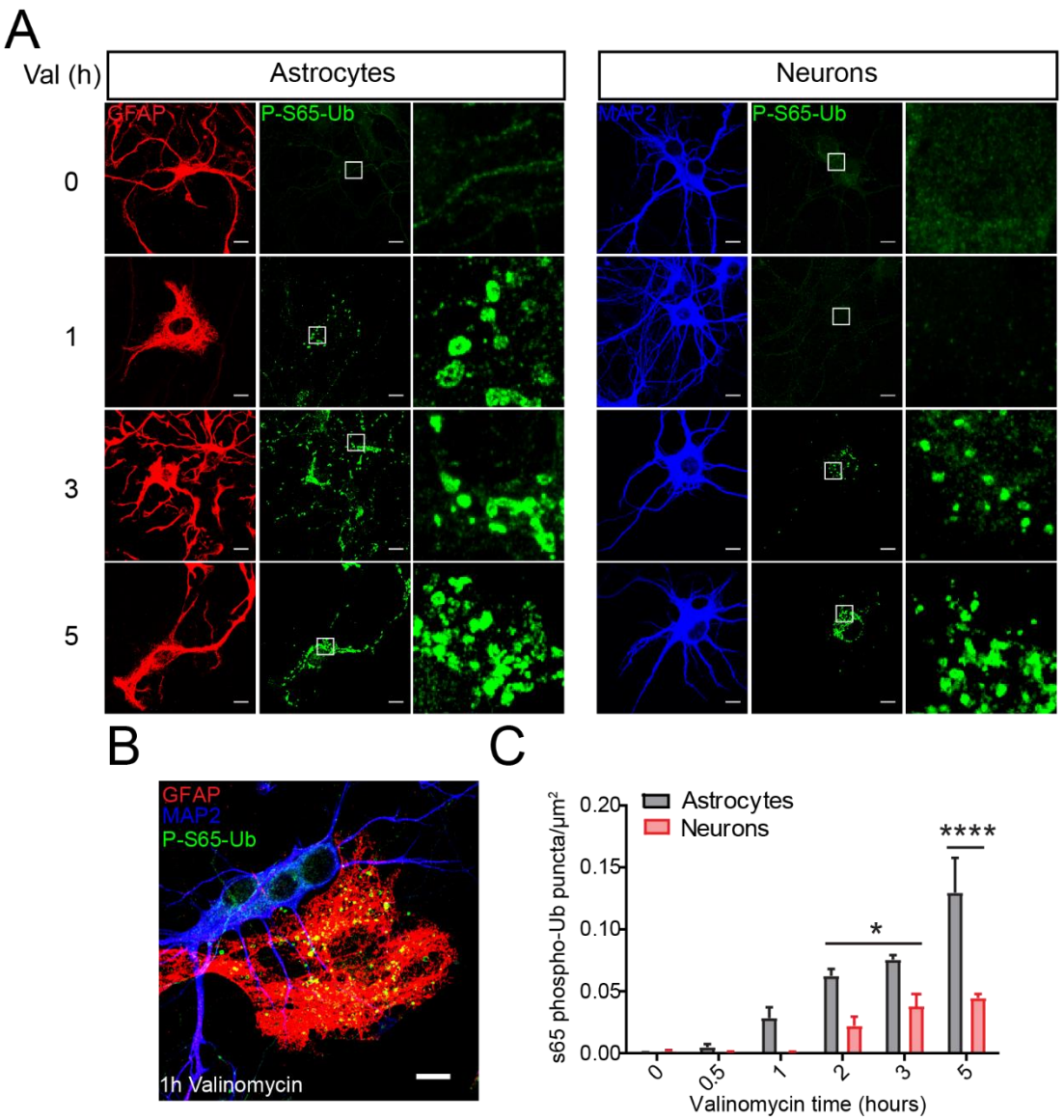

Figure 6: S65-phospho-ubiquitin puncta appear more quickly in astrocytes compared to neurons following mitochondrial damage. A. Representative confocal images of astrocytes and neurons immunostained with GFAP and MAP2, respectively, and s65-phospho-ubiquitin after valinomycin treatment (Scale bars = 10µm) B. Confocal image of an astrocyte-neuron mixed culture immunostained for GFAP, MAP2 and s65-phospho-ubiquitin after 1h valinomycin treatment. (Scale bars = 10µm) C. Quantification of s65 phospho-ubiquitin puncta within neurons and astrocytes following valinomycin treatment (two-way ANOVA, n≥15 cells over 4 different preparations). Error bars represent s.e.m. Significance: *p<0.05 and ****p<0.0001.

3.2.7 Phosphorylated ubiquitin accumulates on the outer membrane of depolarised mitochondria in astrocytes.

To ensure that phospho-Ub signal was specific to depolarised mitochondria, DIV14 astrocyte-neuron cultures were transfected with MtDsRed prior to valinomycin treatment and stained with s65-Phospho-Ub and GFAP following fixation. As expected, valinomycin-induced phospho-Ub puncta colocalised with mitochondria in astrocytes (Figure 7). This could be clearly observed with high resolution (Airyscan) imaging, a method that increases imaging resolution by a factor of 1.7 and showed that P-S65-Ub signal surrounded MtDsRed signal in rings as could be observed by fluorescent linescan (Figure 7A and B). This confirms that phospho-Ub accumulates on the OMM of depolarised mitochondria in astrocytes and underlines the legitimacy of s65-Phospho-Ub as a readout of mitophagy.

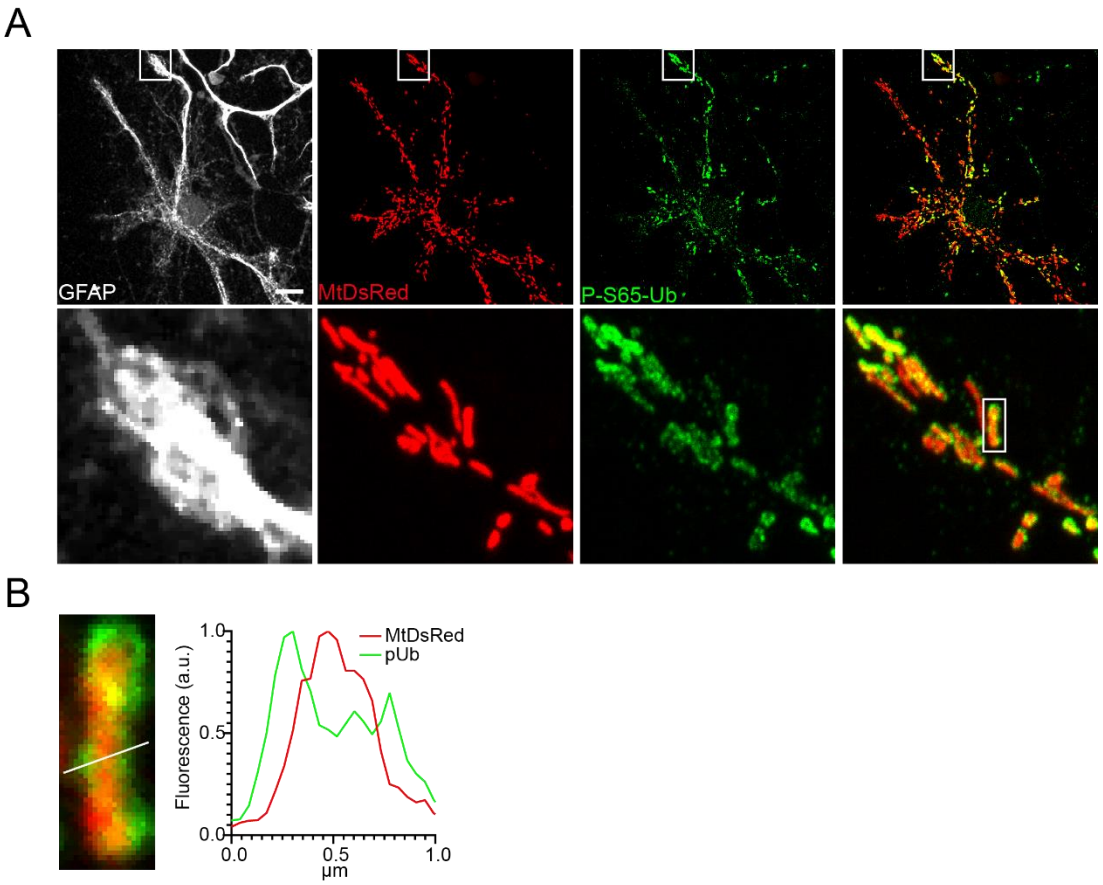

Figure 7: S65-phospho-ubiquitin accumulates on the outer mitochondrial membrane of depolarised mitochondria in astrocytes. A. Airyscan confocal image and zooms of a valinomycin-treated astrocyte expressing MtDsRed and immunostained with GFAP and s65-phospho-ubiquitin. (Scale bars = 10µm) B. Zoomed airyscan confocal image and fluorescent linescan of an individual mitochondrion expressing MtDsRed immunostained with s65-phospho-ubiquitin. This data is purely qualitative and has not been repeated or quantified.

3.2.8 Mitophagy in astrocytes is not spatially restricted.

Previous evidence suggests that mitophagy in neurons is spatially restricted to the somatodendritic region and that mitochondria are retrogradely transported back to the soma to facilitate their clearance (Cai et al., 2012, Zheng et al., 2019), however, less is known about the spatial component of astrocytic mitophagy. Intriguingly, as had been previously observed in the Parkin recruitment experiments, damage-induced phospho-ub puncta did not appear to be spatially restricted in astrocytes. Therefore, sholl analyses was performed in order to quantify the spatial distribution of phospho-Ub accumulations in astrocytes and neurons after 5 hours of valinomycin treatment (Figure 8). The analyses measured the number of phospho-ub puncta present within equidistant concentric circles emanating from the centre of the cell (Figure 8B). The cell area was determined by GFAP or MAP2 signal for astrocytes and neurons, respectively and the cumulative probability of phospho-ub puncta was plotted against the distance from the centre of the cell (Figure 8C). As observed by eye, phospho-ub accumulations were distributed homogenously throughout astrocytes (Figure 8C). Phospho-ub puncta were even present within the very distal processes of astrocytes suggesting that mitophagy can occur irrespective of subcellular compartment. However, this was not the case in neurons, where the majority of phospho-ub signal was positioned close to the centre of the cell, which confirms previous findings (Cai et al., 2012, Zheng et al., 2019) (Figure 8). The vast difference in distribution of phospho-ub between cell types is highlighted by the 60% probability value

which is more than 3x closer to the cell body in neurons than in astrocytes (Figure 8D). Therefore, these findings suggest that, unlike in neurons, mitophagy in astrocytes is initiated regardless of subcellular localisation and mitochondria may not require to be transported to the cell body to facilitate their clearance.

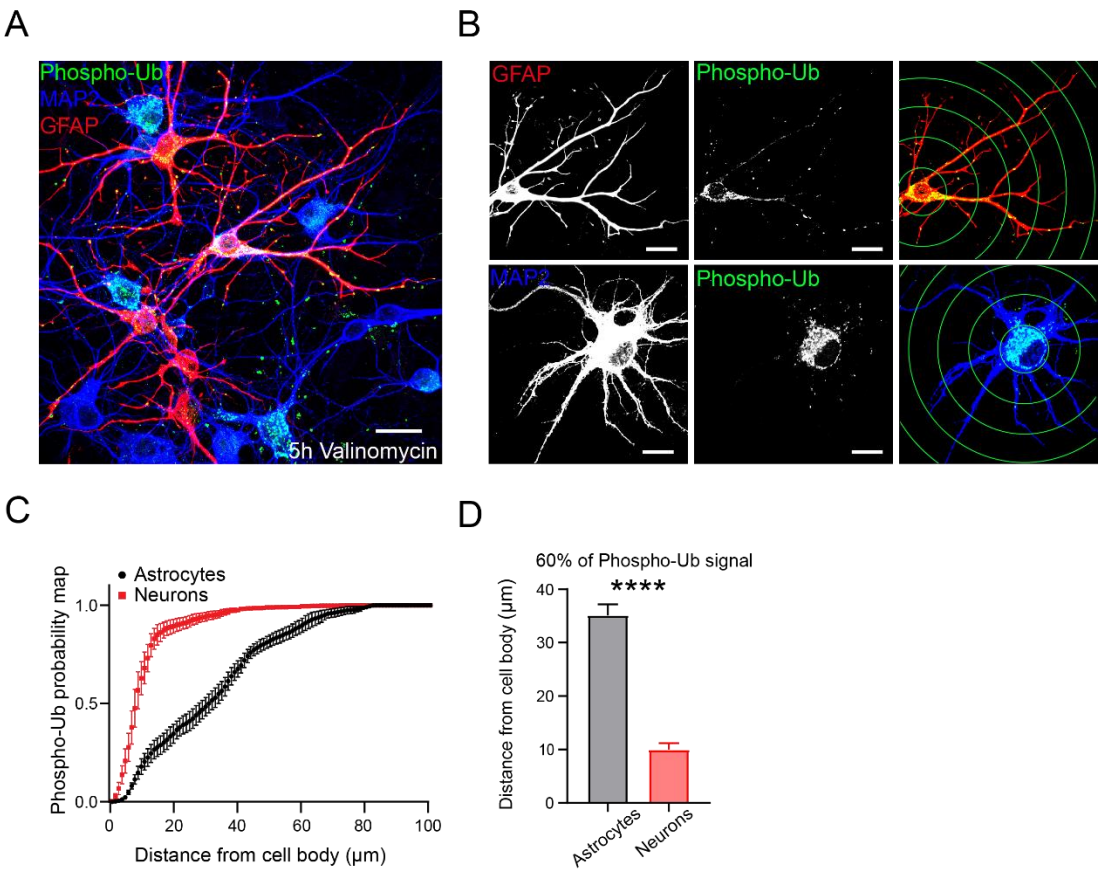

Figure 8: S65-phospho-Ub puncta formation is not spatially restricted in astrocytes, unlike in neurons, following mitochondrial damage. A. Confocal image of an astrocyte-neuron mixed culture immunostained for GFAP, MAP2 and s65-phospho-ubiquitin after 5 hours of 1µM valinomycin treatment. (Scale bars = 10µm) B. Representative confocal images used for sholl analyses of an individual astrocyte and neuron immunostained with GFAP and MAP2, respectively, and s65-phospho-ubiquitin after 5 hours of valinomycin treatment (Circles are for representative only and are not to scale). C. Cumulative plot of s65-phospho-ubiquitin signal distribution in astrocytes and neurons after 5 hours 1µM valinomycin treatment (normalised to GFAP and MAP2 area for astrocytes and neurons, respectively). D. Quantification of mean distance from the cell body that 60% of phopho-ub signal is situated (normalised to GFAP and MAP2 area for astrocytes and neurons, respectively) (unpaired t test, n≥15 cells over 4 different preparations). Error bars represent s.e.m. Significance: ****p<0.0001.

3.2.9 Mitophagy in astrocytes, but not neurons, is detectable by western blot.

Alongside immunocytochemical analysis, the accumulation of phospho-Ub and other common targets of PINK1/Parkin-dependent mitophagy in neurons and astrocytes were assessed by western blot, which may provide a more quantitative readout of mitophagy rates (Figure 9). To do this, pure astrocyte and pure neuronal cultures were generated and treated with 1µM valinomycin at various timepoints as described previously (with an additional 24-hour treatment point), prior to lysing the cells. Samples were probed with S65-phospho ubiquitin, PINK1 and Parkin antibodies alongside other mitochondrial proteins known to be ubiquitinated and degraded during mitophagy; Mfn1, Miro2 and VDAC1. GFAP and Tuj1 (B-III-Tubulin) expression levels were also measured to ensure astrocyte and neuronal enrichment, respectively, and to exclude any confounding effects of contamination from the other cell type (Figure 9A).

Once again, a clear difference was observed between the rates of mitophagy in astrocytes and neurons (Figure 9B-G). In the pure astrocyte cultures, low kDa phospho-Ub signal (<75kDa) started to appear just 30 minutes into valinomycin treatment. Throughout 24 hours of treatment the phospho-Ub signal increased and shifted into higher molecular weights (>75kDa); indicative of the formation of polymeric phospho-Ub chains (Figure 9A and C). The increase in phospho-Ub signal coincided with an increase in PINK1 expression

suggesting that, as expected, the phosphorylation of ubiquitin at serine 65 is dependent on PINK1 activity (Figure 9B). As has been previously reported in cell lines, PINK1 was undetectable in untreated samples. This is due to the constant proteasomal turnover of the non-cleaved version of PINK1 when mitochondrial membrane potential is intact (Figure 9B). The increased expression of PINK1 and phospho-ub was also accompanied by a reduction in the levels of non-ubiquitinated Parkin (52 kDa) in astrocytes (Figure 9D). Parkin is phosphorylated by PINK1 at s65 to activate Parkin's E3 ligase activity enabling Parkin to ubiquitinate various mitochondrial substrates including its own auto-ubiquitination. The formation of ubiquitin chains on Parkin will shift Parkin to a higher molecular weight. Consequently, the reduction in levels of non-ubiquitinated Parkin is indicative of increased levels of PINK1's kinase and Parkin's E3 ligase activity following valinomycin treatment in astrocytes.

Mfn1 is a key Parkin substrate and is rapidly ubiquitinated and degraded by the proteosome to prevent refusion of mitochondria following the induction of mitophagy (Glauser et al., 2011). Therefore, the ubiquitination and degradation of Mfn1 is a robust readout of the early stages of PINK1/Parkin-dependent mitophagy. Ubiquitination of Mfn1 in primary astrocytes (manifested as increased banding at higher molecular weights) occurred within only 1 hour of valinomycin treatment which translated to its degradation at later timepoints. There was an almost complete loss of Mfn1 expression following 24 hours treatment (Figure 9E). Additionally, VDAC1 and Miro2

expression in astrocytes was reduced following longer valinomycin treatment (Figure 8F and G). Like Mfn1, Miro2 and VDAC1 are ubiquitinated by Parkin however they are not degraded proteosomally (Wang et al., 2019a, Geisler et al., 2010). Instead, ubiquitin chains present on VDAC1 bind to autophagosome receptors to facilitate mitochondrial clearance meaning that VDAC1 degradation occurs on a much longer timescale to Mfn1 (Geisler et al., 2010). Thus, the reduction seen in VDAC1 expression after 5 and 24 hours of treatment could reflect the lysosomal degradation of mitochondria in astrocytes (Figure 9F).

In contrast, in the pure neuronal samples PINK1 or phospho-Ub signal was undetectable, even after 24 hours of valinomycin treatment. Transcriptomic and proteomic data shows that neurons express comparable levels of PINK1 to astrocytes (Zhang et al., 2014, Zhang et al., 2016), so this data indicates that PINK1 is uncleaved and inactive in pure neuronal cultures even after ↓ψm (Figure 9B). Alongside this, the levels of Parkin, Mfn1, Miro2 and VDAC1 remained unchanged at each treatment timepoint which suggests that these proteins are not being ubiquitinated and degraded in neurons, at least 24 hours after mitochondrial depolarisation (Figure 9). However, it should be noted there is a clear caveat with the neuronal data. Pure neuronal cultures lack the metabolic and neurotrophic support provided by astrocytes and other glial cells which confer neuronal viability (Enright et al., 2020). Thus, it could be that valinomycin treatment is more neurotoxic in this system which would explain

why readouts of neuronal mitophagy in a pure neuronal culture are non-quantifiable by western blot. Notwithstanding, the pure astrocyte western blot data outlines the kinetics of the mitophagic process in astrocytes and further underlines the rapid induction of this mitophagy following ↓ψm in astrocytes.

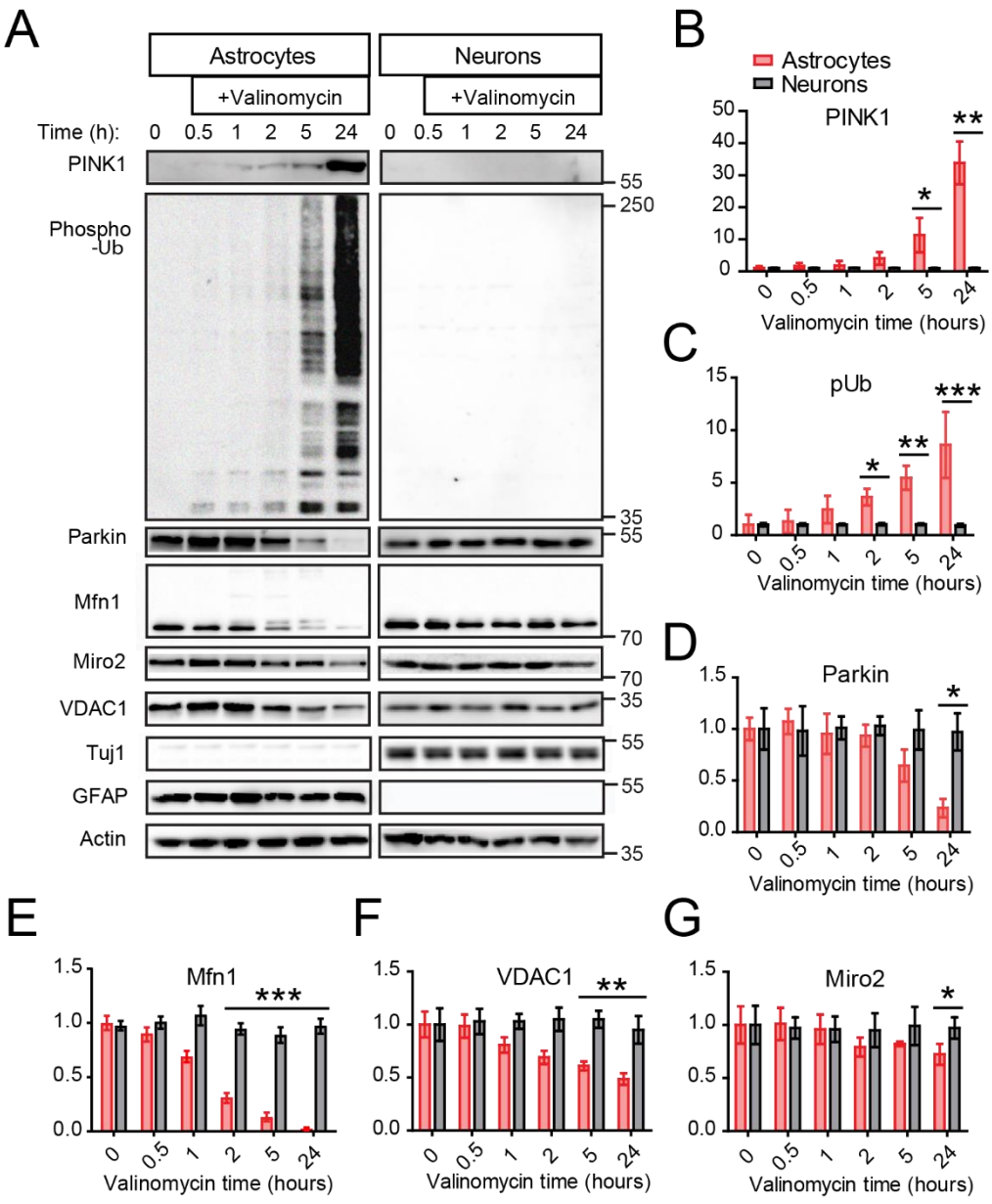

Figure 9: Mitophagy readouts are quantifiable by western blot in astrocytes, but not in neurons. A. Representative western blot images of lysates from pure astrocyte and pure neuronal cultures treated with 1µM valinomycin probed with the primary antibodies stated. B. Quantification of PINK1 band intensity (normalised to timepoint 0h and actin) (two-way ANOVA, n=4). C. Quantification of s65-phospho-ubiquitin band intensity (two-way ANOVA, n=4). D. Quantification of Parkin band intensity (two-way ANOVA, n=4) E. Quantification of Mfn1 band intensity (two-way ANOVA, n=4). F. Quantification of VDAC1 band intensity (two-way ANOVA, n=4). G. Quantification of Miro2 band intensity (two-way ANOVA, n=4). Error bars represent s.e.m. Significance: *p<0.05, **p<0.01, ***p<0.001 and ****p<0.0001.

3.2.10 Damage-induced mitophagy in astrocytes and neurons is dependent on PINK1.

Recently, the loss of PINK1 was shown to be the biggest decelerator of damage-induced mitophagy in a whole-genome CRISPR knockout screen in Parkin-overexpressing mouse myoblasts (Hoshino et al., 2019). Yet, the role of PINK1 in astrocytic mitophagy has not been well studied. Therefore, to establish the role of PINK1 in mitophagy in astrocytes and neurons and to ensure previous findings were properly controlled, the previous experiments were repeated in astrocytes and neurons lacking PINK1. To do this, a global PINK1^{KO} mouse line that displays a complete loss of PINK1 expression in the cortex, hippocampus and cerebellum was utilised (Figure 10). These mice display no obvious signs of pathology although a decreased mean platelet volume has been reported (Smith and Eppig, 2012).

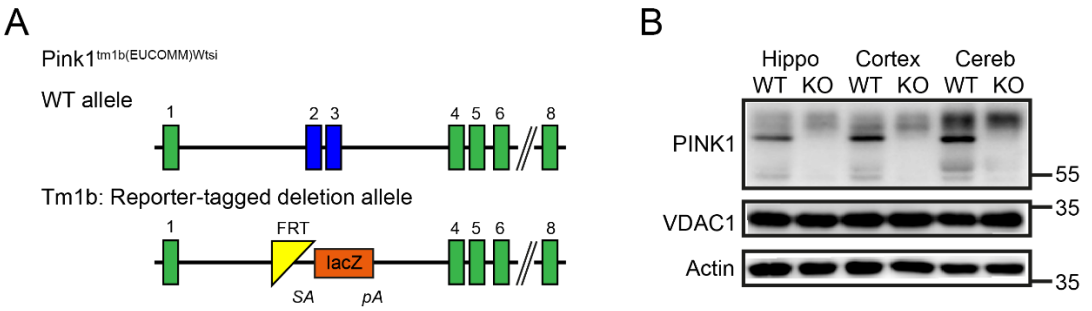

Figure 10: Global PINK1^{KO} mouse line. A. Genetic allele map of a WT and Tm1b PINK1 allele. B. Western blot image of hippocampal, cortical and cerebellar lysates taken from a WT and PINK1^{KO} mouse probed with anti-PINK1, VDAC1 and actin antibodies.

Firstly, astrocyte-neuron cultures were generated from E16.5 PINK1^{KO} and WT embryos and transfected with ^{YFP}Parkin and MtDsRed prior to valinomycin treatment, as previously described (Figure 11). As expected, the loss of PINK1 completely blocked Parkin recruitment to mitochondria in both astrocytes and neurons (Figure 11 A-C). Importantly, damage-induced mitochondrial clearance was also blocked in PINK1^{KO} astrocytes. Mitochondrial area in WT astrocytes was near to half that in astrocytes lacking PINK1 after 5 hours of valinomycin treatment (Figure 11D). Additionally, there was a near to significant difference in mitochondrial occupancy between WT and PINK1^{KO} neurons which could suggest there is some level of mitochondrial clearance in WT neurons after 5 hours of valinomycin treatment (Figure 11E). However, there was no difference in mitochondrial area between WT and PINK1^{KO} astrocytes and neurons for the first 3 hours of valinomycin treatment. Mitochondria became fragmented and mitochondrial area was reduced irrespective of PINK1 expression suggesting that damage-induced remodelling of mitochondria in astrocytes and neurons occurs independently to PINK1 (Figure 11D and E). This also confirms that the reduction in mitochondrial area seen after 5 hours of valinomycin treatment is mitophagy-dependent and distinct to the remodelling seen at previous timepoints.

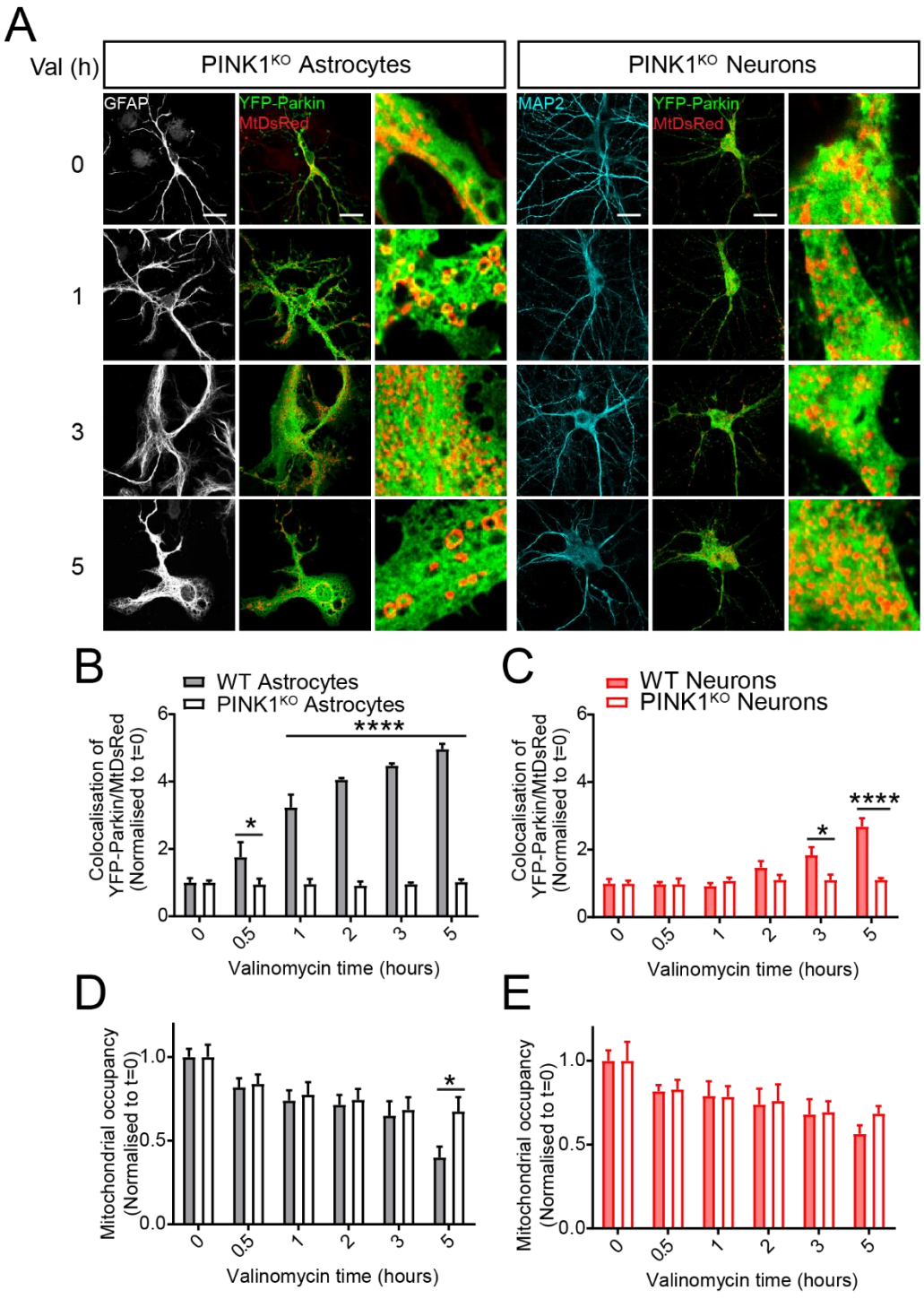

Figure 11: Parkin recruitment and mitophagy is dependent on PINK1 in astrocytes and neurons. A. Representative confocal images of GFAP-positive astrocytes and MAP2-positive neurons present in a PINK1^{KO} astrocyte-neuron mixed culture expressing YFP-Parkin and MtDsRed treated with 1µM valinomycin. (Scale

bars = 10µm) B. Quantification of Parkin recruitment to mitochondria (Integrated YFP-Parkin signal overlapping MtDsred signal normalised to t=0) in WT and PINK1^{KO} astrocytes following 1µM valinomycin treatment (two-way ANOVA, n≥12 cells all conditions over 3 different preparations). C. Quantification of Parkin recruitment to mitochondria in WT and PINK1^{KO} neurons following 1µM valinomycin treatment (two-way ANOVA, n≥12 cells all conditions over 3 different preparations). D. Quantification of mitochondrial occupancy (Area of MtDsRed signal in GFAP area of cell) in WT and PINK1^{KO} astrocytes following 1µM valinomycin treatment (two-way ANOVA, n≥12 cells all conditions over 3 different preparations). E. Quantification of mitochondrial occupancy (Area of MtDsRed signal in MAP2 area of cell) in WT and PINK1^{KO} neurons following 1µM valinomycin treatment (two-way ANOVA, n≥12 cells all conditions over 3 different preparations). Error bars represent s.e.m. Significance: *p<0.05 and ****p<0.0001.

Next, the specificity and validity of the S65-phospho ubiquitin antibody as a readout of mitophagy in astrocytes and neurons was assessed (Figure 12). As PINK1 is the only known kinase to phosphorylate ubiquitin, the formation of phospho-ubiquitin puncta should be entirely dependent on PINK1 expression. Therefore, WT and PINK1^{KO} astrocyte-neuron cultures were treated with valinomycin, fixed and stained with GFAP, MAP2 and s65-phospho-ubiquitin, as previously described (Figure 12A). Accordingly, s65-phospho-ubiquitin immunoreactivity was undetectable in PINK1^{KO} astrocyte-neuron cultures throughout the valinomycin treatment regimen. In contrast, phospho-ubiquitin puncta began to appear after 1 hour in WT cultures and increased in number with treatment time (Figure 12B). Thus, S65-phospho ubiquitin immunoreactivity was deemed to be a specific readout of PINK1-dependent mitophagy in astrocytes and neurons.

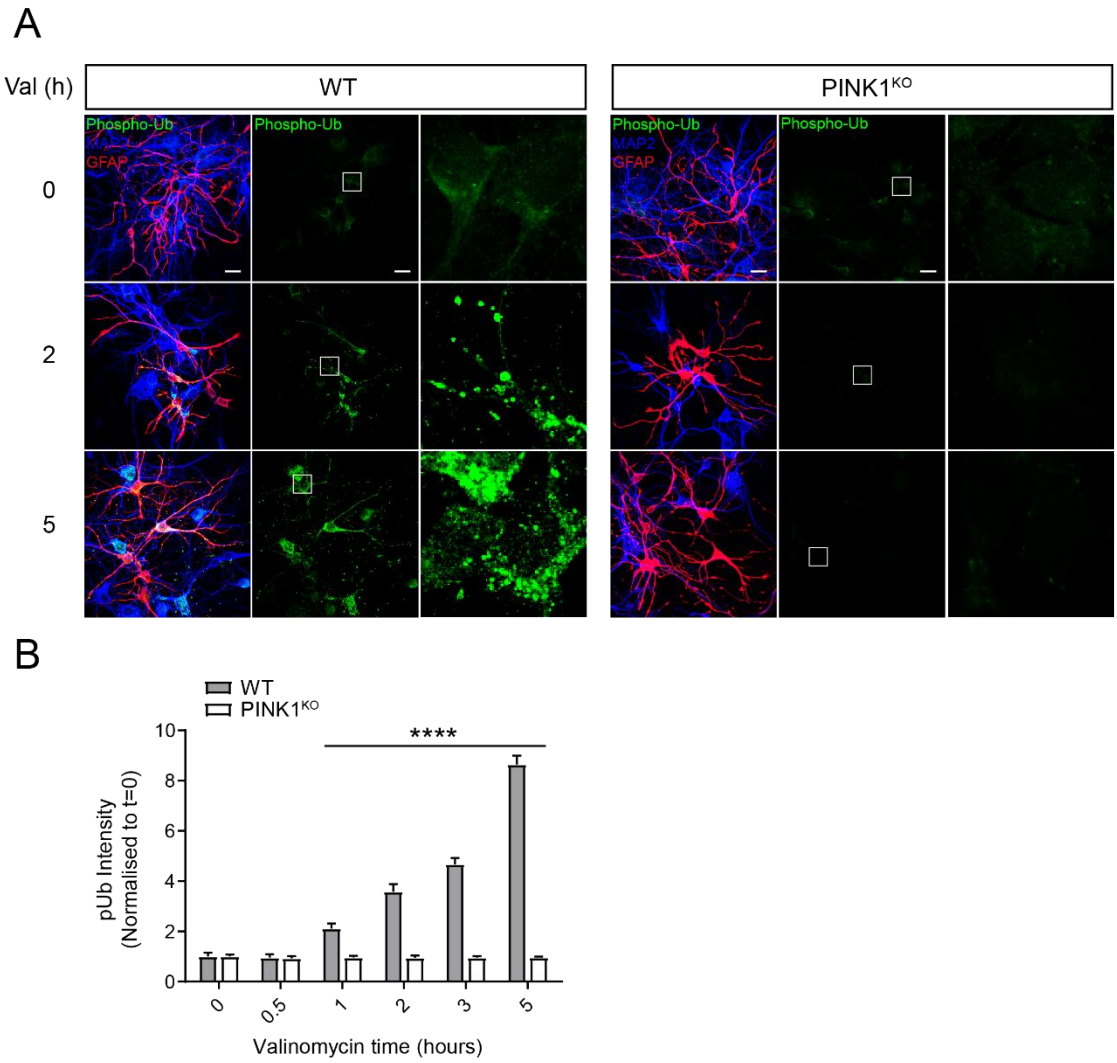

Figure 12: S65-phospho-ubiquitin puncta formation is dependent on PINK1 in astrocytes and neurons. A. Representative confocal images of WT and PINK1^{KO} astrocyte-neuron cultures treated with 1µM valinomycin immunostained with GFAP, MAP2 and s65-phospho-ubiquitin. (Scale bars = 10µm) B. Quantification of s65-phospho-ubiquitin signal intensity in WT and PINK1^{KO} astrocyte-neuron cultures treated with 1µM valinomycin (normalised to control) (two-way ANOVA, n≥15 ROIs all conditions over 3 different preparations) Error bars represent s.e.m. Significance: ****p<0.0001.

Finally, pure astrocyte cultures were generated from WT and PINK1^{KO} mice and lysates were produced following valinomycin treatment (Figure 13). Western analysis was performed and PINK1, s65-phospho-ub and Mfn1 levels were measured as readouts of mitophagy alongside the levels of total ubiquitin as a control measure (Figure 13A). In contrast to WT samples, no PINK1 or s65-phospho-ub signal was observed in all the samples derived from PINK1^{KO} mice confirming both the loss of PINK1 in astrocytes and the specificity of the pS65-Ub antibody by western blot (Figure 13B and C). Importantly, there was no change in the amount of total ubiquitin between WT and KO astrocytes indicating that the lack of phospho-ubiquitin signal seen in the KO is not the result of altered total ubiquitin levels (Figure 13A). Additionally, there was no sign of ubiquitination or degradation of Mfn1 following valinomycin treatment in PINK1^{KO} astrocytes (Figure 13C).

Taken together, this triad of experiments establishes the importance of PINK1 for mitophagy in both astrocytes and neurons. Additionally, this data adds further weight to the previous findings showing that PINK1/Parkin-mediated mitophagy occurs more readily in astrocytes than in neurons.

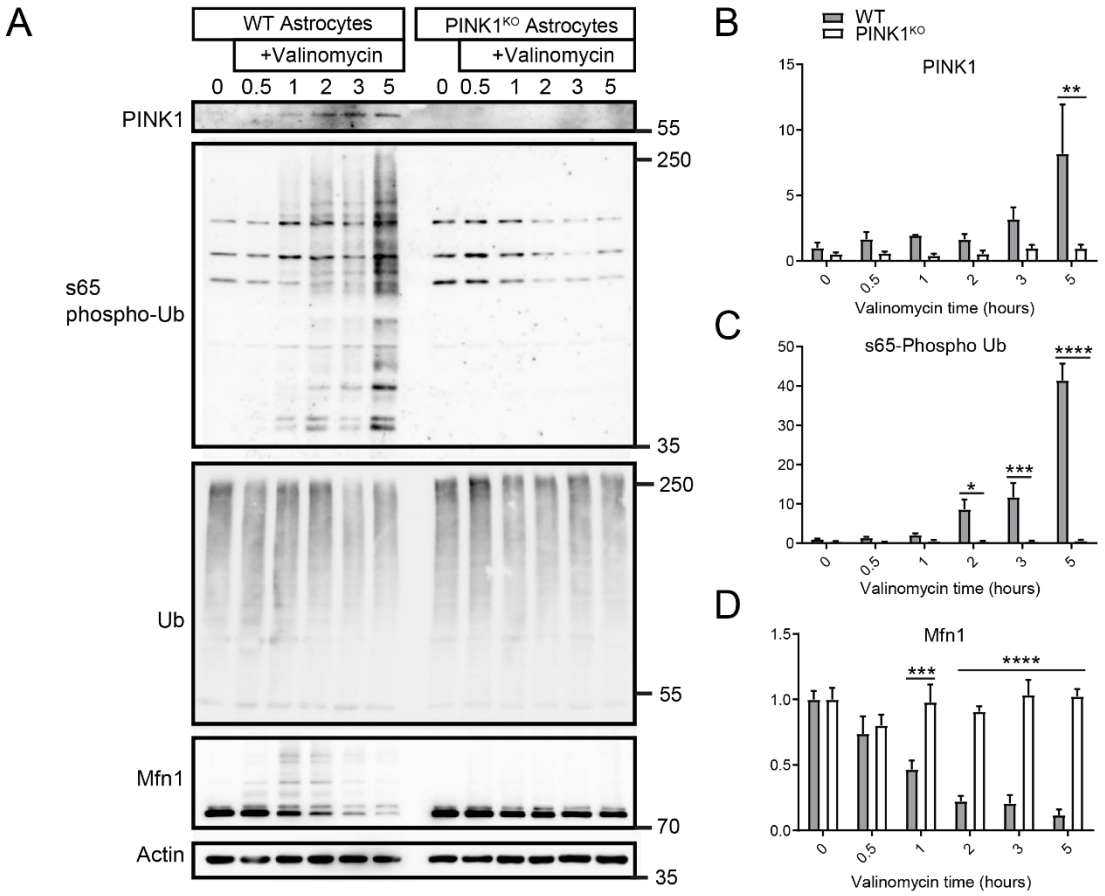

Figure 13: Damage-induced mitophagy in pure astrocyte cultures is dependent on PINK1. A. Representative western blot images of lysates from WT and PINK1^{KO} astrocyte cultures treated with 1µM valinomycin probed with the primary antibodies stated. B. Quantification of PINK1 band intensity (normalised to actin and WT timepoint 0h) (two-way ANOVA, n=5 all conditions and genotypes) C. Quantification of s65-phospho-ubiquitin band intensity (normalised to WT timepoint 0h) (two-way ANOVA, n=5 all conditions and genotypes) D. Quantification of Mfn1 band intensity (normalised to WT timepoint 0h) (two-way ANOVA, n=5 all conditions and genotypes). Error bars represent s.e.m. Significance: *p<0.05, **p<0.01, ***p<0.001 and ****p<0.0001.

3.2.11 Glycolysis inhibition blocks damage-induced Parkin recruitment to mitochondria in astrocytes and neurons.

A clear difference has been identified in the rates of damage-induced PINK1/Parkin-mediated mitophagy in neurons and astrocytes. Therefore, it was important to understand how and why this is the case. One proposed hypothesis is that astrocytes are more metabolically flexible than neurons meaning that they are able to utilise glycolysis as their primary source of ATP following mitochondrial insult. This would ensure that astrocytes could continue to adequately produce energy while undergoing mitophagy to re-establish a healthy mitochondrial network. To test this theory, glycolysis was blocked in astrocyte-neuron cultures by replacing glucose with 2-Deoxy-D-glucose (2DG) in the culture medium (Figure 14). 2DG is a glucose molecule which has the 2-hydroxyl group replaced by hydrogen, so that it cannot undergo further glycolysis. Consequently, cells cultured in 2DG have to meet their energy demands through non-glycolytic means and are more reliant on mitochondrial respiration. Glucose or 2DG astrocyte-neuron cultures were transfected with ^{YFP}Parkin and MtDsRed and treated them with valinomycin as previously described (Figure 14). Intriguingly, the robust recruitment of Parkin to depolarised mitochondria observed after 1, 2 and 3 hours of valinomycin treatment in glucose-cultured astrocytes was completely absent in 2DG-cultured astrocytes (Figure 14A and B). Additionally, there was a small yet significant reduction in the amount of Parkin on mitochondria after 3 hours of treatment in neurons cultured in 2DG rather than glucose (Figure 14A and C).

Interestingly, the rate of Parkin recruitment to mitochondria after 5 hours of valinomycin treatment was unquantifiable due to excess cytotoxicity (manifested as a loss of MAP2 and GFAP immunoreactivity) reaffirming that mitophagy is a vital protective and pro-survival mechanism in astrocytes and neurons. Therefore, this data suggests that the induction of damage-induced mitophagy in astrocytes and neurons is dependent on the glycolytic capacity of the cells.

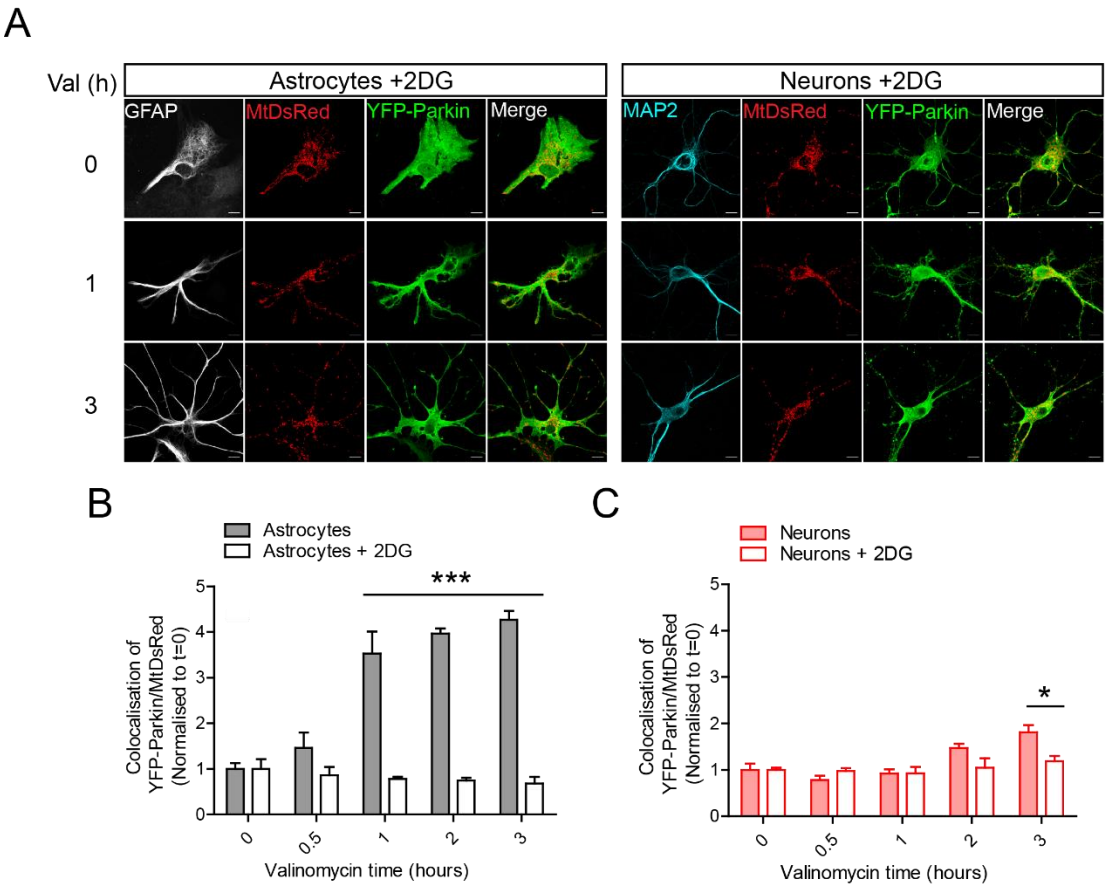

Figure 14: Glycolytic inhibition blocks Parkin recruitment to depolarised mitochondria in neurons and astrocytes. A. Representative confocal images of GFAP-positive astrocytes and MAP2-positive neurons present in a 2DG astrocyte-neuron mixed culture expressing YFP-Parkin and MtDsRed after 1µM valinomycin treatment. (Scale bars = 10µm) B. Quantification of Parkin recruitment to mitochondria (Integrated YFP-Parkin signal overlapping MtDsred signal normalised to t=0) in glucose and 2DG astrocytes following 1µM valinomycin treatment (two-way ANOVA, n≥12 cells all conditions over 3 different preparations). C. Quantification of Parkin recruitment to mitochondria in glucose and 2DG neurons following 1µM valinomycin treatment (two-way ANOVA, n≥12 cells all conditions over 3 different preparations). Error bars represent s.e.m. Significance: *p<0.05 and ***p<0.001.

3.2.12 Glycolysis inhibition completely blocks damage-induced mitochondrial clearance in primary astrocytes.

Although this data suggests that glucose metabolism is required for the induction of Parkin-dependent mitophagy in astrocytes, the latter readouts of mitophagy, including mitochondrial clearance, were unquantifiable in a mixed culture system (Figure 15). Therefore, due to their increased resilience to insult when cultured alone, pure astrocytes were cultured in either glucose or 2DG-containing medium. The pure astrocytes were then transfected with ^{YFP}Parkin and MtDsRed and treated with valinomycin for various timepoints in a 24-hour treatment regimen (Figure 15A). Consistent with the findings in the astrocyte-neuron cultures, Parkin translocated to mitochondria following 1 hour of valinomycin treatment and colocalisation between ^{YFP}Parkin and MtDsRed signal increased with increasing treatment time up to 5 hours (Figure 15B). Parkin was cytosolically distributed following 24 hours of treatment, however this was accompanied by an almost complete loss of MtDsRed signal suggesting that substantial mitochondrial degradation had already occurred (Figure 15A and C). On the other hand, Parkin recruitment to depolarised mitochondria was completely blocked in non-glycolytic astrocytes throughout the entire 24 hours of valinomycin treatment. Remarkably, there was no sign of any level of mitochondrial degradation in 2DG astrocytes even after 24 hours of valinomycin treatment (Figure 15A and C).

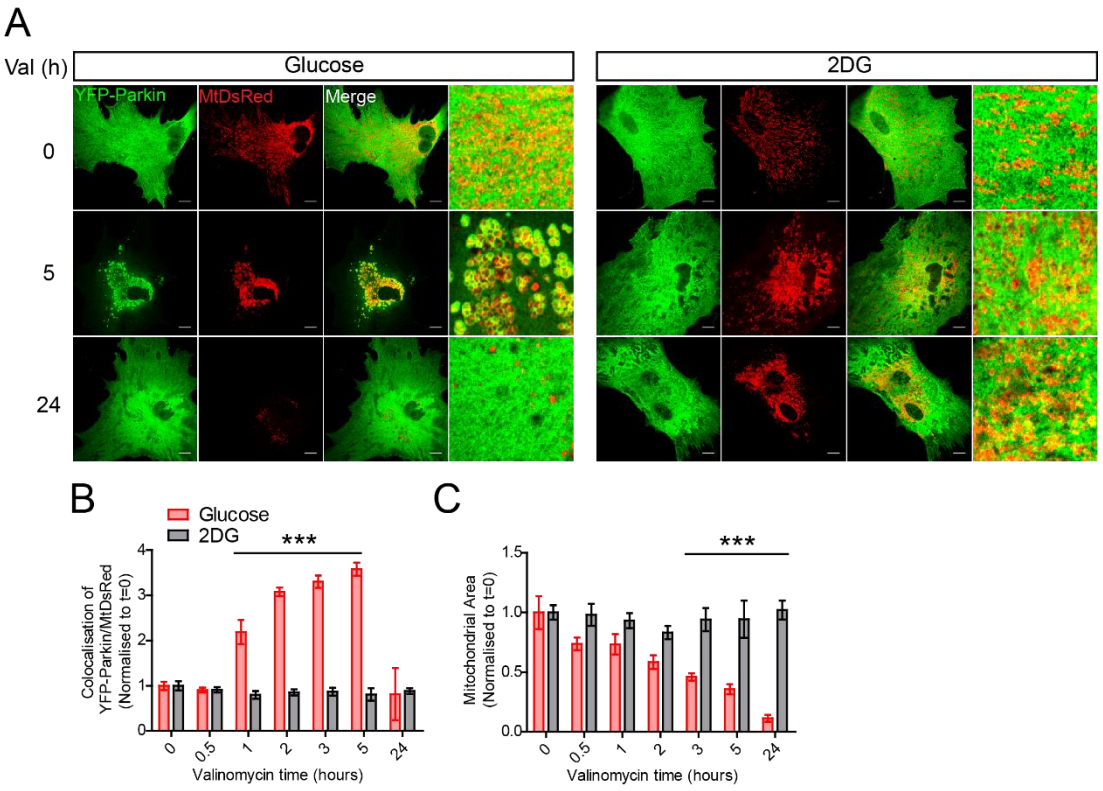

Figure 15: Glycolytic inhibition blocks Parkin recruitment to depolarised mitochondria and mitophagy in astrocytes. A. Representative confocal images of astrocytes cultured in either glucose-containing or 2DG-containing medium. B. Quantification of Parkin recruitment to mitochondria in glucose and 2DG-cultured astrocytes following 1µM valinomycin treatment (Normalised to 0h timepoint) (two-way ANOVA, n≥12 cells all conditions over 3 different preparations). C. Quantification of mitochondrial occupancy (Area of MtDsRed) in glucose and 2DG-cultured astrocytes following 1µM valinomycin treatment (Normalised to 0h timepoint) (two-way ANOVA, n≥12 cells all conditions over 3 different preparations). Error bars represent s.e.m. Significance: ***p<0.001.

Alongside the Parkin recruitment experiment, lysates were produced from valinomycin-treated glucose- and 2DG-cultured astrocytes for western analysis (Figure 16). Once again, there was an absence of any mitophagy signals in the non-glycolytic astrocytes. PINK1 and s65-phospho-ub signal was undetectable and Mfn1 signal was unchanged throughout 24 hours of valinomycin treatment (Figure 16B-D). This was in stark contrast to glucose cultured astrocytes that displayed increasing levels of PINK1 and phospho-ub throughout 24 hours of valinomycin treatment which coincided with rapid ubiquitination and degradation of Mfn1 (Figure 16B-D).

Altogether, this data establishes astrocytes as a principal site of mitochondrial turnover in the CNS. Furthermore, damage-induced mitophagy was shown to be dependent on glucose metabolism and glycolysis in astrocytes. Consequently, the different bioenergetic/metabolic profile, specifically the increased glycolytic capacity of astrocytes compared to neurons, could underpin the different rates of mitophagy between the two cell types. Therefore, targeting the mitophagic pathway specifically in astrocytes presents an intriguing therapeutic avenue in the treatment of neurodegenerative disease, in particular Parkinson’s Disease.

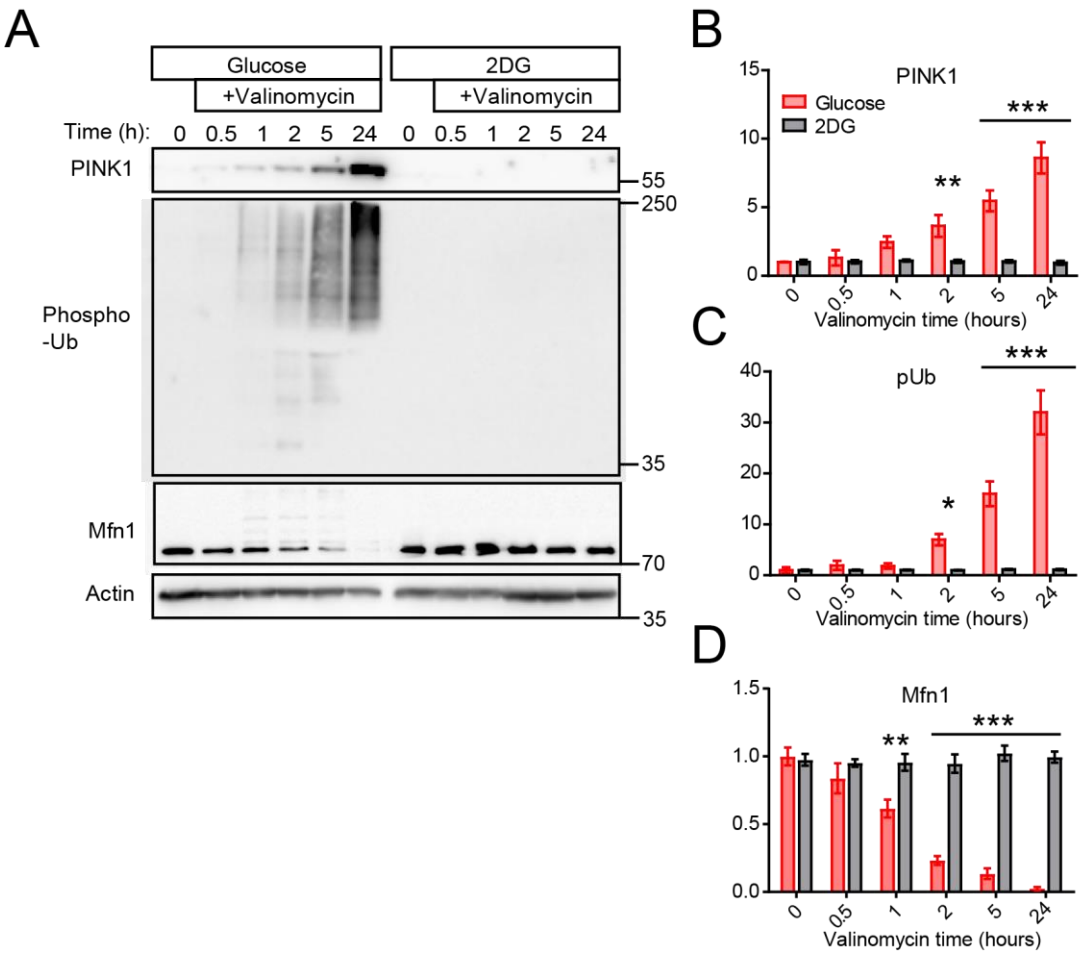

Figure 16: Damage-induced mitophagy in pure astrocyte cultures is dependent on glycolysis. A. Representative western blot images of lysates from glucose and 2DG astrocyte cultures treated with 1µM valinomycin probed with the primary antibodies stated. B. Quantification of PINK1 band intensity (normalised to actin and glucose timepoint 0h) (two-way ANOVA, n=5 all conditions) C. Quantification of s65-Phospho-Ubiquitin band intensity (normalised to glucose timepoint 0h) (two-way ANOVA, n=5 all conditions) D. Quantification of Mfn1 band intensity (normalised to glucose timepoint 0h) (two-way ANOVA, n=5 all conditions and genotypes). Error bars represent s.e.m. Significance: *p<0.05, **p<0.01 and ***p<0.001.

3.3 Discussion

Maintaining mitochondrial function through quality control methods, including mitophagy, is extremely important for CNS health and function. This is highlighted by mutations in the mitophagy machinery leading to familial forms of Parkinson's Disease. Yet, despite the obvious pathological relevance, previous evidence suggests that neuronal mitophagy occurs less readily than in non-neuronal cell lines (Van Laar et al., 2011, Cai et al., 2012). However, very little is known about the mitophagic process in the other cell types of the brain, including astrocytes, despite the potential pathological implications. Therefore, this chapter examined the spatiotemporal regulation of the PINK1/Parkin mitochondrial quality control pathway in astrocytes and compared that to the same pathway in neurons.

Firstly, optimal conditions were established to depolarise the mitochondrial network in both astrocytes and neurons and allow for robust Parkin translocation and accumulation of S65-phospho-Ub with the use of the mitochondrial uncoupler valinomycin, without causing the significant neuronal death observed with other commonly used inducers of mitophagy such as CCCP/FCCP or antimycin-A. This allowed for the visualisation of the mitophagic process in astrocytes and neurons present within the same culture which was physiologically important as it has previously been shown that both astrocytes and neurons are morphologically and transcriptionally altered when

cultured without the presence of the other cell type (Hasel et al., 2017, Enright et al., 2020).

Intriguingly, PINK1/Parkin-dependent mitophagy was rapidly induced in astrocytes and at a much quicker rate than in neurons following valinomycin-induced damage. This was displayed by the rapid mitochondrial localisation of Parkin and the formation of S65-phospho-Ub clusters in astrocyte-neuron cultures, both of which occurred quicker in astrocytes than in neurons. Importantly, this also correlated with increased mitochondrial clearance in astrocytes at later timepoints and was backed up by western blot data showing increased expression of PINK1 and S65-phospho-Ub alongside rapid ubiquitination and degradation of key mitochondrial Parkin substrates in pure astrocyte cultures following valinomycin treatment. Significantly, these processes were occluded in PINK1^{KO} astrocytes and neurons.

These findings are in agreement with a previous report using primary cultures that shows that ubiquitin is more readily phosphorylated in astrocytes than in neurons following mitochondrial depolarisation (Barodia et al., 2019). However, in that study they find no evidence of mitophagy induction in neurons whereas the data presented here indicates that even though mitophagy induction is delayed in comparison to astrocytes, neuronal mitophagy does occur. This could be due to differences in experimental setup. In the previous study, neurons are cultured without the presence of astrocytes and other glia meaning that they may lack the neurotrophic and metabolic support required

to adequately perform mitophagy; a theory backed up by data presented in this chapter showing that mitophagy readouts are undetectable in pure neuronal cultures by western blot. Notwithstanding, the data presented in this chapter, backed up by previous data, suggests that the rate of PINK1/Parkin-dependent mitophagy is higher in astrocytes than it is in neurons.

On the other hand, it was found that mitochondrial damage-induced remodelling occurred quicker and more readily in neurons compared to astrocytes. This was shown by the rapid decrease in mitochondrial diameter and rounding of neuronal mitochondria at early valinomycin treatment timepoints. Damage-induced mitochondrial remodelling has been widely reported in non-neuronal cell lines and occurs following the dissipation of mitochondrial membrane potential (Miyazono et al., 2018). It was previously thought that mitochondrial fragmentation is a prerequisite for mitophagy (Twig et al., 2008), yet recent evidence outlines that the fragmentation of mitochondria does not accelerate mitophagy (Yamashita et al., 2016) and the loss of DRP1 actually enhances the recruitment of Parkin to depolarised yet fused mitochondria and increases the rate of mitophagy (Burman et al., 2017). Thus, a new model suggests that instead of promoting mitophagy, damage-induced fragmentation attempts to segregate healthy mitochondrial domains from elimination by PINK1 and Parkin (Burman et al., 2017). Intriguingly, mitochondrial remodelling preceded Parkin translocation in neurons but not in astrocytes. Therefore, this could suggest that neurons prioritise mitochondrial

fragmentation over whole organellar mitophagy to maintain mitochondrial fidelity following insult and only proceed with mitophagy following prolonged damage. This proposed mechanism, that occurs independently to PINK1, could be favoured by neurons in order to prevent an energy deficit following mitochondrial damage as they are heavily reliant on mitochondrial ATP production to meet their energy demands.

Moreover, it was then identified that the spatial regulation of mitophagy differed vastly between astrocytes and neurons. Following valinomycin treatment, s65-phospho-Ub puncta were distributed evenly throughout astrocytes and were even present within the distal processes. In contrast, s65-phospho-Ub signal was restricted mainly to the somatic region in neurons, which backs up previous findings indicating that neuronal mitochondria are retrogradely transported to the soma to facilitate their clearance (Cai et al., 2012, Zheng et al., 2019) . These findings could be the result of altered degradative lysosomal distribution between the two cell types. Whereas neuronal lysosomes are, in the main (Farfel-Becker et al., 2019), restricted to the somatic and proximal dendritic regions (Peters, 1991, Maday et al., 2012, Maday and Holzbaur, 2016, Yap et al., 2018, Cai et al., 2012), degradative lysosomes in astrocytes are distributed uniformly and are present within even the finest of astrocytic processes *in vivo* (Damisah et al., 2020). Thus, this suggests that mitochondria in astrocytes may be able to rapidly undergo mitophagy irrespective of their subcellular localisation whereas neuronal mitochondria have to be

retrogradely transported to the soma prior to the induction of mitophagy to facilitate their clearance; a phenomenon that could, in some part, explain the difference in timescale of mitophagy induction in astrocytes and neurons. However, it was observed that there is also a delay in Parkin recruitment to mitochondria already present within neuronal somas and thus, other mechanisms are likely to be involved.

Accordingly, it was found that damage-induced mitophagy progression is dependent on glucose uptake and glycolytic capacity in astrocytes. Through replacing glucose with 2DG, which inhibits the hexokinase-dependent glucose phosphorylation step of glycolysis, valinomycin-induced Parkin translocation, s65-phospho-Ub formation and mitochondrial clearance was completely inhibited in astrocytes, even after 24 hours of treatment. Astrocytes are extremely metabolically flexible and have a high glycolytic capacity due to contact with vasculature *in vivo*, which provides a rapid source of glucose, and through increased expression of specific glycolytic enzymes including PFKFB3 and HK2 (Herrero-Mendez et al., 2009, Zhang et al., 2014, Zhang et al., 2016). Previous evidence shows that astrocytes metabolically switch from oxidative phoshorylation to glycolysis following insult (cortical stab wound, LPS/IFNγ), which coincides with DRP1-dependent fragmentation of mitochondria (Motori et al., 2013). In fact, although astrocytes display high rates of oxidative phosphorylation, they can function purely glycolytically and mice expressing respiration-deficient astrocytes display no signs of pathology

(Supplie et al., 2017). On the other hand, neuronal glycolysis is limited, and neurons rely heavily on mitochondrial respiration to meet their energy demands. It has previously been shown that Parkin translocation to depolarised mitochondria is dependent on cellular ATP levels and that some level of glycolysis is required to adequately perform mitophagy upon loss of mitochondrial ATP production (Van Laar et al., 2011). Therefore, unlike neurons, it could be that due to their metabolic flexibility, astrocytes are able to meet their energy demands through non-mitochondrial sources following mitochondrial damage and therefore readily and robustly undergo mitophagy. However, it should be noted that replacing glucose with 2DG could also be indirectly impacting mitochondrial oxidative phosphorylation in astrocytes. Glycolysis produces two ATP molecules alongside two pyruvate molecules that help to fuel mitochondrial OXPHOS, yet this is blocked when 2DG is present. Previous evidence shows that 2DG replacement in Z138 cells partially inhibited glycolytic-dependent oxidative phosphorylation on top of blocking glycolysis (Robinson et al., 2012). Thus, going forward it will be important to assess the impact of 2DG replacement on the mitochondrial respiratory capacity of astrocytes.

Intriguingly, recent evidence suggests that neuronal mitochondria can be dynamically transferred to astrocytes to facilitate their clearance. Studies have shown that mitochondria can be released from neurons extracellularly and taken up and internalised by nearby astrocytes (Gao et al., 2019, Davis et al.,

2014, Morales et al., 2020). The internalised neuronal mitochondria can then be degraded by the autophagy-lysosomal system in astrocytes. This has been termed transmitophagy and may be a key process in conferring neuroprotection following neuronal insult. Conversely, healthy mitochondria can be transported back to neurons from astrocytes to support neuronal viability (Hayakawa et al., 2016, English et al., 2020, Gao et al., 2019). Therefore, the findings in this chapter showing that mitophagy occurs quicker, more readily and is less spatially restricted in astrocytes compared to neurons outlines why astrocytes are the perfect candidate for a hub of mitochondrial turnover in the CNS.

Chapter 4 - The role of Miro1 in the mitophagy pathway in astrocytes and neurons

4.1 Introduction

A key target of Parkin-mediated ubiquitination is the Miro (mitochondrial Rho) family of GTPases. In mammals there are two members of the family, Miro1 and Miro2, which contain two GTPase domains flanking two Ca^{2+}-sensing EF-hand motifs and a transmembrane domain that anchors them to the OMM (Fransson et al., 2003). Miro proteins have emerged as critical regulators of neuronal and astrocytic mitochondrial trafficking and distribution (Fransson et al., 2006, Macaskill et al., 2009, Guo et al., 2005, Stephen et al., 2015, Lopez-Domenech et al., 2016) and may also have other important roles for mitochondrial function as components of mitochondria-ER contact sites and as regulators of mitochondrial calcium homeostasis (Kornmann et al., 2011, Lee et al., 2016b, Modi et al., 2019, Niescier et al., 2018). Under mitochondrial damage Miro proteins are rapidly ubiquitinated and degraded by a PINK1/Parkin-dependent mechanism (Birsa et al., 2014, Ordureau et al., 2018, Liu et al., 2012, Wang et al., 2011b). Regulation of the Miro trafficking complex by PINK1 and Parkin may serve to dissociate damaged mitochondria from the microtubule and actin transport pathways (Lopez-Domenech et al., 2018, Wang et al., 2011b), helping to isolate the damaged organelles from the functional mitochondrial network prior to their clearance.

In addition to acting as a Parkin substrate, it has been reported that Miro proteins might directly act as receptors for Parkin on the OMM to facilitate Parkin recruitment and stabilisation on the OMM (Birsa et al., 2014, Safiulina et al., 2019, Shlevkov et al., 2016). Other OMM proteins, namely Mfn2, have previously been identified as Parkin receptors (Chen and Dorn, 2013, Okatsu et al., 2015, Wang et al., 2019a, McLelland et al., 2018). The rapid formation of phospho-ubiquitin chains on Mfn2 acts as a signal to recruit more Parkin to the OMM to accelerate mass mitochondrial ubiquitination (McLelland et al., 2018, Chen and Dorn, 2013, Okatsu et al., 2015) However, whether this is also the case for Miro1 remains to be established.

Furthermore, Miro degradation was shown to be impaired in PD-patient derived fibroblasts (Hsieh et al., 2016) and several Miro1 mutations have been identified as risk factors in patients with PD, further supporting the involvement of Miro1 in the pathogenesis of the disease (Grossmann et al., 2019, Berenguer-Escuder et al., 2019, Grossmann et al., 2020). Despite the emerging role for Miro1 in the regulation of mitophagy and the growing links between Miro1 and human PD pathology, the role of Miro1 in the mitophagic process in the CNS remains poorly understood.

Therefore, by using Miro1 knockout mouse primary astrocyte-neuron cultures, the role of Miro1 in the mitophagic process in astrocytes and neurons will be identified. Furthermore, through the expression of less- and non-ubiquitinable

mutant versions of Miro1, the importance of Miro1 ubiquitination for the progression of mitophagy will be assessed.

4.2 Results

4.2.1 Parkin-dependent mitophagy in astrocytes is not dependent on Miro1.

To establish the role of Miro1 in mitophagy in astrocytes and neurons a global Miro1^{KO} mouse line that exhibits a complete loss of Miro1 expression in embryonic brain lysates was utilised (Figure 1). Miro1^{KO} mice display preweaning lethality with complete penetrance (Smith and Eppig, 2012).

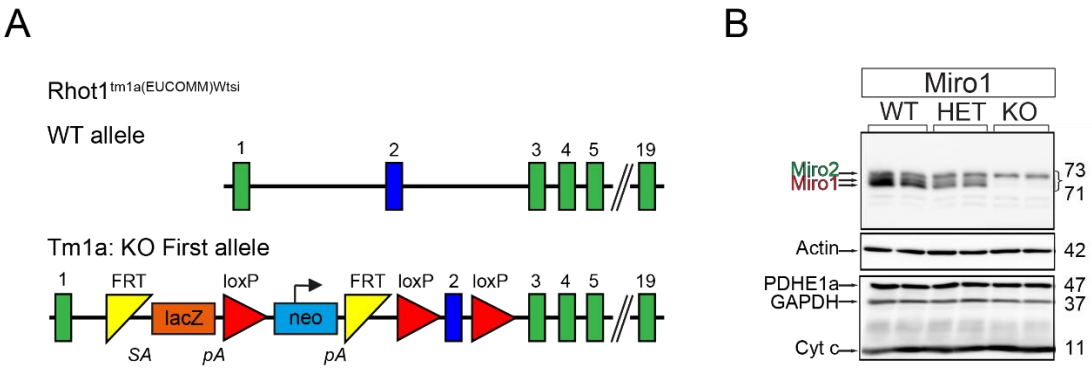

Figure 1: Global Miro1 knockout model. A. Genetic allele map of a WT and Tm1a Miro1 alleles. B. Western blot image of brain lysates taken from a WT and Miro1^{KO} hetero- and homozygote mouse embryos probed with anti-Miro, PDHE1a, GAPDH, cytochrome c and actin antibodies.

Using this mouse line, astrocyte-neuron cultures were generated from E16.5 WT and Miro1^{KO} embryos and transfected with ^{YFP}Parkin and MtDsRed prior to valinomycin treatment, as previously described. Firstly, the role of Miro1 in mitophagy in astrocytes, which display a robust and rapid induction of the mitophagic process following mitochondrial depolarisation, was assessed (Figure 2). Surprisingly, no difference in the rate of Parkin recruitment to depolarised mitochondria was observed between WT and Miro1^{KO} astrocytes (Figure 2A and B). Colocalisation of YFP-Parkin and MtDsRed signal increased with valinomycin treatment time irrespective of the expression of Miro1 (Figure 2B). In addition, there was no change in mitochondrial area at early valinomycin treatment timepoints following the loss of Miro1 in astrocytes suggesting that damage-induced mitochondrial remodelling occurs independently of Miro1 in astrocytes (Figure 2C). Importantly, there was also no difference in the amount of mitochondrial clearance seen after 5 hours of valinomycin treatment in WT and Miro1^{KO} astrocytes indicating that the mitophagic process in astrocytes is not Miro1-dependent (Figure 2C).

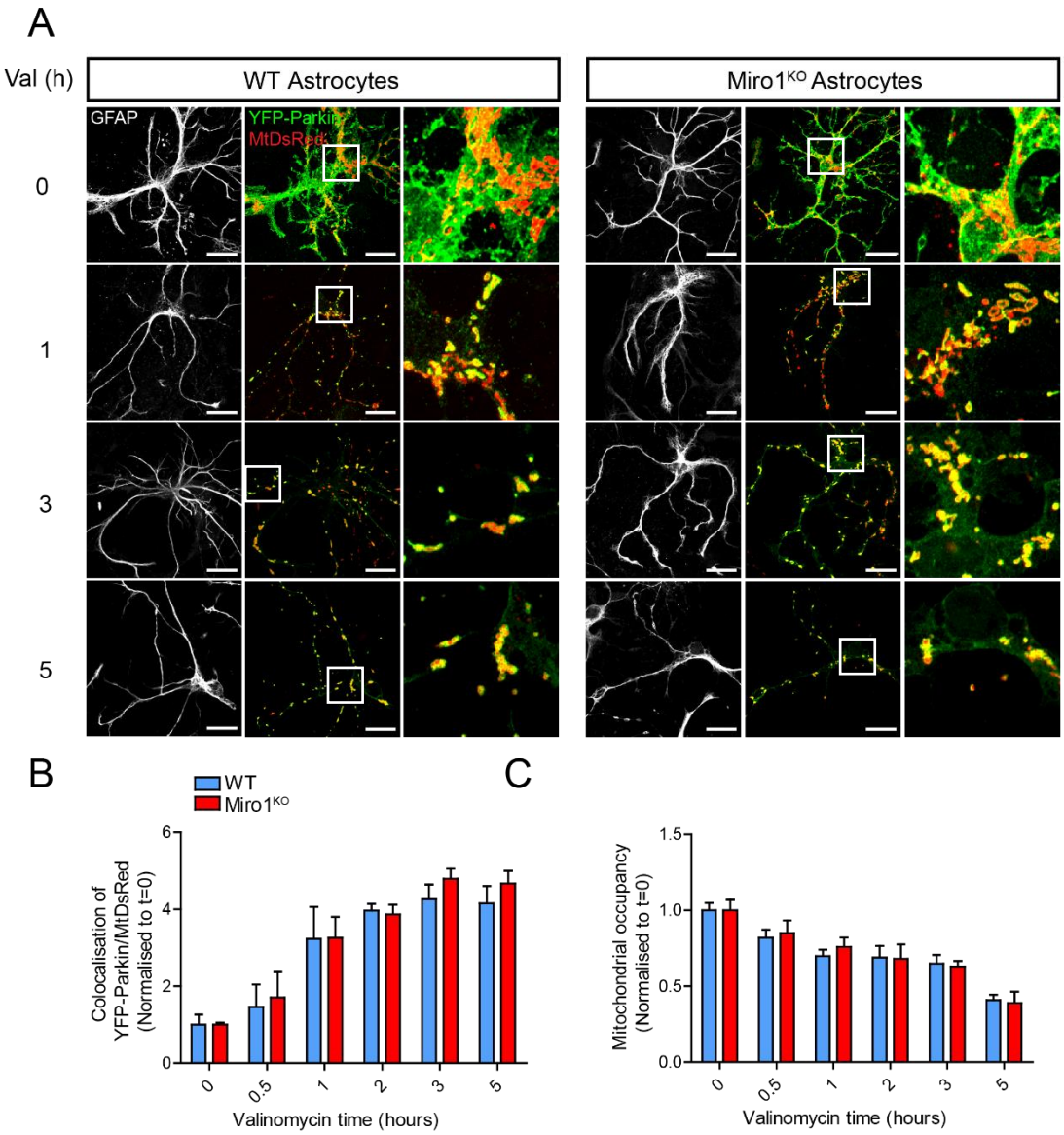

Figure 2: Parkin translocation to depolarised mitochondria in astrocytes is unaffected by the loss of Miro1. A. Representative confocal images of WT and Miro1^{KO} GFAP-positive astrocytes present in astrocyte-neuron mixed cultures expressing YFP-Parkin and MtDsRed treated with 1µM valinomycin. (Scale bars = 10µm) B. Quantification of Parkin recruitment to mitochondria (Integrated YFP-Parkin signal overlapping MtDsRed signal normalised to t=0) in WT and Miro1^{KO} astrocytes following 1µM valinomycin treatment (two-way ANOVA, n≥15 cells all conditions over 4 different preparations). D. Quantification of mitochondrial occupancy (Area of MtDsRed signal in GFAP area of cell) in WT and Miro1^{KO} astrocytes following 1µM valinomycin treatment (two-way ANOVA, n≥15 cells all conditions over 4 different preparations). Error bars represent s.e.m.

4.2.2 Mitophagy in astrocytes occurs independently of Miro1 under endogenous conditions.

Following this, to validate the findings in Parkin-overexpressing astrocytes, western analysis of astrocyte lysates expressing endogenous levels of Parkin was performed (Figure 3). Therefore, pure astrocyte cultures were generated from WT and Miro1^{KO} embryos and treated with valinomycin, as previously described, prior to lysis and western blot. The samples were probed with antibodies specific to Miro1, alongside s65-phospho-Ub and Mfn1 as specific readouts of PINK1/Parkin-dependent mitophagy (Figure 3A). Importantly, the loss of Miro1 expression was confirmed with a complete loss of Miro1 immunoreactivity in Miro1^{KO} astrocytes (Figure 3B). Once again, no significant differences in mitophagy readouts between WT and Miro1^{KO} astrocytes were observed (Figure 3C and D). S65-phospho-ubiquitin signal appeared following valinomycin treatment and the levels increased with treatment time in both WT and Miro1^{KO} astrocytes (Figure 3C). Accordingly, Mfn1 was rapidly ubiquitinated and later degraded following valinomycin treatment in astrocytes irrespective of Miro1 expression (Figure 3D). Therefore, taken together, these findings indicate that PINK1/Parkin-mediated mitophagy in astrocytes is not dependent on Miro1 expression.

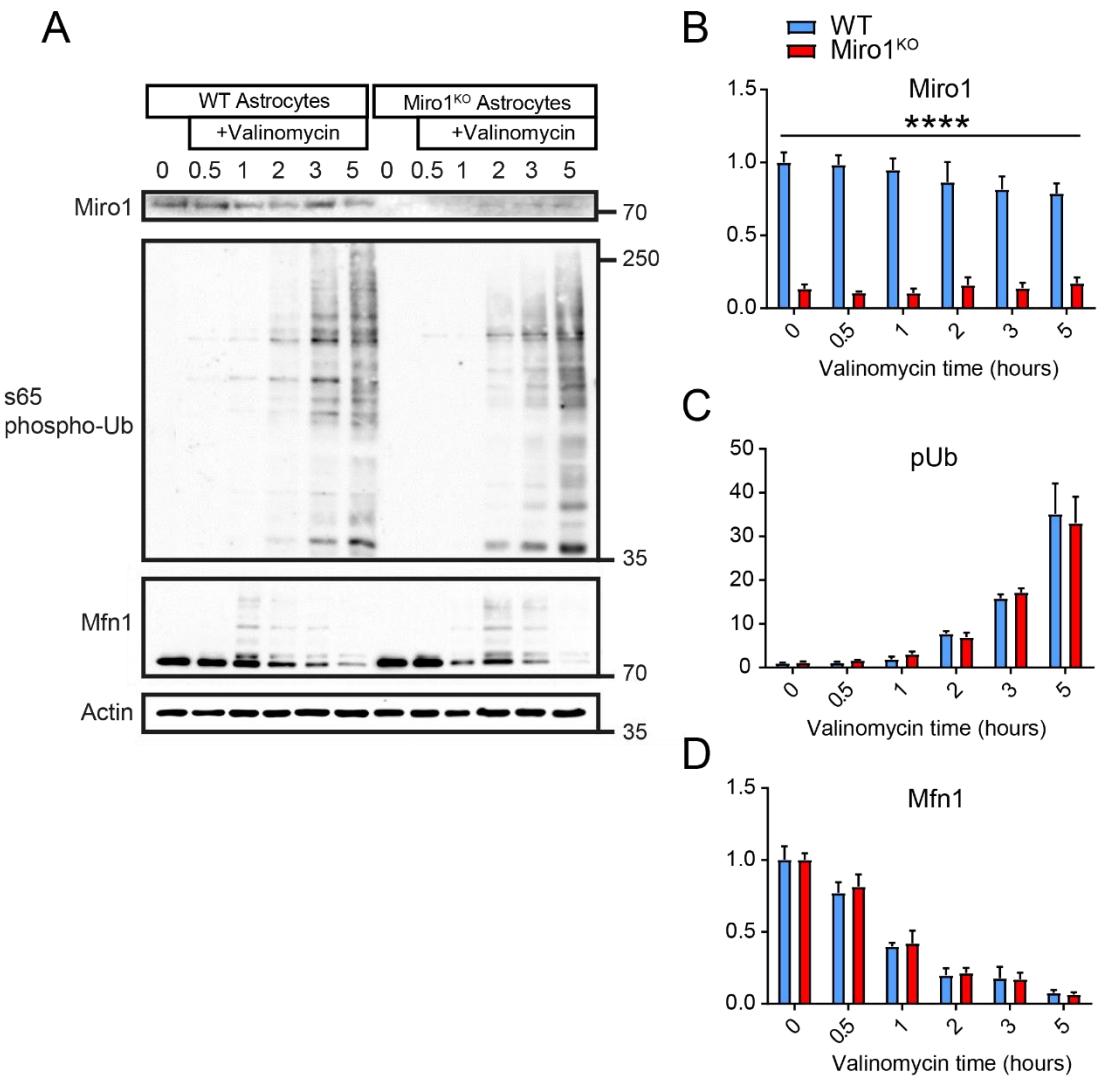

Figure 3: Western blot mitophagy readouts are unchanged in Miro1^{KO} astrocytes. A. Representative western blot images of lysates from WT and Miro1^{KO} astrocyte cultures treated with 1µM valinomycin probed with the primary antibodies stated. B. Quantification of Miro1 band intensity (normalised to actin and WT timepoint 0h) (two-way ANOVA, n=4 all conditions and genotypes) C. Quantification of s65-phospho-ubiquitin band intensity (normalised to WT timepoint 0h) (two-way ANOVA, n=4 all conditions and genotypes) D. Quantification of Mfn1 band intensity (normalised to WT timepoint 0h) (two-way ANOVA, n=4 all conditions and genotypes). Error bars represent s.e.m. Significance: ****p<0.0001.

4.2.3 Miro1 is critically important to recruit Parkin to mitochondria to trigger mitophagy in neurons.

As clear differences between the spatiotemporal regulation of mitophagy in astrocytes and neurons had already been established, it was examined if Miro1 played a role in the mitophagic process in neurons. Firstly, the rate of Parkin recruitment to depolarised mitochondria was quantified in ^{YFP}Parkin/MtDsRed-expressing neurons in astrocyte-neuron cultures. Remarkably, unlike in astrocytes, a dramatic delay in Parkin translocation to mitochondria in Miro1^{KO} neurons (Figure 4A and D) compared to WT neurons was observed. This could also be seen by reduced overlap between Parkin and the mitochondrial marker MtDsRed in fluorescent linescans (Figure 4B and C). Moreover, this was accompanied by a reduction in somatic mitochondrial clearance in the absence of Miro1 in neurons. Due to previous observations, changes in mitochondrial area up to 3 hours of valinomycin treatment were defined as mitochondrial remodelling and changes post 3 hours as mitochondrial clearance. Additionally, as it had already been shown that mitophagy in neurons principally takes place proximally, only the somatic mitochondrial signal was used for this analysis. In Miro1^{KO} neurons, mitochondria became fragmented following valinomycin treatment, similarly to those in WT neurons. Yet, there was no further decrease in somatic mitochondrial content in Miro1^{KO} neurons following 3 hours of treatment compared to a 30% reduction in WT neurons indicating that the mitophagic process in neurons is dependent on the presence of Miro1 (Figure 4E and F).

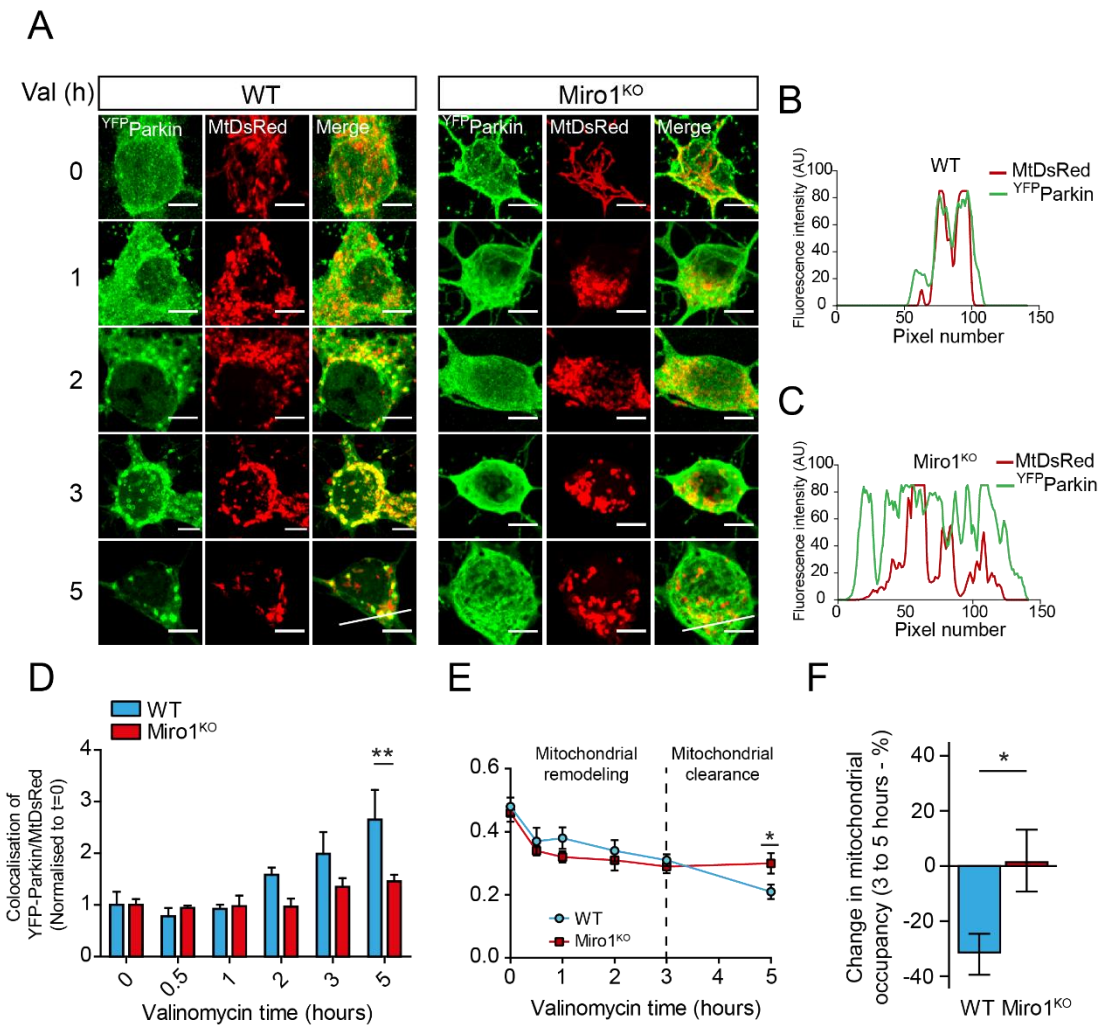

Figure 4: Loss of Miro1 delays Parkin recruitment to depolarised mitochondria in neurons. A. Representative confocal images of the soma of WT and Miro1^{KO} neurons expressing YFP-Parkin and MtDsRed after 1µM valinomycin treatment (Scale bars = 5µM). B-C. Fluorescent linescans of YFP-Parkin and MtDsRed signal in (B) WT and (C) Miro1^{KO} neurons after 5 hours of valinomycin treatment (Lines shown in A). D. Quantification of Parkin recruitment to mitochondria (Integrated YFP-Parkin signal overlapping MtDsred signal normalised to t=0) in WT and Miro1^{KO} neurons following valinomycin treatment (two-way ANOVA, n≥15 cells all conditions). E. Quantification of mitochondrial occupancy (Area of MtDsRed signal in soma / Entire area of soma) in the soma of WT and Miro1^{KO} neurons following valinomycin treatment. F. Percentage change in mitochondrial occupancy in the soma of WT and Miro1^{KO} neurons between 3 and 5 hours of valinomycin treatment (Unpaired t-test). Error bars represent s.e.m. Significance: *p<0.05 and **p<0.01.

4.2.4 Miro1 is critically important to the damage-induced formation of phospho-ubiquitin in neurons.

Next, to validate the delay in Parkin recruitment to neuronal mitochondria in the absence of Miro1, valinomycin-treated WT and Miro1^{KO} neurons were immunostained with antibodies specific to pS65-Ub without exogenous expression of fluorescently tagged Parkin that could alter mitophagy kinetics. The neuronal specificity of phospho-ub signal was established by MAP2 staining. In WT neurons, pS65-Ub appeared in somatodendritic clusters following valinomycin treatment and increased in number with longer treatment time. In contrast, the appearance of pS65-Ub puncta in Miro1^{KO} neurons was severely delayed and pS65-Ub puncta were sparse even after 5 hours of valinomycin treatment. It is worth noting that unlike in PINK1^{KO} neurons, there was not a complete absence of pS65-Ub signal, rather there was significant delay in the formation of pS65-Ub following valinomycin treatment in Miro1^{KO} neurons (Figure 5A and B). Thus, unlike in astrocytes (Figure 5C), Miro1 appears to be critically important for the stabilisation of Parkin on the OMM and for the formation of pS65-Ub chains upon mitochondrial damage in neurons, which are critical steps for damage-induced mitochondrial clearance.

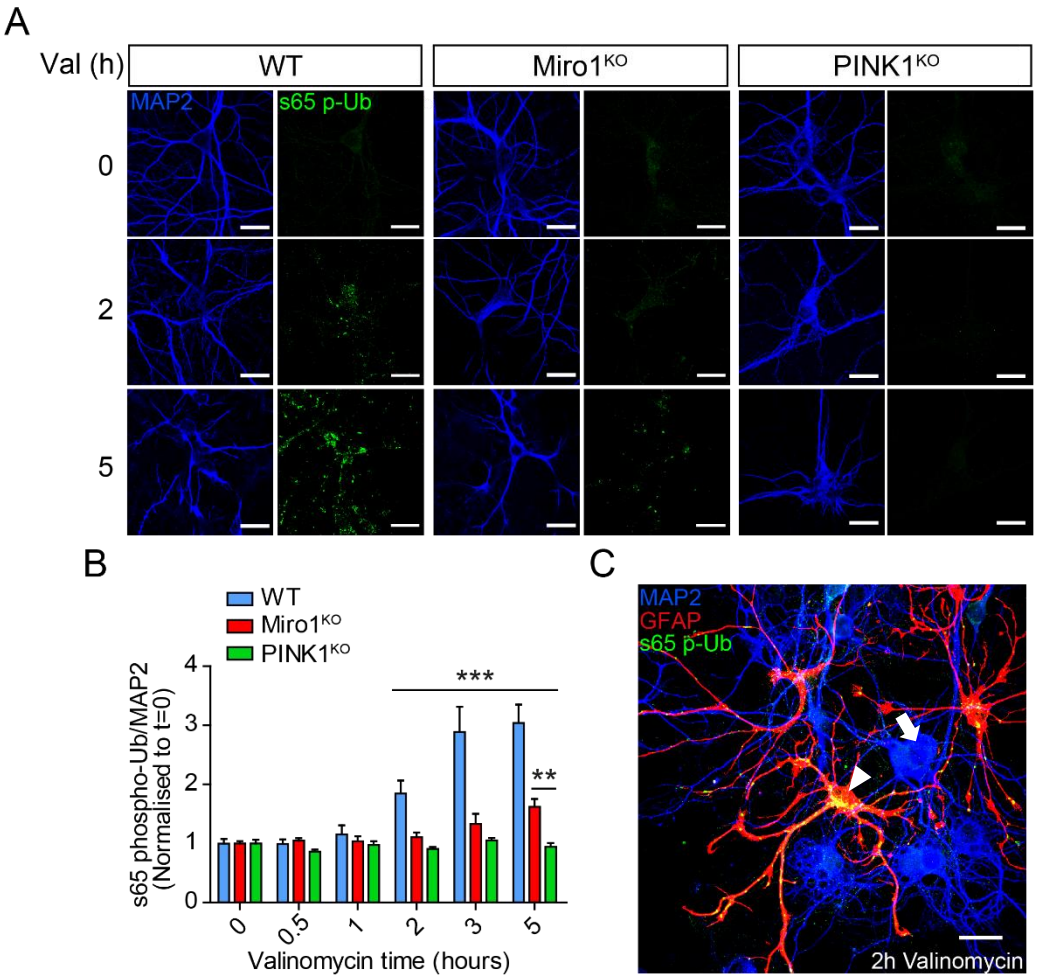

Figure 5: Damage-induced s65-phospho-ubiquitin puncta formation is delayed in Miro1^{KO} neurons. A. Representative confocal images of WT, Miro1^{KO} and PINK1^{KO} neurons immunostained with MAP2 (blue) and s65-phospho-ubiquitin (green) after 1µM valinomycin treatment (Scale bars = 20µm). B. Quantification of s65-phospho-ubiquitin signal intensity within MAP2 signal (normalised to MAP2 area and t=0) in Miro1^{WT}, Miro1^{KO} and PINK1^{KO} neurons following 1µM valinomycin treatment (two-way ANOVA, n= 3, 4 and 3 embryos from WT, Miro1^{KO} and PINK1^{KO} embryos, respectively, 6 ROIs per condition). C. Confocal image of a Miro1^{KO} astrocyte-neuron mixed culture immunostained for GFAP (red), MAP2 (blue) and s65-phospho-ubiquitin (green) after 2h valinomycin treatment. Neuron (arrow), astrocyte (arrowhead). (Scale bars = 10µm) Error bars represent s.e.m. Significance: **p<0.01 and ***p<0.001.

4.2.5 Miro1 is promiscuously ubiquitinated by Parkin.

To further investigate the mechanisms underlying the role of Miro1 in the mitophagic process in neurons, rescue experiments were performed in Miro1^{KO} neurons by expressing human WT or mutant forms of Miro1. Alongside WT Miro1, Miro1 mutants that are less- or non-ubiquitinated by Parkin following mitochondrial damage, Miro1^{5R}, Miro1^{AllR} and Miro1$^{\Delta EF}$ were expressed (Figure 6A). Several lysine residues have been identified as potential sites for Miro1 ubiquitination, both from *in vitro* studies (Kazlauskaite, Kelly et al., 2014) and from unbiased mass spectrometric approaches (Table 4).

	Lysine (Human)	Lysine (Mouse)	Steady State	Mitochondrial Damage	Other
Miro1	**K92**	K105	(Akimov et al., 2018)		
	K107	K120			(Boeing et al., 2016)[a]
	K153	K166	(Wagner et al., 2012, Wagner et al., 2011)	(Sarraf et al., 2013, Kazlauskaite et al., 2014)	
	K182	K195	(Wagner et al., 2012, Akimov et al., 2018)		
	K187	K200	(Udeshi et al., 2013, Wagner et al., 2011, Wagner et al., 2012, Mertins et al., 2013, Akimov et al., 2018)	(Ordureau et al., 2015, Ordureau et al., 2014b, Ordureau et al., 2018)	(Boeing et al., 2016)[a]; (Wu et al., 2015)[b]; (Povlsen et al., 2012)[a]
	K194	K207	(Wagner et al., 2012, Akimov et al., 2018)	(Sarraf et al., 2013)	
	K230	K243	(Akimov et al., 2018)	(Kazlauskaite et al., 2014)	
	K235	K248	(Akimov et al., 2018)	(Kazlauskaite et al., 2014, Sarraf et al., 2013)	
	K249	(K to R)		(Ordureau et al., 2014b)	
	K330	K343	(Akimov et al., 2018)	(Kazlauskaite et al., 2014)	
	K427	K440	(Akimov et al., 2018)		
	K512	K525	(Wagner et al., 2012, Udeshi et al., 2013)	(Ordureau et al., 2018)	
	K535	K548	(Akimov et al., 2018)		
	K572	K585		(Kazlauskaite et al., 2014, Sarraf et al., 2013, Ordureau et al., 2014b, Ordureau et al., 2018)	

Table 4: Lysine residues identified as potential sites for ubiquitination.

Miro1^{5R} contains a compound mutation in which five key potential sites were replaced by arginine. K153, K187 and K572 were chosen because they were identified in several studies as being ubiquitinated upon mitochondrial damage, and K182 and K194 due to their close proximity to K187, likely a

critical ubiquitination target. Miro1^{AllR} is a Miro1 mutant construct in which all lysine residues (except K612 and K616 to avoid mistargeted localisation) were replaced by arginine. Previous work in the lab tested the ability of these constructs to be ubiquitinated by inducing mitochondrial damage in non-neuronal cell lines (Figure 6B). The Miro1^{5R} construct led to a significant (but only partial) decrease in the levels of damage-induced Miro ubiquitination suggesting that multiple lysine residues may serve as substrates for Miro1 ubiquitination. Only by mutating all potential Miro1 ubiquitination sites (Miro1^{AllR}) could the damage-induced ubiquitination of Miro1 be blocked. Therefore, Parkin exhibits significant promiscuity in targeting lysine residues on Miro1 for ubiquitination. Lysine 572 (K572) was previously demonstrated to be a key site for Parkin dependent ubiquitination (Kazlauskaite et al., 2014, Klosowiak et al., 2016, Safiulina et al., 2019). Yet, reintroduction of this residue on the Miro1^{allR} backbone (Miro1^{R572K}) was unable to rescue damage-induced ubiquitination of Miro1. A Miro1 construct with mutations (E208K and E328K) in both EF-hand motifs (Miro1$^{\Delta EF}$), which abolish Ca^{2+} binding and renders Miro1 insensitive to calcium (Fransson et al., 2006) and that was recently shown to be poorly ubiquitinated and unable to recruit Parkin to mitochondria was also included (Safiulina et al., 2019) (Figure 6A).

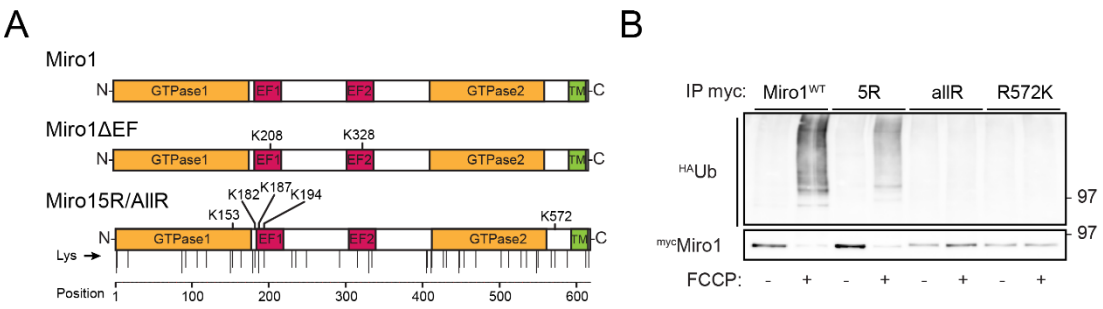

Figure 6: Miro1 ubiquitin mutants. A. Schematic representation of human WT and mutant Miro1 sequences highlighting domains and lysine residues (Lys) in its sequence. Key lysine residues reported to be ubiquitinated upon mitochondrial damage and mutated to generate the $^{myc}Miro1^{5R}$ mutant construct are highlighted. Lines indicate all lysine residues that are mutated in the $^{myc}Miro1^{AllR}$ mutant. B. Ubiquitination assay showing that Miro1 lysine mutants have reduced ubiquitination upon FCCP treatment (1h, 10 µM) in ^{Flag}Parkin overexpressing SH-SY5Y cells (Taken from (Lopez-Domenech et al., 2021)).

4.2.6 Expression of Miro1^{5R} but not Miro1^{AllR} rescues mitochondrial distribution in Miro1^{KO} neurons.

Firstly, to identify any confounding variables, it was established whether the introduction of these mutations had any effect on the intrinsic properties of Miro1 to regulate the trafficking and distribution of mitochondria in neurons. To do this the Miro1 constructs described above were expressed alongside GFP and MtDsRed in Miro1^{KO} neurons and mitochondrial sholl analysis was performed (Figure 7). As previously reported, the loss of Miro1 dramatically reduced the distribution of mitochondria in neurons. The defect in distribution was rescued by the expression of WT Miro1 and Miro1^{5R} but not Miro1^{AllR} or Miro1$^{\Delta EF}$ (Figure 7A and B). Miro1 regulates mitochondrial trafficking in a Ca^{2+}-dependent manner through its Ca^{2+}-sensing EF hands, hence why the reintroduction of Miro1$^{\Delta EF}$ does not rescue mitochondrial distribution in the absence of Miro1. In addition, this could also explain why mitochondrial distribution is not rescued upon expression of Miro1^{AllR}. Miro1^{AllR} contains mutations in both EF-hand domains which may affect the Ca^{2+}-sensing properties of Miro1.

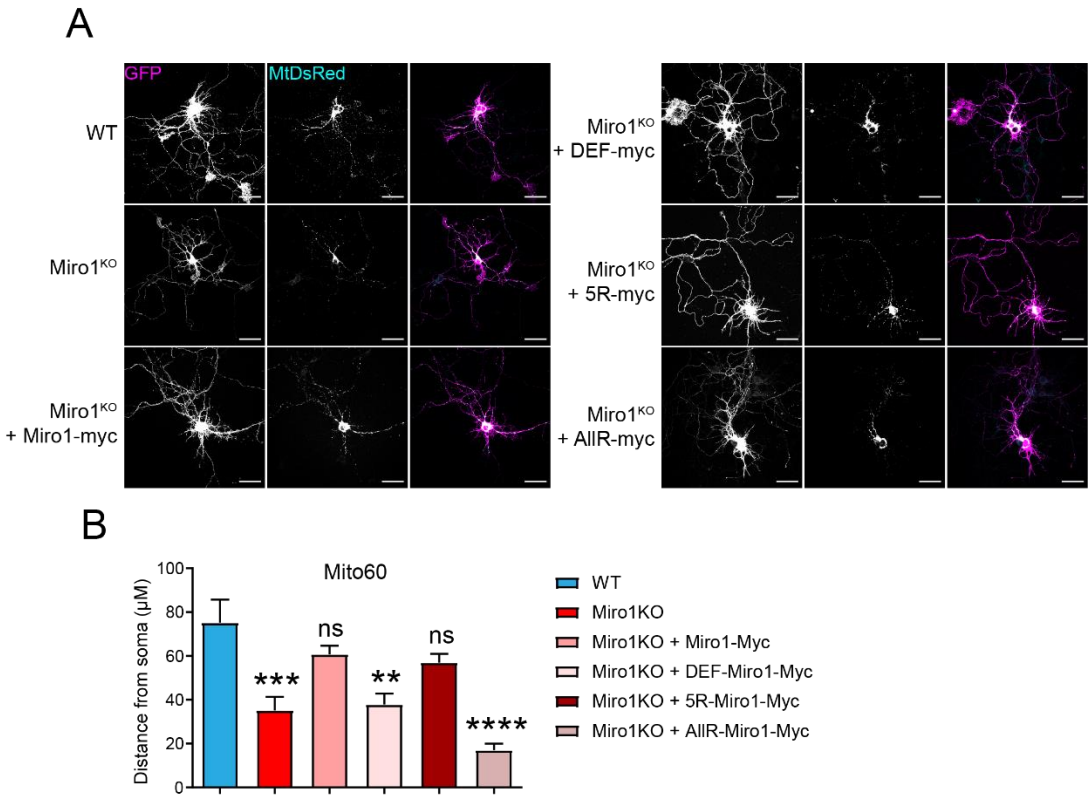

Figure 7: Miro1^{5R} but not Miro1^{AllR} rescues mitochondrial distribution in Miro1^{KO} neurons. A. Representative confocal images of WT and Miro1^{KO} neurons expressing WT and mutant forms of Miro1 alongside GFP (magenta) and MtDsRed (cyan). (Scale bars = 50µm) B. Quantification of mean distance from the soma that 60% of MtDsRed signal is situated (unpaired t test, n≥12 cells over 3 different preparations). Error bars represent s.e.m. Significance: **p<0.01, p<0.001, ****p<0.0001.

4.2.7 Miro1 recruits Parkin to polarised mitochondria in neurons.

Next, it was determined whether expression of any of the Miro1 constructs could rescue the defects in Parkin translocation to depolarised mitochondria in Miro1^{KO} neurons. To do this Miro1^{KO} neurons were transfected with myc-tagged WT Miro1, Miro1^{5R}, Miro1^{AllR} or Miro1 $^{\Delta EF}$ alongside ^{YFP}Parkin and MtDsRed and treated with valinomycin for 2 and 5 hours (Figure 8). Intriguingly, when performing untreated control experiments, it was observed that exogenous expression of WT Miro1 in Miro1^{KO} neurons induced Parkin recruitment to mitochondria even in the absence of valinomycin treatment (Figure 8A and B). In these experiments, Parkin was enriched onto tubular, elongated and reticular mitochondria unlike the rings of Parkin surrounding fragmented mitochondria after valinomycin-induced damage (Figure 8A and B). Similar to WT Miro1, expression of Miro1^{5R} also induced a near to 3-fold enrichment of Parkin onto polarised mitochondria, suggesting that the ubiquitination defect introduced in Miro1^{5R} does not block the ability of Miro1 to bind Parkin on healthy mitochondria (Figure 8B). The Miro1-dependent recruitment of Parkin to polarised mitochondria was recently shown to be dependent on the ability Ca^{2+}-sensing EF hands of Miro1 in non-neuronal cell lines (Safiulina et al., 2019). Accordingly, the expression of Miro1$^{\Delta EF}$ did not induce the translocation of Parkin to polarised mitochondria in neurons (Figure 8B). This was also the case for the expression of Miro1^{AllR}, which again could be the result of mutations in the EF-hand domains.

4.2.8 Parkin recruitment to depolarised mitochondria in neurons is dependent on Miro1 ubiquitination.

During valinomycin treatment, only expression of WT Miro1, but not Miro1^{5R}, in Miro1^{KO} neurons significantly increased Parkin translocation to mitochondria after 2 and 5 hours (Figure 8A and C) indicating that the correct ubiquitination of Miro1 is critical to efficiently recruit Parkin to depolarised mitochondria in neurons. Interestingly, it was also observed that the expression of Miro1^{AllR} delayed the damage-induced translocation of Parkin to a greater extent than the absence of Miro1 after 5 hours of valinomycin treatment, suggesting that Miro1 not only acts as a receptor for Parkin translocation but may interfere with the normal progression of mitophagy by additional means when not ubiquitinated, effectively blocking Parkin translocation (Figure 8A and C). Thus, Miro1 can bind and enrich Parkin on mitochondria in the absence of mitochondrial damage and independently of the activation of the mitophagic process in neurons, while during mitophagy activation, the ubiquitination of Miro1 is paramount for the enrichment of Parkin onto depolarised mitochondria (Figure 8). Therefore, the presence of Miro1 and its correct ubiquitination appear to be equally important for ensuring the recruitment and stabilisation of Parkin on the mitochondrial membrane during mitochondrial damage in neurons.

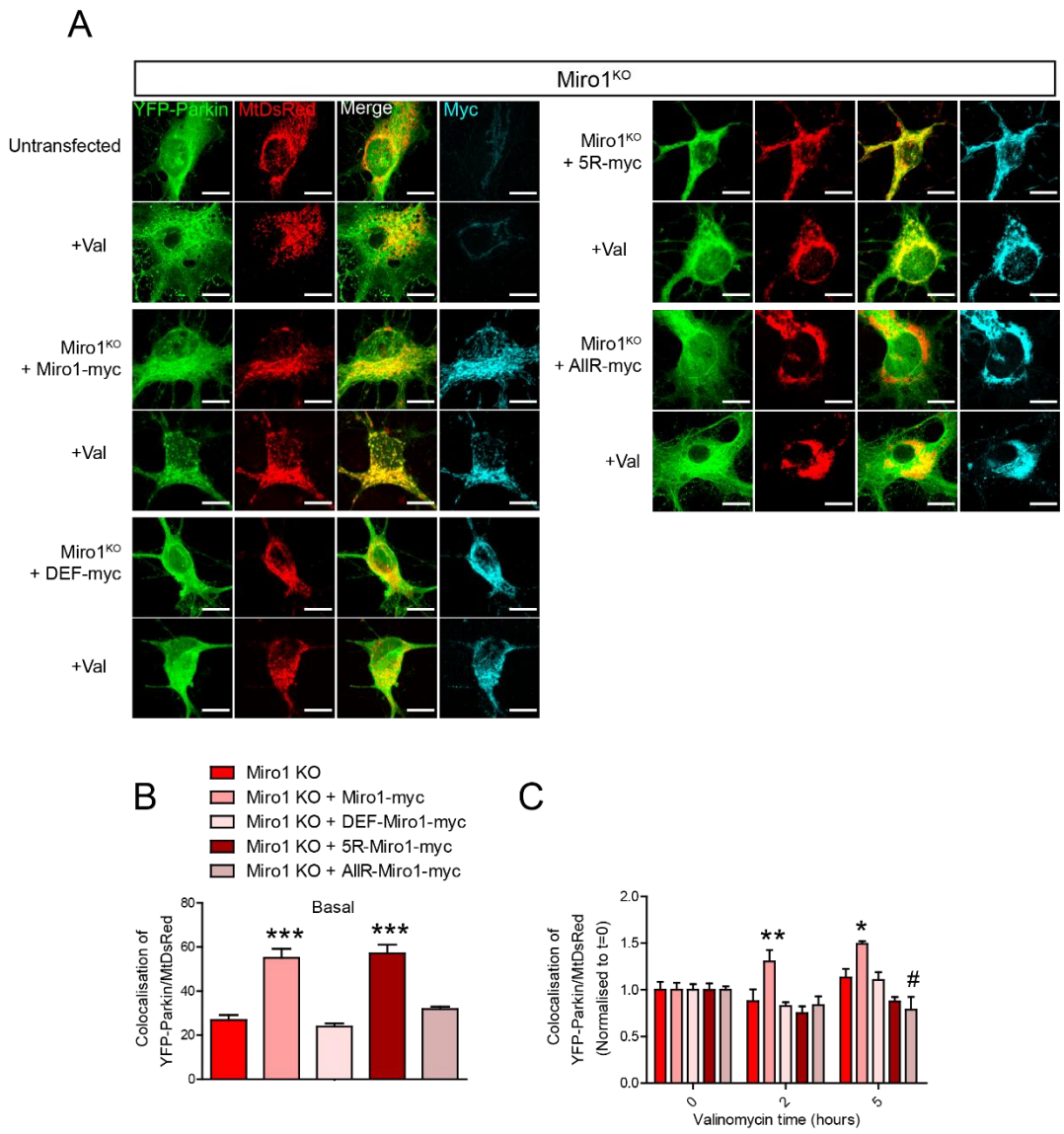

Figure 8: Exogenous expression of Miro1 recruits Parkin to polarised mitochondria and Miro1 ubiquitination is required for damage-induced Parkin recruitment in neurons. A. Representative confocal images of the soma of Miro1^{KO} neurons expressing Miro1^{WT} and mutant forms of Miro1, ^{YFP}Parkin and MtDsRed with and without 5h valinomycin treatment (Scale bars=10µm). B. Quantification of Parkin colocalization with MtDsRed (^{YFP}Parkin signal overlapping MtDsRed signal – intensity-adjusted) in the soma of WT and Miro1^{KO} neurons without valinomycin treatment (one-way ANOVA, n≥12 cells all conditions per genotype over 3 different preparations). C. Quantification of Parkin recruitment to mitochondria (Normalised to t=0) in WT and Miro1^{KO} neurons following valinomycin treatment (two-way ANOVA, n≥12 cells all conditions per genotype over 3 preparations). Error bars represent s.e.m. Significance: *p<0.05 (increase), #p<0.05 (decrease), **p<0.01 and ***p<0.001.

4.2.9 Overexpression of Miro1 recruits Parkin to polarised mitochondria in the absence of PINK1 but does not compensate for the loss of PINK1 in damage-induced mitophagy in neurons.

To establish whether Miro1-dependent Parkin recruitment to polarised and depolarised mitochondria is dependent on PINK1, WT and mutant forms of Miro1 were expressed in ^{YFP}Parkin/MtDsRed-expressing PINK1^{KO} neurons and treated with valinomycin for 2 and 5 hours, as previously described. Importantly, it was found that Parkin recruitment to polarised mitochondria was not dependent on PINK1 as both Miro1^{WT} and Miro1^{5R} were still able to recruit Parkin to polarised mitochondria in PINK1^{KO} neurons (Figure 9A and B), indicating that Parkin recruitment by overexpression of Miro1 occurs independently to PINK1 stabilisation, Parkin's activation and the induction of mitophagy. However, following valinomycin treatment, any further recruitment of Parkin to mitochondria was occluded in PINK1^{KO} neurons overexpressing either WT or mutant forms of Miro1 (Figure 9A and C). This indicates that under mitochondrial damage, Parkin recruitment by Miro1 is dependent on PINK1 stabilisation, the activation of mitophagy and requires Miro1 to be ubiquitinated (Figure 8 and 9).

Altogether, our findings provide new insights into the requirement of Miro1 for mitophagy following mitochondrial damage in astrocytes and neurons. This data identifies a redundancy in the requirement of Miro1 for the mitophagic process in astrocytes yet highlight its importance for neuronal mitophagy. It is

shown that neuronal expression of Miro1 is capable recruiting Parkin in the absence of mitochondrial damage and that the correct ubiquitination of Miro1 by Parkin is paramount for damage-induced mitophagy in neurons.

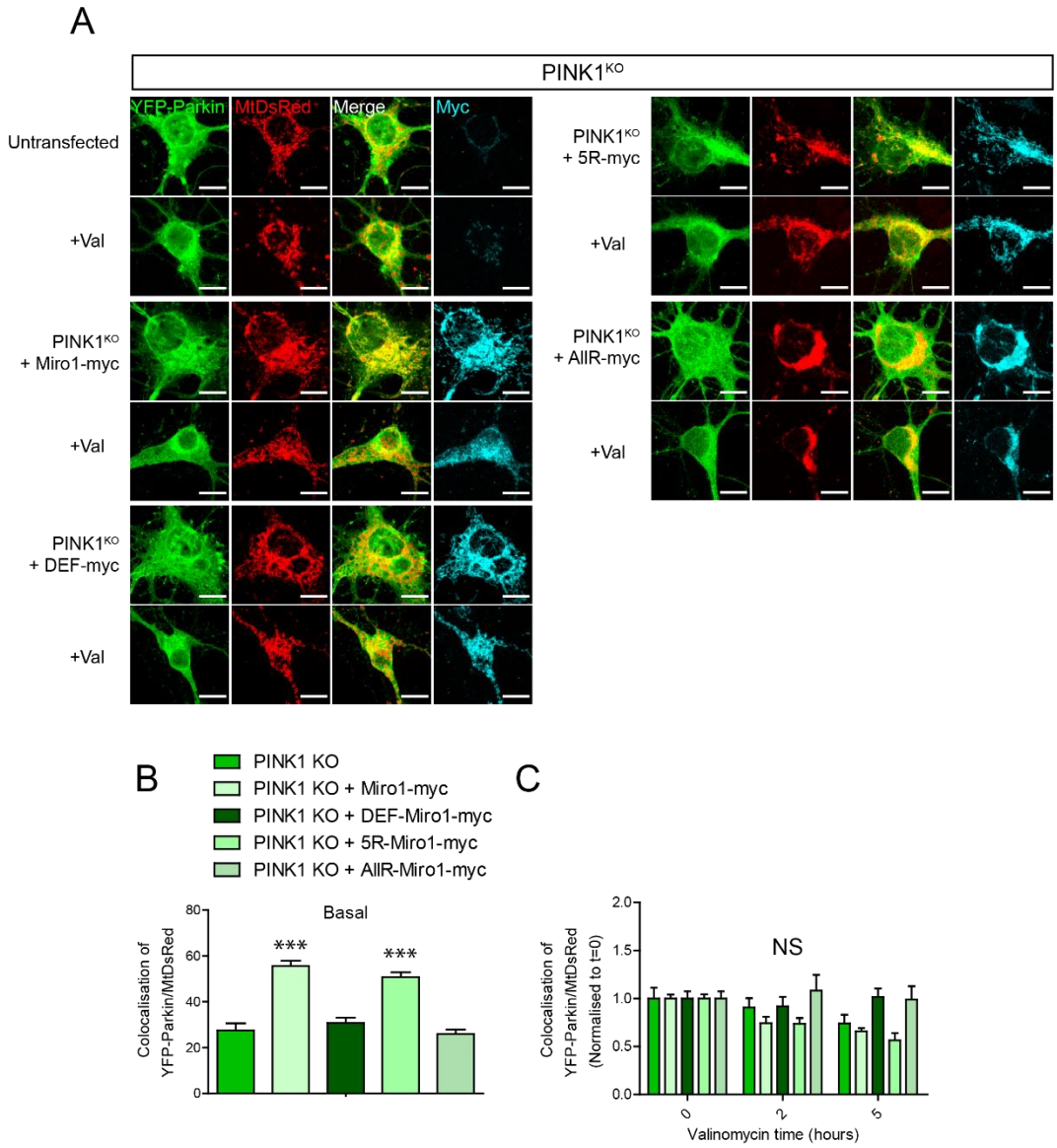

Figure 9: Exogenous expression of Miro1 recruits Parkin to polarised mitochondria in the absence of PINK1 but PINK1 is required for damage-induced Parkin recruitment in neurons. A. Representative confocal images of the soma of PINK1^{KO} neurons expressing Miro1^{WT} and mutant forms of Miro1, ^{YFP}Parkin and MtDsRed with and without 5h valinomycin treatment (Scale bars=10µm). B. Quantification of Parkin colocalization with MtDsRed (^{YFP}Parkin signal overlapping MtDsRed signal – intensity-adjusted) in the soma of WT and PINK1^{KO} neurons without valinomycin treatment (one-way ANOVA, n≥12 cells all conditions per genotype over 3 different preparations). C. Quantification of Parkin recruitment to mitochondria (Normalised to t=0) in WT and PINK1^{KO} neurons following valinomycin treatment (two-way ANOVA, n≥12 cells all conditions per genotype over 3 preparations). Error bars represent s.e.m. Significance: ***p<0.001, NS = not significant.

4.3 Discussion

Defects in mitophagy are a key part of the aetiology of neurodegenerative diseases, for example, mutations in PINK1 and Parkin are associated with early onset familial Parkinson's disease (PD). Recently, loss of function mutations in Miro1 have also been identified in PD patients (Grossmann et al., 2019, Berenguer-Escuder et al., 2019, Grossmann et al., 2020) and it has been previously shown that Miro1 promotes the recruitment and stabilisation of Parkin onto depolarised mitochondria (Birsa et al., 2014, Safiulina et al., 2019, Shlevkov et al., 2016). This would suggest that Parkin binding by Miro1, in conjunction with Parkin activation by PINK1 phosphorylation, could act together to stabilize Parkin on the OMM, providing a mechanism to tune Parkin levels on the OMM.

With the use of a knockout mouse model, the role of Miro1 in PINK1/Parkin dependent mitophagy in astrocytes and neurons was investigated. Surprisingly, it was found that the mitophagic process in astrocytes is unaffected by the loss of Miro1. On the other hand, Miro1 was found to be critically important for mitophagy in neurons which further outlines the cell type heterogeneity in the mitophagic pathway in astrocytes and neurons. Miro1^{KO} neurons exhibited dramatically reduced Parkin translocation onto mitochondria compared to wild type neurons and a considerable delay in the appearance of s65-phospho-Ub clusters following damage. This also correlated with reduced mitochondrial clearance at later time points. Thus,

these results, supported by previous proposals in cell lines, demonstrate that Miro1 forms part of a Parkin receptor complex on the OMM, important for tuning Parkin-mediated mitochondrial quality control in neurons.

Disruption of mitochondrial trafficking may also contribute to the defects in mitophagy in Miro1^{KO} neurons. The findings in the previous chapter and the work of others have shown that neuronal mitophagy is, in the main, restricted to the somatic region (Cai et al., 2012, Zheng et al., 2019, Evans and Holzbaur, 2020). In agreement with this, it has been shown that neuronal mitophagy relies on axonal retrograde transport of mitochondria to the soma prior to degradation following mitochondrial damage (Zheng et al., 2019). It is likely that Miro1 is involved in this process as the loss of Miro1 in neurons reduces axonal retrograde transport of mitochondria (Nguyen et al., 2014). Although it has been shown that mitochondria can undergo mitophagy in the distal axon following localised damage (Ashrafi et al., 2014), inhibition of mitochondrial motility post-damage, by overexpression of the mitochondrial anchor, SNPH, completely blocks the clearance of mitochondria (Zheng et al., 2019). Thus, Miro1's role in neuronal mitophagy may be particularly important as it could link retrograde mitochondrial trafficking to Parkin-mediated clearance of mitochondria in neuronal somas.

This could also serve to explain why the loss of Miro1 does not affect mitophagy rates in astrocytes. Data presented in the previous chapter has shown that mitophagy is not spatially restricted in astrocytes and thus,

astrocytic mitochondria may be less reliant on Miro1-dependent retrograde trafficking to facilitate their clearance. On top of this, although transcriptomic studies suggest that Miro1 gene expression levels are similar between neurons and astrocytes (Zhang et al., 2014, Zhang et al., 2016), a recent proteomic study using the MitoTag mouse line, which enables mitochondrial profiling *in vivo*, indicates that astrocytic mitochondria express relatively low amounts of Miro1 compared to neuronal mitochondria in the cerebellum (Fecher et al., 2019). Consequently, this could explain the redundancy of Miro1 for astrocytic mitophagy and may suggest the presence of distinct mitochondrial Parkin receptors in astrocytes.

Moreover, rescue experiments outline that the damage-induced Parkin recruitment to mitochondria and progression of mitophagy in neurons is dependent on the ubiquitination of Miro1. These findings indicate that Miro1 ubiquitination may directly act as a rapid signal on the OMM for the mitophagic process in neurons. It has been suggested that the rapid ubiquitination of certain Parkin substrates can facilitate the release of dysfunctional mitochondria from the ER in a p97-dependent manner which acts as a gating mechanism to allow widespread Parkin ubiquitination of other mitochondrial substrates and facilitate the progression of mitophagy (McLelland et al., 2018). In support of this view, neuronal expression of PTPIP51, an ER/Mitochondrial anchoring protein, results in the suppression of Parkin-mediated mitophagy, highlighting the role of the Mitochondria-ER contact sites (MERCS) in the

regulation of mitophagy progression in neurons (Puri et al., 2019). Recently, it has been shown that Miro1 is present at MERCS (Modi et al., 2019) and alongside Mfn2, is one of two mitochondrial targets of p97 (Ordureau et al., 2020). Thus, it could be that the ubiquitination and subsequent degradation of Miro1 is required to release damaged mitochondria from the ER to facilitate their clearance in neurons; a process that cannot occur when the non-ubiquitinable form of Miro1, Miro1^{AllR}, is present on mitochondria. Intriguingly, defects in damage-induced Miro1 degradation have been identified in cells derived from PD patients and reducing Miro1 levels has been suggested as a potential therapeutic strategy (Hsieh et al., 2016, Hsieh et al., 2019).

Interestingly, when performing the rescue experiments, it was found that Parkin is recruited to polarised mitochondria when Miro1 is exogenously expressed in Miro1^{KO} neurons, consistent with previous findings in non-neuronal cells (Safiulina et al., 2019). As this Parkin recruitment was still observed in the absence of PINK1 (in PINK1^{KO} neurons), this is unlikely to result in degradation of mitochondria as Parkin's E3-ligase activity is dependent on its phosphorylation by PINK1. However, Parkin is not recruited when the Ca^{2+}-insensitive mutant, Miro1$^{\Delta EF}$ is expressed. This is consistent with previous findings in non-neuronal cells (Safiulina et al., 2019) and suggests Miro1, through its EF-hand domains, interacts with a small pool of Parkin at the OMM prior to damage, priming neuronal mitochondria for mitophagy. Further Parkin can then be recruited upon damage-induced

stabilisation of PINK1 on the OMM and ubiquitination of Miro1, thus facilitating mass-ubiquitination of Parkin substrates and the clearance of neuronal mitochondria.

Chapter 5 – The role of Miro1 in the regulation of neuronal mitochondrial homeostasis *in vivo*

5.1 Introduction

Although embryonic cultures provide a powerful and amenable system to investigate the mitophagy pathway in neurons they are unable to develop over the extended timescales that are associated with neurodegenerative disease. Inadequate mitophagy can lead to neuronal death through bioenergetic deficiencies, imbalanced intracellular Ca^{2+} homeostasis and oxidative stress as a result of mitochondrial dysfunction and the accumulation of mtDNA mutations that build up over time (Lin and Beal, 2006).

In addition, long term mitophagic dysfunction *in vivo* can lead to the age-dependent accumulation of key PINK1/Parkin substrates due to inefficient targeting by the ubiquitin/proteosomal system (Sarraf et al., 2013). This can result in the pathological reconfiguration of the mitochondrial network due to the dysregulation and accumulation of proteins involved in regulating mitochondrial dynamics (Celardo et al., 2016, Yamada et al., 2018). This has previously been observed for the mitochondrial proteins VDAC1, Miro1 and Mfn1/2 in both sporadic and genetic PD postmortem brains and PINK1 and Parkin mutant models (Hsieh et al., 2016, Shaltouki et al., 2018, Hsieh et al., 2019, Celardo et al., 2016). In PINK1 and Parkin mutant drosophila, neurodegeneration is triggered by the upregulation of Mfn (orthologue of

Mfn1/2) which causes the pathological reconfiguration of the mitochondrial network due to an altered balance of the fission/fusion dynamics and disrupted MERCS (Celardo et al., 2016). On the other hand, due to the vast bioenergetic needs of neurons, excessive neuronal mitophagy could also lead to neurodegeneration through bioenergetic deficiencies if degraded mitochondria are not replaced (Doxaki and Palikaras, 2020). Therefore, there needs to be a balance between maintaining mitochondrial health and mitophagy, which is likely the final resort once other mitochondrial quality control mechanisms have failed in neurons.

Thus, to provide an accurate representation of age-dependent mitochondrial dysfunction that is associated with neurodegenerative disease, biochemical postmortem experiments can be performed on tissue acquired from aged animals. However, the loss of Miro1 is lethal perinatally (Lopez-Domenech et al., 2016, Nguyen et al., 2014) meaning that global Miro1^{KO} mice are an unviable model to study progressive neurodegeneration. To bypass the requirement of Miro1 for normal development, a conditional knockout model has previously been developed that exhibits the loss of Miro1 expression exclusively in the principal neurons of the hippocampus and cortex (Miro1^{cKO}) (Lopez-Domenech et al., 2016). Previous work with the Miro1^{cKO} model has shown that the loss of Miro1 in principal neurons leads to progressive dendritic and neuronal degeneration, although how and why degeneration occurs is not entirely clear (Lopez-Domenech et al., 2016).

Therefore, given the defects in mitophagy caused upon loss of Miro1 in neurons *in vitro*, this chapter aimed to identify any signs of aberrant mitochondrial quality control/homeostasis in the brains of Miro1^{cKO} mice *in vivo.* Additionally, by crossing Miro1^{cKO} mice with mice expressing a fluorescent mitochondrial reporter, MitoDendra, the impact of Miro1 loss on neuronal mitochondrial morphology will be explored and any pathological hallmarks will be identified.

5.2 Results

5.2.1 Conditional knockout of Miro1 in forebrain neurons.

The loss of Miro1 is lethal in the late embryonic stage (Lopez-Domenech et al., 2016, Nguyen et al., 2014). Therefore, to bypass the requirement of Miro1 for normal development and study the impact of Miro1 deletion in mitochondrial homeostasis in mature neurons *in vivo* a conditional Miro1 knockout model crossed with a mouse line expressing the Cre recombinase under the control of the CaMKIIα promoter (Miro1^{cKO} from hereon) was utilised (Lopez-Domenech et al., 2016) (Figure 1A and C-F). CaMKIIα is abundantly expressed in the excitatory neurons of the forebrain meaning that Miro1^{cKO} mice exhibit a significant reduction in expression of Miro1 in lysates from the hippocampus and cortex but not the cerebellum (Figure 1D). In addition, to determine the Miro subtype specificity of any effects, the impact of knocking out Miro2 was analyzed, which can also be a substrate for damage-induced Parkin ubiquitination (Mertins et al., 2013, Sarraf et al., 2013, Udeshi et al., 2013). A global Miro2^{KO} mouse model was used as, unlike Miro1^{KO}, Miro2^{KO} mice are viable (Figure 1B and F). Miro2^{KO} mice display no serious signs of pathology, although a slightly decreased body weight has been reported (Smith and Eppig, 2012).

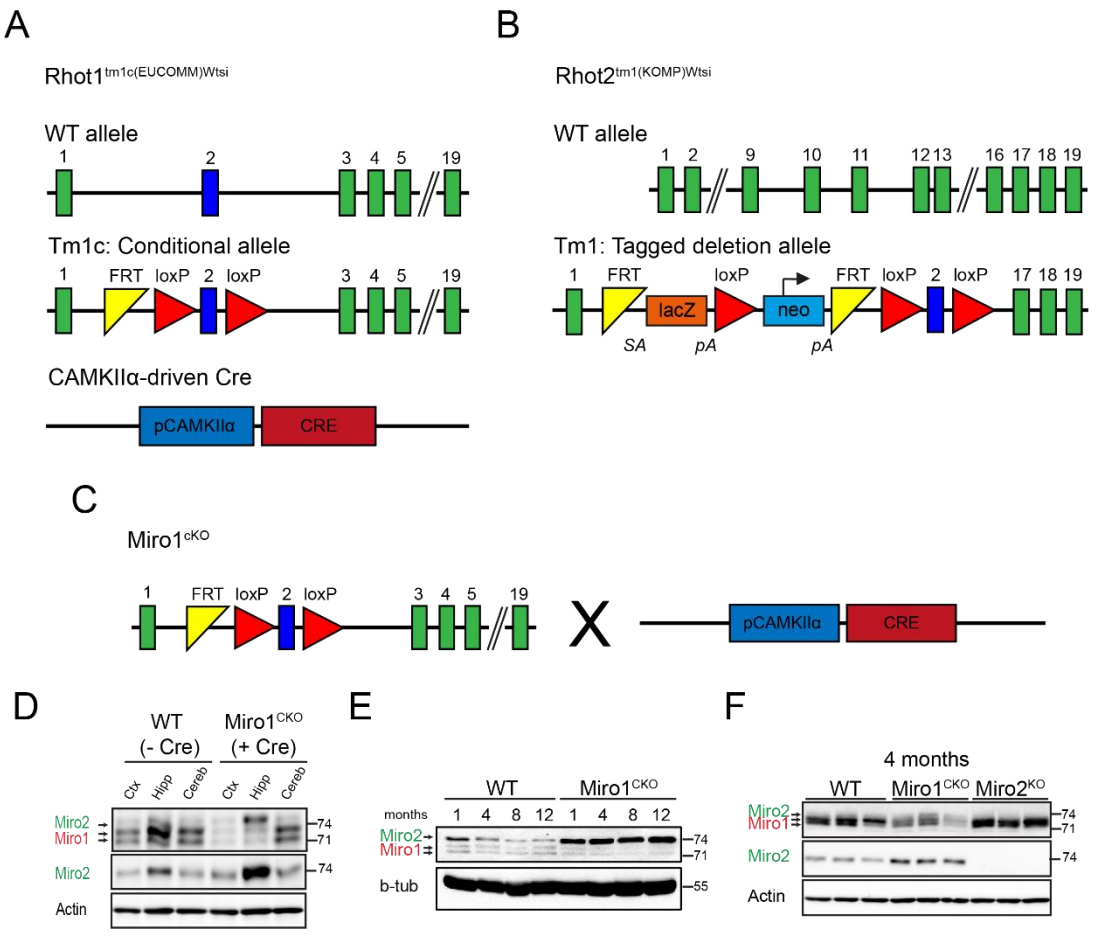

Figure 1: Conditional Miro1 knockout and global Miro2 knockout models A. Genetic allele map of a WT, Tm1c Miro1 and CAMKIIα-driven Cre alleles. B. Genetic allele map of a WT and Tm1 Miro2 alleles. C. Schematic representation of breeding schedule to develop Miro1^{cKO} mice D. Western blot image of cortical, hippocampal and cerebellar lysates taken from 1-month-old WT and Miro1^{cKO} mouse brains probed with anti-Miro, Miro2 and actin antibodies. E. Western blot image of lysates taken from 1, 4, 8 and 12-month-old WT and Miro1^{cKO} mouse brains probed with anti-Miro, β-tubulin antibodies. F. Western blot image of lysates taken from 4-month-old WT Miro1^{cKO} and Miro2^{KO} mouse brains probed with anti-Miro, Miro2 and actin antibodies. D-F taken from (Lopez-Domenech et al., 2016).

5.2.2 Deletion of Miro1 leads to an upregulation of mitofusins and the mitophagic machinery in vivo.

Defects in mitophagy can lead to an age-dependent accumulation of mitochondrial dysfunction due to aberrant mitochondrial homeostasis; a phenomenon that underpins neurodegenerative disease. To investigate whether altered mitophagy induced by the loss of Miro1 affects mitochondrial homeostasis under more physiological conditions *in vivo,* the expression levels of key mitophagy substrates in mouse brain were investigated, where neurons can develop on an extended timescale compared to primary cells. Hippocampal lysates were generated from 4- and 12-month-old WT, Miro1^{cKO} and Miro2^{KO} animals and western analysis was performed with antibodies specific to PINK1, Parkin, Mfn1, Mfn2 and VDAC1 (Figure 2). At 4 months of age, no difference in Parkin and PINK1 levels were observed between WT, Miro1^{cKO} and Miro2^{KO} animals (Figure 2A and B), however, western blot analysis at 12 months of age revealed that there was a significant increase in PINK1 levels and the appearance of an upper band of Parkin, indicative of Parkin auto-ubiquitination (Chaugule et al., 2011, Wauer and Komander, 2013) (Figure 2C and D). This could indicate that Miro1^{cKO} neurons sustain a compensatory over-activation of the mitophagic pathway in an effort to counteract accumulated mitochondrial damage. To further establish differences in neuronal Parkin-dependent mitophagy following the loss of Miro1 *in vivo,* the levels of Mfn1, Mfn2 and VDAC1 - well characterized Parkin substrates - were also probed (Chen and Dorn, 2013, Gegg et al., 2010,

Geisler et al., 2010, Sarraf et al., 2013). Interestingly, at 4 months, an increase in Mfn1 was observed in Miro1^{cKO} in comparison to WT animals, though no increase in VDAC1 and DRP1 was observed (Figure 2A and B). Strikingly, the levels of both Mfn1 and Mfn2 in the Miro1^{cKO} at 12 months were substantially and consistently increased around 2- and 5-fold, respectively, in comparison to WT hippocampal lysates; an effect that was not observed in the Miro2^{KO} mice (Figure 2C and D).

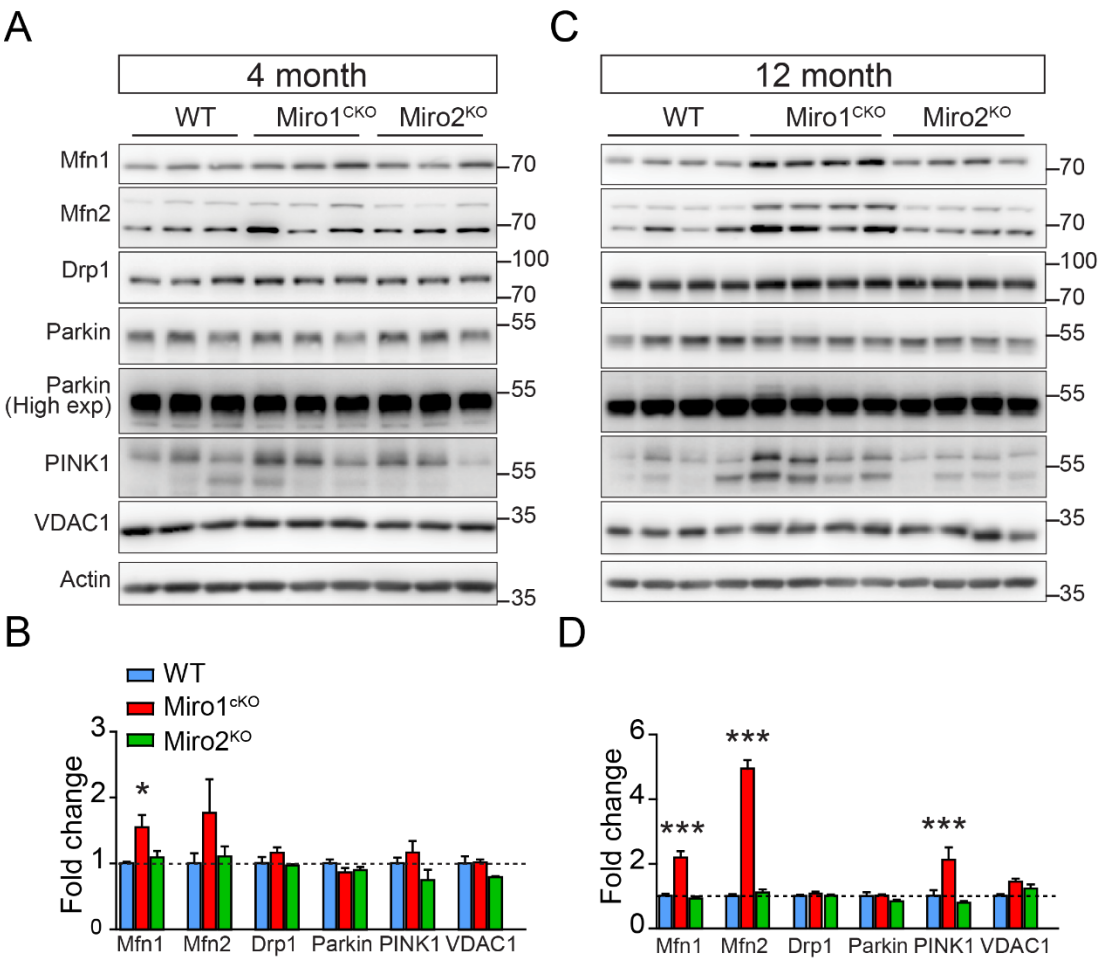

Figure 2: Age-dependent upregulation of mitophagy related proteins in Miro1^{cKO}, but not Miro2^{KO}, hippocampal lysates by western blot. A. Representative blots of 4 months old hippocampal lysates from WT, Miro1^{cKO} and Miro2^{KO} brains probed with the stated antibodies. B. Quantification of protein levels in 4-month lysates (normalised to actin and WT) (unpaired t test, n=3 animals/genotype). C. Representative blots of 12 months old hippocampal lysates from control, Miro1^{cKO} and Miro2^{KO} brains. D. Quantification of protein levels in 12-month lysates (unpaired t test, n=4 animals/genotype). Error bars represent s.e.m. Significance: *p<0.05 and ***p<0.001. Data obtained in collaboration with Christian Covill-Cooke.

5.2.3 The upregulation of mitofusins in Miro1^{cKO} brains is the result of dysfunctional ubiquitination not transcriptional changes.

Next, it was investigated whether the upregulation of the mitofusins was indeed due to aberrant mitochondrial quality control mechanisms and not the result of transcriptional changes following the loss of Miro1. To assess this, first a ubiquitination assay was performed in Miro1^{KO} neurons *in vitro*. Mature neurons (DIV14) cultured from Miro1^{KO} embryos and litter matched WT controls were treated with MG-132, a proteasomal inhibitor, for 4 hours to prevent the clearance of ubiquitinated substrates via the proteasome. Immunoprecipitation of Mfn2 followed by western blotting for ubiquitin revealed that Mfn2 is significantly less ubiquitinated in Miro1^{KO} neurons compared to WT controls (Figure 3A and B). On top of this, Mfn1 and Mfn2 gene expression levels in WT and Miro1^{cKO} brain samples were determined by reverse transcription quantitative PCR (RT-qPCR). Importantly, expression levels of the mitofusins were unchanged between WT and Miro1^{cKO} brains. Thus, the upregulation of Mfn1 and Mfn2 was not due to increased transcription (Figure 3C and D) suggesting that their upregulation is a response to inefficient maintenance by the PINK1/Parkin pathway. Therefore, in summary, *in vivo* disruption of PINK1/Parkin-dependent mitophagy as a result of neuronal Miro1 deletion in leads to an upregulation of the mitofusins in an age-dependent manner.

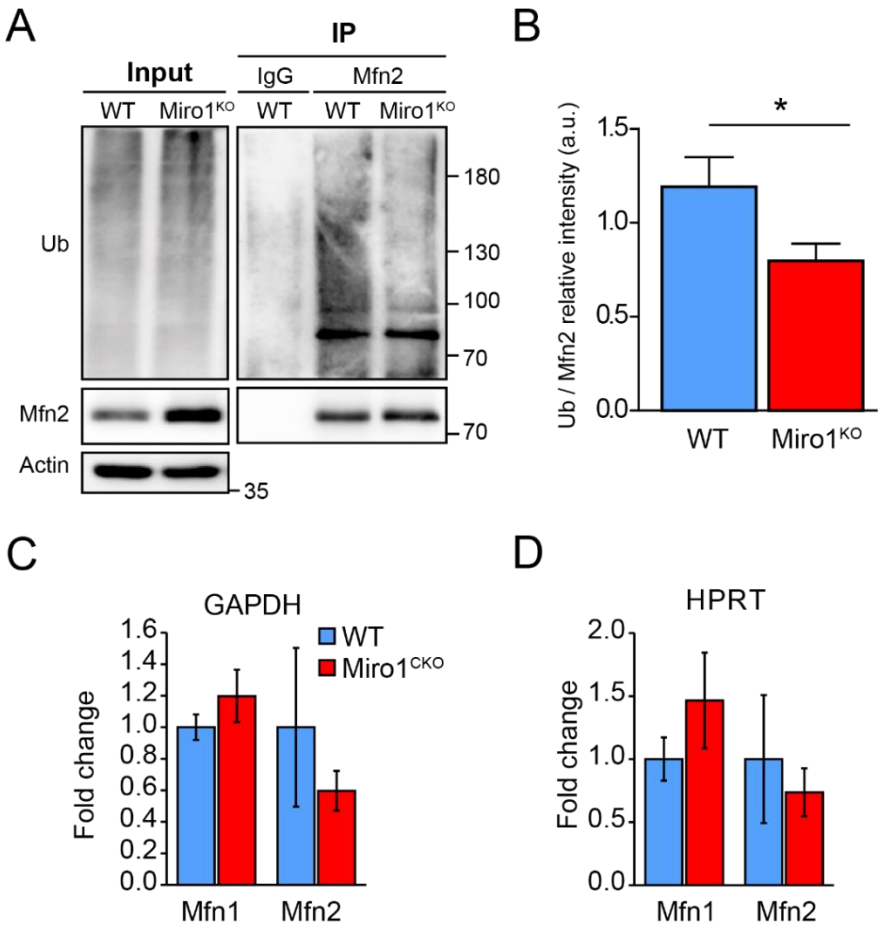

Figure 3: Ubiquitination of Mfn2 is reduced in Miro1^{KO} neurons and Mfn1 and Mfn2 transcription levels are unchanged in Miro1^{cKO} brains. A. Representative western blot images of lysates from WT and Miro1^{KO} cortical neurons immunoprecipitated with an anti-Mfn2 antibody and immunoblotted with the antibodies stated. (D) Quantification of ubiquitin band intensity (60-250 kDa) normalised to Mfn2 band intensity from WT and Miro1^{KO} cortical neurons (unpaired t-test, n=2 WT and n=4 Miro1^{KO} preparations;). C-D. Quantification of Mitofusin1 and Mitofusin2 mRNA levels in 12-month-old WT and Miro1^{cKO} hippocampus using GAPDH (C) or HPRT (D) as housekeeping genes. (unpaired t test, n=4 animals per genotype). Error bars represent s.e.m. Significance: *p<0.05. qPCR performed by William Andrews.

5.2.4 Loss of Miro1 in principal neurons induces the appearance of hyperfused megamitochondria.

The dramatic upregulation in Mfn1 and Mfn2 in Miro1^{cKO} principal neurons suggests a pathological re-configuration of the mitochondrial network due to an altered balance of the fission/fusion dynamics caused by disruption of PINK1/Parkin-mediated mitophagy. To further address this *in vivo* the Miro1^{cKO} mouse was crossed with a mouse line that allows conditional Cre-recombinase-dependent expression of the fluorescent mitochondrial reporter mitoDendra (Figure 4). Crossing the mitoDendra line with Cre recombinase led to robust expression of mitoDendra in CamKIIα-driven Cre expressing cells. This approach allowed visualisation of the mitochondrial network, specifically in principal neurons of cortex and hippocampus from aged animals (Figure 4B).

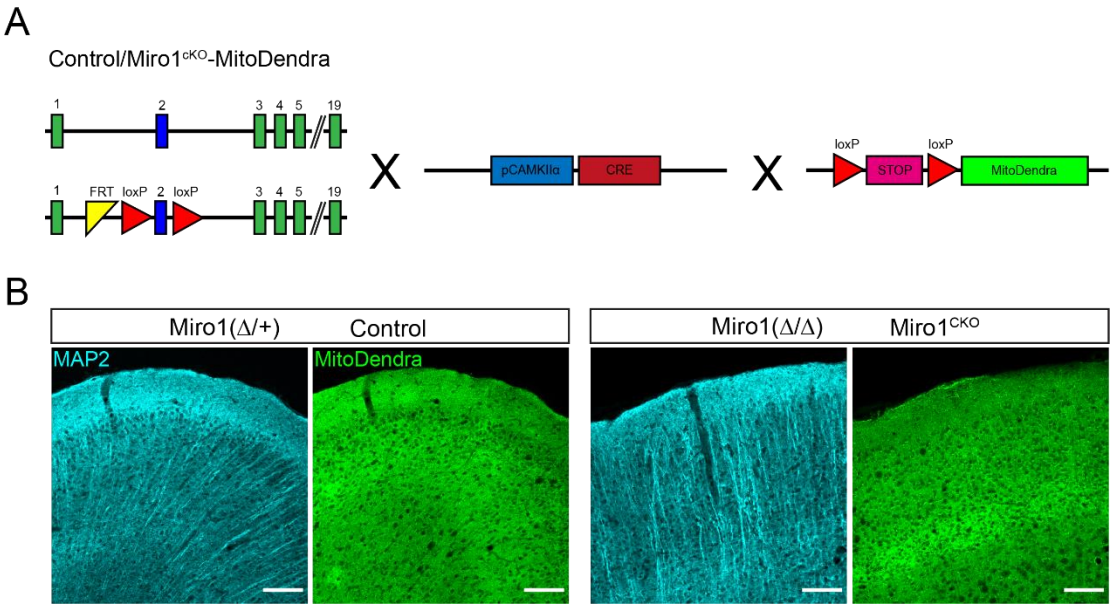

Figure 4: Miro1^{cKO}-MitoDendra model. A. Schematic representation of breeding schedule to develop Control and Miro1^{cKO}-MitoDendra mice. B. Representative confocal images of cortical regions from control and Miro1^{cKO} crossed with MitoDendra animals immunostained with MAP2. (Scale bars = 100µm).

In control mice (heterozygous for the Miro1 conditional allele - Miro1(Δ/+)) mitoDendra labelled mitochondria appeared as an elongated network of various sized mitochondrial elements (Figure 5A). In stark contrast, mitoDendra labelled mitochondria in Miro1^{cKO} cells at 1 year exhibited a dramatic remodelling of somatic mitochondria revealing large mitochondrial units that were absent in cell somas of control neurons (Figure 5A). Importantly, immunostaining with an antibody specific to the OMM protein, Tomm20, confirmed that these units are in fact mitochondria (Figure 5B). The mitochondrial phenotype induced by Miro1 deletion is similar to previous reports of accumulated and hyperfused “megamitochondria” identified in a number of models where either mitochondrial fission / fusion proteins or mitophagy have been altered (Chen et al., 2007, El Fissi et al., 2018, Kageyama et al., 2012, Kageyama et al., 2014, Yamada et al., 2018).

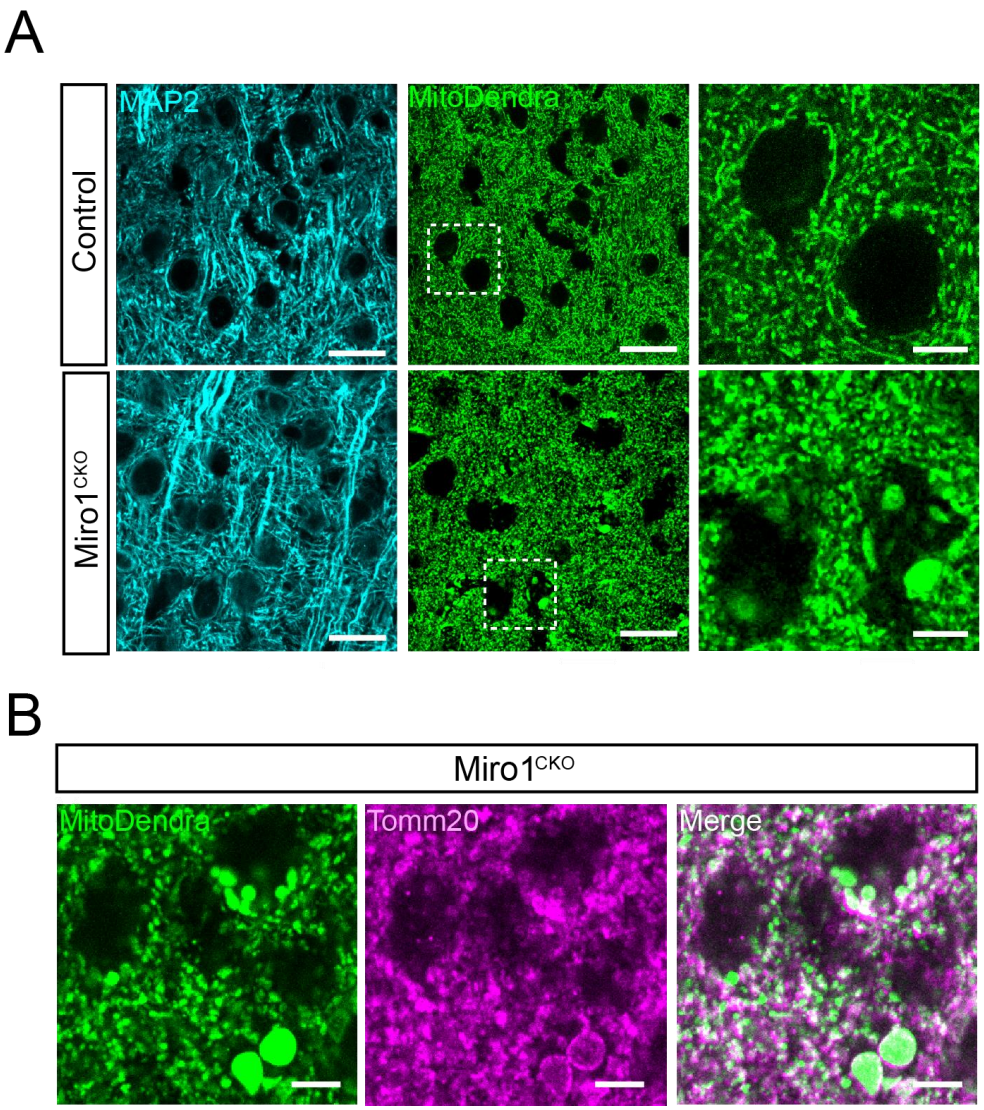

Figure 5: Loss of Miro1 in principal neurons induces the appearance of hyperfused megamitochondria. A. Representative confocal images of cortical regions from control and Miro1^{cKO} crossed with MitoDendra mice immunostained with MAP2 (cyan). (Scale bars = 20µm; Zoom = 5µm) B. Representative confocal images of cortical regions from Miro1^{cKO} crossed with MitoDendra mice immunostained with Tomm20 (magenta). (Scale bars = 5µm). This data is purely qualitative and has not been quantified.

Following this, immunohistochemistry was performed to confirm the upregulation of the mitofusins in Miro1^{cKO} brains in Miro1^{cKO}-MitoDendra neurons (Figure 6). Expression of MitoDendra enabled visualization of only the Cre-expressing cells. Immunostaining of coronal brain slices from 12 months old animals showed a large increase in both Mfn1 and Mfn2 levels on the mitochondria of principal neurons from the Miro1^{cKO} brains when compared to control neurons (Figure 6A-D) with an enrichment of signal on megamitochondria. This confirms that increased mitofusin levels are specific to the Miro1 knockout neurons and are not due to a dysregulation of tissue homeostasis. Taken together, the dysregulation of mitofusin levels and the severe mitochondrial remodelling observed in Miro1^{cKO} neurons *in vivo* suggests that mitochondrial homeostasis is compromised by the loss of Miro1 in mature neurons.

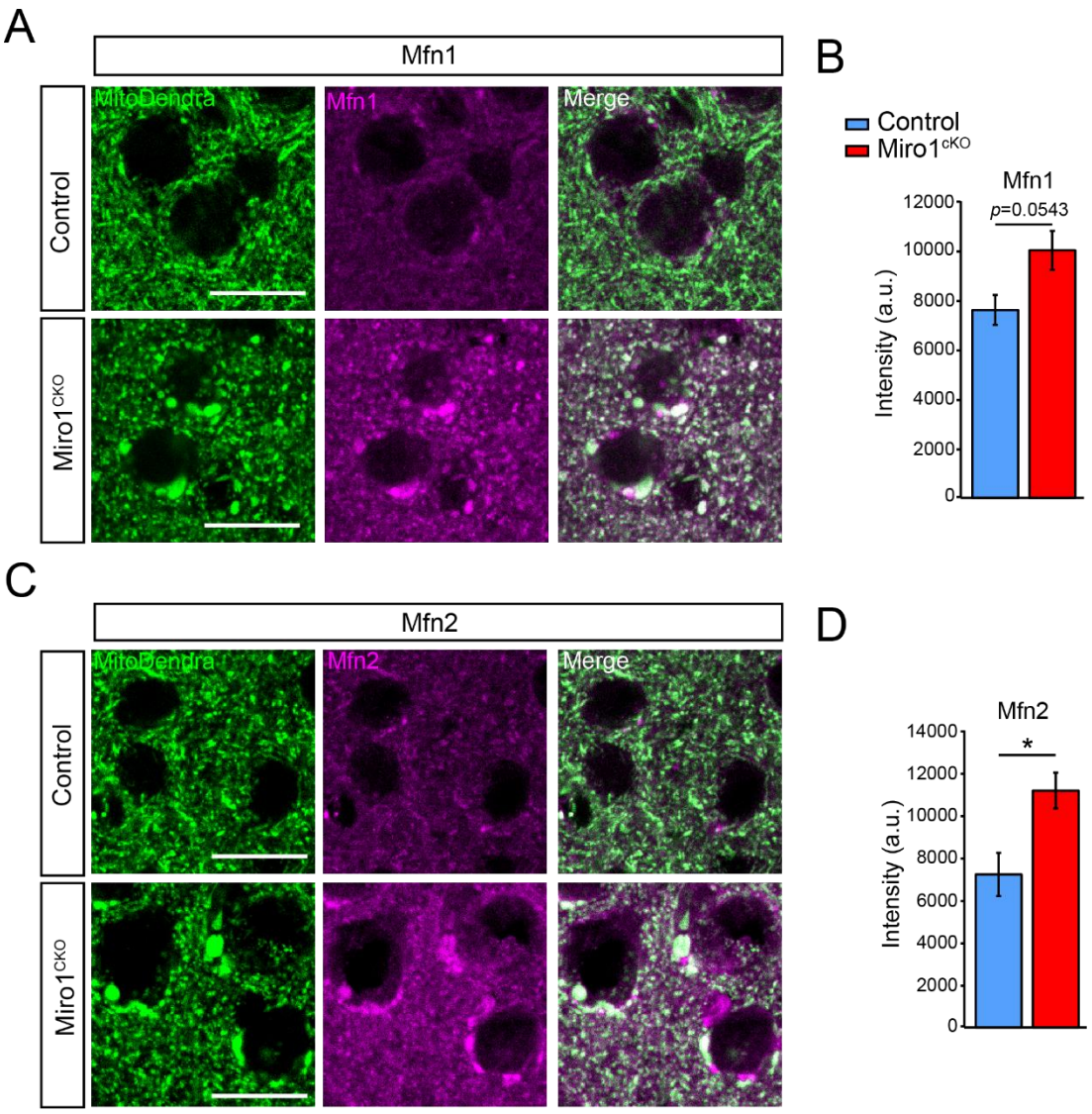

Figure 6: The mitofusins are enriched in Miro1^{cKO}-MitoDendra brains. A. Representative confocal images of Mfn1 (magenta) immunostaining in cortical sections from 12-month control and Miro1^{cKO}-MitoDendra mice (Scale bars = 10µm) B. Quantification of Mfn1 signal intensity in 12-month control and Miro1^{cKO}-MitoDendra cortical sections (unpaired t-test, n=4 animals per genotype, 12 ROIs per animal). C. Representative confocal images of Mfn2 (magenta) immunostaining in cortical slices from 12-month control and Miro1^{cKO}-MitoDendra mice (Scale bars = 10µm) D. Quantification of Mfn2 signal intensity in 12-month control and Miro1^{cKO}-MitoDendra cortical sections (unpaired t-test, n=4 animals per genotype, 12 ROIs per animal). Error bars represent s.e.m. Significance: *p<0.05. Data collected in collaboration with Guillermo Lopez-Domenech.

5.2.5 S65-Phospho-ubiquitin colocalises with a proportion of megamitochondria in Miro1^{cKO} brains.

The pathological relevance of the formation of megamitochondria in Miro1^{cKO} neurons *in vivo* was then investigated. S65-Phospho-Ubiquitin formation can serve as a biomarker for mitochondrial damage in aging and disease (Hou et al., 2018). Therefore, coronal brain slices from control-and Miro1^{cKO}-MitoDendra expressing mice were immunostained (Figure 7). Although no significant change in the total levels of p-S65-Ubiquitin was identified (Figure 6B), interestingly, it was observed that a proportion of Miro1^{cKO} cells presenting giant mitochondria showed an accumulation of p-S65-Ubiquitin surrounding the aberrant mitochondrial particles (Figure 7A and B). This is similar to previous findings in aged or Lewy Body Disease post-mortem brains (Hou et al., 2018) and suggests that the formation of megamitochondria in Miro1^{cKO} neurons could be triggering a disease-like phenotype.

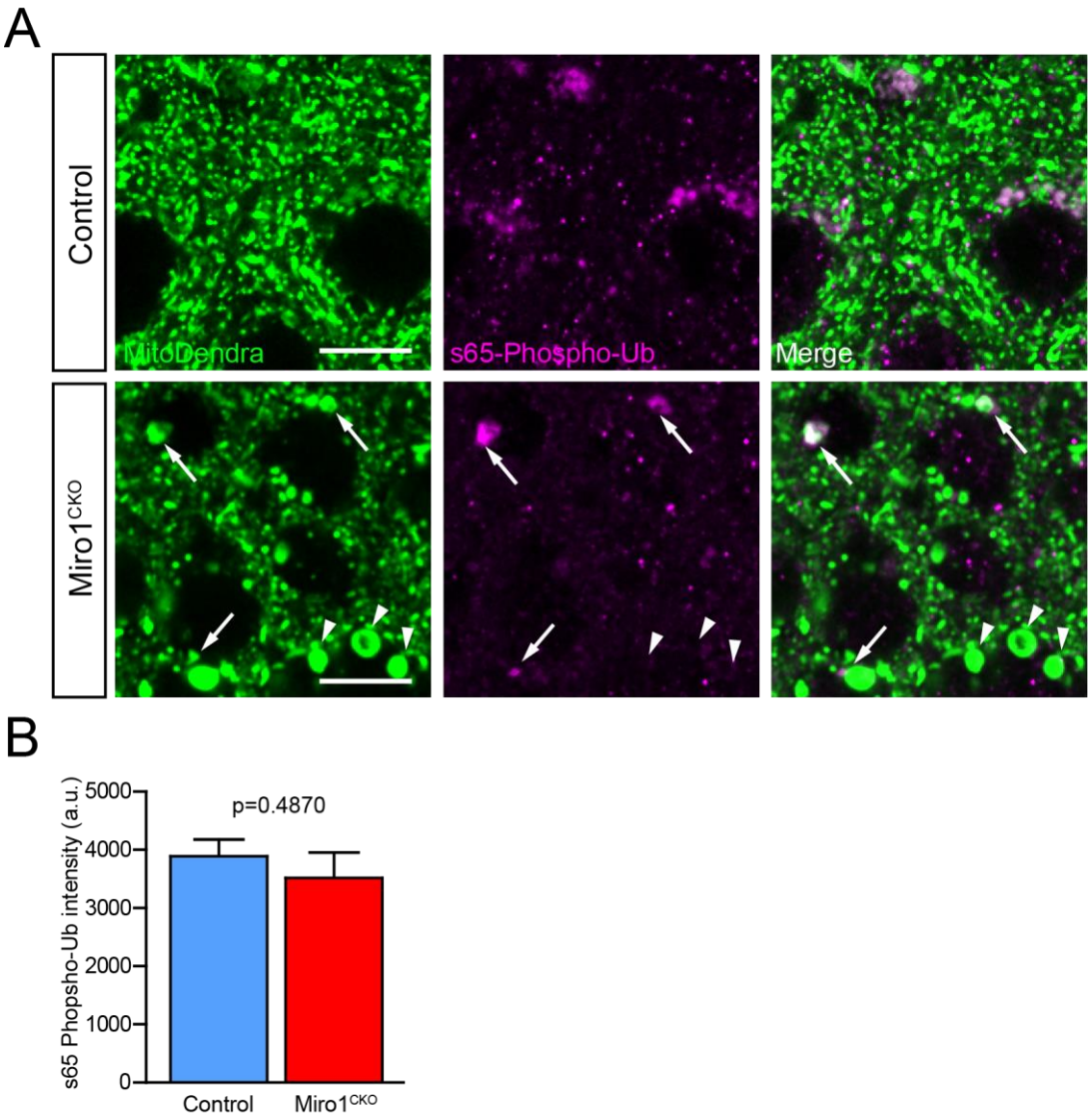

Figure 7: S65-Phospho-ubiquitin colocalises with a proportion of megamitochondria in Miro1^{cKO} brains. A. Representative confocal images of s65-phospho-ubiquitin immunostaining in cortical sections from 12-month control and Miro1^{cKO} crossed with Mitodendra mice (Arrow indicates colocalization between megamitochondria and s65-p-Ub, arrowhead indicates non-colocalization) (Scale bars = 10µm) B. Quantification of s65-phospho-ubiqutin signal intensity in 12-month WT and Miro1^{cKO} cortical sections (unpaired t-test, n=4 animals per genotype, 12 ROIs per animal). Error bars represent s.e.m

5.2.6 Long-term loss of Miro1 in vivo leads to the initiation of the integrated stress response.

Animal models in which either mitochondrial fission and fusion or mitophagy have been altered have been shown to induce the integrated stress response (ISR), a protective pathway that leads to a reduction in global protein synthesis rates (Smith and Mallucci, 2016, Costa-Mattioli and Walter, 2020). However, sustained activation of this pathway leading to a chronic reduction in the translation of vital proteins can lead to neuronal death (Celardo et al., 2016, Munoz et al., 2013, Restelli et al., 2018). Activation of the ISR is mediated by the activity of 4 discrete kinases (PERK, HRI, PKR and GCN2) which all converge onto one phosphorylation site at serine 51 of the Eukaryotic Initiation Factor 2 alpha (eIF2α) (Wek, 2018). Therefore, antibodies specific to pS51-eIF2α can be used as a measure of activation of the ISR. Strikingly, the levels of pS51-eIF2α in 4-month-old Miro1^{cKO} hippocampal lysates were substantially and consistently increased in comparison to WT hippocampal lysates; an effect that was not observed in the Miro2^{KO} mice (Figure 8A and B). The increase in pS51-eIF2α was further exacerbated in 12-month-old Miro1^{cKO} hippocampal lysates which correlates with the age-dependent increase in mitofusin levels (Figure 8C and D). Total levels of eIF2α were unchanged between all 3 genotypes allowing us to conclude that the increase of pS51-eIF2α seen in Miro1^{cKO} brains is due to an increase in phosphorylation of eIF2α (Figure 8).

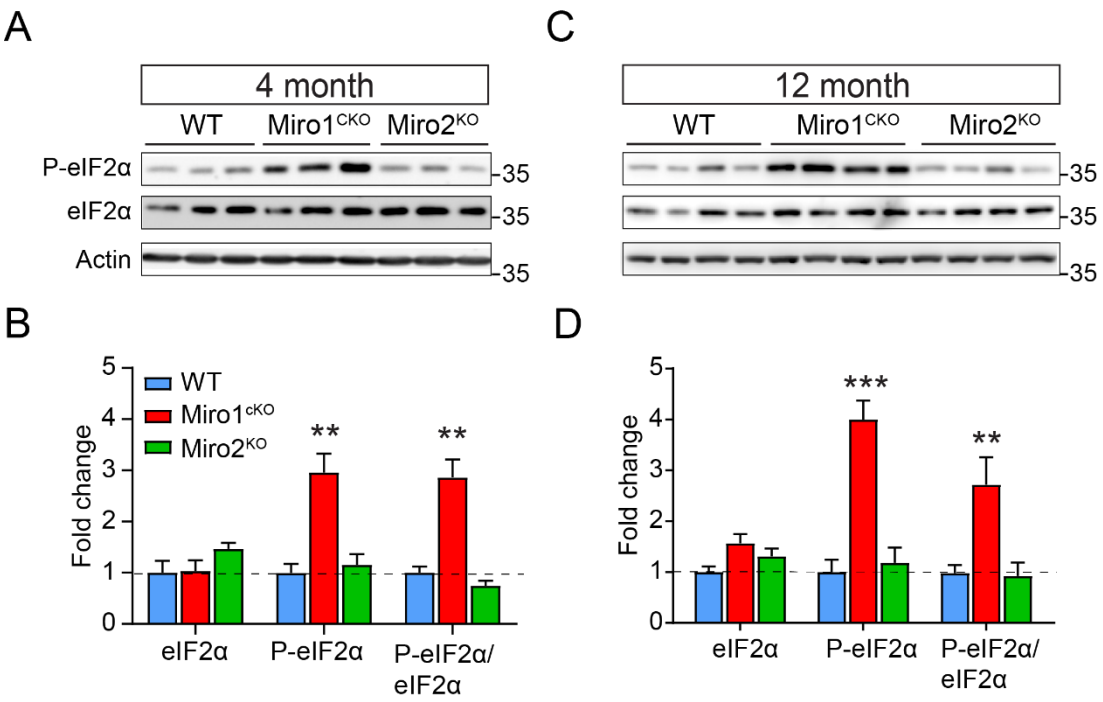

Figure 8: Loss of Miro1, but not Miro2, in principal neurons induces the activation of the integrated stress response. A. Representative western blot images of brain lysates from 4-month WT, Miro1^{cKO} and Miro2^{KO} mice immunoblotted with the antibodies stated. (B) Quantification of eIF2α and P-eIF2α band intensity (normalised to actin and WT) from 4-month WT, Miro1^{cKO} and Miro2^{KO} brain lysates. Phosphorylation of eIF2α is defined as P-eIF2α/eIF2α (unpaired t-test, n=3 mice per genotype). (A) Representative western blot images of brain lysates from 12-month WT, Miro1^{cKO} and Miro2^{KO} mice immunoblotted with the antibodies stated. (B) Quantification of eIF2α and P-eIF2α band intensity (normalised to actin band intensity) from 12-month WT, Miro1^{cKO} and Miro2^{KO} brain lysates. Phosphorylation of eIF2α is defined as P-eIF2α/eIF2α (unpaired t-test, n=4 mice per genotype). Error bars represent s.e.m. Significance: **p<0.01, ***p<0.001.

To confirm the western blot data, coronal brain slices from 12-month-old control and Miro1^{cKO} MitoDendra-expressing mice were immunostained with pS51-eIF2α (Figure 9). In agreement with the previous data, there was a large and consistent increase in pS51-eIF2α staining in the soma of MitoDendra- and MAP2-expressing neurons in the cortex of Miro1^{cKO} mice compared with control mice (Figure 9A and B).

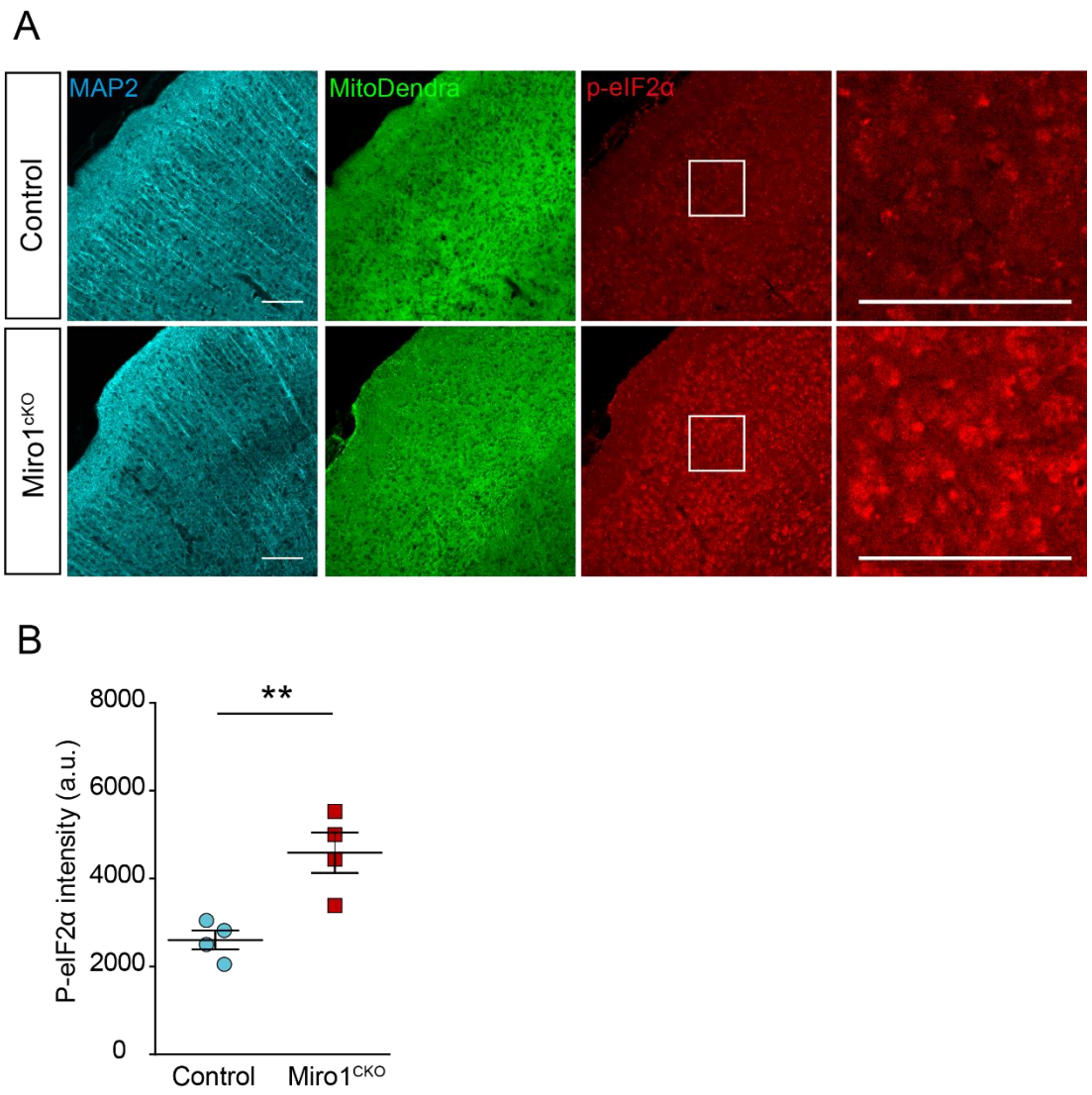

Figure 9: Loss of Miro1 in principal neurons increases pS51-eIF2α staining in neuronal somas. A. Representative confocal images of cortical regions of 12-month mitoDendra-crossed control and Miro1^{cKO} mice stained with MAP2 and P-eIF2α. (Scale bars = 100µm) B. Quantification of P-eIF2α signal intensity from cortical regions of 12-month mitoDendra-crossed control and Miro1^{cKO} mice (unpaired t-test, n=4 mice per genotype). Error bars represent s.e.m. Significance: **p<0.01.

5.2.7 The initiation of the integrated stress response correlates with the formation of megamitochondria in Miro1^{cKO} neurons in vivo.

In order to establish whether initiation of the ISR in Miro1^{cKO} brains correlates with the formation of megamitochondria in neurons, two populations of neurons within Miro1^{cKO} brains were established: those with megamitochondria and those without (Figure 10). Using MitoDendra signal, megamitochondria were defined as mitochondria with an area greater than 2.5µm^2, consistent with previous reports (Yamada et al., 2018). Strikingly, there was a significant increase in pS51-eIF2α staining in neuronal soma containing megamitochondria compared to those without (Figure 10B and C) suggesting that activation of the ISR in Miro1^{cKO} brains is dependent on the formation of hyperfused megamitochondria in neurons. Collectively, this data indicates that long-term disruption of mitochondrial homeostasis *in vivo* by Miro1 deletion, leads to increased levels of mitofusins, formation of megamitochondria and ISR activation.

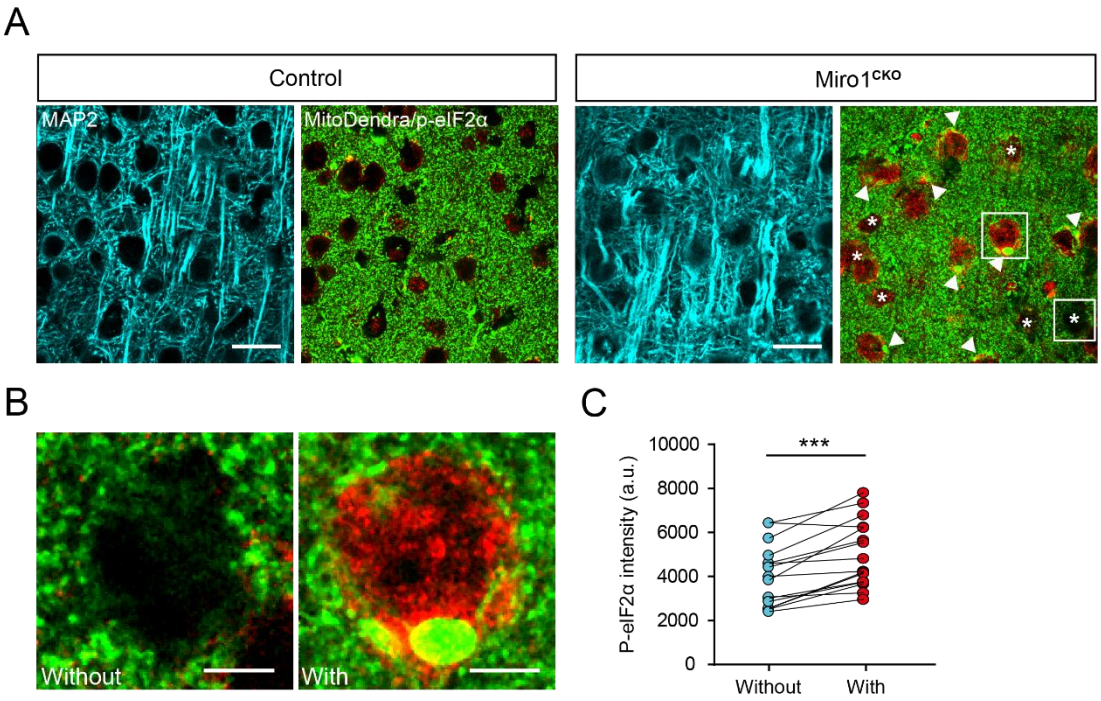

Figure 10: The initiation of the integrated stress response correlates with the formation of megamitochondria in Miro1^{cKO} neurons. A. Representative confocal images (63x) of cortical regions of 12-month control and Miro1^{cKO}-MitoDendra mice stained with MAP2 and P-eIF2α. Arrows indicate the presence of megamitochondria (>2.5 µm^2), stars indicate neuronal somas without megamitochondria. (Scale bars = 20µm) B. Example zoom images of neuronal somas with and without megamitochondria from cortical regions of 12-month Miro1^{cKO}-mitoDendra mice stained with P-eIF2α. (Scale bars = 5µm) C. Quantification P-eIF2α signal intensity (a.u.) from neuronal somas with and without megamitochondria from cortical regions of 12-month Miro1^{cKO}-MitoDendra (paired t-test, n=16 sections from 4 mice). Error bars represent s.e.m. Significance: p<0.001.

5.3 Discussion

The late onset of many neurodegenerative diseases suggests that damage can accumulate with time because of long-term defects in cellular processes. Given the defects in mitophagy caused upon loss of Miro1 in neurons, the *in vivo* consequences of the loss of neuronal Miro1 in aged animals were studied. Importantly, this study identified hallmarks of altered neuronal mitochondrial quality control *in vivo*. For example, a significant increase in PINK1 levels and the appearance of an upper band of Parkin, suspected of being an auto-ubiquitinated form of Parkin was observed in 12-month-old Miro1^{cKO} mice (Chaugule et al., 2011, Wauer and Komander, 2013). Parkin auto-ubiquitination leads to the activation of Parkin E3-ligase activity, with sustained auto-ubiquitination being proposed to be indicative of a pathological state of Parkin activation (Chaugule et al., 2011). Moreover, overexpression of PINK1 is known to cause mitochondrial dysfunction (Yang et al., 2008). Alongside the changes in PINK1 and Parkin in 12-month-old Miro1^{cKO} mice, a dramatic increase in the expression levels of Mfn1 and Mfn2 were also revealed. Furthermore, it was found that Mfn1 and Mfn2 gene expression are unaltered in Miro1^{cKO} brains and that ubiquitination of Mfn2 is significantly decreased when Miro1 is knocked out in cortical neurons *in vitro*. Therefore, the upregulation of the mitofusins in Miro1^{cKO} brains is likely a consequence of reduced Parkin E3-ligase activity in Miro1^{KO} neurons due to delayed Parkin recruitment to mitochondria. It is worth noting that the mitofusins are also

ubiquitination targets of another mitochondrial E3 ligase, Mul1 (Yun et al., 2014), so alterations Mul1 activity in Miro1^{KO} neurons may also contribute.

Interestingly, alterations in Mfn1 and Mfn2 have been observed in several models of mitophagic dysfunction and neurodegeneration (Chen and Dorn, 2013, Gong et al., 2015, Rocha et al., 2018, Wang et al., 2015). Additionally, overexpression and reduced ubiquitination of Mfn2 repress mitophagy (McLelland et al., 2018), perhaps further exacerbating the defects in mitophagy in Miro1^{cKO} animals. Therefore, these findings indicate that the long-term loss of Miro1 in neurons leads to profound changes in mitophagy and consequently, the mitochondrial fusion machinery.

Upregulation of the mitochondrial fusion machinery and in particular gain of function mutations of Mfn2 associated with Charcot Marie Tooth-2 (CMT2) pathology lead to mitochondrial remodelling and the accumulation of hyperfused “megamitochondria” in neuronal somas (El Fissi et al., 2018, Santel and Fuller, 2001). Interestingly, studying mitochondrial morphology in aged Miro1^{cKO}-MitoDendra neurons *in vivo* revealed a dramatic hyperfusion of the mitochondrial network and large mitochondrial structures located in neuronal somas. This is similar to previous reports of mitochondrial structures identified in a number of models where either mitochondrial fission / fusion proteins or mitophagy have been altered (Chen and Dorn, 2013, El Fissi et al., 2018, Kageyama et al., 2012, Kageyama et al., 2014, Yamada et al., 2018). Intriguingly, a proportion of the megamitochondria associated with phospho-

S65-Ubiquitin that surrounded the aberrant mitochondrial particles. Phospho-S65-Ubiquitin formation can serve as a biomarker for mitochondrial damage in aging and disease (Hou et al., 2018). However, it is not definitively known whether the megamitochondria present within Miro1^{cKO} neurons are indeed damaged.

Mouse models with disrupted mitochondrial dynamics in neurons can present sustained levels of cellular stress that lead to the activation of the integrated stress response (ISR) (Restelli et al., 2018, Celardo et al., 2016, Mick et al., 2020). Alterations in Mfns either directly, in Mfn2 ablated MEFs, or as a consequence of dysfunctional mitophagy, in PD mutant flies, are known to induce the ISR, a protective pathway that leads to a reduction in global protein synthesis rates upon detection of cellular stress (Celardo et al., 2016, Munoz et al., 2013). The ISR is implicated in the pathology of numerous neurodegenerative diseases where the chronic reduction in translation of vital proteins leads to neuronal death (Halliday and Mallucci, 2015). Intriguingly, it was found that the formation of hyperfused megamitochondria in Miro1^{cKO} brains correlated with the initiation of the ISR *in vivo*, providing further links between the loss of Miro1 and neurodegeneration. The induction of the ISR is mediated by the activity of four discrete kinases, PERK, HRI, PKR and GCN2, all of which converge onto a single phosphorylation site of eIF2α at Serine 51 (Wek, 2018, Costa-Mattioli and Walter, 2020); however, it is currently unclear which of these kinases is responsible for the increase observed in Miro1^{cKO}

neurons. Recent studies have shown that HRI and GCN2 can act as sensors for mitochondrial stress (Fessler et al., 2020, Guo et al., 2020, Mick et al., 2020), however the majority of ISR activation seen in models of neurodegenerative disease is dependent on PERK (Smith and Mallucci, 2016). Interestingly, this includes mutant PINK1 and Parkin drosophila models of genetic Parkinson's Disease (Celardo et al., 2016). In these models, PERK is activated via the upregulation of Mfn and formation of Mfn bridges between damaged mitochondria and the ER. Inhibiting PERK activity or knocking down Mfn prevented ISR activation and was neuroprotective, irrespective of the mitochondrial dysfunction that remained (Celardo et al., 2016). In Miro1^{cKO} brains, P-eIF2α expression is significantly higher in neurons containing megamitochondria compared to those without. Additionally, it was observed that Mfn expression is enriched on megamitochondria. Therefore, it may be that the ISR is activated via a similar Mfn- and PERK-dependent mechanism in the brains of Miro1^{cKO} mice Taken together, these findings further implicate Miro1 dysfunction in the pathogenesis of neurodegenerative diseases, including Parkinson's Disease, and provides additional evidence of a pathological activation of the ISR as a result of dysfunctional mitochondrial homeostasis underlying this pathology.

Chapter 6- Discussion

6.1 Summary

By studying PINK1/Parkin-mediated mitophagy in astrocytes and neurons, the work contained in this thesis identified new insights into mitochondrial quality control in the central nervous system (CNS). Firstly, with the use of mixed and single cell culture systems, the PINK1/Parkin-mediated mitophagy pathway was further characterised in primary astrocytes and neurons. Intriguingly, this work identified clear differences between the spatial and temporal regulation of the mitophagy pathway in astrocytes and neurons showing that mitophagy occurs quicker, more readily and is less spatially restricted in astrocytes compared to neurons. Furthermore, it was identified that astrocytic PINK1/Parkin-mediated mitophagy is dependent on glucose metabolism and the glycolytic capacity of astrocytes. Next, with the use of a constitutive knockout mouse line, this thesis investigated the role of the mitochondrial Rho GTPase, Miro1, in the mitophagic process in astrocytes and neurons. Interestingly, this work identified that the loss of Miro1 did not affect mitophagy rates in astrocytes yet outlined a cell type-specific role for Miro1 and its ubiquitination in the regulation of PINK1/Parkin-mediated mitophagy in neurons. Finally, with the use of a conditional knockout mouse line, this thesis investigated the long-term impact of loss of neuronal Miro1 on mitochondrial homeostasis *in vivo* and revealed a dramatic hyperfusion of somatic mitochondria as a result of dysregulation of the mitochondrial fusion

machinery. Importantly, this work found that disrupted neuronal mitochondrial homeostasis *in vivo* triggered the activation of the neurodegeneration-associated integrated stress response (ISR) pathway that correlated with the formation of “megamitochondria” in Miro1 conditional knockout brains. Taken together, this thesis provides important new insights into the cell type-specific regulation of mitochondrial quality control in astrocytes and neurons and outlines how disrupted mitochondrial homeostasis in the CNS can lead to neurodegenerative pathology.

6.2 Astrocytes: A hub of mitophagy in the CNS?

The first results chapter focussed on characterising the PINK1/Parkin-dependent mitophagy pathway in astrocytes and comparing that to the same pathway in neurons. Previous work had compared mitophagy in astrocyte and neuronal monocultures, however this may not provide a physiologically accurate model of both astrocytic and neuronal biology (Enright et al., 2020, Hasel et al., 2017). Therefore, with the use of fluorescently tagged Parkin and antibodies specific to s65-phospho-ubiquitin, which mitigates the need for overexpression of Parkin, PINK1/Parkin-dependent mitophagy was shown to occur quicker, more readily and was less spatially restricted in astrocytes compared to neurons present within the same culture system. Furthermore, it was shown that astrocytic damage-induced mitophagy is dependent on PINK1 and the glycolytic capacity of astrocytes. These findings backed up by previous

evidence (Barodia et al., 2019, O'Donnell et al., 2016), establish astrocytes as a principal site of mitophagy in the CNS.

Recently, it has been shown that damaged neuronal mitochondria can be transferred to astrocytes to facilitate their clearance (Gao et al., 2019, Davis et al., 2014, Morales et al., 2020) and that healthy mitochondria can be sent from astrocytes to neurons to support neuronal viability (Hayakawa et al., 2016, English et al., 2020, Gao et al., 2019). The concept of “transmitophagy” is an intriguing one, however, until now, it wasn’t known why this happened and how astrocytes went about performing this role. The findings in this thesis show that due to their glycolytic capacity, astrocytes are able to rapidly and robustly perform mitophagy. Additionally, the lack of spatial constraints to astrocytic mitophagy means that mitochondria taken up by astrocytes can readily be turned over irrespective of their subcellular localisation. Therefore, these findings outline why astrocytes could be the perfect candidate to act as a hub of mitophagy in the CNS.

Neuron-astrocyte transmitophagy has previously been explored in the context of ischemic insult but could also be a key process in the constant regulation of synaptic function. Synaptic transmission and plasticity rely heavily on the presence of healthy mitochondria at pre- and post-synapses (Devine and Kittler, 2018, Seager et al., 2020). On the other hand, the presence of dysfunctional synaptic mitochondria can result in aberrant synaptic function through inadequate ATP production, Ca^{2+} buffering and the production of

harmful reactive oxygen species and have been heavily implicated in neurological disease (Lin and Beal, 2006). Therefore, damaged synaptic mitochondria need to be removed via quality control mechanisms. However, the findings in this thesis and work by others indicate that neuronal mitophagy is, in the main, spatially confined to the proximal somatodendritic regions where the majority of degradative lysosomes are situated (Evans and Holzbaur, 2020, Cai et al., 2012, Zheng et al., 2019). Yet synapses are positioned throughout neuronal processes including the most distal regions. Consequently, the cell autonomous turnover of distal neuronal mitochondria could require mitochondria to be transported over extremely long distances to facilitate their clearance. Whereas the uptake of neuronal mitochondria by perisynaptic astrocytic processes and consequent rapid turnover could expedite the process of removing dysfunctional mitochondria from synapses to confer neuronal protection.

On top of facilitating the turnover of neuronal mitochondria, the robust mitophagy pathway in astrocytes would allow for the constant maintenance of the astrocytic mitochondrial network. Astrocytes heavily rely on mitochondria to buffer Ca^{2+}, to modulate intracellular Ca^{2+} homeostasis, and provide ATP for glutamate uptake, a process key to preventing excitotoxicity and maintaining synaptic function (Jackson and Robinson, 2018). Thus, it is vitally important that astrocytes are able to maintain a healthy mitochondrial network

as astrocytic mitochondrial dysfunction in astrocytes could impact both astrocyte and neuronal function.

On the other hand, dysfunctional astrocytic mitophagy could have serious implications in the pathogenesis of neurodegenerative disease. Previous evidence has shown that mitochondrial dysfunction in astrocytes leads to the propagation of disease to neurons through the release of inflammatory cytokines (Joshi et al., 2019). Accordingly, Parkin dysfunction has been shown to impair astrocyte mitochondrial function and contribute to the pathogenesis of PD through astrocytic, but not neuronal, upregulation of the unfolded protein response (Ledesma et al., 2002). Intriguingly, recent evidence suggests that mitophagy does not occur within DA neurons of the SNc *in vivo* (Katayama et al., 2020) which could explain the selective susceptibility of DA neurons in PD pathology. Therefore, the support of neighbouring astrocytes in the SN and the striatum may take on increased importance and the failure of maintaining both neuronal and astrocytic mitochondria in these cells could accelerate PD progression.

The work in this thesis establishes astrocytes as the prime candidate to act as a hub of mitophagy in the CNS. Consequently, dysfunctional astrocytic mitophagy could have implications for astrocytes and neurons but also for the health of the entire CNS. Therefore, specifically targeting mitophagy in astrocytes provides a novel therapeutic avenue in the treatment of CNS disease.

Notwithstanding, the work in the later chapters outlined the importance of cell autonomous mitochondrial quality control in neurons.

6.3 Miro1: The missing link between mitochondrial trafficking and mitophagy in neurons?

The second results chapter focussed on defining the role of the mitochondrial Rho GTPase, Miro1, in the PINK1/Parkin-dependent mitophagy pathway in astrocytes and neurons. Miro1 has well established roles in the regulation of mitochondrial trafficking in both neurons and astrocytes yet, until now, its role in the regulation of PINK1/Parkin-mediated mitophagy in these cells was unclear.

Under mitochondrial damage Miro1 is ubiquitinated and degraded by a PINK1/Parkin-dependent mechanism (Birsa et al., 2014, Ordureau et al., 2018, Liu et al., 2012, Wang et al., 2011b) that may serve to dissociate damaged mitochondria from the microtubule and actin transport pathways (Lopez-Domenech et al., 2018, Wang et al., 2011b). Additionally, it has been shown that Miro1 promotes the recruitment and stabilisation of Parkin onto depolarised mitochondria in cell lines (Birsa et al., 2014, Safiulina et al., 2019, Shlevkov et al., 2016) and recently, loss of function mutations in Miro1 have also been identified in PD patients (Grossmann et al., 2019, Berenguer-Escuder et al., 2019, Grossmann et al., 2020).

Surprisingly, this thesis revealed a cell-type specific role of Miro1 in mitophagy in astrocytes and neurons. Despite Miro1's previously reported role in the

regulation of astrocytic mitochondrial trafficking (Stephen et al., 2015), the loss of Miro1 had minimal effect on the PINK1/Parkin-dependent mitophagy pathway in astrocytes. In stark contrast, Miro1 loss severely delayed Parkin recruitment to depolarised mitochondria, the formation of s65-phospho-ubiqutin clusters and mitophagy progression in neurons. These findings further underline the differences between the mitophagy pathway in astrocytes and neurons that were set out in chapter 3.

Moreover, this thesis went on to show that Miro1 interacts with a small proportion of Parkin on healthy neuronal mitochondria and that Parkin recruitment to depolarised mitochondria in neurons is dependent on the ubiquitination of Miro1. This suggests that Miro1 could prime neuronal mitochondria for mitophagy prior to further Parkin being recruited upon damage-induced stabilisation of PINK1 on the OMM and ubiquitination of Miro1, thus facilitating mass-ubiquitination of Parkin substrates and the clearance of neuronal mitochondria.

These findings also further implicate the involvement of mitochondrial trafficking in neuronal mitophagy. Previous evidence, backed up by work in this thesis, suggests that depolarised neuronal mitochondria are, in the main, retrogradely trafficked to the soma, where the majority of lysosomes are present (Becker et al., 1960, Yap et al., 2018, Peters, 1991, Cai et al., 2012), to facilitate their clearance (Zheng et al., 2019, Cai et al., 2012). A previous study has shown that Miro1 remains present on damaged axonal mitochondria

following the release of syntaphilin and subsequent retrograde movement, only later to be degraded (Lin et al., 2017). Thus, this could indicate that Miro1 is required to facilitate the trafficking of depolarised mitochondria to neuronal somas and may also explain the redundancy of Miro1 for astrocytic mitophagy which appears to be spatially unrestricted.

Consequently, it could be that Miro1 plays two essential roles in neuronal mitophagy. First to retrogradely transport depolarised mitochondria to somas where the majority of lysosomes are present. Once in the soma, Parkin-dependent ubiquitination of Miro1 facilitates the feedforward mass-ubiquitination of OMM substrates and the subsequent clearance of mitochondria. The importance of the second step is highlighted by work in this thesis showing that expression of the Miro1 ubiquitination mutant, Miro1^{5R}, which rescues defects in mitochondrial distribution, does not rescue damage-induced Parkin recruitment to mitochondria in Miro1^{KO} neurons.

Therefore, this thesis establishes Miro1 as a critical molecular player in the mitophagy pathway in neurons that could provide the missing link between damage-induced retrograde mitochondrial trafficking of neuronal mitochondria and Parkin-mediated clearance of mitochondria in neuronal somas.

6.4 The loss of neuronal Miro1 in vivo disrupts mitochondrial homeostasis and triggers the integrated stress response: implications for neurodegenerative disease.

Given the defects in mitophagy caused upon loss of Miro1 in neurons *in vitro*, the third results chapter aimed to identify signs of aberrant dysfunctional mitochondrial quality control in the brains of mice lacking neuronal Miro1 *in vivo.* Many studies have explored neuronal mitochondrial dynamics and quality control mechanisms *in vitro*, but the majority lack translation to neurodegenerative pathology *in vivo*. Importantly, this thesis identified hallmarks of altered neuronal mitochondrial homeostasis in Miro1^{cKO} brains *in vivo* including the age-dependent upregulation of PINK1 and the mitofusins, the formation of hyperfused megamitochondria in neuronal somas and activation of the ISR.

The mitofusins are important targets of PINK1/Parkin ubiquitination and their upregulation has been observed in several models of mitophagic dysfunction and neurodegeneration (Chen and Dorn, 2013, Gong et al., 2015, Rocha et al., 2018, Wang et al., 2015) including PINK1 and Parkin models of PD (Celardo et al., 2016, Ziviani et al., 2010). Accordingly, Mfn2 ubiquitination was found to be reduced in Miro1^{KO} neurons and Mfn1 and 2 gene expression levels unaltered in Miro1^{cKO} brains indicating that the Mfns are ineffectively targeted by the PINK1/Parkin pathway in the absence of Miro1 in neurons *in vivo*. Interestingly, by crossing Miro1^{cKO} mice with mice expressing a

fluorescent mitochondrial reporter, MitoDendra, revealed that the dysregulation of the Mfns was associated with remodelling of the mitochondrial network and the formation of hyperfused megamitochondria in neuronal somas. Mitochondrial hyperfusion is associated with neurodegenerative disease (El Fissi et al., 2018, Yamada et al., 2018, Santel and Fuller, 2001, Kageyama et al., 2012, Kageyama et al., 2014). Loss of function mutations in DRP1 are associated with ADOA (Gerber et al., 2017) and gain of function mutations in Mfn2 are associated with CMT2A (El Fissi et al., 2018), both of which result in the hyper-fusion of neuronal mitochondria although how this results in neuronal death is less clear.

Hallmarks of neurodegeneration including significant neuronal loss and severe astrogliosis have previously been identified in Miro1^{cKO} brains but until now the underlying cause of neurodegeneration remained unknown (Lopez-Domenech et al., 2016). Intriguingly, the formation of megamitochondria in Miro1^{cKO} brains correlated with activation of the ISR, a protective pathway that leads to a reduction in global protein synthesis rates. However, sustained activation of this pathway can lead to neuronal death due to a chronic reduction in the translation of vital proteins; a phenomenon that has been implicated in the pathology of various neurodegenerative diseases including PD (Halliday and Mallucci, 2015, Smith and Mallucci, 2016).

In drosophila models of PD, ISR activation is triggered by the upregulation of Mfn (the drosophila orthologue of Mfn1/2) and the activation of the ER stressor

sensor kinase, PERK (Celardo et al., 2016). In these models, PERK is activated via the upregulation of Mfn and formation of Mfn bridges between damaged mitochondria and the ER. Accordingly, Mfn2 has been shown to be a regulator of PERK in mammalian cells (Munoz et al., 2013). Thus, it may be that the ISR is activated via a similar Mfn- and PERK-dependent mechanism in the brains of Miro1^{cKO} mice. However, loss of Miro1 in forebrain neurons may induce a wide spectrum of stress conditions. Conditional knockout of Drp1 in the adult mouse forebrain, which ablates mitochondrial fission, induces the ISR through the activity of HRI and GCN2, which are sensors for mitochondrial dysfunction and amino acid deprivation, respectively, as well as PERK (Restelli et al., 2018). Therefore, going forward it will be important to establish which of these kinases mediates the activation of the ISR in Miro1^{cKO} neurons and what impact blockade of this pathway has on the neurodegeneration previously described in this model (Lopez-Domenech et al., 2016).

Defects in damage-induced Miro1 degradation have been linked to PD pathology and pharmacologically reducing Miro1 levels has been suggested as a therapeutic strategy (Hsieh et al., 2016, Hsieh et al., 2019). However, the findings here indicate the importance of the presence of Miro1 for functional mitochondrial homeostasis and that the loss of Miro1 is detrimental to neuronal health. Thus, caution needs to be exercised when altering Miro1 expression levels.

Taken together, this thesis provides new insights into the requirement of Miro1 for mitophagy following mitochondrial damage in astrocytes and neurons. This data identifies a redundancy in the requirement of Miro1 for the mitophagic process in astrocytes yet highlights its importance for neuronal mitochondrial homeostasis *in vitro* and *in vivo*. Moreover, a role for Miro1 as part of the Parkin receptor complex on the OMM and its potential role in priming neuronal mitochondria for Parkin-mediated mitochondrial quality was uncovered. Long-term disruption of mitochondrial quality control in mature neurons lacking Miro1 *in vivo* leads to upregulation of Mfn1/2, remodelling of the mitochondrial network and induction of the integrated stress response. These findings further implicate Miro1 dysfunction in the pathogenesis of neurodegenerative diseases, including PD, and provides additional evidence of a pathological activation of the ISR as a common theme in neurodegenerative pathology. Going forward, this may open new strategies to target mitochondrial dysfunction in PD pathogenesis and other related diseases with alterations in the clearance of dysfunctional mitochondria.

6.5 Future Directions

The work in this thesis outlined the mitophagy pathway in astrocytes present within mixed glial and neuronal cultures. Astrocytes in co-culture are more complex than their counterparts present in monocultures however, a single astrocyte can contact up to 2 million synapses in the human brain *in vivo* (Oberheim et al., 2009). Therefore, going forward it will be important to

characterise the mitophagy pathway in astrocytes *in vivo* to answer the following questions: Does mitophagy occur rapidly in astrocytes *in vivo*? And does mitophagy occur even in the finest of perisynaptic PAPs *in vivo*?

The redundancy of Miro1 for mitophagy in astrocytes suggests the involvement of other molecular players in the PINK1/Parkin-dependent mitophagy pathway in astrocytes. One possible candidate is hexokinase II (HK2). 2DG blocks glycolytic flux via inhibition of the hexokinases that phosphorylate glucose in the first step of glycolysis. HK2 is an OMM-residing enzyme that is exclusively expressed in glia but not in neurons (Zhang et al., 2014, Zhang et al., 2016). Intriguingly, recent evidence suggests that HK2 could also play a key role in the PINK1/Parkin-mediated mitophagy pathway (McCoy et al., 2014, Heo et al., 2019). In cell lines, HK2, but not HK1, that is expressed in neurons, promotes the stabilisation of PINK1 on the OMM following mitochondrial damage and its loss delays the accumulation of 65-phospho-ubiquitin on depolarised mitochondria (Heo et al., 2019). Therefore, going forward it will be important to establish what role, if any, HK2 plays in the mitophagic process in astrocytes. Could HK2 link astrocytic metabolism to the PINK1/Parkin mitophagy pathway? Could the presence of HK2 on astrocytic mitochondria explain the redundancy of Miro1 for mitophagy?

This thesis has shown the impact of dysfunctional mitophagy in neurons *in vivo* but what is not known is what happens when mitochondrial homeostasis is specifically disrupted in astrocytes *in vivo*. Intriguing recent evidence has

shown that activating the ISR specifically in astrocytes induces a specific reactivity state that causes non-cell-autonomous neurodegeneration through secretome alterations (Smith et al., 2020). Therefore, it will be important to know if disrupting astrocytic mitochondrial quality control *in vivo* triggers a similar phenotype.

What role does Miro1 play in the retrograde transport of depolarised neuronal mitochondria back to soma? Although the involvement of Miro1 in this phenomenon is yet to be elucidated, the multifaceted roles of Miro1 offer various intriguing hypotheses. Firstly, Miro1 could potentially sense energetic stress (ie. inadequate ATP production/cristae alterations) through its interaction with the MICOS complex on the IMM (Modi et al., 2019). This could facilitate disengagement from the actin cytoskeleton (Lopez-Domenech et al., 2018) to increase retrograde microtubular transport to the soma. Once in soma, ubiquitination and degradation of Miro1 could enable mitochondria to disengage from the microtubular trafficking machinery and gate wholesale mitochondrial ubiquitination and facilitate clearance, potentially through p97 mediated release from the ER (Ordureau et al., 2020).

The findings in chapter 4 show that mitophagy is disrupted in Miro1^{KO} neurons *in vitro* and the findings in chapter 5 indicate that aberrant mitochondrial quality control mechanisms contribute to the mitochondrial hyperfusion and consequent activation of the ISR seen in Miro1^{cKO} brains. However, it is not definitive that there is reduced levels of mitophagy in Miro1^{cKO} neurons *in vivo.*

Therefore, through the expression of mitophagy reporters (ie. Mito-Keima, Mito-QC, Mito-SRAI) the rates of mitophagy in Miro1^{cKO} neurons *in vivo* should be established, both basally and following stress (ie. exhaustive exercise (Sliter et al., 2018)). These reporters have been widely used *in vivo* however, there is controversy when it comes to which are true readouts of mitophagy (Katayama et al., 2020, Ganley et al., 2021, Liu et al., 2021) so this will need to be considered.

As the loss of Miro1-dependent anterograde mitochondrial trafficking could also contribute to the somatic accumulation of mitochondria in Miro1^{cKO} neurons it will be important to separate these effects from dysfunctional mitochondrial quality control. To do this, Miro1^{5R} could be expressed in the brains of Miro1^{cKO} mice *in vivo* (eg. by viral transduction or *in utero* electroporation) as this version of Miro rescues defects in mitochondrial distribution but is less ubiquitinated by Parkin upon mitochondrial damage.

Additionally, it will be important to further elucidate the mechanism of ISR activation in Miro1^{cKO} brains – is it indeed PERK dependent as a result of Mfn upregulation and mitochondrial hyperfusion causing ER stress? Can knockdown of the Mfns or PERK inhibition reverse ISR activation? And/or is there a role for the other ISR stressor kinases? The HRI-DELE1 axis has been specifically linked to mitochondrial dysfunction (Fessler et al., 2020, Guo et al., 2020) and GCN2 activity is increased upon electron transport chain inhibition (Mick et al., 2020). Are these also activated in Miro1^{cKO} brains?

Finally, what happens when you inhibit the ISR pathway in Miro1^{cKO} brains? Either through pharmacological or genetic inhibition of the specific stressor kinases or via application of ISRIB, that suppresses the entire pathway (Rabouw et al., 2019). Is it possible to reverse neurodegeneration?

References

Agarwal, A., Wu, P. H., Hughes, E. G., Fukaya, M., Tischfield, M. A., Langseth, A. J., Wirtz, D. & Bergles, D. E. 2017. Transient Opening of the Mitochondrial Permeability Transition Pore Induces Microdomain Calcium Transients in Astrocyte Processes. *Neuron,* 93**,** 587-605 e7.

Agulhon, C., Sun, M. Y., Murphy, T., Myers, T., Lauderdale, K. & Fiacco, T. A. 2012. Calcium Signaling and Gliotransmission in Normal vs. Reactive Astrocytes. *Front Pharmacol,* 3**,** 139.

Akimov, V., Barrio-Hernandez, I., Hansen, S. V. F., Hallenborg, P., Pedersen, A. K., Bekker-Jensen, D. B., Puglia, M., Christensen, S. D. K., Vanselow, J. T., Nielsen, M. M., Kratchmarova, I., Kelstrup, C. D., Olsen, J. V. & Blagoev, B. 2018. UbiSite approach for comprehensive mapping of lysine and N-terminal ubiquitination sites. *Nat Struct Mol Biol,* 25**,** 631-640.

Akundi, R. S., Huang, Z., Eason, J., Pandya, J. D., Zhi, L., Cass, W. A., Sullivan, P. G. & Bueler, H. 2011. Increased mitochondrial calcium sensitivity and abnormal expression of innate immunity genes precede dopaminergic defects in Pink1-deficient mice. *PLoS One,* 6**,** e16038.

Al Awabdh, S., Gupta-Agarwal, S., Sheehan, D. F., Muir, J., Norkett, R., Twelvetrees, A. E., Griffin, L. D. & Kittler, J. T. 2016. Neuronal activity mediated regulation of glutamate transporter GLT-1 surface diffusion in rat astrocytes in dissociated and slice cultures. *Glia,* 64**,** 1252-64.

Alexander, C., Votruba, M., Pesch, U. E., Thiselton, D. L., Mayer, S., Moore, A., Rodriguez, M., Kellner, U., Leo-Kottler, B., Auburger, G., Bhattacharya, S. S. & Wissinger, B. 2000. OPA1, encoding a dynamin-related GTPase, is mutated in autosomal dominant optic atrophy linked to chromosome 3q28. *Nat Genet,* 26**,** 211-5.

Allen, N. J. 2014. Astrocyte regulation of synaptic behavior. *Annu Rev Cell Dev Biol,* 30**,** 439-63.

Allen, N. J. & Lyons, D. A. 2018. Glia as architects of central nervous system formation and function. *Science,* 362**,** 181-185.

Almeida, A., Almeida, J., Bolanos, J. P. & Moncada, S. 2001. Different responses of astrocytes and neurons to nitric oxide: the role of glycolytically generated ATP in astrocyte protection. *Proc Natl Acad Sci U S A,* 98**,** 15294-9.

Amiri, M. & Hollenbeck, P. J. 2008. Mitochondrial biogenesis in the axons of vertebrate peripheral neurons. *Dev Neurobiol,* 68**,** 1348-61.

Ashrafi, G., de Juan-Sanz, J., Farrell, R. J. & Ryan, T. A. 2020. Molecular Tuning of the Axonal Mitochondrial $Ca^{(2+)}$ Uniporter Ensures Metabolic Flexibility of Neurotransmission. *Neuron,* 105**,** 678-687 e5.

Ashrafi, G., Schlehe, J. S., LaVoie, M. J. & Schwarz, T. L. 2014. Mitophagy of damaged mitochondria occurs locally in distal neuronal axons and requires PINK1 and Parkin. *J Cell Biol,* 206**,** 655-70.

Attwell, D. & Laughlin, S. B. 2001. An energy budget for signaling in the grey matter of the brain. *J Cereb Blood Flow Metab,* 21**,** 1133-45.

Baas, P. W., Deitch, J. S., Black, M. M. & Banker, G. A. 1988. Polarity orientation of microtubules in hippocampal neurons: uniformity in the axon and nonuniformity in the dendrite. *Proc Natl Acad Sci U S A,* 85**,** 8335-9.

Babic, M., Russo, G. J., Wellington, A. J., Sangston, R. M., Gonzalez, M. & Zinsmaier, K. E. 2015. Miro's N-terminal GTPase domain is required for transport of mitochondria into axons and dendrites. *J Neurosci,* 35**,** 5754-71.

Badimon, A., Strasburger, H. J., Ayata, P., Chen, X., Nair, A., Ikegami, A., Hwang, P., Chan, A. T., Graves, S. M., Uweru, J. O., Ledderose, C., Kutlu, M. G., Wheeler, M. A., Kahan, A., Ishikawa, M., Wang, Y. C., Loh, Y. E., Jiang, J. X., Surmeier, D. J., Robson, S. C., Junger, W. G., Sebra, R., Calipari, E. S., Kenny, P. J., Eyo, U. B., Colonna, M., Quintana, F. J., Wake, H., Gradinaru, V. & Schaefer, A. 2020. Negative feedback control of neuronal activity by microglia. *Nature,* 586**,** 417-423.

Balaban, R. S. 2009. The role of Ca($^{2+}$) signaling in the coordination of mitochondrial ATP production with cardiac work. *Biochim Biophys Acta,* 1787**,** 1334-41.

Ballabio, A. & Bonifacino, J. S. 2020. Lysosomes as dynamic regulators of cell and organismal homeostasis. *Nat Rev Mol Cell Biol,* 21**,** 101-118.

Baranov, S. V., Baranova, O. V., Yablonska, S., Suofu, Y., Vazquez, A. L., Kozai, T. D. Y., Cui, X. T., Ferrando, L. M., Larkin, T. M., Tyurina, Y. Y., Kagan, V. E., Carlisle, D. L., Kristal, B. S. & Friedlander, R. M. 2019. Mitochondria modulate programmed neuritic retraction. *Proc Natl Acad Sci U S A,* 116**,** 650-659.

Barodia, S. K., McMeekin, L. J., Creed, R. B., Quinones, E. K., Cowell, R. M. & Goldberg, M. S. 2019. PINK1 phosphorylates ubiquitin predominantly in astrocytes. *NPJ Parkinsons Dis,* 5**,** 29.

Bartolome, F., Wu, H. C., Burchell, V. S., Preza, E., Wray, S., Mahoney, C. J., Fox, N. C., Calvo, A., Canosa, A., Moglia, C., Mandrioli, J., Chio, A., Orrell, R. W., Houlden, H., Hardy, J., Abramov, A. Y. & Plun-Favreau, H. 2013. Pathogenic VCP mutations induce mitochondrial uncoupling and reduced ATP levels. *Neuron,* 78**,** 57-64.

Basso, V., Marchesan, E. & Ziviani, E. 2020. A trio has turned into a quartet: DJ-1 interacts with the IP3R-Grp75-VDAC complex to control ER-mitochondria interaction. *Cell Calcium,* 87**,** 102186.

Becker, N. H., Goldfischer, S., Shin, W. Y. & Novikoff, A. B. 1960. The localization of enzyme activities in the rat brain. *J Biophys Biochem Cytol,* 8**,** 649-63.

Berenguer-Escuder, C., Grossmann, D., Massart, F., Antony, P., Burbulla, L. F., Glaab, E., Imhoff, S., Trinh, J., Seibler, P., Grunewald, A. & Kruger, R. 2019. Variants in Miro1 Cause Alterations of ER-Mitochondria Contact Sites in Fibroblasts from Parkinson's Disease Patients. *J Clin Med,* 8.

Bergami, M. & Motori, E. 2020. Reweaving the Fabric of Mitochondrial Contact Sites in Astrocytes. *Front Cell Dev Biol,* 8**,** 592651.

Bernier, L. P., York, E. M., Kamyabi, A., Choi, H. B., Weilinger, N. L. & MacVicar, B. A. 2020. Microglial metabolic flexibility supports immune surveillance of the brain parenchyma. *Nat Commun,* 11**,** 1559.

Billups, B. & Forsythe, I. D. 2002. Presynaptic mitochondrial calcium sequestration influences transmission at mammalian central synapses. *J Neurosci,* 22**,** 5840-7.

Birsa, N., Norkett, R., Higgs, N., Lopez-Domenech, G. & Kittler, J. T. 2013. Mitochondrial trafficking in neurons and the role of the Miro family of GTPase proteins. *Biochem Soc Trans,* 41**,** 1525-31.

Birsa, N., Norkett, R., Wauer, T., Mevissen, T. E., Wu, H. C., Foltynie, T., Bhatia, K., Hirst, W. D., Komander, D., Plun-Favreau, H. & Kittler, J. T. 2014. Lysine 27 ubiquitination of the mitochondrial transport protein Miro is dependent on serine 65 of the Parkin ubiquitin ligase. *J Biol Chem,* 289**,** 14569-82.

Boeing, S., Williamson, L., Encheva, V., Gori, I., Saunders, R. E., Instrell, R., Aygun, O., Rodriguez-Martinez, M., Weems, J. C., Kelly, G. P., Conaway, J. W., Conaway, R. C., Stewart, A., Howell, M., Snijders, A. P. & Svejstrup, J. Q. 2016. Multiomic Analysis of the UV-Induced DNA Damage Response. *Cell Rep,* 15**,** 1597-1610.

Boitier, E., Rea, R. & Duchen, M. R. 1999. Mitochondria exert a negative feedback on the propagation of intracellular Ca^{2+} waves in rat cortical astrocytes. *J Cell Biol,* 145**,** 795-808.

Brown, G. C., Bolanos, J. P., Heales, S. J. & Clark, J. B. 1995. Nitric oxide produced by activated astrocytes rapidly and reversibly inhibits cellular respiration. *Neurosci Lett,* 193**,** 201-4.

Bruzzone, S., Verderio, C., Schenk, U., Fedele, E., Zocchi, E., Matteoli, M. & De Flora, A. 2004. Glutamate-mediated overexpression of CD38 in astrocytes cultured with neurones. *J Neurochem,* 89**,** 264-72.

Burman, J. L., Pickles, S., Wang, C., Sekine, S., Vargas, J. N. S., Zhang, Z., Youle, A. M., Nezich, C. L., Wu, X., Hammer, J. A. & Youle, R. J. 2017.

Mitochondrial fission facilitates the selective mitophagy of protein aggregates. *J Cell Biol,* 216**,** 3231-3247.

Bushong, E. A., Martone, M. E. & Ellisman, M. H. 2004. Maturation of astrocyte morphology and the establishment of astrocyte domains during postnatal hippocampal development. *Int J Dev Neurosci,* 22**,** 73-86.

Cai, Q., Davis, M. L. & Sheng, Z. H. 2011. Regulation of axonal mitochondrial transport and its impact on synaptic transmission. *Neurosci Res,* 70**,** 9-15.

Cai, Q., Zakaria, H. M., Simone, A. & Sheng, Z. H. 2012. Spatial parkin translocation and degradation of damaged mitochondria via mitophagy in live cortical neurons. *Curr Biol,* 22**,** 545-52.

Celardo, I., Costa, A. C., Lehmann, S., Jones, C., Wood, N., Mencacci, N. E., Mallucci, G. R., Loh, S. H. & Martins, L. M. 2016. Mitofusin-mediated ER stress triggers neurodegeneration in pink1/parkin models of Parkinson's disease. *Cell Death Dis,* 7**,** e2271.

Cha, G. H., Kim, S., Park, J., Lee, E., Kim, M., Lee, S. B., Kim, J. M., Chung, J. & Cho, K. S. 2005. Parkin negatively regulates JNK pathway in the dopaminergic neurons of Drosophila. *Proc Natl Acad Sci U S A,* 102**,** 10345-50.

Chan, N. C., Salazar, A. M., Pham, A. H., Sweredoski, M. J., Kolawa, N. J., Graham, R. L., Hess, S. & Chan, D. C. 2011. Broad activation of the ubiquitin-proteasome system by Parkin is critical for mitophagy. *Hum Mol Genet,* 20**,** 1726-37.

Chang, C. H., Curtis, J. D., Maggi, L. B., Jr., Faubert, B., Villarino, A. V., O'Sullivan, D., Huang, S. C., van der Windt, G. J., Blagih, J., Qiu, J., Weber, J. D., Pearce, E. J., Jones, R. G. & Pearce, E. L. 2013. Posttranscriptional control of T cell effector function by aerobic glycolysis. *Cell,* 153**,** 1239-51.

Chang, D. T., Honick, A. S. & Reynolds, I. J. 2006. Mitochondrial trafficking to synapses in cultured primary cortical neurons. *J Neurosci,* 26**,** 7035-45.

Chaugule, V. K., Burchell, L., Barber, K. R., Sidhu, A., Leslie, S. J., Shaw, G. S. & Walden, H. 2011. Autoregulation of Parkin activity through its ubiquitin-like domain. *EMBO J,* 30**,** 2853-67.

Chen, H., Detmer, S. A., Ewald, A. J., Griffin, E. E., Fraser, S. E. & Chan, D. C. 2003. Mitofusins Mfn1 and Mfn2 coordinately regulate mitochondrial fusion and are essential for embryonic development. *J Cell Biol,* 160**,** 189-200.

Chen, H., McCaffery, J. M. & Chan, D. C. 2007. Mitochondrial fusion protects against neurodegeneration in the cerebellum. *Cell,* 130**,** 548-62.

Chen, Y. & Dorn, G. W., 2nd 2013. PINK1-phosphorylated mitofusin 2 is a Parkin receptor for culling damaged mitochondria. *Science,* 340**,** 471-5.

Chen, Y. & Sheng, Z. H. 2013. Kinesin-1-syntaphilin coupling mediates activity-dependent regulation of axonal mitochondrial transport. *J Cell Biol,* 202**,** 351-64.

Chicurel, M. E. & Harris, K. M. 1992. Three-dimensional analysis of the structure and composition of CA3 branched dendritic spines and their synaptic relationships with mossy fiber boutons in the rat hippocampus. *J Comp Neurol,* 325**,** 169-82.

Choi, I., Choi, D. J., Yang, H., Woo, J. H., Chang, M. Y., Kim, J. Y., Sun, W., Park, S. M., Jou, I., Lee, S. H. & Joe, E. H. 2016. PINK1 expression increases during brain development and stem cell differentiation, and affects the development of GFAP-positive astrocytes. *Mol Brain,* 9**,** 5.

Choi, I., Kim, J., Jeong, H. K., Kim, B., Jou, I., Park, S. M., Chen, L., Kang, U. J., Zhuang, X. & Joe, E. H. 2013. PINK1 deficiency attenuates astrocyte proliferation through mitochondrial dysfunction, reduced AKT and increased p38 MAPK activation, and downregulation of EGFR. *Glia,* 61**,** 800-12.

Chu, C. T., Ji, J., Dagda, R. K., Jiang, J. F., Tyurina, Y. Y., Kapralov, A. A., Tyurin, V. A., Yanamala, N., Shrivastava, I. H., Mohammadyani, D., Wang, K. Z. Q., Zhu, J., Klein-Seetharaman, J., Balasubramanian, K.,

Amoscato, A. A., Borisenko, G., Huang, Z., Gusdon, A. M., Cheikhi, A., Steer, E. K., Wang, R., Baty, C., Watkins, S., Bahar, I., Bayir, H. & Kagan, V. E. 2013. Cardiolipin externalization to the outer mitochondrial membrane acts as an elimination signal for mitophagy in neuronal cells. *Nat Cell Biol,* 15**,** 1197-1205.

Chung, E., Choi, Y., Park, J., Nah, W., Park, J., Jung, Y., Lee, J., Lee, H., Park, S., Hwang, S., Kim, S., Lee, J., Min, D., Jo, J., Kang, S., Jung, M., Lee, P. H., Ruley, H. E. & Jo, D. 2020. Intracellular delivery of Parkin rescues neurons from accumulation of damaged mitochondria and pathological alpha-synuclein. *Sci Adv,* 6**,** eaba1193.

Chung, K. W., Kim, S. B., Park, K. D., Choi, K. G., Lee, J. H., Eun, H. W., Suh, J. S., Hwang, J. H., Kim, W. K., Seo, B. C., Kim, S. H., Son, I. H., Kim, S. M., Sunwoo, I. N. & Choi, B. O. 2006. Early onset severe and late-onset mild Charcot-Marie-Tooth disease with mitofusin 2 (MFN2) mutations. *Brain,* 129**,** 2103-18.

Cioni, J. M., Lin, J. Q., Holtermann, A. V., Koppers, M., Jakobs, M. A. H., Azizi, A., Turner-Bridger, B., Shigeoka, T., Franze, K., Harris, W. A. & Holt, C. E. 2019. Late Endosomes Act as mRNA Translation Platforms and Sustain Mitochondria in Axons. *Cell,* 176**,** 56-72 e15.

Cipolat, S., Martins de Brito, O., Dal Zilio, B. & Scorrano, L. 2004. OPA1 requires mitofusin 1 to promote mitochondrial fusion. *Proc Natl Acad Sci U S A,* 101**,** 15927-32.

Clark, I. E., Dodson, M. W., Jiang, C., Cao, J. H., Huh, J. R., Seol, J. H., Yoo, S. J., Hay, B. A. & Guo, M. 2006. Drosophila pink1 is required for mitochondrial function and interacts genetically with parkin. *Nature,* 441**,** 1162-6.

Cobley, J. N. 2018. Synapse Pruning: Mitochondrial ROS with Their Hands on the Shears. *Bioessays,* 40**,** e1800031.

Cornelissen, T., Vilain, S., Vints, K., Gounko, N., Verstreken, P. & Vandenberghe, W. 2018. Deficiency of parkin and PINK1 impairs age-dependent mitophagy in Drosophila. *Elife,* 7.

Costa-Mattioli, M. & Walter, P. 2020. The integrated stress response: From mechanism to disease. *Science,* 368.

Covill-Cooke, C., Howden, J. H., Birsa, N. & Kittler, J. T. 2018. Ubiquitination at the mitochondria in neuronal health and disease. *Neurochem Int,* 117**,** 55-64.

Covill-Cooke, C., Toncheva, V. S., Drew, J., Birsa, N., Lopez-Domenech, G. & Kittler, J. T. 2020. Peroxisomal fission is modulated by the mitochondrial Rho-GTPases, Miro1 and Miro2. *EMBO Rep,* 21**,** e49865.

Creed, R. B. & Goldberg, M. S. 2018. Analysis of alpha-Synuclein Pathology in PINK1 Knockout Rat Brains. *Front Neurosci,* 12**,** 1034.

Creed, R. B. & Goldberg, M. S. 2020. Enhanced Susceptibility of PINK1 Knockout Rats to alpha-Synuclein Fibrils. *Neuroscience,* 437**,** 64-75.

Cserep, C., Posfai, B., Lenart, N., Fekete, R., Laszlo, Z. I., Lele, Z., Orsolits, B., Molnar, G., Heindl, S., Schwarcz, A. D., Ujvari, K., Kornyei, Z., Toth, K., Szabadits, E., Sperlagh, B., Baranyi, M., Csiba, L., Hortobagyi, T., Magloczky, Z., Martinecz, B., Szabo, G., Erdelyi, F., Szipocs, R., Tamkun, M. M., Gesierich, B., Duering, M., Katona, I., Liesz, A., Tamas, G. & Denes, A. 2020. Microglia monitor and protect neuronal function through specialized somatic purinergic junctions. *Science,* 367**,** 528-537.

Culmsee, C., Michels, S., Scheu, S., Arolt, V., Dannlowski, U. & Alferink, J. 2018. Mitochondria, Microglia, and the Immune System-How Are They Linked in Affective Disorders? *Front Psychiatry,* 9**,** 739.

D'Este, E., Kamin, D., Gottfert, F., El-Hady, A. & Hell, S. W. 2015. STED nanoscopy reveals the ubiquity of subcortical cytoskeleton periodicity in living neurons. *Cell Rep,* 10**,** 1246-51.

Damisah, E. C., Hill, R. A., Rai, A., Chen, F., Rothlin, C. V., Ghosh, S. & Grutzendler, J. 2020. Astrocytes and microglia play orchestrated roles and respect phagocytic territories during neuronal corpse removal in vivo. *Sci Adv,* 6**,** eaba3239.

Danbolt, N. C. 2001. Glutamate uptake. *Prog Neurobiol,* 65**,** 1-105.

Dani, J. W., Chernjavsky, A. & Smith, S. J. 1992. Neuronal activity triggers calcium waves in hippocampal astrocyte networks. *Neuron,* 8**,** 429-40.

Dave, K. D., De Silva, S., Sheth, N. P., Ramboz, S., Beck, M. J., Quang, C., Switzer, R. C., 3rd, Ahmad, S. O., Sunkin, S. M., Walker, D., Cui, X., Fisher, D. A., McCoy, A. M., Gamber, K., Ding, X., Goldberg, M. S., Benkovic, S. A., Haupt, M., Baptista, M. A., Fiske, B. K., Sherer, T. B. & Frasier, M. A. 2014. Phenotypic characterization of recessive gene knockout rat models of Parkinson's disease. *Neurobiol Dis,* 70**,** 190-203.

Davies, V. J., Hollins, A. J., Piechota, M. J., Yip, W., Davies, J. R., White, K. E., Nicols, P. P., Boulton, M. E. & Votruba, M. 2007. Opa1 deficiency in a mouse model of autosomal dominant optic atrophy impairs mitochondrial morphology, optic nerve structure and visual function. *Hum Mol Genet,* 16**,** 1307-18.

Davis, A. F. & Clayton, D. A. 1996. In situ localization of mitochondrial DNA replication in intact mammalian cells. *J Cell Biol,* 135**,** 883-93.

Davis, C. H., Kim, K. Y., Bushong, E. A., Mills, E. A., Boassa, D., Shih, T., Kinebuchi, M., Phan, S., Zhou, Y., Bihlmeyer, N. A., Nguyen, J. V., Jin, Y., Ellisman, M. H. & Marsh-Armstrong, N. 2014. Transcellular degradation of axonal mitochondria. *Proc Natl Acad Sci U S A,* 111**,** 9633-8.

de Brito, O. M. & Scorrano, L. 2008. Mitofusin 2 tethers endoplasmic reticulum to mitochondria. *Nature,* 456**,** 605-10.

De Vos, K. J., Morotz, G. M., Stoica, R., Tudor, E. L., Lau, K. F., Ackerley, S., Warley, A., Shaw, C. E. & Miller, C. C. 2012. VAPB interacts with the mitochondrial protein PTPIP51 to regulate calcium homeostasis. *Hum Mol Genet,* 21**,** 1299-311.

Delettre, C., Lenaers, G., Griffoin, J. M., Gigarel, N., Lorenzo, C., Belenguer, P., Pelloquin, L., Grosgeorge, J., Turc-Carel, C., Perret, E., Astarie-Dequeker, C., Lasquellec, L., Arnaud, B., Ducommun, B., Kaplan, J. &

Hamel, C. P. 2000. Nuclear gene OPA1, encoding a mitochondrial dynamin-related protein, is mutated in dominant optic atrophy. *Nat Genet,* 26**,** 207-10.

Denton, R. M. 2009. Regulation of mitochondrial dehydrogenases by calcium ions. *Biochim Biophys Acta,* 1787**,** 1309-16.

Denton, R. M., Randle, P. J. & Martin, B. R. 1972. Stimulation by calcium ions of pyruvate dehydrogenase phosphate phosphatase. *Biochem J,* 128**,** 161-3.

Derouiche, A., Haseleu, J. & Korf, H. W. 2015. Fine Astrocyte Processes Contain Very Small Mitochondria: Glial Oxidative Capability May Fuel Transmitter Metabolism. *Neurochem Res,* 40**,** 2402-13.

Devine, M. J., Birsa, N. & Kittler, J. T. 2016. Miro sculpts mitochondrial dynamics in neuronal health and disease. *Neurobiol Dis,* 90**,** 27-34.

Devine, M. J. & Kittler, J. T. 2018. Mitochondria at the neuronal presynapse in health and disease. *Nat Rev Neurosci,* 19**,** 63-80.

Dickey, A. S. & Strack, S. 2011. PKA/AKAP1 and PP2A/Bbeta2 regulate neuronal morphogenesis via Drp1 phosphorylation and mitochondrial bioenergetics. *J Neurosci,* 31**,** 15716-26.

Disatnik, M. H., Joshi, A. U., Saw, N. L., Shamloo, M., Leavitt, B. R., Qi, X. & Mochly-Rosen, D. 2016. Potential biomarkers to follow the progression and treatment response of Huntington's disease. *J Exp Med,* 213**,** 2655-2669.

Dityatev, A. & Rusakov, D. A. 2011. Molecular signals of plasticity at the tetrapartite synapse. *Curr Opin Neurobiol,* 21**,** 353-9.

Divakaruni, S. S., Van Dyke, A. M., Chandra, R., LeGates, T. A., Contreras, M., Dharmasri, P. A., Higgs, H. N., Lobo, M. K., Thompson, S. M. & Blanpied, T. A. 2018. Long-Term Potentiation Requires a Rapid Burst of Dendritic Mitochondrial Fission during Induction. *Neuron,* 100**,** 860-875 e7.

Doxaki, C. & Palikaras, K. 2020. Neuronal Mitophagy: Friend or Foe? *Front Cell Dev Biol,* 8**,** 611938.

El Fissi, N., Rojo, M., Aouane, A., Karatas, E., Poliacikova, G., David, C., Royet, J. & Rival, T. 2018. Mitofusin gain and loss of function drive pathogenesis in Drosophila models of CMT2A neuropathy. *EMBO Rep,* 19.

English, K., Shepherd, A., Uzor, N. E., Trinh, R., Kavelaars, A. & Heijnen, C. J. 2020. Astrocytes rescue neuronal health after cisplatin treatment through mitochondrial transfer. *Acta Neuropathol Commun,* 8**,** 36.

Enright, H. A., Lam, D., Sebastian, A., Sales, A. P., Cadena, J., Hum, N. R., Osburn, J. J., Peters, S. K. G., Petkus, B., Soscia, D. A., Kulp, K. S., Loots, G. G., Wheeler, E. K. & Fischer, N. O. 2020. Functional and transcriptional characterization of complex neuronal co-cultures. *Sci Rep,* 10**,** 11007.

Erturk, A., Wang, Y. & Sheng, M. 2014. Local pruning of dendrites and spines by caspase-3-dependent and proteasome-limited mechanisms. *J Neurosci,* 34**,** 1672-88.

Evans, C. S. & Holzbaur, E. L. 2020. Degradation of engulfed mitochondria is rate-limiting in Optineurin-mediated mitophagy in neurons. *Elife,* 9.

Evans, C. S. & Holzbaur, E. L. F. 2019. Autophagy and mitophagy in ALS. *Neurobiol Dis,* 122**,** 35-40.

Faits, M. C., Zhang, C., Soto, F. & Kerschensteiner, D. 2016. Dendritic mitochondria reach stable positions during circuit development. *Elife,* 5**,** e11583.

Farfel-Becker, T., Roney, J. C., Cheng, X. T., Li, S., Cuddy, S. R. & Sheng, Z. H. 2019. Neuronal Soma-Derived Degradative Lysosomes Are Continuously Delivered to Distal Axons to Maintain Local Degradation Capacity. *Cell Rep,* 28**,** 51-64 e4.

Fecher, C., Trovo, L., Muller, S. A., Snaidero, N., Wettmarshausen, J., Heink, S., Ortiz, O., Wagner, I., Kuhn, R., Hartmann, J., Karl, R. M., Konnerth, A., Korn, T., Wurst, W., Merkler, D., Lichtenthaler, S. F., Perocchi, F. & Misgeld, T. 2019. Cell-type-specific profiling of brain mitochondria reveals functional and molecular diversity. *Nat Neurosci,* 22**,** 1731-1742.

Feely, S. M., Laura, M., Siskind, C. E., Sottile, S., Davis, M., Gibbons, V. S., Reilly, M. M. & Shy, M. E. 2011. MFN2 mutations cause severe phenotypes in most patients with CMT2A. *Neurology,* 76**,** 1690-6.

Felber, S. M. & Brand, M. D. 1982. Valinomycin Can Depolarize Mitochondria in Intact Lymphocytes without Increasing Plasma-Membrane Potassium Fluxes. *Febs Letters,* 150**,** 122-124.

Ferree, A. & Shirihai, O. 2012. Mitochondrial dynamics: the intersection of form and function. *Adv Exp Med Biol,* 748**,** 13-40.

Fessler, E., Eckl, E. M., Schmitt, S., Mancilla, I. A., Meyer-Bender, M. F., Hanf, M., Philippou-Massier, J., Krebs, S., Zischka, H. & Jae, L. T. 2020. A pathway coordinated by DELE1 relays mitochondrial stress to the cytosol. *Nature,* 579**,** 433-437.

Fields, R. D. & Stevens-Graham, B. 2002. New insights into neuron-glia communication. *Science,* 298**,** 556-62.

Fiesel, F. C. & Springer, W. 2015. Disease relevance of phosphorylated ubiquitin (p-S65-Ub). *Autophagy,* 11**,** 2125-2126.

Filichia, E., Hoffer, B., Qi, X. & Luo, Y. 2016. Inhibition of Drp1 mitochondrial translocation provides neural protection in dopaminergic system in a Parkinson's disease model induced by MPTP. *Sci Rep,* 6**,** 32656.

Fransson, A., Ruusala, A. & Aspenstrom, P. 2003. Atypical Rho GTPases have roles in mitochondrial homeostasis and apoptosis. *J Biol Chem,* 278**,** 6495-502.

Fransson, S., Ruusala, A. & Aspenstrom, P. 2006. The atypical Rho GTPases Miro-1 and Miro-2 have essential roles in mitochondrial trafficking. *Biochem Biophys Res Commun,* 344**,** 500-10.

Freitag, H., Janes, M. & Neupert, W. 1982. Biosynthesis of mitochondrial porin and insertion into the outer mitochondrial membrane of Neurospora crassa. *Eur J Biochem,* 126**,** 197-202.

Fukumitsu, K., Fujishima, K., Yoshimura, A., Wu, Y. K., Heuser, J. & Kengaku, M. 2015. Synergistic action of dendritic mitochondria and creatine kinase maintains ATP homeostasis and actin dynamics in growing neuronal dendrites. *J Neurosci,* 35**,** 5707-23.

Ganjam, G. K., Bolte, K., Matschke, L. A., Neitemeier, S., Dolga, A. M., Hollerhage, M., Hoglinger, G. U., Adamczyk, A., Decher, N., Oertel, W. H. & Culmsee, C. 2019. Mitochondrial damage by alpha-synuclein causes cell death in human dopaminergic neurons. *Cell Death Dis,* 10**,** 865.

Ganley, I. G., Whitworth, A. J. & McWilliams, T. G. 2021. Comment on "mt-Keima detects PINK1-PRKN mitophagy in vivo with greater sensitivity than mito-QC". *Autophagy***,** 1-3.

Gao, L., Zhang, Z., Lu, J. & Pei, G. 2019. Mitochondria Are Dynamically Transferring Between Human Neural Cells and Alexander Disease-Associated GFAP Mutations Impair the Astrocytic Transfer. *Front Cell Neurosci,* 13**,** 316.

Gegg, M. E., Cooper, J. M., Chau, K. Y., Rojo, M., Schapira, A. H. & Taanman, J. W. 2010. Mitofusin 1 and mitofusin 2 are ubiquitinated in a PINK1/parkin-dependent manner upon induction of mitophagy. *Hum Mol Genet,* 19**,** 4861-70.

Geisler, S., Holmstrom, K. M., Skujat, D., Fiesel, F. C., Rothfuss, O. C., Kahle, P. J. & Springer, W. 2010. PINK1/Parkin-mediated mitophagy is dependent on VDAC1 and p62/SQSTM1. *Nat Cell Biol,* 12**,** 119-31.

Gerber, S., Charif, M., Chevrollier, A., Chaumette, T., Angebault, C., Kane, M. S., Paris, A., Alban, J., Quiles, M., Delettre, C., Bonneau, D., Procaccio,

V., Amati-Bonneau, P., Reynier, P., Leruez, S., Calmon, R., Boddaert, N., Funalot, B., Rio, M., Bouccara, D., Meunier, I., Sesaki, H., Kaplan, J., Hamel, C. P., Rozet, J. M. & Lenaers, G. 2017. Mutations in DNM1L, as in OPA1, result in dominant optic atrophy despite opposite effects on mitochondrial fusion and fission. *Brain,* 140**,** 2586-2596.

Ghosh, S., Castillo, E., Frias, E. S. & Swanson, R. A. 2018. Bioenergetic regulation of microglia. *Glia,* 66**,** 1200-1212.

Giacomello, M. & Pellegrini, L. 2016. The coming of age of the mitochondria-ER contact: a matter of thickness. *Cell Death Differ,* 23**,** 1417-27.

Giguere, N., Burke Nanni, S. & Trudeau, L. E. 2018. On Cell Loss and Selective Vulnerability of Neuronal Populations in Parkinson's Disease. *Front Neurol,* 9**,** 455.

Gimeno-Bayon, J., Lopez-Lopez, A., Rodriguez, M. J. & Mahy, N. 2014. Glucose pathways adaptation supports acquisition of activated microglia phenotype. *J Neurosci Res,* 92**,** 723-31.

Gispert, S., Brehm, N., Weil, J., Seidel, K., Rub, U., Kern, B., Walter, M., Roeper, J. & Auburger, G. 2015. Potentiation of neurotoxicity in double-mutant mice with Pink1 ablation and A53T-SNCA overexpression. *Hum Mol Genet,* 24**,** 1061-76.

Glancy, B. & Balaban, R. S. 2012. Role of mitochondrial Ca^{2+} in the regulation of cellular energetics. *Biochemistry,* 51**,** 2959-73.

Glater, E. E., Megeath, L. J., Stowers, R. S. & Schwarz, T. L. 2006. Axonal transport of mitochondria requires milton to recruit kinesin heavy chain and is light chain independent. *J Cell Biol,* 173**,** 545-57.

Glauser, L., Sonnay, S., Stafa, K. & Moore, D. J. 2011. Parkin promotes the ubiquitination and degradation of the mitochondrial fusion factor mitofusin 1. *J Neurochem,* 118**,** 636-45.

Gogvadze, V., Zhivotovsky, B. & Orrenius, S. 2010. The Warburg effect and mitochondrial stability in cancer cells. *Mol Aspects Med,* 31**,** 60-74.

Goldberg, M. S., Fleming, S. M., Palacino, J. J., Cepeda, C., Lam, H. A., Bhatnagar, A., Meloni, E. G., Wu, N., Ackerson, L. C., Klapstein, G. J., Gajendiran, M., Roth, B. L., Chesselet, M. F., Maidment, N. T., Levine, M. S. & Shen, J. 2003. Parkin-deficient mice exhibit nigrostriatal deficits but not loss of dopaminergic neurons. *J Biol Chem,* 278**,** 43628-35.

Gomez-Suaga, P., Perez-Nievas, B. G., Glennon, E. B., Lau, D. H. W., Paillusson, S., Morotz, G. M., Cali, T., Pizzo, P., Noble, W. & Miller, C. C. J. 2019. The VAPB-PTPIP51 endoplasmic reticulum-mitochondria tethering proteins are present in neuronal synapses and regulate synaptic activity. *Acta Neuropathol Commun,* 7**,** 35.

Gong, G., Song, M., Csordas, G., Kelly, D. P., Matkovich, S. J. & Dorn, G. W., 2nd 2015. Parkin-mediated mitophagy directs perinatal cardiac metabolic maturation in mice. *Science,* 350**,** aad2459.

Gordaliza-Alaguero, I., Canto, C. & Zorzano, A. 2019. Metabolic implications of organelle-mitochondria communication. *EMBO Rep,* 20**,** e47928.

Grohm, J., Kim, S. W., Mamrak, U., Tobaben, S., Cassidy-Stone, A., Nunnari, J., Plesnila, N. & Culmsee, C. 2012. Inhibition of Drp1 provides neuroprotection in vitro and in vivo. *Cell Death Differ,* 19**,** 1446-58.

Grossmann, D., Berenguer-Escuder, C., Bellet, M. E., Scheibner, D., Bohler, J., Massart, F., Rapaport, D., Skupin, A., Fouquier d'Herouel, A., Sharma, M., Ghelfi, J., Rakovic, A., Lichtner, P., Antony, P., Glaab, E., May, P., Dimmer, K. S., Fitzgerald, J. C., Grunewald, A. & Kruger, R. 2019. Mutations in RHOT1 Disrupt Endoplasmic Reticulum-Mitochondria Contact Sites Interfering with Calcium Homeostasis and Mitochondrial Dynamics in Parkinson's Disease. *Antioxid Redox Signal,* 31**,** 1213-1234.

Grossmann, D., Berenguer-Escuder, C., Chemla, A., Arena, G. & Kruger, R. 2020. The Emerging Role of RHOT1/Miro1 in the Pathogenesis of Parkinson's Disease. *Front Neurol,* 11**,** 587.

Guo, X., Aviles, G., Liu, Y., Tian, R., Unger, B. A., Lin, Y. T., Wiita, A. P., Xu, K., Correia, M. A. & Kampmann, M. 2020. Mitochondrial stress is relayed to the cytosol by an OMA1-DELE1-HRI pathway. *Nature,* 579**,** 427-432.

Guo, X., Disatnik, M. H., Monbureau, M., Shamloo, M., Mochly-Rosen, D. & Qi, X. 2013. Inhibition of mitochondrial fragmentation diminishes Huntington's disease-associated neurodegeneration. *J Clin Invest,* 123**,** 5371-88.

Guo, X., Macleod, G. T., Wellington, A., Hu, F., Panchumarthi, S., Schoenfield, M., Marin, L., Charlton, M. P., Atwood, H. L. & Zinsmaier, K. E. 2005. The GTPase dMiro is required for axonal transport of mitochondria to Drosophila synapses. *Neuron,* 47**,** 379-93.

Gyorffy, B. A., Kun, J., Torok, G., Bulyaki, E., Borhegyi, Z., Gulyassy, P., Kis, V., Szocsics, P., Micsonai, A., Matko, J., Drahos, L., Juhasz, G., Kekesi, K. A. & Kardos, J. 2018. Local apoptotic-like mechanisms underlie complement-mediated synaptic pruning. *Proc Natl Acad Sci U S A,* 115**,** 6303-6308.

Halassa, M. M., Fellin, T., Takano, H., Dong, J. H. & Haydon, P. G. 2007. Synaptic islands defined by the territory of a single astrocyte. *J Neurosci,* 27**,** 6473-7.

Hall, C. N., Klein-Flugge, M. C., Howarth, C. & Attwell, D. 2012. Oxidative phosphorylation, not glycolysis, powers presynaptic and postsynaptic mechanisms underlying brain information processing. *J Neurosci,* 32**,** 8940-51.

Halliday, M. & Mallucci, G. R. 2015. Review: Modulating the unfolded protein response to prevent neurodegeneration and enhance memory. *Neuropathol Appl Neurobiol,* 41**,** 414-27.

Han, Y., Li, M., Qiu, F., Zhang, M. & Zhang, Y. H. 2017. Cell-permeable organic fluorescent probes for live-cell long-term super-resolution imaging reveal lysosome-mitochondrion interactions. *Nat Commun,* 8**,** 1307.

Harland, M., Torres, S., Liu, J. & Wang, X. 2020. Neuronal Mitochondria Modulation of LPS-Induced Neuroinflammation. *J Neurosci,* 40**,** 1756-1765.

Harris, J. J., Jolivet, R. & Attwell, D. 2012. Synaptic energy use and supply. *Neuron,* 75**,** 762-77.

Hasel, P., Dando, O., Jiwaji, Z., Baxter, P., Todd, A. C., Heron, S., Markus, N. M., McQueen, J., Hampton, D. W., Torvell, M., Tiwari, S. S., McKay, S., Eraso-Pichot, A., Zorzano, A., Masgrau, R., Galea, E., Chandran, S., Wyllie, D. J. A., Simpson, T. I. & Hardingham, G. E. 2017. Neurons and neuronal activity control gene expression in astrocytes to regulate their development and metabolism. *Nat Commun,* 8**,** 15132.

Hayakawa, K., Esposito, E., Wang, X., Terasaki, Y., Liu, Y., Xing, C., Ji, X. & Lo, E. H. 2016. Transfer of mitochondria from astrocytes to neurons after stroke. *Nature,* 535**,** 551-5.

Henrichs, V., Grycova, L., Barinka, C., Nahacka, Z., Neuzil, J., Diez, S., Rohlena, J., Braun, M. & Lansky, Z. 2020. Mitochondria-adaptor TRAK1 promotes kinesin-1 driven transport in crowded environments. *Nat Commun,* 11**,** 3123.

Heo, J. M., Harper, N. J., Paulo, J. A., Li, M., Xu, Q., Coughlin, M., Elledge, S. J. & Harper, J. W. 2019. Integrated proteogenetic analysis reveals the landscape of a mitochondrial-autophagosome synapse during PARK2-dependent mitophagy. *Sci Adv,* 5**,** eaay4624.

Herrero-Mendez, A., Almeida, A., Fernandez, E., Maestre, C., Moncada, S. & Bolanos, J. P. 2009. The bioenergetic and antioxidant status of neurons is controlled by continuous degradation of a key glycolytic enzyme by APC/C-Cdh1. *Nat Cell Biol,* 11**,** 747-52.

Hertz, L., Peng, L. & Dienel, G. A. 2007. Energy metabolism in astrocytes: high rate of oxidative metabolism and spatiotemporal dependence on glycolysis/glycogenolysis. *J Cereb Blood Flow Metab,* 27**,** 219-49.

Hirokawa, N. & Takemura, R. 2005. Molecular motors and mechanisms of directional transport in neurons. *Nat Rev Neurosci,* 6**,** 201-14.

Hollenbeck, P. J. 1993. Products of endocytosis and autophagy are retrieved from axons by regulated retrograde organelle transport. *J Cell Biol,* 121**,** 305-15.

Hoshino, A., Wang, W. J., Wada, S., McDermott-Roe, C., Evans, C. S., Gosis, B., Morley, M. P., Rathi, K. S., Li, J., Li, K., Yang, S., McManus, M. J., Bowman, C., Potluri, P., Levin, M., Damrauer, S., Wallace, D. C., Holzbaur, E. L. F. & Arany, Z. 2019. The ADP/ATP translocase drives mitophagy independent of nucleotide exchange. *Nature,* 575**,** 375-379.

Hou, X., Fiesel, F. C., Truban, D., Castanedes Casey, M., Lin, W. L., Soto, A. I., Tacik, P., Rousseau, L. G., Diehl, N. N., Heckman, M. G., Lorenzo-Betancor, O., Ferrer, I., Arbelo, J. M., Steele, J. C., Farrer, M. J., Cornejo-Olivas, M., Torres, L., Mata, I. F., Graff-Radford, N. R., Wszolek, Z. K., Ross, O. A., Murray, M. E., Dickson, D. W. & Springer, W. 2018. Age- and disease-dependent increase of the mitophagy marker phospho-ubiquitin in normal aging and Lewy body disease. *Autophagy,* 14**,** 1404-1418.

Houlden, H. & Singleton, A. B. 2012. The genetics and neuropathology of Parkinson's disease. *Acta Neuropathol,* 124**,** 325-38.

Hsieh, C. H., Li, L., Vanhauwaert, R., Nguyen, K. T., Davis, M. D., Bu, G., Wszolek, Z. K. & Wang, X. 2019. Miro1 Marks Parkinson's Disease Subset and Miro1 Reducer Rescues Neuron Loss in Parkinson's Models. *Cell Metab,* 30**,** 1131-1140 e7.

Hsieh, C. H., Shaltouki, A., Gonzalez, A. E., Bettencourt da Cruz, A., Burbulla, L. F., St Lawrence, E., Schule, B., Krainc, D., Palmer, T. D. & Wang, X. 2016. Functional Impairment in Miro Degradation and Mitophagy Is a Shared Feature in Familial and Sporadic Parkinson's Disease. *Cell Stem Cell,* 19**,** 709-724.

Ishihara, N., Eura, Y. & Mihara, K. 2004. Mitofusin 1 and 2 play distinct roles in mitochondrial fusion reactions via GTPase activity. *J Cell Sci,* 117**,** 6535-46.

Ishihara, N., Nomura, M., Jofuku, A., Kato, H., Suzuki, S. O., Masuda, K., Otera, H., Nakanishi, Y., Nonaka, I., Goto, Y., Taguchi, N., Morinaga, H., Maeda, M., Takayanagi, R., Yokota, S. & Mihara, K. 2009. Mitochondrial fission factor Drp1 is essential for embryonic development and synapse formation in mice. *Nat Cell Biol,* 11**,** 958-66.

Itoh, K., Nakamura, K., Iijima, M. & Sesaki, H. 2013. Mitochondrial dynamics in neurodegeneration. *Trends Cell Biol,* 23**,** 64-71.

Jackson, J. G., O'Donnell, J. C., Takano, H., Coulter, D. A. & Robinson, M. B. 2014. Neuronal activity and glutamate uptake decrease mitochondrial mobility in astrocytes and position mitochondria near glutamate transporters. *J Neurosci,* 34**,** 1613-24.

Jackson, J. G. & Robinson, M. B. 2015. Reciprocal Regulation of Mitochondrial Dynamics and Calcium Signaling in Astrocyte Processes. *J Neurosci,* 35**,** 15199-213.

Jackson, J. G. & Robinson, M. B. 2018. Regulation of mitochondrial dynamics in astrocytes: Mechanisms, consequences, and unknowns. *Glia,* 66**,** 1213-1234.

Jahn, R. & Fasshauer, D. 2012. Molecular machines governing exocytosis of synaptic vesicles. *Nature,* 490**,** 201-7.

Joselin, A. P., Hewitt, S. J., Callaghan, S. M., Kim, R. H., Chung, Y. H., Mak, T. W., Shen, J., Slack, R. S. & Park, D. S. 2012. ROS-dependent regulation of Parkin and DJ-1 localization during oxidative stress in neurons. *Hum Mol Genet,* 21**,** 4888-903.

Joshi, A. U., Minhas, P. S., Liddelow, S. A., Haileselassie, B., Andreasson, K. I., Dorn, G. W., 2nd & Mochly-Rosen, D. 2019. Fragmented mitochondria released from microglia trigger A1 astrocytic response and propagate inflammatory neurodegeneration. *Nat Neurosci,* 22**,** 1635-1648.

Joshi, A. U., Saw, N. L., Vogel, H., Cunnigham, A. D., Shamloo, M. & Mochly-Rosen, D. 2018. Inhibition of Drp1/Fis1 interaction slows progression of amyotrophic lateral sclerosis. *EMBO Mol Med,* 10.

Kageyama, Y., Hoshijima, M., Seo, K., Bedja, D., Sysa-Shah, P., Andrabi, S. A., Chen, W., Hoke, A., Dawson, V. L., Dawson, T. M., Gabrielson, K., Kass, D. A., Iijima, M. & Sesaki, H. 2014. Parkin-independent mitophagy requires Drp1 and maintains the integrity of mammalian heart and brain. *EMBO J,* 33**,** 2798-813.

Kageyama, Y., Zhang, Z., Roda, R., Fukaya, M., Wakabayashi, J., Wakabayashi, N., Kensler, T. W., Reddy, P. H., Iijima, M. & Sesaki, H. 2012. Mitochondrial division ensures the survival of postmitotic neurons by suppressing oxidative damage. *J Cell Biol,* 197**,** 535-51.

Kane, L. A., Lazarou, M., Fogel, A. I., Li, Y., Yamano, K., Sarraf, S. A., Banerjee, S. & Youle, R. J. 2014. PINK1 phosphorylates ubiquitin to activate Parkin E3 ubiquitin ligase activity. *J Cell Biol,* 205**,** 143-53.

Kang, J. S., Tian, J. H., Pan, P. Y., Zald, P., Li, C., Deng, C. & Sheng, Z. H. 2008. Docking of axonal mitochondria by syntaphilin controls their mobility and affects short-term facilitation. *Cell,* 132**,** 137-48.

Kano, M., Takanashi, M., Oyama, G., Yoritaka, A., Hatano, T., Shiba-Fukushima, K., Nagai, M., Nishiyama, K., Hasegawa, K., Inoshita, T., Ishikawa, K. I., Akamatsu, W., Imai, Y., Bolognin, S., Schwamborn, J. C. & Hattori, N. 2020. Reduced astrocytic reactivity in human brains and midbrain organoids with PRKN mutations. *NPJ Parkinsons Dis,* 6**,** 33.

Karcher, R. L., Deacon, S. W. & Gelfand, V. I. 2002. Motor-cargo interactions: the key to transport specificity. *Trends Cell Biol,* 12**,** 21-7.

Kasthuri, N., Hayworth, K. J., Berger, D. R., Schalek, R. L., Conchello, J. A., Knowles-Barley, S., Lee, D., Vazquez-Reina, A., Kaynig, V., Jones, T. R., Roberts, M., Morgan, J. L., Tapia, J. C., Seung, H. S., Roncal, W. G., Vogelstein, J. T., Burns, R., Sussman, D. L., Priebe, C. E., Pfister, H. & Lichtman, J. W. 2015. Saturated Reconstruction of a Volume of Neocortex. *Cell,* 162**,** 648-61.

Katayama, H., Hama, H., Nagasawa, K., Kurokawa, H., Sugiyama, M., Ando, R., Funata, M., Yoshida, N., Homma, M., Nishimura, T., Takahashi, M., Ishida, Y., Hioki, H., Tsujihata, Y. & Miyawaki, A. 2020. Visualizing and Modulating Mitophagy for Therapeutic Studies of Neurodegeneration. *Cell,* 181**,** 1176-1187 e16.

Katayama, H., Kogure, T., Mizushima, N., Yoshimori, T. & Miyawaki, A. 2011. A sensitive and quantitative technique for detecting autophagic events based on lysosomal delivery. *Chem Biol,* 18**,** 1042-52.

Katoh, M., Wu, B., Nguyen, H. B., Thai, T. Q., Yamasaki, R., Lu, H., Rietsch, A. M., Zorlu, M. M., Shinozaki, Y., Saitoh, Y., Saitoh, S., Sakoh, T., Ikenaka, K., Koizumi, S., Ransohoff, R. M. & Ohno, N. 2017. Polymorphic regulation of mitochondrial fission and fusion modifies phenotypes of microglia in neuroinflammation. *Sci Rep,* 7**,** 4942.

Kazlauskaite, A., Kelly, V., Johnson, C., Baillie, C., Hastie, C. J., Peggie, M., Macartney, T., Woodroof, H. I., Alessi, D. R., Pedrioli, P. G. & Muqit, M. M. 2014. Phosphorylation of Parkin at Serine65 is essential for activation: elaboration of a Miro1 substrate-based assay of Parkin E3 ligase activity. *Open Biol,* 4**,** 130213.

Kenwood, B. M., Weaver, J. L., Bajwa, A., Poon, I. K., Byrne, F. L., Murrow, B. A., Calderone, J. A., Huang, L., Divakaruni, A. S., Tomsig, J. L., Okabe, K., Lo, R. H., Cameron Coleman, G., Columbus, L., Yan, Z., Saucerman, J. J., Smith, J. S., Holmes, J. W., Lynch, K. R., Ravichandran, K. S., Uchiyama, S., Santos, W. L., Rogers, G. W., Okusa, M. D., Bayliss, D. A. & Hoehn, K. L. 2014. Identification of a novel mitochondrial uncoupler that does not depolarize the plasma membrane. *Mol Metab,* 3**,** 114-23.

Kerr, J. S., Adriaanse, B. A., Greig, N. H., Mattson, M. P., Cader, M. Z., Bohr, V. A. & Fang, E. F. 2017. Mitophagy and Alzheimer's Disease: Cellular and Molecular Mechanisms. *Trends Neurosci,* 40**,** 151-166.

Kettenmann, H. & Verkhratsky, A. 2008. Neuroglia: the 150 years after. *Trends Neurosci,* 31**,** 653-9.

Kety, S. S. 1963. The circulation and energy metabolism of the brain. *Clin Neurosurg,* 9**,** 56-66.

Khalil, B., El Fissi, N., Aouane, A., Cabirol-Pol, M. J., Rival, T. & Lievens, J. C. 2015. PINK1-induced mitophagy promotes neuroprotection in Huntington's disease. *Cell Death Dis,* 6**,** e1617.

Kim, S., Wong, Y. C., Gao, F. & Krainc, D. 2021. Dysregulation of mitochondria-lysosome contacts by GBA1 dysfunction in dopaminergic neuronal models of Parkinson's disease. *Nat Commun,* 12**,** 1807.

Kirichok, Y., Krapivinsky, G. & Clapham, D. E. 2004. The mitochondrial calcium uniporter is a highly selective ion channel. *Nature,* 427**,** 360-4.

Kitada, T., Asakawa, S., Hattori, N., Matsumine, H., Yamamura, Y., Minoshima, S., Yokochi, M., Mizuno, Y. & Shimizu, N. 1998. Mutations in the parkin gene cause autosomal recessive juvenile parkinsonism. *Nature,* 392**,** 605-8.

Kitada, T., Pisani, A., Karouani, M., Haburcak, M., Martella, G., Tscherter, A., Platania, P., Wu, B., Pothos, E. N. & Shen, J. 2009. Impaired dopamine release and synaptic plasticity in the striatum of parkin-/- mice. *J Neurochem,* 110**,** 613-21.

Kitada, T., Pisani, A., Porter, D. R., Yamaguchi, H., Tscherter, A., Martella, G., Bonsi, P., Zhang, C., Pothos, E. N. & Shen, J. 2007. Impaired dopamine release and synaptic plasticity in the striatum of PINK1-deficient mice. *Proc Natl Acad Sci U S A,* 104**,** 11441-6.

Klosowiak, J. L., Park, S., Smith, K. P., French, M. E., Focia, P. J., Freymann, D. M. & Rice, S. E. 2016. Structural insights into Parkin substrate lysine targeting from minimal Miro substrates. *Sci Rep,* 6**,** 33019.

Knott, A. B., Perkins, G., Schwarzenbacher, R. & Bossy-Wetzel, E. 2008. Mitochondrial fragmentation in neurodegeneration. *Nat Rev Neurosci,* 9**,** 505-18.

Kondapalli, C., Kazlauskaite, A., Zhang, N., Woodroof, H. I., Campbell, D. G., Gourlay, R., Burchell, L., Walden, H., Macartney, T. J., Deak, M., Knebel, A., Alessi, D. R. & Muqit, M. M. 2012. PINK1 is activated by mitochondrial membrane potential depolarization and stimulates Parkin E3 ligase activity by phosphorylating Serine 65. *Open Biol,* 2**,** 120080.

Kornmann, B., Osman, C. & Walter, P. 2011. The conserved GTPase Gem1 regulates endoplasmic reticulum-mitochondria connections. *Proc Natl Acad Sci U S A,* 108**,** 14151-6.

Kraus, F., Roy, K., Pucadyil, T. J. & Ryan, M. T. 2021. Function and regulation of the divisome for mitochondrial fission. *Nature,* 590**,** 57-66.

Kremneva, E., Kislin, M., Kang, X. Y. & Khiroug, L. 2013. Motility of astrocytic mitochondria is arrested by Ca^{2+}-dependent interaction between mitochondria and actin filaments. *Cell Calcium,* 53**,** 85-93.

Kuzniewska, B., Cysewski, D., Wasilewski, M., Sakowska, P., Milek, J., Kulinski, T. M., Winiarski, M., Kozielewicz, P., Knapska, E., Dadlez, M., Chacinska, A., Dziembowski, A. & Dziembowska, M. 2020. Mitochondrial protein biogenesis in the synapse is supported by local translation. *EMBO Rep,* 21**,** e48882.

Kwon, S. K., Sando, R., 3rd, Lewis, T. L., Hirabayashi, Y., Maximov, A. & Polleux, F. 2016. LKB1 Regulates Mitochondria-Dependent Presynaptic Calcium Clearance and Neurotransmitter Release Properties at Excitatory Synapses along Cortical Axons. *PLoS Biol,* 14**,** e1002516.

Lauro, C. & Limatola, C. 2020. Metabolic Reprograming of Microglia in the Regulation of the Innate Inflammatory Response. *Front Immunol,* 11**,** 493.

Lawson, L. J., Perry, V. H. & Gordon, S. 1992. Turnover of resident microglia in the normal adult mouse brain. *Neuroscience,* 48**,** 405-15.

Lazarou, M., Sliter, D. A., Kane, L. A., Sarraf, S. A., Wang, C., Burman, J. L., Sideris, D. P., Fogel, A. I. & Youle, R. J. 2015. The ubiquitin kinase PINK1 recruits autophagy receptors to induce mitophagy. *Nature,* 524**,** 309-314.

Ledesma, M. D., Galvan, C., Hellias, B., Dotti, C. & Jensen, P. H. 2002. Astrocytic but not neuronal increased expression and redistribution of parkin during unfolded protein stress. *J Neurochem,* 83**,** 1431-40.

Lee, J. E., Westrate, L. M., Wu, H., Page, C. & Voeltz, G. K. 2016a. Multiple dynamin family members collaborate to drive mitochondrial division. *Nature,* 540**,** 139-143.

Lee, J. J., Sanchez-Martinez, A., Martinez Zarate, A., Beninca, C., Mayor, U., Clague, M. J. & Whitworth, A. J. 2018. Basal mitophagy is widespread

in Drosophila but minimally affected by loss of Pink1 or parkin. *J Cell Biol,* 217**,** 1613-1622.

Lee, S., Lee, K. S., Huh, S., Liu, S., Lee, D. Y., Hong, S. H., Yu, K. & Lu, B. 2016b. Polo Kinase Phosphorylates Miro to Control ER-Mitochondria Contact Sites and Mitochondrial $Ca^{(2+)}$ Homeostasis in Neural Stem Cell Development. *Dev Cell,* 37**,** 174-189.

Lee, S., Sterky, F. H., Mourier, A., Terzioglu, M., Cullheim, S., Olson, L. & Larsson, N. G. 2012. Mitofusin 2 is necessary for striatal axonal projections of midbrain dopamine neurons. *Hum Mol Genet,* 21**,** 4827-35.

Lepekhin, E. A., Eliasson, C., Berthold, C. H., Berezin, V., Bock, E. & Pekny, M. 2001. Intermediate filaments regulate astrocyte motility. *J Neurochem,* 79**,** 617-25.

Levy, M., Faas, G. C., Saggau, P., Craigen, W. J. & Sweatt, J. D. 2003. Mitochondrial regulation of synaptic plasticity in the hippocampus. *J Biol Chem,* 278**,** 17727-34.

Lewis, T. L., Jr., Kwon, S. K., Lee, A., Shaw, R. & Polleux, F. 2018. MFF-dependent mitochondrial fission regulates presynaptic release and axon branching by limiting axonal mitochondria size. *Nat Commun,* 9**,** 5008.

Lewis, T. L., Jr., Turi, G. F., Kwon, S. K., Losonczy, A. & Polleux, F. 2016. Progressive Decrease of Mitochondrial Motility during Maturation of Cortical Axons In Vitro and In Vivo. *Curr Biol,* 26**,** 2602-2608.

Li, Q. & Barres, B. A. 2018. Microglia and macrophages in brain homeostasis and disease. *Nat Rev Immunol,* 18**,** 225-242.

Li, S., Xiong, G. J., Huang, N. & Sheng, Z. H. 2020. The cross-talk of energy sensing and mitochondrial anchoring sustains synaptic efficacy by maintaining presynaptic metabolism. *Nat Metab,* 2**,** 1077-1095.

Li, Z., Okamoto, K., Hayashi, Y. & Sheng, M. 2004. The importance of dendritic mitochondria in the morphogenesis and plasticity of spines and synapses. *Cell,* 119**,** 873-87.

Lie, P. P. Y., Yang, D. S., Stavrides, P., Goulbourne, C. N., Zheng, P., Mohan, P. S., Cataldo, A. M. & Nixon, R. A. 2021. Post-Golgi carriers, not lysosomes, confer lysosomal properties to pre-degradative organelles in normal and dystrophic axons. *Cell Rep,* 35**,** 109034.

Lin, M. T. & Beal, M. F. 2006. Mitochondrial dysfunction and oxidative stress in neurodegenerative diseases. *Nature,* 443**,** 787-95.

Lin, M. Y., Cheng, X. T., Tammineni, P., Xie, Y., Zhou, B., Cai, Q. & Sheng, Z. H. 2017. Releasing Syntaphilin Removes Stressed Mitochondria from Axons Independent of Mitophagy under Pathophysiological Conditions. *Neuron,* 94**,** 595-610 e6.

Lin, T. H., Bis-Brewer, D. M., Sheehan, A. E., Townsend, L. N., Maddison, D. C., Zuchner, S., Smith, G. A. & Freeman, M. R. 2021. TSG101 negatively regulates mitochondrial biogenesis in axons. *Proc Natl Acad Sci U S A,* 118.

Liu, L., Sakakibara, K., Chen, Q. & Okamoto, K. 2014. Receptor-mediated mitophagy in yeast and mammalian systems. *Cell Res,* 24**,** 787-95.

Liu, S., Sawada, T., Lee, S., Yu, W., Silverio, G., Alapatt, P., Millan, I., Shen, A., Saxton, W., Kanao, T., Takahashi, R., Hattori, N., Imai, Y. & Lu, B. 2012. Parkinson's disease-associated kinase PINK1 regulates Miro protein level and axonal transport of mitochondria. *PLoS Genet,* 8**,** e1002537.

Liu, Y., Ma, X., Fujioka, H., Liu, J., Chen, S. & Zhu, X. 2019. DJ-1 regulates the integrity and function of ER-mitochondria association through interaction with IP3R3-Grp75-VDAC1. *Proc Natl Acad Sci U S A,* 116**,** 25322-25328.

Liu, Y. T., Sliter, D. A., Shammas, M. K., Huang, X., Wang, C., Calvelli, H., D, S. M. & D, P. N. 2021. Mt-Keima detects PINK1-PRKN mitophagy in vivo with greater sensitivity than mito-QC. *Autophagy***,** 1-10.

Llorente-Folch, I., Rueda, C. B., Pardo, B., Szabadkai, G., Duchen, M. R. & Satrustegui, J. 2015. The regulation of neuronal mitochondrial metabolism by calcium. *J Physiol,* 593**,** 3447-62.

Lopez-Domenech, G., Covill-Cooke, C., Ivankovic, D., Halff, E. F., Sheehan, D. F., Norkett, R., Birsa, N. & Kittler, J. T. 2018. Miro proteins coordinate microtubule- and actin-dependent mitochondrial transport and distribution. *EMBO J,* 37**,** 321-336.

Lopez-Domenech, G., Higgs, N. F., Vaccaro, V., Ros, H., Arancibia-Carcamo, I. L., MacAskill, A. F. & Kittler, J. T. 2016. Loss of Dendritic Complexity Precedes Neurodegeneration in a Mouse Model with Disrupted Mitochondrial Distribution in Mature Dendrites. *Cell Rep,* 17**,** 317-327.

Lopez-Domenech, G., Howden, J. H., Covill-Cooke, C., Morfill, C., Patel, J. V., Burli, R., Crowther, D., Birsa, N., Brandon, N. J. & Kittler, J. T. 2021. Loss of neuronal Miro1 disrupts mitophagy and induces hyperactivation of the integrated stress response. *EMBO J***,** e100715.

Lovatt, D., Sonnewald, U., Waagepetersen, H. S., Schousboe, A., He, W., Lin, J. H., Han, X., Takano, T., Wang, S., Sim, F. J., Goldman, S. A. & Nedergaard, M. 2007. The transcriptome and metabolic gene signature of protoplasmic astrocytes in the adult murine cortex. *J Neurosci,* 27**,** 12255-66.

Lull, M. E. & Block, M. L. 2010. Microglial activation and chronic neurodegeneration. *Neurotherapeutics,* 7**,** 354-65.

Luongo, T. S., Lambert, J. P., Gross, P., Nwokedi, M., Lombardi, A. A., Shanmughapriya, S., Carpenter, A. C., Kolmetzky, D., Gao, E., van Berlo, J. H., Tsai, E. J., Molkentin, J. D., Chen, X., Madesh, M., Houser, S. R. & Elrod, J. W. 2017. The mitochondrial Na(+)/Ca($^{2+}$) exchanger is essential for Ca($^{2+}$) homeostasis and viability. *Nature,* 545**,** 93-97.

Luth, E. S., Stavrovskaya, I. G., Bartels, T., Kristal, B. S. & Selkoe, D. J. 2014. Soluble, prefibrillar alpha-synuclein oligomers promote complex I-dependent, Ca^{2+}-induced mitochondrial dysfunction. *J Biol Chem,* 289**,** 21490-507.

Ma, H., Cai, Q., Lu, W., Sheng, Z. H. & Mochida, S. 2009. KIF5B motor adaptor syntabulin maintains synaptic transmission in sympathetic neurons. *J Neurosci,* 29**,** 13019-29.

MacAskill, A. F. & Kittler, J. T. 2010. Control of mitochondrial transport and localization in neurons. *Trends Cell Biol,* 20**,** 102-12.

Macaskill, A. F., Rinholm, J. E., Twelvetrees, A. E., Arancibia-Carcamo, I. L., Muir, J., Fransson, A., Aspenstrom, P., Attwell, D. & Kittler, J. T. 2009. Miro1 is a calcium sensor for glutamate receptor-dependent localization of mitochondria at synapses. *Neuron,* 61**,** 541-55.

Maday, S. & Holzbaur, E. L. 2016. Compartment-Specific Regulation of Autophagy in Primary Neurons. *J Neurosci,* 36**,** 5933-45.

Maday, S., Wallace, K. E. & Holzbaur, E. L. 2012. Autophagosomes initiate distally and mature during transport toward the cell soma in primary neurons. *J Cell Biol,* 196**,** 407-17.

Madry, C., Kyrargyri, V., Arancibia-Carcamo, I. L., Jolivet, R., Kohsaka, S., Bryan, R. M. & Attwell, D. 2018. Microglial Ramification, Surveillance, and Interleukin-1beta Release Are Regulated by the Two-Pore Domain K(+) Channel THIK-1. *Neuron,* 97**,** 299-312 e6.

Maeder, C. I., Shen, K. & Hoogenraad, C. C. 2014. Axon and dendritic trafficking. *Curr Opin Neurobiol,* 27**,** 165-70.

Martin, M., Iyadurai, S. J., Gassman, A., Gindhart, J. G., Jr., Hays, T. S. & Saxton, W. M. 1999. Cytoplasmic dynein, the dynactin complex, and kinesin are interdependent and essential for fast axonal transport. *Mol Biol Cell,* 10**,** 3717-28.

Martinez-Vicente, M. 2017. Neuronal Mitophagy in Neurodegenerative Diseases. *Front Mol Neurosci,* 10**,** 64.

Mathiisen, T. M., Lehre, K. P., Danbolt, N. C. & Ottersen, O. P. 2010. The perivascular astroglial sheath provides a complete covering of the brain

microvessels: an electron microscopic 3D reconstruction. *Glia,* 58**,** 1094-103.

Matsutani, S. & Yamamoto, N. 1997. Neuronal regulation of astrocyte morphology in vitro is mediated by GABAergic signaling. *Glia,* 20**,** 1-9.

McCoy, M. K., Kaganovich, A., Rudenko, I. N., Ding, J. & Cookson, M. R. 2014. Hexokinase activity is required for recruitment of parkin to depolarized mitochondria. *Hum Mol Genet,* 23**,** 145-56.

McLelland, G. L., Goiran, T., Yi, W., Dorval, G., Chen, C. X., Lauinger, N. D., Krahn, A. I., Valimehr, S., Rakovic, A., Rouiller, I., Durcan, T. M., Trempe, J. F. & Fon, E. A. 2018. Mfn2 ubiquitination by PINK1/parkin gates the p97-dependent release of ER from mitochondria to drive mitophagy. *Elife,* 7.

McWilliams, T. G., Prescott, A. R., Allen, G. F., Tamjar, J., Munson, M. J., Thomson, C., Muqit, M. M. & Ganley, I. G. 2016. mito-QC illuminates mitophagy and mitochondrial architecture in vivo. *J Cell Biol,* 214**,** 333-45.

McWilliams, T. G., Prescott, A. R., Montava-Garriga, L., Ball, G., Singh, F., Barini, E., Muqit, M. M. K., Brooks, S. P. & Ganley, I. G. 2018. Basal Mitophagy Occurs Independently of PINK1 in Mouse Tissues of High Metabolic Demand. *Cell Metab,* 27**,** 439-449 e5.

Meng, L., Mulcahy, B., Cook, S. J., Neubauer, M., Wan, A., Jin, Y. & Yan, D. 2015. The Cell Death Pathway Regulates Synapse Elimination through Cleavage of Gelsolin in Caenorhabditis elegans Neurons. *Cell Rep,* 11**,** 1737-48.

Mertins, P., Qiao, J. W., Patel, J., Udeshi, N. D., Clauser, K. R., Mani, D. R., Burgess, M. W., Gillette, M. A., Jaffe, J. D. & Carr, S. A. 2013. Integrated proteomic analysis of post-translational modifications by serial enrichment. *Nat Methods,* 10**,** 634-7.

Mick, E., Titov, D. V., Skinner, O. S., Sharma, R., Jourdain, A. A. & Mootha, V. K. 2020. Distinct mitochondrial defects trigger the integrated stress response depending on the metabolic state of the cell. *Elife,* 9.

Miller, K. E. & Sheetz, M. P. 2004. Axonal mitochondrial transport and potential are correlated. *J Cell Sci,* 117**,** 2791-804.

Misko, A., Jiang, S., Wegorzewska, I., Milbrandt, J. & Baloh, R. H. 2010. Mitofusin 2 is necessary for transport of axonal mitochondria and interacts with the Miro/Milton complex. *J Neurosci,* 30**,** 4232-40.

Miyazono, Y., Hirashima, S., Ishihara, N., Kusukawa, J., Nakamura, K. I. & Ohta, K. 2018. Uncoupled mitochondria quickly shorten along their long axis to form indented spheroids, instead of rings, in a fission-independent manner. *Sci Rep,* 8**,** 350.

Modi, S., Lopez-Domenech, G., Halff, E. F., Covill-Cooke, C., Ivankovic, D., Melandri, D., Arancibia-Carcamo, I. L., Burden, J. J., Lowe, A. R. & Kittler, J. T. 2019. Miro clusters regulate ER-mitochondria contact sites and link cristae organization to the mitochondrial transport machinery. *Nat Commun,* 10**,** 4399.

Montagna, E., Crux, S., Luckner, M., Herber, J., Colombo, A. V., Marinkovic, P., Tahirovic, S., Lichtenthaler, S. F., Wanner, G., Muller, U. C., Sgobio, C. & Herms, J. 2019. In vivo $Ca(^{2+})$ imaging of astrocytic microdomains reveals a critical role of the amyloid precursor protein for mitochondria. *Glia,* 67**,** 985-998.

Morales, I., Sanchez, A., Puertas-Avendano, R., Rodriguez-Sabate, C., Perez-Barreto, A. & Rodriguez, M. 2020. Neuroglial transmitophagy and Parkinson's disease. *Glia,* 68**,** 2277-2299.

Morris, R. L. & Hollenbeck, P. J. 1993. The regulation of bidirectional mitochondrial transport is coordinated with axonal outgrowth. *J Cell Sci,* 104 (Pt 3)**,** 917-27.

Morris, R. L. & Hollenbeck, P. J. 1995. Axonal transport of mitochondria along microtubules and F-actin in living vertebrate neurons. *J Cell Biol,* 131**,** 1315-26.

Motori, E., Puyal, J., Toni, N., Ghanem, A., Angeloni, C., Malaguti, M., Cantelli-Forti, G., Berninger, B., Conzelmann, K. K., Gotz, M., Winklhofer, K. F., Hrelia, S. & Bergami, M. 2013. Inflammation-induced alteration of

astrocyte mitochondrial dynamics requires autophagy for mitochondrial network maintenance. *Cell Metab,* 18**,** 844-59.

Mozdy, A. D., McCaffery, J. M. & Shaw, J. M. 2000. Dnm1p GTPase-mediated mitochondrial fission is a multi-step process requiring the novel integral membrane component Fis1p. *J Cell Biol,* 151**,** 367-80.

Munoz, J. P., Ivanova, S., Sanchez-Wandelmer, J., Martinez-Cristobal, P., Noguera, E., Sancho, A., Diaz-Ramos, A., Hernandez-Alvarez, M. I., Sebastian, D., Mauvezin, C., Palacin, M. & Zorzano, A. 2013. Mfn2 modulates the UPR and mitochondrial function via repression of PERK. *EMBO J,* 32**,** 2348-61.

Nair, S., Sobotka, K. S., Joshi, P., Gressens, P., Fleiss, B., Thornton, C., Mallard, C. & Hagberg, H. 2019. Lipopolysaccharide-induced alteration of mitochondrial morphology induces a metabolic shift in microglia modulating the inflammatory response in vitro and in vivo. *Glia,* 67**,** 1047-1061.

Naon, D., Zaninello, M., Giacomello, M., Varanita, T., Grespi, F., Lakshminaranayan, S., Serafini, A., Semenzato, M., Herkenne, S., Hernandez-Alvarez, M. I., Zorzano, A., De Stefani, D., Dorn, G. W., 2nd & Scorrano, L. 2016. Critical reappraisal confirms that Mitofusin 2 is an endoplasmic reticulum-mitochondria tether. *Proc Natl Acad Sci U S A,* 113**,** 11249-11254.

Narendra, D., Tanaka, A., Suen, D. F. & Youle, R. J. 2008. Parkin is recruited selectively to impaired mitochondria and promotes their autophagy. *J Cell Biol,* 183**,** 795-803.

Nguyen, T. T., Oh, S. S., Weaver, D., Lewandowska, A., Maxfield, D., Schuler, M. H., Smith, N. K., Macfarlane, J., Saunders, G., Palmer, C. A., Debattisti, V., Koshiba, T., Pulst, S., Feldman, E. L., Hajnoczky, G. & Shaw, J. M. 2014. Loss of Miro1-directed mitochondrial movement results in a novel murine model for neuron disease. *Proc Natl Acad Sci U S A,* 111**,** E3631-40.

Niescier, R. F., Hong, K., Park, D. & Min, K. T. 2018. MCU Interacts with Miro1 to Modulate Mitochondrial Functions in Neurons. *J Neurosci,* 38**,** 4666-4677.

Nirschl, J. J., Ghiretti, A. E. & Holzbaur, E. L. F. 2017. The impact of cytoskeletal organization on the local regulation of neuronal transport. *Nat Rev Neurosci,* 18**,** 585-597.

Nistico, R., Mehdawy, B., Piccirilli, S. & Mercuri, N. 2011. Paraquat- and rotenone-induced models of Parkinson's disease. *Int J Immunopathol Pharmacol,* 24**,** 313-22.

O'Donnell, J. C., Jackson, J. G. & Robinson, M. B. 2016. Transient Oxygen/Glucose Deprivation Causes a Delayed Loss of Mitochondria and Increases Spontaneous Calcium Signaling in Astrocytic Processes. *J Neurosci,* 36**,** 7109-27.

Oberheim, N. A., Takano, T., Han, X., He, W., Lin, J. H., Wang, F., Xu, Q., Wyatt, J. D., Pilcher, W., Ojemann, J. G., Ransom, B. R., Goldman, S. A. & Nedergaard, M. 2009. Uniquely hominid features of adult human astrocytes. *J Neurosci,* 29**,** 3276-87.

Oberheim, N. A., Wang, X., Goldman, S. & Nedergaard, M. 2006. Astrocytic complexity distinguishes the human brain. *Trends Neurosci,* 29**,** 547-53.

Okatsu, K., Koyano, F., Kimura, M., Kosako, H., Saeki, Y., Tanaka, K. & Matsuda, N. 2015. Phosphorylated ubiquitin chain is the genuine Parkin receptor. *J Cell Biol,* 209**,** 111-28.

Oliveras-Salva, M., Macchi, F., Coessens, V., Deleersnijder, A., Gerard, M., Van der Perren, A., Van den Haute, C. & Baekelandt, V. 2014. Alpha-synuclein-induced neurodegeneration is exacerbated in PINK1 knockout mice. *Neurobiol Aging,* 35**,** 2625-2636.

Ordureau, A., Heo, J. M., Duda, D. M., Paulo, J. A., Olszewski, J. L., Yanishevski, D., Rinehart, J., Schulman, B. A. & Harper, J. W. 2015. Defining roles of PARKIN and ubiquitin phosphorylation by PINK1 in mitochondrial quality control using a ubiquitin replacement strategy. *Proc Natl Acad Sci U S A,* 112**,** 6637-42.

Ordureau, A., Paulo, J. A., Zhang, J., An, H., Swatek, K. N., Cannon, J. R., Wan, Q., Komander, D. & Harper, J. W. 2020. Global Landscape and

Dynamics of Parkin and USP30-Dependent Ubiquitylomes in iNeurons during Mitophagic Signaling. *Mol Cell,* 77**,** 1124-1142 e10.

Ordureau, A., Paulo, J. A., Zhang, W., Ahfeldt, T., Zhang, J., Cohn, E. F., Hou, Z., Heo, J. M., Rubin, L. L., Sidhu, S. S., Gygi, S. P. & Harper, J. W. 2018. Dynamics of PARKIN-Dependent Mitochondrial Ubiquitylation in Induced Neurons and Model Systems Revealed by Digital Snapshot Proteomics. *Mol Cell,* 70**,** 211-227 e8.

Ordureau, A., Sarraf, S. A., Duda, D. M., Heo, J. M., Jedrychowski, M. P., Sviderskiy, V. O., Olszewski, J. L., Koerber, J. T., Xie, T., Beausoleil, S. A., Wells, J. A., Gygi, S. P., Schulman, B. A. & Harper, J. W. 2014a. Quantitative proteomics reveal a feedforward mechanism for mitochondrial PARKIN translocation and ubiquitin chain synthesis. *Mol Cell,* 56**,** 360-375.

Ordureau, A., Sarraf, S. A., Duda, D. M., Heo, J. M., Jedrychowski, M. P., Sviderskiy, V. O., Olszewski, J. L., Koerber, J. T., Xie, T., Beausoleil, S. A., Wells, J. A., Gygi, S. P., Schulman, B. A. & Harper, J. W. 2014b. Quantitative proteomics reveal a feedforward mechanism for mitochondrial PARKIN translocation and ubiquitin chain synthesis. *Mol Cell,* 56**,** 360-75.

Orihuela, R., McPherson, C. A. & Harry, G. J. 2016. Microglial M1/M2 polarization and metabolic states. *Br J Pharmacol,* 173**,** 649-65.

Otera, H., Miyata, N., Kuge, O. & Mihara, K. 2016. Drp1-dependent mitochondrial fission via MiD49/51 is essential for apoptotic cristae remodeling. *J Cell Biol,* 212**,** 531-44.

Otera, H., Wang, C., Cleland, M. M., Setoguchi, K., Yokota, S., Youle, R. J. & Mihara, K. 2010. Mff is an essential factor for mitochondrial recruitment of Drp1 during mitochondrial fission in mammalian cells. *J Cell Biol,* 191**,** 1141-58.

Padman, B. S., Nguyen, T. N., Uoselis, L., Skulsuppaisarn, M., Nguyen, L. K. & Lazarou, M. 2019. LC3/GABARAPs drive ubiquitin-independent recruitment of Optineurin and NDP52 to amplify mitophagy. *Nat Commun,* 10**,** 408.

Paillusson, S., Stoica, R., Gomez-Suaga, P., Lau, D. H. W., Mueller, S., Miller, T. & Miller, C. C. J. 2016. There's Something Wrong with my MAM; the ER-Mitochondria Axis and Neurodegenerative Diseases. *Trends Neurosci,* 39**,** 146-157.

Pakos-Zebrucka, K., Koryga, I., Mnich, K., Ljujic, M., Samali, A. & Gorman, A. M. 2016. The integrated stress response. *EMBO Rep,* 17**,** 1374-1395.

Palikaras, K. & Tavernarakis, N. 2012. Mitophagy in neurodegeneration and aging. *Front Genet,* 3**,** 297.

Paolicelli, R. C., Bolasco, G., Pagani, F., Maggi, L., Scianni, M., Panzanelli, P., Giustetto, M., Ferreira, T. A., Guiducci, E., Dumas, L., Ragozzino, D. & Gross, C. T. 2011. Synaptic pruning by microglia is necessary for normal brain development. *Science,* 333**,** 1456-8.

Park, J., Min, J. S., Kim, B., Chae, U. B., Yun, J. W., Choi, M. S., Kong, I. K., Chang, K. T. & Lee, D. S. 2015. Mitochondrial ROS govern the LPS-induced pro-inflammatory response in microglia cells by regulating MAPK and NF-kappaB pathways. *Neurosci Lett,* 584**,** 191-6.

Park, J. H., Burgess, J. D., Faroqi, A. H., DeMeo, N. N., Fiesel, F. C., Springer, W., Delenclos, M. & McLean, P. J. 2020. Alpha-synuclein-induced mitochondrial dysfunction is mediated via a sirtuin 3-dependent pathway. *Mol Neurodegener,* 15**,** 5.

Park, K. S., Jo, I., Pak, K., Bae, S. W., Rhim, H., Suh, S. H., Park, J., Zhu, H., So, I. & Kim, K. W. 2002. FCCP depolarizes plasma membrane potential by activating proton and Na+ currents in bovine aortic endothelial cells. *Pflugers Arch,* 443**,** 344-52.

Parnis, J., Montana, V., Delgado-Martinez, I., Matyash, V., Parpura, V., Kettenmann, H., Sekler, I. & Nolte, C. 2013. Mitochondrial exchanger NCLX plays a major role in the intracellular Ca^{2+} signaling, gliotransmission, and proliferation of astrocytes. *J Neurosci,* 33**,** 7206-19.

Parton, R. G., Simons, K. & Dotti, C. G. 1992. Axonal and dendritic endocytic pathways in cultured neurons. *J Cell Biol,* 119**,** 123-37.

Pathak, D., Shields, L. Y., Mendelsohn, B. A., Haddad, D., Lin, W., Gerencser, A. A., Kim, H., Brand, M. D., Edwards, R. H. & Nakamura, K. 2015. The role of mitochondrially derived ATP in synaptic vesicle recycling. *J Biol Chem,* 290**,** 22325-36.

Patron, M., Granatiero, V., Espino, J., Rizzuto, R. & De Stefani, D. 2019. MICU3 is a tissue-specific enhancer of mitochondrial calcium uptake. *Cell Death Differ,* 26**,** 179-195.

Pellerin, L., Bouzier-Sore, A. K., Aubert, A., Serres, S., Merle, M., Costalat, R. & Magistretti, P. J. 2007. Activity-dependent regulation of energy metabolism by astrocytes: an update. *Glia,* 55**,** 1251-62.

Peng, W., Wong, Y. C. & Krainc, D. 2020. Mitochondria-lysosome contacts regulate mitochondrial Ca($^{2+}$) dynamics via lysosomal TRPML1. *Proc Natl Acad Sci U S A,* 117**,** 19266-19275.

Perez, F. A. & Palmiter, R. D. 2005. Parkin-deficient mice are not a robust model of parkinsonism. *Proc Natl Acad Sci U S A,* 102**,** 2174-9.

Perkins, G. A., Tjong, J., Brown, J. M., Poquiz, P. H., Scott, R. T., Kolson, D. R., Ellisman, M. H. & Spirou, G. A. 2010. The micro-architecture of mitochondria at active zones: electron tomography reveals novel anchoring scaffolds and cristae structured for high-rate metabolism. *J Neurosci,* 30**,** 1015-26.

Peters, A. 1991. A Guide to the Cellular Structure of the Nervous-System - 2 Citation-Classic Commentary on the Fine-Structure of the Nervous-System - the Neurons and Supporting Cells by Peters,A., Palay,S.L., and Webster,H.D. *Current Contents/Life Sciences***,** 9-9.

Pham, A. H., Meng, S., Chu, Q. N. & Chan, D. C. 2012. Loss of Mfn2 results in progressive, retrograde degeneration of dopaminergic neurons in the nigrostriatal circuit. *Hum Mol Genet,* 21**,** 4817-26.

Pickrell, A. M. & Youle, R. J. 2015. The roles of PINK1, parkin, and mitochondrial fidelity in Parkinson's disease. *Neuron,* 85**,** 257-73.

Polymeropoulos, M. H., Higgins, J. J., Golbe, L. I., Johnson, W. G., Ide, S. E., Di Iorio, G., Sanges, G., Stenroos, E. S., Pho, L. T., Schaffer, A. A., Lazzarini, A. M., Nussbaum, R. L. & Duvoisin, R. C. 1996. Mapping of a gene for Parkinson's disease to chromosome 4q21-q23. *Science,* 274**,** 1197-9.

Povlsen, L. K., Beli, P., Wagner, S. A., Poulsen, S. L., Sylvestersen, K. B., Poulsen, J. W., Nielsen, M. L., Bekker-Jensen, S., Mailand, N. & Choudhary, C. 2012. Systems-wide analysis of ubiquitylation dynamics reveals a key role for PAF15 ubiquitylation in DNA-damage bypass. *Nat Cell Biol,* 14**,** 1089-98.

Puri, R., Cheng, X. T., Lin, M. Y., Huang, N. & Sheng, Z. H. 2019. Mul1 restrains Parkin-mediated mitophagy in mature neurons by maintaining ER-mitochondrial contacts. *Nat Commun,* 10**,** 3645.

Puschmann, A., Fiesel, F. C., Caulfield, T. R., Hudec, R., Ando, M., Truban, D., Hou, X., Ogaki, K., Heckman, M. G., James, E. D., Swanberg, M., Jimenez-Ferrer, I., Hansson, O., Opala, G., Siuda, J., Boczarska-Jedynak, M., Friedman, A., Koziorowski, D., Rudzinska-Bar, M., Aasly, J. O., Lynch, T., Mellick, G. D., Mohan, M., Silburn, P. A., Sanotsky, Y., Vilarino-Guell, C., Farrer, M. J., Chen, L., Dawson, V. L., Dawson, T. M., Wszolek, Z. K., Ross, O. A. & Springer, W. 2017. Heterozygous PINK1 p.G411S increases risk of Parkinson's disease via a dominant-negative mechanism. *Brain,* 140**,** 98-117.

Qi, X., Qvit, N., Su, Y. C. & Mochly-Rosen, D. 2013. A novel Drp1 inhibitor diminishes aberrant mitochondrial fission and neurotoxicity. *J Cell Sci,* 126**,** 789-802.

Quintero, O. A., DiVito, M. M., Adikes, R. C., Kortan, M. B., Case, L. B., Lier, A. J., Panaretos, N. S., Slater, S. Q., Rengarajan, M., Feliu, M. & Cheney, R. E. 2009. Human Myo19 is a novel myosin that associates with mitochondria. *Curr Biol,* 19**,** 2008-13.

Rabouw, H. H., Langereis, M. A., Anand, A. A., Visser, L. J., de Groot, R. J., Walter, P. & van Kuppeveld, F. J. M. 2019. Small molecule ISRIB suppresses the integrated stress response within a defined window of activation. *Proc Natl Acad Sci U S A,* 116**,** 2097-2102.

Rangaraju, V., Calloway, N. & Ryan, T. A. 2014. Activity-driven local ATP synthesis is required for synaptic function. *Cell,* 156**,** 825-35.

Rangaraju, V., Lauterbach, M. & Schuman, E. M. 2019. Spatially Stable Mitochondrial Compartments Fuel Local Translation during Plasticity. *Cell,* 176**,** 73-84 e15.

Reddy, P. H. 2014. Increased mitochondrial fission and neuronal dysfunction in Huntington's disease: implications for molecular inhibitors of excessive mitochondrial fission. *Drug Discov Today,* 19**,** 951-5.

Reddy, P. H., Reddy, T. P., Manczak, M., Calkins, M. J., Shirendeb, U. & Mao, P. 2011. Dynamin-related protein 1 and mitochondrial fragmentation in neurodegenerative diseases. *Brain Res Rev,* 67**,** 103-18.

Restelli, L. M., Oettinghaus, B., Halliday, M., Agca, C., Licci, M., Sironi, L., Savoia, C., Hench, J., Tolnay, M., Neutzner, A., Schmidt, A., Eckert, A., Mallucci, G., Scorrano, L. & Frank, S. 2018. Neuronal Mitochondrial Dysfunction Activates the Integrated Stress Response to Induce Fibroblast Growth Factor 21. *Cell Rep,* 24**,** 1407-1414.

Reyes, R. C. & Parpura, V. 2008. Mitochondria modulate Ca^{2+}-dependent glutamate release from rat cortical astrocytes. *J Neurosci,* 28**,** 9682-91.

Roberts, R. F., Tang, M. Y., Fon, E. A. & Durcan, T. M. 2016. Defending the mitochondria: The pathways of mitophagy and mitochondrial-derived vesicles. *Int J Biochem Cell Biol,* 79**,** 427-436.

Robinson, G. L., Dinsdale, D., Macfarlane, M. & Cain, K. 2012. Switching from aerobic glycolysis to oxidative phosphorylation modulates the sensitivity of mantle cell lymphoma cells to TRAIL. *Oncogene,* 31**,** 4996-5006.

Rocha, A. G., Franco, A., Krezel, A. M., Rumsey, J. M., Alberti, J. M., Knight, W. C., Biris, N., Zacharioudakis, E., Janetka, J. W., Baloh, R. H., Kitsis, R. N., Mochly-Rosen, D., Townsend, R. R., Gavathiotis, E. & Dorn, G. W., 2nd 2018. MFN2 agonists reverse mitochondrial defects in preclinical models of Charcot-Marie-Tooth disease type 2A. *Science,* 360**,** 336-341.

Rolfe, D. F. & Brown, G. C. 1997. Cellular energy utilization and molecular origin of standard metabolic rate in mammals. *Physiol Rev,* 77**,** 731-58.

Russo, G. J., Louie, K., Wellington, A., Macleod, G. T., Hu, F., Panchumarthi, S. & Zinsmaier, K. E. 2009. Drosophila Miro is required for both anterograde and retrograde axonal mitochondrial transport. *J Neurosci,* 29**,** 5443-55.

Safiulina, D., Kuum, M., Choubey, V., Gogichaishvili, N., Liiv, J., Hickey, M. A., Cagalinec, M., Mandel, M., Zeb, A., Liiv, M. & Kaasik, A. 2019. Miro proteins prime mitochondria for Parkin translocation and mitophagy. *EMBO J,* 38.

Sakai, J. 2020. Core Concept: How synaptic pruning shapes neural wiring during development and, possibly, in disease. *Proc Natl Acad Sci U S A,* 117**,** 16096-16099.

Santel, A. & Fuller, M. T. 2001. Control of mitochondrial morphology by a human mitofusin. *J Cell Sci,* 114**,** 867-74.

Santos, R. X., Correia, S. C., Wang, X., Perry, G., Smith, M. A., Moreira, P. I. & Zhu, X. 2010. A synergistic dysfunction of mitochondrial fission/fusion dynamics and mitophagy in Alzheimer's disease. *J Alzheimers Dis,* 20 Suppl 2**,** S401-12.

Sarraf, S. A., Raman, M., Guarani-Pereira, V., Sowa, M. E., Huttlin, E. L., Gygi, S. P. & Harper, J. W. 2013. Landscape of the PARKIN-dependent ubiquitylome in response to mitochondrial depolarization. *Nature,* 496**,** 372-6.

Saxton, W. M. & Hollenbeck, P. J. 2012. The axonal transport of mitochondria. *J Cell Sci,* 125**,** 2095-104.

Scaduto, R. C., Jr. & Grotyohann, L. W. 1999. Measurement of mitochondrial membrane potential using fluorescent rhodamine derivatives. *Biophys J,* 76**,** 469-77.

Schett, G. & Neurath, M. F. 2018. Resolution of chronic inflammatory disease: universal and tissue-specific concepts. *Nat Commun,* 9**,** 3261.

Schwarz, T. L. 2013. Mitochondrial trafficking in neurons. *Cold Spring Harb Perspect Biol,* 5.

Scott, I. & Youle, R. J. 2010. Mitochondrial fission and fusion. *Essays Biochem,* 47**,** 85-98.

Scudamore, O. & Ciossek, T. 2018. Increased Oxidative Stress Exacerbates alpha-Synuclein Aggregation In Vivo. *J Neuropathol Exp Neurol,* 77**,** 443-453.

Seager, R., Lee, L., Henley, J. M. & Wilkinson, K. A. 2020. Mechanisms and roles of mitochondrial localisation and dynamics in neuronal function. *Neuronal Signal,* 4**,** NS20200008.

Shaltouki, A., Hsieh, C. H., Kim, M. J. & Wang, X. 2018. Alpha-synuclein delays mitophagy and targeting Miro rescues neuron loss in Parkinson's models. *Acta Neuropathol,* 136**,** 607-620.

Sheng, Z. H. 2014. Mitochondrial trafficking and anchoring in neurons: New insight and implications. *J Cell Biol,* 204**,** 1087-98.

Shlevkov, E., Kramer, T., Schapansky, J., LaVoie, M. J. & Schwarz, T. L. 2016. Miro phosphorylation sites regulate Parkin recruitment and mitochondrial motility. *Proc Natl Acad Sci U S A,* 113**,** E6097-E6106.

Sidlauskaite, E., Gibson, J. W., Megson, I. L., Whitfield, P. D., Tovmasyan, A., Batinic-Haberle, I., Murphy, M. P., Moult, P. R. & Cobley, J. N. 2018. Mitochondrial ROS cause motor deficits induced by synaptic inactivity: Implications for synapse pruning. *Redox Biol,* 16**,** 344-351.

Sliter, D. A., Martinez, J., Hao, L., Chen, X., Sun, N., Fischer, T. D., Burman, J. L., Li, Y., Zhang, Z., Narendra, D. P., Cai, H., Borsche, M., Klein, C. & Youle, R. J. 2018. Parkin and PINK1 mitigate STING-induced inflammation. *Nature,* 561**,** 258-262.

Smirnova, E., Griparic, L., Shurland, D. L. & van der Bliek, A. M. 2001. Dynamin-related protein Drp1 is required for mitochondrial division in mammalian cells. *Mol Biol Cell,* 12**,** 2245-56.

Smit-Rigter, L., Rajendran, R., Silva, C. A., Spierenburg, L., Groeneweg, F., Ruimschotel, E. M., van Versendaal, D., van der Togt, C., Eysel, U. T., Heimel, J. A., Lohmann, C. & Levelt, C. N. 2016. Mitochondrial Dynamics in Visual Cortex Are Limited In Vivo and Not Affected by Axonal Structural Plasticity. *Curr Biol,* 26**,** 2609-2616.

Smith, C. L. & Eppig, J. T. 2012. The Mammalian Phenotype Ontology as a unifying standard for experimental and high-throughput phenotyping data. *Mamm Genome,* 23**,** 653-68.

Smith, H. L., Freeman, O. J., Butcher, A. J., Holmqvist, S., Humoud, I., Schatzl, T., Hughes, D. T., Verity, N. C., Swinden, D. P., Hayes, J., de Weerd, L., Rowitch, D. H., Franklin, R. J. M. & Mallucci, G. R. 2020. Astrocyte Unfolded Protein Response Induces a Specific Reactivity State that Causes Non-Cell-Autonomous Neuronal Degeneration. *Neuron,* 105**,** 855-866 e5.

Smith, H. L. & Mallucci, G. R. 2016. The unfolded protein response: mechanisms and therapy of neurodegeneration. *Brain,* 139**,** 2113-21.

Solano, R. M., Casarejos, M. J., Menendez-Cuervo, J., Rodriguez-Navarro, J. A., Garcia de Yebenes, J. & Mena, M. A. 2008. Glial dysfunction in parkin null mice: effects of aging. *J Neurosci,* 28**,** 598-611.

Sorbara, M. T. & Girardin, S. E. 2011. Mitochondrial ROS fuel the inflammasome. *Cell Res,* 21**,** 558-60.

Stephan, A. H., Barres, B. A. & Stevens, B. 2012. The complement system: an unexpected role in synaptic pruning during development and disease. *Annu Rev Neurosci,* 35**,** 369-89.

Stephen, T. L., Gupta-Agarwal, S. & Kittler, J. T. 2014. Mitochondrial dynamics in astrocytes. *Biochem Soc Trans,* 42**,** 1302-10.

Stephen, T. L., Higgs, N. F., Sheehan, D. F., Al Awabdh, S., Lopez-Domenech, G., Arancibia-Carcamo, I. L. & Kittler, J. T. 2015. Miro1 Regulates Activity-Driven Positioning of Mitochondria within Astrocytic Processes Apposed to Synapses to Regulate Intracellular Calcium Signaling. *J Neurosci,* 35**,** 15996-6011.

Stoica, R., De Vos, K. J., Paillusson, S., Mueller, S., Sancho, R. M., Lau, K. F., Vizcay-Barrena, G., Lin, W. L., Xu, Y. F., Lewis, J., Dickson, D. W., Petrucelli, L., Mitchell, J. C., Shaw, C. E. & Miller, C. C. 2014. ER-mitochondria associations are regulated by the VAPB-PTPIP51 interaction and are disrupted by ALS/FTD-associated TDP-43. *Nat Commun,* 5**,** 3996.

Stowers, R. S., Megeath, L. J., Gorska-Andrzejak, J., Meinertzhagen, I. A. & Schwarz, T. L. 2002. Axonal transport of mitochondria to synapses depends on milton, a novel Drosophila protein. *Neuron,* 36**,** 1063-77.

Strappazzon, F., Nazio, F., Corrado, M., Cianfanelli, V., Romagnoli, A., Fimia, G. M., Campello, S., Nardacci, R., Piacentini, M., Campanella, M. & Cecconi, F. 2015. AMBRA1 is able to induce mitophagy via LC3 binding, regardless of PARKIN and p62/SQSTM1. *Cell Death Differ,* 22**,** 517.

Styr, B., Gonen, N., Zarhin, D., Ruggiero, A., Atsmon, R., Gazit, N., Braun, G., Frere, S., Vertkin, I., Shapira, I., Harel, M., Heim, L. R., Katsenelson, M., Rechnitz, O., Fadila, S., Derdikman, D., Rubinstein, M., Geiger, T., Ruppin, E. & Slutsky, I. 2019. Mitochondrial Regulation of the Hippocampal Firing Rate Set Point and Seizure Susceptibility. *Neuron,* 102**,** 1009-1024 e8.

Sudhof, T. C. 2012. The presynaptic active zone. *Neuron,* 75**,** 11-25.

Sun, N., Yun, J., Liu, J., Malide, D., Liu, C., Rovira, II, Holmstrom, K. M., Fergusson, M. M., Yoo, Y. H., Combs, C. A. & Finkel, T. 2015. Measuring In Vivo Mitophagy. *Mol Cell,* 60**,** 685-96.

Sun, T., Qiao, H., Pan, P. Y., Chen, Y. & Sheng, Z. H. 2013. Motile axonal mitochondria contribute to the variability of presynaptic strength. *Cell Rep,* 4**,** 413-419.

Supplie, L. M., Duking, T., Campbell, G., Diaz, F., Moraes, C. T., Gotz, M., Hamprecht, B., Boretius, S., Mahad, D. & Nave, K. A. 2017. Respiration-Deficient Astrocytes Survive As Glycolytic Cells In Vivo. *J Neurosci,* 37**,** 4231-4242.

Szabadkai, G., Bianchi, K., Varnai, P., De Stefani, D., Wieckowski, M. R., Cavagna, D., Nagy, A. I., Balla, T. & Rizzuto, R. 2006. Chaperone-mediated coupling of endoplasmic reticulum and mitochondrial Ca^{2+} channels. *J Cell Biol,* 175**,** 901-11.

Szalay, G., Martinecz, B., Lenart, N., Kornyei, Z., Orsolits, B., Judak, L., Csaszar, E., Fekete, R., West, B. L., Katona, G., Rozsa, B. & Denes, A. 2016. Microglia protect against brain injury and their selective elimination dysregulates neuronal network activity after stroke. *Nat Commun,* 7**,** 11499.

Tanaka, A., Cleland, M. M., Xu, S., Narendra, D. P., Suen, D. F., Karbowski, M. & Youle, R. J. 2010. Proteasome and p97 mediate mitophagy and degradation of mitofusins induced by Parkin. *J Cell Biol,* 191**,** 1367-80.

Tilokani, L., Nagashima, S., Paupe, V. & Prudent, J. 2018. Mitochondrial dynamics: overview of molecular mechanisms. *Essays Biochem,* 62**,** 341-360.

Twig, G., Elorza, A., Molina, A. J., Mohamed, H., Wikstrom, J. D., Walzer, G., Stiles, L., Haigh, S. E., Katz, S., Las, G., Alroy, J., Wu, M., Py, B. F., Yuan, J., Deeney, J. T., Corkey, B. E. & Shirihai, O. S. 2008. Fission and selective fusion govern mitochondrial segregation and elimination by autophagy. *EMBO J,* 27**,** 433-46.

Udeshi, N. D., Svinkina, T., Mertins, P., Kuhn, E., Mani, D. R., Qiao, J. W. & Carr, S. A. 2013. Refined preparation and use of anti-diglycine remnant (K-epsilon-GG) antibody enables routine quantification of 10,000s of ubiquitination sites in single proteomics experiments. *Mol Cell Proteomics,* 12**,** 825-31.

Ugbode, C. I., Hirst, W. D. & Rattray, M. 2014. Neuronal influences are necessary to produce mitochondrial co-localization with glutamate transporters in astrocytes. *J Neurochem,* 130**,** 668-77.

Umpierre, A. D., Bystrom, L. L., Ying, Y., Liu, Y. U., Worrell, G. & Wu, L. J. 2020. Microglial calcium signaling is attuned to neuronal activity in awake mice. *Elife,* 9.

Vaccaro, V., Devine, M. J., Higgs, N. F. & Kittler, J. T. 2017. Miro1-dependent mitochondrial positioning drives the rescaling of presynaptic Ca^{2+} signals during homeostatic plasticity. *EMBO Rep,* 18**,** 231-240.

Valente, E. M., Salvi, S., Ialongo, T., Marongiu, R., Elia, A. E., Caputo, V., Romito, L., Albanese, A., Dallapiccola, B. & Bentivoglio, A. R. 2004. PINK1 mutations are associated with sporadic early-onset parkinsonism. *Ann Neurol,* 56**,** 336-41.

Valm, A. M., Cohen, S., Legant, W. R., Melunis, J., Hershberg, U., Wait, E., Cohen, A. R., Davidson, M. W., Betzig, E. & Lippincott-Schwartz, J. 2017. Applying systems-level spectral imaging and analysis to reveal the organelle interactome. *Nature,* 546**,** 162-167.

Van Laar, V. S., Arnold, B., Cassady, S. J., Chu, C. T., Burton, E. A. & Berman, S. B. 2011. Bioenergetics of neurons inhibit the translocation response of Parkin following rapid mitochondrial depolarization. *Hum Mol Genet,* 20**,** 927-40.

van Spronsen, M., Mikhaylova, M., Lipka, J., Schlager, M. A., van den Heuvel, D. J., Kuijpers, M., Wulf, P. S., Keijzer, N., Demmers, J., Kapitein, L. C., Jaarsma, D., Gerritsen, H. C., Akhmanova, A. & Hoogenraad, C. C. 2013. TRAK/Milton motor-adaptor proteins steer mitochondrial trafficking to axons and dendrites. *Neuron,* 77**,** 485-502.

Verstreken, P., Ly, C. V., Venken, K. J., Koh, T. W., Zhou, Y. & Bellen, H. J. 2005. Synaptic mitochondria are critical for mobilization of reserve pool vesicles at Drosophila neuromuscular junctions. *Neuron,* 47**,** 365-78.

Villa, E., Marchetti, S. & Ricci, J. E. 2018. No Parkin Zone: Mitophagy without Parkin. *Trends in Cell Biology,* 28**,** 882-895.

Voloboueva, L. A., Emery, J. F., Sun, X. & Giffard, R. G. 2013. Inflammatory response of microglial BV-2 cells includes a glycolytic shift and is

modulated by mitochondrial glucose-regulated protein 75/mortalin. *FEBS Lett,* 587**,** 756-62.

Wagner, S. A., Beli, P., Weinert, B. T., Nielsen, M. L., Cox, J., Mann, M. & Choudhary, C. 2011. A proteome-wide, quantitative survey of in vivo ubiquitylation sites reveals widespread regulatory roles. *Mol Cell Proteomics,* 10**,** M111 013284.

Wagner, S. A., Beli, P., Weinert, B. T., Scholz, C., Kelstrup, C. D., Young, C., Nielsen, M. L., Olsen, J. V., Brakebusch, C. & Choudhary, C. 2012. Proteomic analyses reveal divergent ubiquitylation site patterns in murine tissues. *Mol Cell Proteomics,* 11**,** 1578-85.

Wakabayashi, J., Zhang, Z., Wakabayashi, N., Tamura, Y., Fukaya, M., Kensler, T. W., Iijima, M. & Sesaki, H. 2009. The dynamin-related GTPase Drp1 is required for embryonic and brain development in mice. *J Cell Biol,* 186**,** 805-16.

Wang, J. Q., Zhu, S., Wang, Y. H., Wang, F. L., An, C. Q., Jiang, D. F., Gao, L. J., Tu, Y. F., Zhu, X. F., Wang, Y., Liu, H. M., Gong, J. J., Sun, Z. S., Wang, X., Liu, L. M., Yang, K. Y., Guo, C. X. & Tang, T. S. 2019a. Miro2 supplies a platform for Parkin translocation to damaged mitochondria. *Science Bulletin,* 64**,** 730-747.

Wang, K. & Klionsky, D. J. 2011. Mitochondria removal by autophagy. *Autophagy,* 7**,** 297-300.

Wang, S. H., Martin, S. M., Harris, P. S. & Knudson, C. M. 2011a. Caspase inhibition blocks cell death and enhances mitophagy but fails to promote T-cell lymphoma. *PLoS One,* 6**,** e19786.

Wang, W., Zhang, F., Li, L., Tang, F., Siedlak, S. L., Fujioka, H., Liu, Y., Su, B., Pi, Y. & Wang, X. 2015. MFN2 couples glutamate excitotoxicity and mitochondrial dysfunction in motor neurons. *J Biol Chem,* 290**,** 168-82.

Wang, X., Becker, K., Levine, N., Zhang, M., Lieberman, A. P., Moore, D. J. & Ma, J. 2019b. Pathogenic alpha-synuclein aggregates preferentially bind to mitochondria and affect cellular respiration. *Acta Neuropathol Commun,* 7**,** 41.

Wang, X. & Schwarz, T. L. 2009. The mechanism of Ca^{2+} -dependent regulation of kinesin-mediated mitochondrial motility. *Cell,* 136**,** 163-74.

Wang, X., Winter, D., Ashrafi, G., Schlehe, J., Wong, Y. L., Selkoe, D., Rice, S., Steen, J., LaVoie, M. J. & Schwarz, T. L. 2011b. PINK1 and Parkin target Miro for phosphorylation and degradation to arrest mitochondrial motility. *Cell,* 147**,** 893-906.

Wauer, T. & Komander, D. 2013. Structure of the human Parkin ligase domain in an autoinhibited state. *EMBO J,* 32**,** 2099-112.

Wek, R. C. 2018. Role of eIF2alpha Kinases in Translational Control and Adaptation to Cellular Stress. *Cold Spring Harb Perspect Biol,* 10.

Werth, J. L. & Thayer, S. A. 1994. Mitochondria buffer physiological calcium loads in cultured rat dorsal root ganglion neurons. *J Neurosci,* 14**,** 348-56.

Whitworth, A. J., Theodore, D. A., Greene, J. C., Benes, H., Wes, P. D. & Pallanck, L. J. 2005. Increased glutathione S-transferase activity rescues dopaminergic neuron loss in a Drosophila model of Parkinson's disease. *Proc Natl Acad Sci U S A,* 102**,** 8024-9.

Wilson, C. L., Natarajan, V., Hayward, S. L., Khalimonchuk, O. & Kidambi, S. 2015. Mitochondrial dysfunction and loss of glutamate uptake in primary astrocytes exposed to titanium dioxide nanoparticles. *Nanoscale,* 7**,** 18477-88.

Wilson, E. L. & Metzakopian, E. 2020. ER-mitochondria contact sites in neurodegeneration: genetic screening approaches to investigate novel disease mechanisms. *Cell Death Differ*.

Wong, Y. C., Ysselstein, D. & Krainc, D. 2018. Mitochondria-lysosome contacts regulate mitochondrial fission via RAB7 GTP hydrolysis. *Nature,* 554**,** 382-386.

Wu, Q., Cheng, Z., Zhu, J., Xu, W., Peng, X., Chen, C., Li, W., Wang, F., Cao, L., Yi, X., Wu, Z., Li, J. & Fan, P. 2015. Suberoylanilide hydroxamic acid

treatment reveals crosstalks among proteome, ubiquitylome and acetylome in non-small cell lung cancer A549 cell line. *Sci Rep,* 5**,** 9520.

Yamada, T., Murata, D., Adachi, Y., Itoh, K., Kameoka, S., Igarashi, A., Kato, T., Araki, Y., Huganir, R. L., Dawson, T. M., Yanagawa, T., Okamoto, K., Iijima, M. & Sesaki, H. 2018. Mitochondrial Stasis Reveals p62-Mediated Ubiquitination in Parkin-Independent Mitophagy and Mitigates Nonalcoholic Fatty Liver Disease. *Cell Metab,* 28**,** 588-604 e5.

Yamano, K. & Youle, R. J. 2013. PINK1 is degraded through the N-end rule pathway. *Autophagy,* 9**,** 1758-69.

Yamashita, S. I., Jin, X., Furukawa, K., Hamasaki, M., Nezu, A., Otera, H., Saigusa, T., Yoshimori, T., Sakai, Y., Mihara, K. & Kanki, T. 2016. Mitochondrial division occurs concurrently with autophagosome formation but independently of Drp1 during mitophagy. *J Cell Biol,* 215**,** 649-665.

Yang, Y., Gehrke, S., Imai, Y., Huang, Z., Ouyang, Y., Wang, J. W., Yang, L., Beal, M. F., Vogel, H. & Lu, B. 2006. Mitochondrial pathology and muscle and dopaminergic neuron degeneration caused by inactivation of Drosophila Pink1 is rescued by Parkin. *Proc Natl Acad Sci U S A,* 103**,** 10793-8.

Yang, Y., Ouyang, Y., Yang, L., Beal, M. F., McQuibban, A., Vogel, H. & Lu, B. 2008. Pink1 regulates mitochondrial dynamics through interaction with the fission/fusion machinery. *Proc Natl Acad Sci U S A,* 105**,** 7070-5.

Yap, C. C., Digilio, L., McMahon, L. P., Garcia, A. D. R. & Winckler, B. 2018. Degradation of dendritic cargos requires Rab7-dependent transport to somatic lysosomes. *J Cell Biol,* 217**,** 3141-3159.

Yaron, J. R., Gangaraju, S., Rao, M. Y., Kong, X., Zhang, L., Su, F., Tian, Y., Glenn, H. L. & Meldrum, D. R. 2015. K(+) regulates $Ca^{(2+)}$ to drive inflammasome signaling: dynamic visualization of ion flux in live cells. *Cell Death Dis,* 6**,** e1954.

Ye, J., Jiang, Z., Chen, X., Liu, M., Li, J. & Liu, N. 2016. Electron transport chain inhibitors induce microglia activation through enhancing mitochondrial reactive oxygen species production. *Exp Cell Res,* 340**,** 315-26.

Youle, R. J. & Narendra, D. P. 2011. Mechanisms of mitophagy. *Nat Rev Mol Cell Biol,* 12**,** 9-14.

Yun, J., Puri, R., Yang, H., Lizzio, M. A., Wu, C., Sheng, Z. H. & Guo, M. 2014. MUL1 acts in parallel to the PINK1/parkin pathway in regulating mitofusin and compensates for loss of PINK1/parkin. *Elife,* 3**,** e01958.

Zala, D., Hinckelmann, M. V., Yu, H., Lyra da Cunha, M. M., Liot, G., Cordelieres, F. P., Marco, S. & Saudou, F. 2013. Vesicular glycolysis provides on-board energy for fast axonal transport. *Cell,* 152**,** 479-91.

Zaltieri, M., Longhena, F., Pizzi, M., Missale, C., Spano, P. & Bellucci, A. 2015. Mitochondrial Dysfunction and alpha-Synuclein Synaptic Pathology in Parkinson's Disease: Who's on First? *Parkinsons Dis,* 2015**,** 108029.

Zhang, X. M., Walsh, B., Mitchell, C. A. & Rowe, T. 2005. TBC domain family, member 15 is a novel mammalian Rab GTPase-activating protein with substrate preference for Rab7. *Biochem Biophys Res Commun,* 335**,** 154-61.

Zhang, Y., Chen, K., Sloan, S. A., Bennett, M. L., Scholze, A. R., O'Keeffe, S., Phatnani, H. P., Guarnieri, P., Caneda, C., Ruderisch, N., Deng, S., Liddelow, S. A., Zhang, C., Daneman, R., Maniatis, T., Barres, B. A. & Wu, J. Q. 2014. An RNA-sequencing transcriptome and splicing database of glia, neurons, and vascular cells of the cerebral cortex. *J Neurosci,* 34**,** 11929-47.

Zhang, Y., Sloan, S. A., Clarke, L. E., Caneda, C., Plaza, C. A., Blumenthal, P. D., Vogel, H., Steinberg, G. K., Edwards, M. S., Li, G., Duncan, J. A., 3rd, Cheshier, S. H., Shuer, L. M., Chang, E. F., Grant, G. A., Gephart, M. G. & Barres, B. A. 2016. Purification and Characterization of Progenitor and Mature Human Astrocytes Reveals Transcriptional and Functional Differences with Mouse. *Neuron,* 89**,** 37-53.

Zheng, Y., Wildonger, J., Ye, B., Zhang, Y., Kita, A., Younger, S. H., Zimmerman, S., Jan, L. Y. & Jan, Y. N. 2008. Dynein is required for polarized dendritic transport and uniform microtubule orientation in axons. *Nat Cell Biol,* 10**,** 1172-80.

Zheng, Y., Zhang, X., Wu, X., Jiang, L., Ahsan, A., Ma, S., Xiao, Z., Han, F., Qin, Z. H., Hu, W. & Chen, Z. 2019. Somatic autophagy of axonal mitochondria in ischemic neurons. *J Cell Biol,* 218**,** 1891-1907.

Zhou, B., Yu, P., Lin, M. Y., Sun, T., Chen, Y. & Sheng, Z. H. 2016. Facilitation of axon regeneration by enhancing mitochondrial transport and rescuing energy deficits. *J Cell Biol,* 214**,** 103-19.

Ziviani, E., Tao, R. N. & Whitworth, A. J. 2010. Drosophila parkin requires PINK1 for mitochondrial translocation and ubiquitinates mitofusin. *Proc Natl Acad Sci U S A,* 107**,** 5018-23.

Zuchner, S., De Jonghe, P., Jordanova, A., Claeys, K. G., Guergueltcheva, V., Cherninkova, S., Hamilton, S. R., Van Stavern, G., Krajewski, K. M., Stajich, J., Tournev, I., Verhoeven, K., Langerhorst, C. T., de Visser, M., Baas, F., Bird, T., Timmerman, V., Shy, M. & Vance, J. M. 2006. Axonal neuropathy with optic atrophy is caused by mutations in mitofusin 2. *Ann Neurol,* 59**,** 276-81.

Zuchner, S., Mersiyanova, I. V., Muglia, M., Bissar-Tadmouri, N., Rochelle, J., Dadali, E. L., Zappia, M., Nelis, E., Patitucci, A., Senderek, J., Parman, Y., Evgrafov, O., Jonghe, P. D., Takahashi, Y., Tsuji, S., Pericak-Vance, M. A., Quattrone, A., Battaloglu, E., Polyakov, A. V., Timmerman, V., Schroder, J. M. & Vance, J. M. 2004. Mutations in the mitochondrial GTPase mitofusin 2 cause Charcot-Marie-Tooth neuropathy type 2A. *Nat Genet,* 36**,** 449-51.